School of Biomedical Sciences

Dermal Fibroblast Extracellular Matrix Regulates Keratinocyte Behaviour

Wong Chee Wai

This thesis is presented for the Degree of
Doctor of Philosophy
of
Curtin University

September 2017

Declaration

To the best of my knowledge and belief, this thesis contains no material previously published by any other person except where due acknowledgement has been made. This thesis contains no material which has been accepted for an award of any other degree or diploma in any university.

Signature: Wong Chee Wai

Date: 5th September 2017

Acknowledgements

Firstly, I would like to thank my principal supervisor, Professor Deirdre Coombe sincerely. Deirdre's passion for scientific research and her expertise in cell biology has been invaluable throughout this study. Her constant guidance and support have been very crucial in helping me to complete my doctoral degree. Furthermore, I am very grateful that Deirdre has provided ample directions to keep me focus on the project at hand but still allows me to a degree of freedom to develop as an independent researcher.

I offer my heartfelt gratitude to my co-supervisor, Professor Birgitte Lane at A*STAR Institute of Medical Science, Singapore. She has graciously hosted me for eight months in her lab, providing me with the opportunity to perform experiments that may not have been possible. She also used her precious time to provide valuable comments that were essential in the completion of this study.

I would like to thank my co-supervisor/colleague, Dr Danielle Dye who has been providing advice during my PhD. She has been generous with her time whenever I came to her to discuss problems that have arisen during the study. Her keen insight in solving key issues have been essential in the progress of the project

A very special thank you to Associate Professor Pritinder Kaur. She has been very kind in sharing her knowledge in keratinocyte biology. She has also provided advice on how to approach the massive microarray data that was obtained. Pritinder has also provided valuable comments that have helped me develop a deeper understanding of biological research.

I would like to extend my sincere thanks to the lab members of the Molecular Immunology Group. Ms Beverley Kinnear expertise in tissue culture has been beneficial throughout my PhD studies. Her constant guidance and direction have helped me solve issues that have arisen with regards in culturing keratinocytes. Ms Catherine Legrand, for helping me complete some of the essential experiments. Many thanks to the current and past lab members, who have provided a reason to keep laughing when there is none.

I would like to thank some of my collaborators, who have been essential in completing experiments that are critical to this study. Professor Michael Raghunath, for his advice on the use of macromolecular crowding. Dr Simon Lieven (Birgitte Lane's Lab) in the analysis the microarray data. Dr Radoslaw Mikolaj (A*STAR Institute of Molecular Cell Biology) and Dr Rajkumar Ramalingam (Brian Burke's Lab, A*STAR Institute of Medical Science) for performing the proteomic analysis. Dr Cedric Badowski, who has imparted me his knowledge on using confocal microscopy and image processing. Dr Paula Benny, who has graciously help me during my stay in Birgitte Lane's, even when she was busy completing her thesis.

Finally, while this doctoral degree has taken four years to complete, the journey up to this point has been much longer. I would like to thank my parents, siblings and my uncle from Singapore for their support that they have given to me while I was struggling to arrive at this point. They have been worried that I may fail and end up as a gloried "test tube washer" at a corner of a rundown laboratory. I am hopeful that the resulting work that I have accomplished will do justice of their faith they have in me.

Abstract

The large-scale expansion of human keratinocytes under serum and feeder free conditions has remained a challenge and long-term expansion of keratinocytes under this conditions has resulted in diminished proliferation and an increased commitment towards terminal differentiation. Identification of culture conditions that enable a longer term expansion of keratinocytes than is presently possible would have a dramatic impact on their clinical application. It is believed that the microenvironmental niche in which cells reside is a factor in determining a cell's fate. A key component of the microenvironmental niche is the extracellular matrix (ECM). It is known that the ECM can regulate the cell behaviour such as adhesion and migration, and it is also known that adhesion is essential for keratinocyte survival and proliferation. For these reasons dermal fibroblast-derived matrices prepared under xenogeneic-free conditions were explored as a substrate for keratinocyte expansion *in vitro*.

Cell-derived matrices are attracting attention for tissue engineering because they contain naturally derived complex sets of physiological signals that are capable of directing a cell's fate. While it is possible to generate ECM *in vitro*, the current culture systems do not allow an efficient assembly and deposition of ECM. In **Chapter III**, a method for generating a structured and well assembled ECM under xenogeneic-free conditions is described. The technique is called "macromolecular crowding", which uses inert synthetic, or natural macromolecules to mimic the crowded conditions that occur *in vivo,* in an *in vitro* culture. Here a Ficoll70/400 mixture was used to produce crowded conditions, which resulted in the production of a well assembled ECM by the primary human dermal fibroblasts.

The dermal fibroblasts matrices were decellularised before being used as substrates for keratinocyte cultures. Various decellularisation methods were tested and are described. Of the decellularisation methods that were compared in **Chapter III**, Phospholipase A_2 was found to best remove cellular components, while preserving the integrity of the ECM. Immunofluorescence revealed that the acellular ECM contained ECM proteins such as type I collagen and fibronectin, and proteomic analysis indicated that the acellular matrix contained an ECM profile that resembled what had been

published for skin dermis. Furthermore, using confocal microscopy, the ultrastructure of the ECM was shown to be preserved.

In **Chapter IV**, the functionality of the dermal fibroblast-derived matrix (Fib-Mat) developed in **Chapter III** was assessed. Fib-Mat was shown to be a superior substrate for the growth of primary human keratinocytes in serum free medium compared to a traditional substrate of bovine type-I collagen or tissue culture plastic (TCP). The keratinocytes on Fib-Mat proliferated more rapidly and retained a high level of Ki-67 expression compared to cells cultured on type I collagen or TCP. More keratinocytes were undifferentiated, as indicated by their small size, cell mobility and the expression of p63, suggesting that the dermal ECM supported the retention of undifferentiated/basal keratinocytes during *in vitro* culture.

The importance of ECM composition was further investigated in **Chapter V.** The foetal skin can restore architecture, organisation and function of an injured site without scarring, whereas adult skin repairs with scar formation. Differences in the ECM composition between the adult and foetal dermis was said to be a reason for healing with scar formation in adult skin. In **Chapter V**, the differences in ECM composition between the adult and foetal dermal fibroblast matrices were explored. Quantitative proteomic analysis revealed differences in the composition of the ECM proteins deposited by adult and foetal dermal fibroblasts. When keratinocytes were grown on matrices generated by either adult or foetal dermal fibroblasts, dramatic differences in their gene expression profiles were found. Keratinocytes grown on foetal matrices upregulated the expression of genes involved in cell cycle, whereas, keratinocytes grown on adult matrices expressed a balanced mix of differentiation and cell cycle genes.

Overall, the goal of this project was to explore the use of dermal fibroblast-derived matrices in the expansion of undifferentiated keratinocytes. Data obtained from this study have shown the huge influence that ECM composition has on keratinocyte gene expression. It is hoped that the finding that foetal matrices promote the expansion of adult keratinocytes will assist in the development of cell based therapies for repairing injured skin.

Conference Presentation During Thesis

Oral

- "Dermal Fibroblast-Derived Matrix Modulates Human Keratinocyte Proliferation and Differentiation *In Vitro"* at ASMR Medical Research Week Scientific Symposium 2017, ECU Mount Lawley Campus Perth, WA at 7th June 2017
- "The Matrix Microenvironment Modulates Human Keratinocyte Proliferation and Differentiation *In Vitro*" at The Joint Meeting of AWTRS & MEPSA 2016 in Melbourne Convention Centre, Melbourne from 7th-9th November 2016
- "A Xenogeneic-Free, Fibroblast-Derived Matrix for Keratinocyte Growth" at the Mark Liveris Health Science Research Student Seminar in Curtin University, WA on 1st September 2016 (Oral Session)
- "A Xenogeneic-Free, Fibroblast-Derived Matrix for Keratinocyte Growth" at the Mark Liveris Health Science Research Student Seminar in Curtin University, WA on 11th November 2014 (Poster Blitz Session)

Poster

- **Chee-Wai Wong,** Beverley F Kinnear, Michael Raghunath, Birgitte E Lane and Deirdre R Coombe "A Xenogeneic-Free, Fibroblast-Derived Matrix for Keratinocyte Growth" at the 26th Combined Biological Science Meeting in UWA, Perth on 26th August 2016
- **Chee-Wai Wong,** Danielle Dye, Michael Raghunath, Birgitte E Lane and Deirdre R Coombe "A Xenogeneic-Free, Fibroblast-Derived Matrix for Keratinocyte Growth" at the Mark Liveris Health Science Research Student Seminar in Curtin University, WA on 11th November 2014
- **Chee-Wai Wong,** Beverley F Kinnear, Michael Raghunath, Birgitte E Lane and Deirdre R Coombe "A Xenogeneic-Free, Fibroblast-Derived Matrix for Keratinocyte Growth" at the 38th Annual Scientific Meeting of Matrix Biology Society of Australia and New Zealand, Queenscliff, Melbourne from 25th-28th October 2014

Awards Obtained During This Thesis

- AWTRS Conference Travel Award (2016) for The Joint Meeting of AWTRS & MEPSA 2016 in Melbourne Convention Centre, Melbourne from 7th-9th November 2016
- Best Paper Award (2016) during the Mark Liveris Health Science Research Student Seminar in Curtin University, WA on 1st September 2016 (Oral Session)
- Poster Award for Cell and Developmental Biology (2016) during the 26th Combined Biologic
- Image of the Month of April and May (2016) at Curtin Health Innovation Research Institute-Biosciences
- Curtin Strategic International Research Scholarship (2013-2017)
  This PhD scholarship covered tuition fees and living stipend for 3.5 years

Abbreviation

The following abbreviations are used throughout this thesis:

°C	Degree Celsius
α-SMA	Alpha-Smooth Muscle Actin
AA	Ascorbic Acid
AD-MAT	Adult Dermal Fibroblast-Derived Extracellular Matrix
AH	Ammonia Hydroxide
ANOVA	Analysis of Variance
APS	Ammonium Persulfate
ATCC	American Type Culture Collection
BM	Basement Membrane
BMP	Bone Morphogenic Protein
BSA	Bovine Serum Albumin
$CaCl_2$	Calcium Chloride
CDM	Cell-Derived Matrix
Col I	Type I Collagen
CP	Committed Progenitor
CS	Chondroitin Sulphate
ddH_2O	Double Distilled Water
DKSFM	Defined Keratinocyte Serum Free Media
DMEM	Dulbecco's Modified Eagle's Medium
DMSO	Dimethyl Sufoxide
DS	Dermatan Sulphate
DTT	Dithiothreitol
ECM	Extracellular Matrix
EDTA	Ethylenediamine Tetra-Acetic Acid
EGC	Etched Glass Coverslip
EGF	Epidermal Growth Factor
EGFR	Epidermal Growth Factor Receptor
EPU	Epidermal Proliferation Unit
ESC	Embryonic Stem Cell
FA	Focal Adhesion

FBS	Fetal Bovine Serum
Fib-MAT	Fibroblast-Derived Extracellular Matrix
FITC	Fluorescein Isothiocynate
FGF	Fibroblast Growth Factor
FT-MAT	Foetal Dermal Fibroblast-Derived Extracellular Matrix
GAG	Glycosaminoglycan
GO	Gene Ontology
GORILLA	Gene Ontology Enrichment Analysis and Visualization
HA	Hyaluronan
HEPES	N-2-hydroxyethylpiperazine-N-2-ethane sulfonic acid
HRP	Horseradish Peroxidase
HS	Heparan Sulphate
IGF	Insulin-like Growth Factor
IGFBP	Insulin Growth Factor Binding Protein
IgG	Immunoglobulin Superfamily
IL-6	Interleukin-6
IL-8	Interleukin-8
INV	Involucrin
K5	Cytokeratin 5
K8	Cytokeratin 8
K10	Cytokeratin 10
K14	Cytokeratin 14
K16	Cytokeratin 16
K18	Cytokeratin 18
kDa	Kilodalton
KGF	Keratinocyte Growth Factor
KMM	Keratinocyte Maintenance Media
KS	Keratan Sulphate
µ	Micro
µM	Micro Molar
m	Milli
M	Molar
mA	Milli Amperes
mAb	Monoclonal Antibody

MAL	Megakaryocytic Acute Leukaemia
MAPK	Mitogen Activated Protein Kinase
MCDM	Macromolecular Crowding ECM Deposition Media
$MgCl_2$	Magnesium Chloride
MGP	Matrix GLA Protein
mL	Milli Liter
mM	Milli Molar
MMC	Macromolecular Crowder
MS	Mass Spectrometry
MSC	Mesenchymal Stem Cell
MTG	Monothioglycerol
MW	Molecular Weight
NDM	Normal ECM Deposition Media
nM	Nano Molar
NP40	Nonidet P40
PAGE	Polyacrylamide Gel Electrophoresis
PBS	Phosphate Buffered Saline
PBS-T	PBS-Tween
PCA	Principle Component Analysis
PCP	Procollagen C-Proteinase
PDGF	Platelet-Derived Growth Factor
PI3K	Phosphatidylinositol 3-Kinase
PLA_2	Phospholipase A_2
PM	Post Mitotic
REVIGO	Reduce + Visualise Gene Ontology
RIPA	Radioimmunoprecipitation Assay
ROCK	Rho associated Kinase
RT	Room Temperature
SB	Stratum Basale
SC	Stratum Corneum
SD	Standard Deviation
SDS	Sodium Dodecyl Sulfate
SDS-PAGE	Sodium Dodecyl Sulfate Polyacrylamide Gel Electrophoresis
SG	Stratum Granulosum

SRF	Serum Response Factor
SS	Stratum Spinosum
TA	Transit Amplifying
TCP	Tissue Culture Plastic
TEAB	Triethylammonium Bicarbonate
TEMED	N,N,N',N'-tetramethylethane-1,2-diamine
TGFβ	Transforming Growth Factor β
TMT	Tandem Mass Tag
Tris	Tris (Hydroxymethyl) Aminomethane
TX-100	Triton X-100
U	Unit of Enzyme
WNT	Wingless

Table of Contents

Chapter I:

Introduction and Literature Review

1.0 The Architecture of the Skin

The skin is a complex structure that forms the largest organ of the body. It is an indispensable barrier that protects the body against environmental stresses such as fluid loss, infectious pathogen, mechanical trauma, chemical assaults and radiation (Fig. 1A). Skin is composed of two distinct layers, the epidermis and the dermis, which are separated by a basement membrane[1,2] (Fig. 1B).

1.0.1 Epidermis

Located on the outer layer of the skin, the epidermis is a stratified squamous epithelium that is mainly composed of keratinocytes. Depending on the progression of keratinocyte differentiation, the epidermis can be divided into four distinct layers: stratum basale (SB), stratum spinosum (SS), stratum granulosum (SG) and stratum corneum (SC). The SB is the innermost epidermal layer, and it consists of undifferentiated stem cells and committed progenitor cells that express keratin 5 (K5) and K14[3]. These cells are called basal keratinocytes, and they are primarily responsible for cell renewal of the epidermis. Committed progenitor cells, which are also known as transient amplifying keratinocytes, can divide rapidly but have a reduced capacity for continued proliferation. Upon differentiation, basal keratinocytes detach from the basement membrane and move up through the different layers to begin a gradual process of terminal differentiation. As they move through the SS, the keratinocytes express keratins distinct from those found in the SB, such as K1 and K10. Once in the SG, the cells will synthesise proteins such as involucrin and lipids, which contribute to the barrier function as well as the intercellular cohesion within the SC[3,4]. Finally, at the SC, which is the outermost layer of the epidermis, the keratinocytes become fully mature and transform into corneocytes: dead keratinocyte-derived cells which are devoid of organelles. This layer serves as the body's principal barrier against environmental assaults[2,5]

1.0.3 Dermis

Underlying the epidermis is the dermis, which provides both structural and nutritional support to the epidermal layer. The dermis is predominantly composed of connective tissue and is made up of two main types of fibrous proteins: members of the collagen family and elastin. Both of these protein types are synthesised by fibroblasts and are

arranged in such a way so as to provide tensile strength, elasticity and resilience, thereby protecting the body from mechanical injuries[6,7]. Besides the collagen and elastin, the dermis of functional skin also contains growth factors, proteoglycans and supportive glycosaminoglycans such as hyaluronic acid, dermatan sulphate and heparan sulphate. The resulting structure retains and binds water, thereby facilitating the passage of nutrients and other chemicals, as well as providing a lubricant for skin movement and bulk for shock absorption[4,6,8].

1.0.4 Basement Membrane

The basement membrane (BM) is a thin sheet of specialised extracellular matrix (ECM) that underlies all epithelial cell sheets and tubes; it separates the epithelial layer from the underlying connective tissue. It provides structural support to the cells and is also capable of influencing cell behaviour[9]. In addition, it provides a tissue-specific niche because different combinations of ECM proteins are present in the BMs of different tissues. While there may be a diversity of BM composition at different tissue sites, all BMs have in common the principle structural components of type IV collagen, a laminin family member, nidogen, perlecan and other heparan sulphate proteoglycans[10]. Both laminin and type IV collagen is responsible for the overall structure of the BM, as these two protein types assemble into independent networks. It is thought laminin molecules generate two-dimensional sheet structures by joining/linking to each other whilst still bound, via integrins, to the cells that have synthesised them. In contrast, type IV collagen networks are formed through the covalent crosslinking of their non-collagenous C- and globular N-terminus by disulphide bonds[11]. Nidogen and perlecan link the laminin and type IV collagen networks by binding to both protein networks[12,13]. During development, the presence of laminin is crucial for the formation of the BM, whilst type IV collagen is essential for BM stability and functionality[14,15]. Type IV collagen and laminin are also crucial for the maintenance of the basal keratinocyte's "stemness" in adult skin, as the anchoring of keratinocytes to the BM modulates their differentiation[16-18].

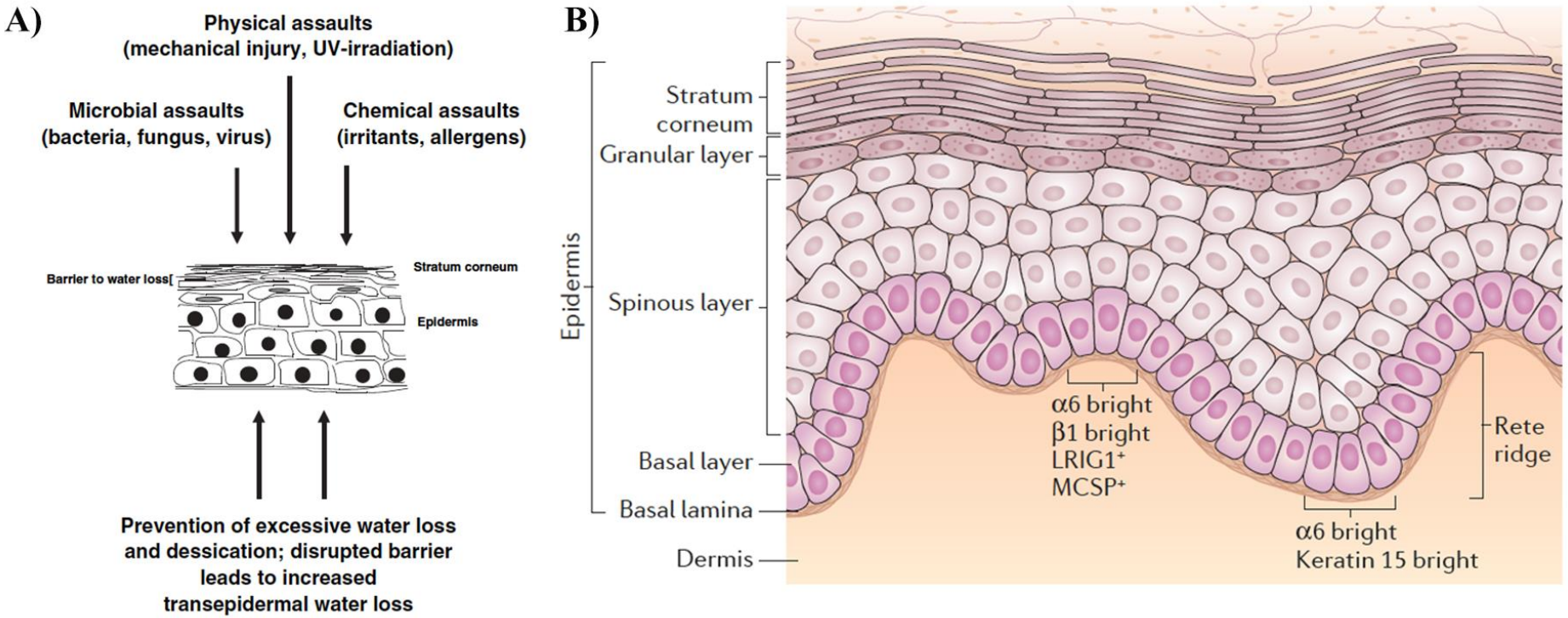

Figure 1.1: Anatomy of the skin. A) The skin protects the body from physical, microbial and chemical assaults, as well as preventing water loss. B) The structure of the skin. The epidermis, which contains the stratum basale, stratum spinosum, stratum granulosum and stratum corneum, serves as the protective layer, whilst the dermis is a connective tissue containing dermal fibroblasts embedded in an extracellular matrix which, provides support and nourishment to keratinocytes. Figures were adapted from Proksch *et al.*[2] *and* Solanas *et al.*[19]

1.1 Development of the Epidermis

The origin of the epidermis lies within the embryonic ectoderm. The embryonic ectoderm has the potential to give rise to the epidermal or neuronal cells[1,20]. The commitment of the ectoderm to either fate is largely a result of the combined effects of wingless (WNT), fibroblast growth factor (FGF) and bone morphogenic protein (BMP) signalling pathways. Under the guidance of the FGF pathway, neuronal induction is the "default" progression pathway of the ectoderm. However, in the presence of WNT, the ectoderm responsiveness shifts towards the BMP pathway. As a consequence, neural induction is blocked, and the cells are directed to an epidermal lineage[21] (Fig. 1.2). This epidermal commitment is marked by a transition of keratin expression patterns from the expression of keratin 8 (K8)/K18 to K5/K14 expression. These cells will form a single layer of proliferating basal keratinocytes, covered by a transient protective layered called the periderm. During the process of epidermal stratification, the periderm acts as a barrier, protecting the developing skin from amniotic fluids. Once epidermal stratification is completed, the periderm sheds and is lost[20].

1.1.1 p63 Signaling

Ectodermal commitment towards an epidermal fate, and epidermal stratification is highly dependent on the transcription factor p63. This protein is a member of the p53 transcription factor family. Evidence indicating the importance of p63 in this regard came from mouse knock-out experiments. Mice in which p63 expression was ablated displayed a defect in initiating epidermal fate commitment. The epidermis in these mice also lacked an ability to stratify and to form a mature epidermis[22,23]. Although a single layer of epithelium was formed, it failed to express the epidermal determination markers, K5 and K14. Instead, this layer still expressed K8 and K18, which is indicative of a failure of the ectoderm to transition into an epidermal lineage[24,25]. Interestingly, the inability to form an epidermis could be rescued, if p63 was exogenously expressed in the K8 and K18 positive epithelial layer, suggesting p63 has a critical role in epidermal determination. The importance of p63 was further demonstrated *in vitro*, by Medawar *et al*.[26] using embryonic stem cells (ESCs). Further investigation showed that K5 and K14 are direct transcriptional targets of p63, and p63 has been shown to interact with a p63-responsive regulatory element located upstream

of the enhancer region in K5 and K14 genes[27,28]. In addition to activating the expression of the epidermal determination markers, K5 and K14, p63 also function to suppress non-epidermal genes, as the aberrant expression of non-epidermal genes was observed when the expression of p63 was lost. The suppression of non-epidermal genes by p63 is through the BMP7/SMAD7 pathway. Rosa *et al.*[29] demonstrated that the p63 transcription factor represses the transcription of the SMAD7 inhibitory factor, which has the effect of ensuring signalling from BMP7 is sustained and the expression of non-epidermal genes is prevented.

The continued development and maturation of the epidermis is dependent on the action of two p63 isoforms, TAp63 and ΔNp63. The existence of these isoforms is due to the presence of two alternative promoters. These alternative promoters generate p63 that contains, or lacks the transactivating domain[30]. Currently, contrasting evidence has led to two different conclusions on the precise contribution of these two p63 isoforms. Koster *et al.*[24] reported that TAp63 is the first isoform to be expressed during early epidermal development and suggested it is required for the initiation of epidermal fate commitment and the inhibition of terminal differentiation. These authors further hypothesised that ΔNp63 expression during late epidermal development counteracts the function of TAp63 to promote the maturation of the embryonic epidermis. An alternative explanation was proposed by Laurikkala *et al.*[31] and Zhao *et al.*[32]. They showed that ΔNp63 is expressed during all stages of epidermal development and that it is required for the ectoderm to commit to an epidermal fate. This view was consistent with studies conducted by Aberdam *et al.*[33] and Medawar *et al.*[26], who indicated that ΔNp63 is required for epidermal commitment of embryonic stem cells. Further studies on mature epidermis showed that ΔNp63 is the main isoform expressed in keratinocytes residing in the proliferative basal layer, and that the expression of ΔNp63 is decreased during terminal differentiation[34].

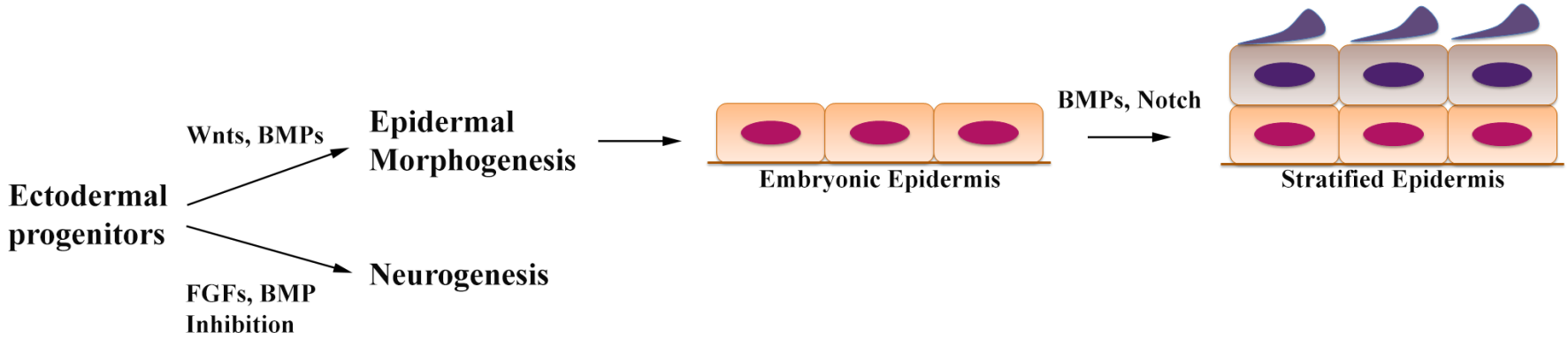

Figure 1.2: Early signalling molecules required to direct the ectodermal progenitors towards an epidermal lineage.

In the absence of WNT, ectodermal progenitors respond to FGFs, downregulates BMP signalling and proceed towards a neuronal lineage through neurogenesis. However, in the presence of WNT, the ability of ectodermal progenitor cells to respond to FGFs are blocked. As a consequence, this allows ectodermal progenitor cells to respond to BMP signalling and adopt an epidermal fate. The figure was adapted from Fuchs[1].

A recent study by Koh *et al.*[35] showed that TAp63 is involved in the transcriptional control of late differentiation pathways in keratinocytes. They found that during keratinocyte differentiation, the expression of TAp63 increases. Their data revealed that TAp63 interacts with Notch signalling pathways to activate several late keratinocyte differentiation genes, including LCE1B, LCE1C, IGFBP3 and SPRR2[35]. Interestingly, Nylander *et al.*[34] observed that TAp63 was located at the suprabasal level in the skin, an observation which supports its involvement in late keratinocyte differentiation. These data suggest that the sequential activation of the p63 isoforms is critical for epidermal development. It is likely that ΔNp63 expression is required for the epidermal fate commitment of the ectoderm layer and the maintenance of keratinocyte stem cells in the basal layer; while a transition of ΔNp63 to TAp63 expression is required during keratinocyte late terminal differentiation for the stratification and maturation of the epidermis.

1.1.2 Notch Signalling

Following ectodermal commitment towards an epidermal fate, the further development of this tissue takes place under the influence of the various p63 isoforms as described above. Importantly, the Notch signalling pathway downstream of TAp63 was also found to play a key role in regulating epidermal differentiation[35,36]. The Notch signalling pathway is a highly conserved molecular network that is involved in directing cell fate decisions such proliferation, migration, differentiation and cell death[36-39]. Signalling within this pathway occurs over a short range as notch receptors and its ligands are transmembrane receptors[35]. The notch ligands have been placed into either the Delta-like or Jagged family of molecules[36,40]. Within the epidermis, the expression of all four Notch receptor homologs has been well-documented. These receptors have been observed to be expressed by keratinocytes located in the suprabasal layer of the epidermis, which is a site where the cells progress towards terminal differentiation[40]. Hence, it has been hypothesized that notch signalling could be involved in initiating keratinocyte terminal differentiation during epidermal development.

A prerequisite of keratinocyte progression toward terminal differentiation is their withdrawal from the cell cycle, and it is believed that Notch signalling is involved in this process[36]. Conditional knockdown of Notch1 in the basal layer of the murine

epidermis has resulted in significant epidermal thickening, which is associated with keratinocyte hyperproliferation. This indicates that Notch signalling provides growth inhibitory signals[41]. Further investigation revealed that Notch1 upregulates the cell cycle regulator p21, and this protein acts to initiate terminal differentiation by inhibiting the cell cycle in proliferating keratinocytes[41]. In addition, Notch has been shown to inhibit p63 activity and so supress keratinocyte stem cell self-renewal and promote differentiation[42]. These data reflect the important role Notch signalling plays in providing signals for cell cycle arrest that result in the progression of keratinocytes towards terminal differentiation.

1.1.3 Rho/Rock Signalling

Rho/Rock signalling is another signalling pathway that is known to be involved in epidermal development. This pathway ensures the proper differentiation and stratification of the epidermis. Rho GTPases are small, evolutionarily conserved proteins, belonging to a unique subgroup within the Ras superfamily of small GTPases[43,44]. Extracellular stimului such as cell-matrix or cell-cell interactions and mechanical stresses have been shown to activate Rho GTPases. These activated Rho GTPases than bind to a variety of effectors to stimulate downstream signalling pathways involved in cell migration, adhesion, proliferation and differentiation[43]. One of the downstream effector molecules is the Rho-associated protein kinase (ROCK). Currently, two isoforms have been identified: ROCKI and ROCKII[45]. Collective studies have shown that the activation of the members of the Rho GTPases family (Rho A, Rho B, Rho C and Rho E) and their downstream effectors, ROCKI and ROCKII is critical to induce keratinocyte terminal differentiation[45-47]. Inhibition of the Rho/ROCK signalling pathway using a pharmacological inhibitor of ROCK, Y-27632, was found to prevent terminal differentiation of keratinocytes. Interestingly, the Y-27632 inhibitor was shown to effectively increase the proliferative capability of keratinocytes during *in vitro* culture[46,48,49]. Further investigation indicates that the attenuation of the Rho/ROCK pathway promotes the expression of genes related to cell division, while reducing the expression of genes involved in keratinocyte terminal differentiation[50]. These data indicate the contribution of the Rho/ROCK signalling pathway is required for keratinocytes to progress to terminal differentiation.

1.2 Maintenance of Adult Epidermis

Upon maturation, the epidermis undergoes homeostatic regulation and continuously replaces cells that are lost by shedding. Homeostatic regulation follows a hierarchal order, whereby quiescent stem cells generate short-lived populations of transit-amplifying (TA) cells that undergo several cell divisions before initiating terminal differentiation and migrating upwards[19,51]. The cells involved in skin homeostatic regulation were believed to be organised as clonal epidermal proliferative units (EPUs), comprising a central slow cycling stem cell, surrounded by TA cells that maintain the overlying differentiated cell layer[52]. Initial evidence for the EPU model came from analysing the histological structure of the mouse epidermis[53]. In this work, the mouse epidermis was described as consisting of a regular array of columns of cells and within the centre of each column was a quiescent epidermal cell, while the adjacent cells were mitotically active. Hence, this led to the proposal that a stem cell was located in the centre of each column of cells and this stem cell generated a short-lived population of clonal TA cells, and these TA cells maintained the column of differentiating cells[53-55]. This arrangement of a stem cell and TA cells into cell columns was called an EPU (Fig. 1.3A). Further evidence supporting the EPU model came from studies of label-retaining cells in the murine ear and dorsal epidermal tissues[56,57]. Cells were labelled with the DNA precursor H^3-thymidine, which became incorporated into the DNA. As the cells underwent division and DNA replication, the amount of H^3-thymidine per cell was halved. This meant that the label was lost when cells are actively proliferating and was only retained in those cells that were quiescent or divided infrequently. Scattered label-retaining cells were observed within the basal epidermal layer, and it was reported that these cells were likely to be slow cycling stem cells. These slow cycling cells were located predominantly in the centre of a cluster of unlabeled cells. Collectively these data were consistent with the EPU model[56,57]. In more recent studies, lineage tracing using genetic labelling similarly found a cell organisation that conformed with the EPU model for maintaining the cells within epidermis[58-60].

An alternative model of epidermal homoeostasis was more recently proposed from the work of Clayton *et al.*[61]. They used an *in vivo* inducible genetic method to label cells in the epidermis of a mouse tail; this allowed a quantitative lineage tracing experiment to be conducted. From these data, they proposed that a single population of committed

progenitor (CP) cells maintained homeostasis in the epidermis[61]. These CP cells had characteristics that did not conform to the classical properties used to describe stem cells or TA cells. The CP cells were not slow-cycling and long-lived like the stem cells, nor did they undergo terminal differentiation after limited cell division like the TA cells. Instead, these CP cells had the potential of unlimited cell division with a random probability of undergoing terminal differentiation[61] (Fig. 1.3B). Doupe *et al.*[62] described that the majority of the cells in a population of CP cells underwent asymmetric division producing a CP cell and a terminally differentiated post-mitotic (PM) cell. While a small proportion of cells in the CP cell population had an equal probability of undergoing symmetric division that either generated two CP cells or two PM cells[62]. Quantitative lineage tracing data of the keratinocytes within the mouse ear epidermis[63] or the oesophagal epithelium of mice[62] were also in agreement with the CP model. Furthermore, when Doupe and Jones[51] revisited earlier literature that described the EPU model, they concluded that the data were entirely consistent with CP behaviour. Interestingly, a recent study by Mascré *et al.*[64] presented quantitative lineage tracing data that supported the EPU model. Thus, it appears that there is no agreement as to whether epidermal homeostasis is achieved by CP cells according to the CP model or stem cells according to the EPU model. However, regardless of the EPU or the CP model presented, these data indicate that there is a population of cells that regulates the epidermal homoeostasis.

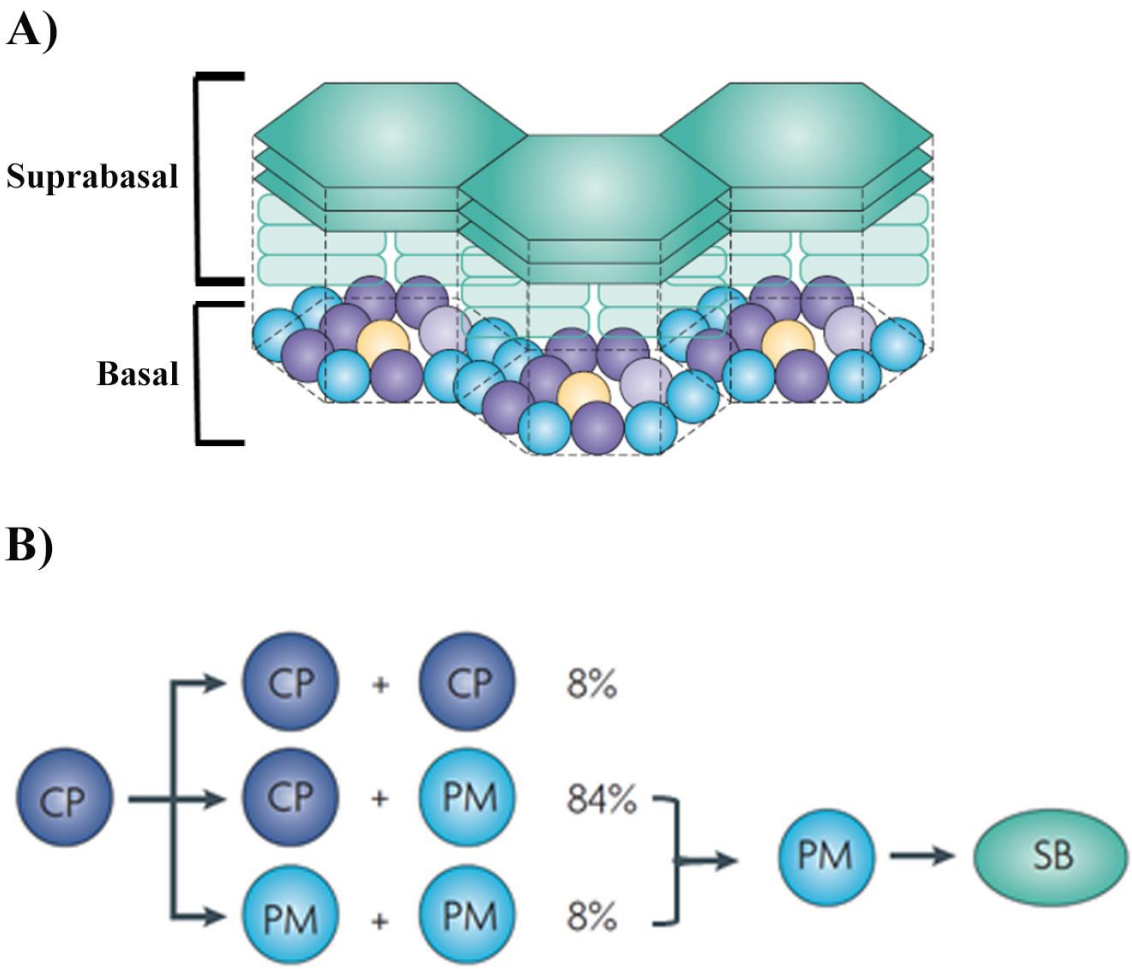

Figure 1.3: Cell Fate Models for Epidermal Homeostasis.

A) Epidermal Proliferation Unit Model. This model hypothesises that the epidermis is maintained by long-lived, slow cycling, self-renewing stem cells (yellow). These stem cells generate a transit-amplifying (TA) cell population (purple) that undergoes a limited number of cell divisions before undergoing terminal differentiation to become post-mitotic (PM) cells (blue). These PM cells subsequently detach from the basal layer and become the suprabasal cells (Green).

B) Committed Progenitor (CP) Model. The CP model describes a population of CP cells (dark blue) that maintain homeostasis of the epidermis. These cells either remain proliferative or becomes terminal differentiating, post-mitotic (PM) cells (blue). These PM cells subsequently detach from the basal layer and become the suprabasal cells (Green). The figure was adapted from Jones and Simons[65].

1.3 The Extracellular Matrix of the Skin

Extracellular matrix (ECM) is an acellular complex network of glycoproteins and carbohydrates that surrounds cells, tissues and organs. Studies over the decades have dramatically altered our knowledge and understanding of the ECM and its role in tissues. Not long ago, the ECM was thought to be a static structure, acting only as a scaffold to which cells adhere. Now, the ECM is viewed as a dynamic structure, providing both biochemical and biomechanical cues for regulating cell behaviours such as adhesion, migration, proliferation, differentiation and survival[66] (Fig. 1.4). Fundamentally, the ECM is composed of several different types of macromolecules; these are the fibrous structural proteins (e.g. collagen, fibronectin, laminin and elastin), specialised proteins (e.g. growth factors) and proteoglycans. However, each tissue has a specific tailored ECM that contains a unique composition and topology, which has been generated during development[67]. The unique matrix composition provides a microenvironmental niche that regulates stem cell homeostasis[68]. Table 1.1 lists some of the known ECM components of the skin.

1.3.1 Composition of the Skin Extracellular Matrix

1.3.1.1 Collagens

Collagens are the dominant structural proteins within the ECM, and they constitute up to 30% of the total proteins in the human body. They are synthesised and secreted into the ECM mainly by fibroblasts[67,69]. While there are up to 28 types of collagens, type I and type III collagen encompasses up to 90% of the total collagen within the skin, and type V collagen represents only 2%[70,71]. Other collagens such as type IV, VII and XVII are also integral in maintaining the proper function of the skin, as demonstrated by the fact that pathological skin conditions that are associated with a mutation in these minor collagens[71]. The collagens can be divided into either fibrillar or non-fibrillar family. The fibrillar collagens were the first members of the collagen superfamily to be discovered. They are characterised by their ability to assemble into highly ordered fibrils, and these fibrils appear to be banded at the ultrastructure level[72,73]. Members of the fibrillar collagens include collagen types I-III, V, XI, XXIV and XXVII[73]. These fibrillar collagens play a crucial role in contributing to the molecular architecture, shape and mechanical properties of tissues. Fibrillar collagens contribute to the tensile strength of skin[74]. The non-fibrillar collagens do not form classical collagen fibrils,

but instead aid the organisation of collagen fibrils into collagen fibres[71]. The tensile strength generated from the organisation of collagen fibrils provides biomechanical cues that control cell behaviour[74].This aspect will be discussed further in later sections.

1.3.1.2 Laminins

Laminins are a family of heterotrimeric multidomain glycoproteins. They are composed of an α-chain, β-chain and γ-chain. Currently, in mammals, genes encoding five α-chains, four β-chains and three γ-chains have been identified. While theoretically 60 trimeric combinations of laminin isoforms could be formed, thus far, only 16 combinations have been discovered[75,76]. Each laminin isoform is named according to its subunit composition; for example, the composition of laminin-111 is α1β1γ1 while laminin-511 is α5β1γ1. Laminins are critical during embryonic development, as naturally occurring or targeted mutations in a laminin gene often lead to embryonic lethality or organ defects[76,77]. During embryonic development, laminins are one of the earlier ECM proteins to appear. Studies have shown that laminins are critical components for the formation of BM. They form independent networks, which interact with other ECM proteins and glycoproteins such as perlecan, nidogen and type IV collagen to form the BM. Laminin-111 is a fundamental component of embryonic BMs and homozygous null mutations of the laminin subunits β1[14] and γ1[78] produces embryos that lack BMs and as a consequence also lack endoderm differentiation, resulting in postimplantation lethality. As mentioned previously, the formation of the BM is also essential for the maintenance of the basal keratinocyte's "stemness" in adult skin, as the anchoring of keratinocytes to the BM modulates their differentiation[16-18]. While laminins are crucial for the formation of BM, they are also critical in providing signals for embryonic development. Mutations in other laminin subunits such as α2, α3, α4, β2 and β3 cause perinatal and postnatal defects in skeletal muscle, nerves, skin, kidney and mucosal blood vessels; these defects occur because the laminin subunit mutation has affected the cell adhesion and tissue maintenance[79].

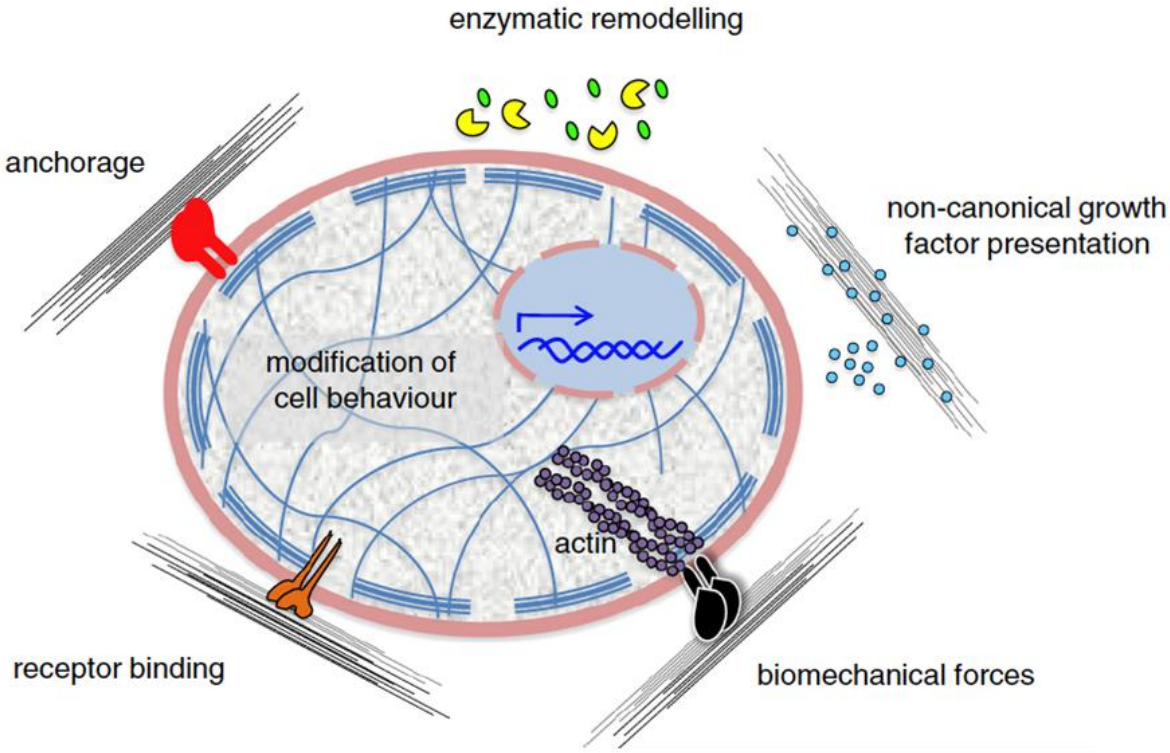

Figure 1.4: The biochemical and biomechanical regulation of cell behaviour by ECM. The ECM can exert its effect on cells by directly binding to the different types of cell surface receptors or co-receptors (red, orange, black), thereby mediating cell anchorage and regulating several pathways involved in intracellular signalling and mechanotransduction. Moreover, the ECM can also act by presenting growth factors (blue), or as a result of being remodelled by active enzymes, functional ECM fragments can be released (green). The figure was adapted from Gattazzo *et al.*[68].

Table 1.1: ECM composition of the Skin: Structural Components.

COMPONENTS	MOLECULAR ORGANISATION	TISSUE DISTRIBUTION	FUNCTIONAL ROLE
COLLAGENS			
TYPE I	[α1(I)]2α2(I)	Ubiquitous in most connective tissues, including skin, bones, tendons, ligaments, etc.	Major component providing tensile strength
TYPE III	[α1(III)]3	Skin, blood vessels, predominant in foetal tissues	Contributes to tensile properties
TYPE IV	[α1(IV)]2α2(IV)	Basement membranes, anchoring plaques	Major structural component of basement membranes
TYPE V	[α1(V)]2α2(V)β [α1(V)]3	Ubiquitous	Pericellular location interfacing the cell surface and the surrounding matrix
TYPE VI	α1(VI)α2(VI)α3(VI)	Extracellular microfibrils	Matrix assembly
TYPE VII	[α1(V)]3	Skin, foetal membranes	Structural component of anchoring fibrils
ELASTIC FIBERS			
ELASTIN	Cross-linked polymer of fibers	Blood vessels, skin and lungs	Resilience and elasticity of the skin
MICROFIBRILLAR COMPONENT	Surrounding the elastic fibers	Same as elastin	Scaffolding in formation of the elastic fibres
FIBRILLIN	Part of the microfibrillar component	Same as microfibrillar component	Stabilization of the microfibril structure
BASEMENT MEMBRANE ASSOCIATED MACROMOLECULES			
PROTEOGLYCANS/GAGS	Complex aggregates	Cartilage, skin	Maintenance of water and ion balance; regulation of growth, migration and attachment of cells
HEPARAN SULFATE PROTEOGLYCAN	Low and high density forms	Basement membranes	
LAMININ	α,β, γ	Basement membranes	Cell attachment and differentiation, neurite outgrowth
NIDOGEN/ENTACTIN	Stoichiometric binding to laminin	Colocalizes with laminin	Cell binding
FIBRONECTIN	Disulfide-linked dimers	Cell surface, plasma	Attachment of cells to the extracellular matrix

This figure was adapted from Uitto *et al.*[80]

1.3.1.3 Fibronectin

Fibronectin is a multifunctional high molecular weight ECM glycoprotein that is widely distributed throughout the body. It is a dimer of two almost identical monomers that are linked by disulphide bonding. Each fibronectin monomer is composed of three types of domains (type I, II and III). Within each fibronectin monomer, there are 12 type I domains, 2 type II domains and 15-17 type III domains, and this accounts for around 90% of the fibronectin sequence[81]. Type I and II domains are stabilised through two intra-chain disulphide bonds. The type III domain is composed of 90 amino acids, which form a beta sandwich fold with one beta sheet containing four strands and the other sheet containing three strands[82-84]. Fibronectin plays a crucial role in the initiation, progression and maturation of matrix assembly. The prominent role of fibronectin in matrix assembly lies in its numerous binding sites for collagen, heparan sulphate proteoglycans and other ECM proteins. This allows fibronectin to interact with these ECM proteins and so assemble the ECM structure[85,86]. Besides fibronectin containing numerous ECM protein binding sites and its involvement in matrix assembly, fibronectin is also known for its RGD binding sites. Integrins bind to the RGD sites, and so stimulate pathways that promote cell attachment, migration and differentiation[85,86]. One of the best known integrins to bind to the fibronectin's RGD sites is the α5β1 integrin. The interaction between α5β1 integrin and fibronectin has shown to inhibit the terminal differentiation of keratinocytes[87]. It was also demonstrated that there is a decrease in the affinity of α5β1 integrin to fibronectin when the keratinocytes are committed to terminal differentiation[88]. These data suggest that fibronectin may play a role in the expansion of undifferentiated keratinocytes.

1.3.1.4 Elastin

Elastin is the ECM component that is critical to the elasticity and resilience of many tissues such as skin, lung, arteries, elastic ligaments and cartilage. It provides these tissues with an ability to resume their original shape after stretching and compression[82,89]. Elastin consists of cross-linked tropoelastin, which interacts with elastin microfibrils to form elastic fibres. Tropoelastin is a ~60kDa unglycosylated protein that is secreted by a variety of cells such as fibroblasts, endothelial cells, chondrocytes, keratinocytes and smooth muscle cells[82,90]. Tropoelastin exists as different alternatively spliced variants, which vary depending

on the tissue site. Approximately 90% of the elastic fibres within a tissue is composed of an elastin core, which is surrounded by a layer of microfibrillar components such as fibrilins, fibulins and emilins. While elastin may only contribute to 2-5% of the total protein in skin, it plays a vital role in maintaining the structure, integrity and function of the skin[90,91]. The low modulus of elasticity and high resilience of elastin complement the tensile strength generated by the fibrillar collagen to provide the biomechanical cues, which can modulate cellular behaviour[92]. The biophysical aspects of the way in which the ECM modulates cell fate will be discussed in later sections.

1.3.1.5 Nidogen

Nidogen is a sulphated monomeric glycoprotein that accounts for 2-3% of all BM proteins[9]. Currently, nidogen-1 and nidogen-2 are the only known isoforms. Nidogen-1 is known to be expressed ubiquitously in all BM, while nidogen-2 has a more restricted expression pattern during development and adulthood. Both isoforms have been shown to interact with BM ECM proteins such as type IV collagen and the laminins. Nidogen acts to link the type IV collagen network with the laminin network to form the superstructure of the BM[9,11]. Studies revealed that nidogen is crucial for the integrity of the BM, as defects in the BM ultrastructure were observed when nidogen was absence. Furthermore, nidogen knockouts are embryonic lethal as a result of abnormal lung and heart development[93]. Interestingly, in nidogen-deficient mice, the gross morphology of the skin, including its appendages and stratification remained normal[94]. However, it has been shown that the absence of nidogen has an impact on the wound healing ability of adult mice. While re-epithelialization of the wounded area in nidogen null mice still occurs, loss of nidogen results in a thinner epidermis, with keratinocytes in the wounded area being less able to differentiate or proliferate[18]. This indicates that nidogen plays a role in modulating keratinocyte differentiation and proliferation. However, it is uncertain whether the modulation of keratinocyte behaviour that was observed is a direct effect from nidogen or is a result of the BM superstructure which is formed from the interaction of nidogen with type IV collagen and laminin networks.

1.3.1.6 Vitronectin

Vitronectin is a multifunctional adhesive matricellular protein that is abundant in blood plasma and is also found associated with the extracellular matrix in most tissues[95-97]. Within an *in vivo* environment, vitronectin can be presented in a monomeric or a multimeric form, depending on its interaction with other proteins or proteolytic enzymes. Hence, numerous vitronectin conformations are possible and these support different biological activities[96]. For example, a physical interaction with proteases or other matricellular proteins induces vitronectin to self-assemble into fibrils, these fibrils then associate with other ECM glycoproteins to form an interconnected network of ECM protein complexes[96,98]. The assembled ECM complex provides a suitable platform to support mammalian cell attachment which triggers the classical "outside-in" signalling cascade mediated by cell surface integrins to enable cell proliferation. This is particularly important for keratinocytes[96,99-101]. During the process of ECM assembly, the presence of vitronectin is critical, as studies have demonstrated that structural ECM proteins are unable to self-assemble into a functional ECM complex in the absence of vitronectin and the resulting provisional ECM is incapable of supporting cell attachment and proliferation[96]. Vitronectin is also known to interact with growth factors to modulate their activities[96]. For example, vitronectin binds to insulin-like growth factors (IGF) to enhance their activities, as demonstrated by Hyde et al[102]. These workers showed that IGFII-vitronectin complexes enhance keratinocyte the protein synthesis and cell migration. In addition, while IGFI does not bind directly to vitronectin, it does indirectly engage with vitronectin as it binds insulin growth factor binding protein-5 (IGFBP-5), forming a complex with vitronectin that also enhances protein synthesis and cell migration by keratinocytes[102]. Hence, it appears vitronectin is critical for forming a correctly assembled ECM, and its interactions with key growth factors enhances their activities; both of these functions are essential to modulate keratinocyte behaviour.

1.3.1.7 Proteoglycans

Proteoglycans are expressed ubiquitously throughout the human body, being present on cell surfaces as well as within the ECM[103]. They play a vital role in modulating signalling pathways during tissue morphogenesis and mammalian development[103,104]. Proteoglycans are comprised of a single core protein, to which are covalently attached with one or more glycosaminoglycan (GAG) chains. GAGs have a considerable

amount of structural heterogeneity, due to the diversity of their disaccharide compositions, glycosidic linkages and the level/position of their sulphate residues. As such, many of the biological functions of proteoglycans are derived from their physiochemical characteristics and the protein binding capabilities of their GAG chains which are attached to the core protein[103,105]. Some of the proteoglycans expressed within the skin are versican, perlecan and decorin.

Versican

Versican is a large chondroitin sulphate proteoglycan that belongs to the hyalectan family. It is comprised of a core protein with two covalently attached chondroitin sulphate chains[106,107]. Versican is known to be present within the ECM surrounding the cells in a variety of tissues and organs[107]. The hygroscopic properties of versican is a result from the negative charge of versican's GAG chains, and this contributes to the viscoelasticity of the pericellular microenvironment, which is necessary to support key events in development[106,108]. Furthermore, versican is known to interact with other ECM components such as hyaluronan (HA), tenascin, thrombospondin 1, fibronectin, and fibrillin to create a microenvironment that influences the ability of cells to change shape, adhere, proliferate, migrate, differentiate and survive[107,109-111]. Furthermore, depending on the ECM proteins that interact with versican, the mechanical properties of the matrix surrounding the cell may be altered and this difference in mechanotransduction influences cell behaviour[107]. It is known that the accumulation of versican at certain tissue sites occurs in regions where cells are undergoing active proliferation. At these sites, versican’s interaction with HA increases the viscoelastic nature of the pericellular matrix, and this creates a high malleable matrix microenvironment that supports changes in cell shape and enables cell proliferation[107]. Furthermore, versican could also influence cell proliferation by acting as a mitogen as it is known to bind to the G3 domain of the epidermal growth factor receptor(EGFR)[109], and EGFR is known to activate pathways for the expansion of undifferentiated keratinocytes[112]. Zimmermann *et al.*[113] showed that versican is located in the proliferative zone within the basal layer of the skin. Hence, versican is likely to play a critical role in modulating the proliferation of keratinocytes at the basal layer of the skin; by either creating a matrix microenvironment suitable for cell proliferation or acting as a mitogen as a consequence of its interaction with EGFR.

Perlecan

Perlecan is a modular heparan sulphate proteoglycan that has a ~500kDa core protein containing five potential attachment sites for GAGs such as chondroitin sulphate, heparan sulphate and keratan sulphate[104,114]. It is known to be expressed in both vascular and avascular tissues, and it is ubiquitously located within the BM. Perlecan is known to play a critical role in the formation of BMs. A deficiency in perlecan is lethal during embryonic development. Knock-out mouse models have shown that the loss of perlecan does not affect the initial deposition of BM, but defects in the BM ultrastructure were observed, which led to the abnormal development of certain organs such as the heart and skin[11,115]. Interestingly, while perlecan-deficient keratinocytes do not alter the deposition of the BM, they do lead to a thin and poorly organised epidermis[17]. Furthermore, it has been shown that a perlecan-deficiency also leads to the enhanced apoptosis of epithelial cells, which in turn leads to a failure of epithelial cell stratification[11,17]. Thus, perlecan contributes to the proper stratification of the epidermis.

Decorin

Decorin is a proteoglycan that has a core protein with a single chondroitin sulphate or dermatan sulphate chain attached[104]. The binding of decorin to collagen regulates the rate and degree of collagen fibrillogenesis. In the presence of decorin, collagen fibres are thinner and of a more uniform fibril diameter[116]. In the absence of decorin, collagen fibrils of varying thickness were observed, and the assembly of the collagen fibrils was shown to have a loose and irregular distribution, which resulted in a decrease in the tensile strength of tissue like skin, blood vessels and smooth muscle. Hence, it was proposed that decorin promotes collagen maturation through correct fibril formation and organisation[117,118]. The formation of uniform and correctly sized collagen fibrils have been shown to be important during skin development and in wound healing[104,116].

1.3.1.7 Glycosaminoglycans

Glycosaminoglycans are large, complex, negatively charged polysaccharides that are present in every mammalian tissue. They are composed of repeating disaccharide units of an amino acid sugar(N-acetyl glucosamine or N-acetyl galactosamine) and a uronic acid (glucuronic acid or iduronic acid)[119,120]. Differences in the composition of the monosaccharides in these disaccharide repeating units, as well as differences in the

sulphation patterns of these monosaccharides results in the following major categories of GAGs: hyaluronan (HA), chondroitin sulphate (CS), dermatan sulphate (DS), heparan sulphate (HS) and keratan sulphate (KS). With the exception of HA, all GAG chains are covalently linked to a serine residue on a core protein via a tetrasaccharide linkage, which consists of xylose, two galactose residues and glucuronic acid[119-121]. Within an aqueous environment, cations such as Ca^{2+} and Na^{+} are attracted to polyanionic GAGs causing them to absorb water which gives rise to a high hydrodynamic volume combined with low compressibility[119]. These properties enable GAGs to restrict and modulate the bioavailability of molecules such as water, cations and proteins like cytokines, chemokines and growth factors[119].

In addition to regulating the availability of the cytokines, chemokines and growth factors, GAGs also play a role in the activation of these molecules. A well-studied example is the binding of fibroblast growth factors (FGFs) to HS chains. The binding of FGFs to HS in the matrix locates these growth factors near the cell surface, and as a result, a more efficient binding of the FGFs to their cell surface receptors is facilitated. In addition, evidence indicates that HS is part of the FGF-FGF receptor complex and is required for activation of signalling cascades triggered by FGF binding[122]. The signalling cascade triggered by the binding of FGFs to their receptors is a key component of the differentiation of many tissues. An interaction, which is critical for keratinocytes, is that which occurs between HS and FGF2 and its receptor, as it has been shown that FGF2 is essential for the proliferation and migration of keratinocytes[123,124].

1.3.2 Biophysical Properties of the Extracellular Matrix

1.3.2.1 Cell Shape

Many events during embryonic development suggest that cell shape is a potent regulator of cell growth, survival and differentiation. Changes in cell shape enable the cells to better perform their specific functions. For example, the spherical shape that adipocytes adopt, maximises lipid storage, while neurones have a long axon that transmits signals over long distance[125]. Thus, it is plausible that the regulation of cell shape may be a key component in controlling cell fate. Initial indications for the potential of cell shape as a regulator of cell fate was shown in the studies on

keratinocytes conducted by Watt *et al.*[126]. By using microcontact printing, these authors generated distinct patterns of adhesive ECM "islands" that controlled the keratinocyte's ability to spread. An inverse correlation between the size of the ECM "islands" and the differentiation status of the keratinocytes was observed. When the keratinocytes resided on small islands their capability to spread was restricted, and they had a rounded morphology. These keratinocytes underwent terminal differentiation as indicated by their expression of involucrin and the inhibition of DNA synthesis[126]. Further investigations showed that keratinocytes residing on the small islands formed less focal adhesions, had less distinct F-actin stress fibres and had a lower level of G-actin compared to their counterparts residing on larger islands[127]. Furthermore, inhibition of cytoskeleton assembly using either Cytochalasin D, an actin depolymerization agent, or Jasplakinolide, an actin stabilising agent promoted terminal differentiation of the keratinocytes. From these data, the cytoskeleton and cell spreading appear to play a role in the directing keratinocyte fate. The actin cytoskeleton-mediated shape-induced differentiation of keratinocytes is regulated by the Serum Response Factor (SRF) transcriptional activity. The activity of SRF or its co-factor myocardin-related transcription factor-A (MRTF-A) has been shown to correlate with keratinocyte differentiation. It has been demonstrated by Connelly *et al.*[127] that G-actin plays a crucial role in preventing keratinocyte differentiation by inhibiting SRF activity through sequestering the MRTF-A and reducing its availability. These data showed how changes in cell shape and cytoskeletal rearrangement could affect keratinocyte differentiation.

1.3.2.2 Matrix Stiffness and Stem Cell Fate

Changes in cell shape and the modulation of cytoskeletal contraction occur in response to biophysical cues from the matrix such as stiffness. The stiffness of the matrix is detected by stem cells through their focal adhesions (FAs). FAs are the mechanical link between the ECM and the cell's actin cytoskeleton. In response to the varying stiffness of the ECM, the integrins are activated, thus promoting the recruitment of signalling proteins to strengthen the FAs. The increase in FAs results in higher cytoskeleton contraction, which results in a mechanotransduction signalling that dictates the stem cell fate[102]. Evidence of the effect of matrix stiffness on stem cell fate was obtained in a landmark study conducted by Engler *et al.*[105]. These authors showed that lineage specification of mesenchymal stem cell (MSC) changed according to the

matrix stiffness. On a soft matrix that mimics the ECM of the brain, MSCs under went differentiation along a neuronal lineage. As the stiffness of the matrix increased to mimic that of muscle or the bone, MSCs were biased towards a myogenic or an osteogenic differentiation pathway respectively. Interestingly, when keratinocytes were maintained on a soft matrix, they were induced to undergo terminal differentiation, but an increase in matrix stiffness was found to prevent keratinocyte differentiation[106]. The keratinocytes cultured on these soft matrixes were rounded and less spread, which agrees with previous reports on how cell shape affects keratinocyte differentiation[104]. Furthermore, recent studies by Le et al[128] demonstrated that increase mechanical strain can induce transcriptional repression of gene associated keratinocyte differentiation. Their finding also indicated that the attenuation of gene transcription is mediated by polycomb repressive complex 2 (PRC2), which is known to repress the expression of keratinocyte differentiation genes[128]. These findings suggest that matrix stiffness adds another dimension to how cell fate is controlled. This further emphasises the complexity of the interactions between the stem cells and their microenvironment in determining their fate[107].

1.3.3 Integrins and Cell-ECM Signalling

The complex biochemical and biophysical properties of the ECM results in a plethora of biological information that have a profound effect on cell behaviours such as adhesion, migration, proliferation and differentiation. To recognise and interpret this biological information, cells have receptors such as integrins that interact with the surrounding ECM proteins[129]. Integrins are a large family of heterodimeric transmembrane receptors, consisting of noncovalently association of α and β subunits. Currently, around 18 α subunits and 8 β subunits have been identified, and they are known to assemble into 24 different integrin heterodimers, each with a distinct but overlapping specificity for ECM proteins[130,131] (Fig. 1.5). The extracellular domains of integrins directly link specific ECM proteins to the internal cytoskeleton via the integrin's cytoplasmic domains. These interactions allow the bi-directional transduction of biochemical and biomechanical signals across a cell's plasma membrane, which gives rise to signalling events that trigger changes in cell behaviour[132,133]. Furthermore, dynamic changes in the qualitative and quantitative presentation of integrins by a cell enables a cell to modulate its affinity towards

specific ECM components, which in turn regulates its responsiveness to the surrounding matrix[133].

In the epidermis, it has been established for some time that changes in integrin expressions and activity occur as keratinocytes undergo terminal differentiation. These changes in integrin expression are accompanied by a decrease in cell proliferation, followed by a loss of adhesion towards the BM[16,132]. Amongst the integrins, α2β1 (collagen receptor), α3β1 (laminin 5 receptor) and α6β4 (laminin receptor) are the most abundant constitutive integrins within the epidermis[16,134]. In normal undamaged skin, these integrins are primarily located at the BM, where undifferentiated and proliferating keratinocytes are located. Studies have shown the importance of these integrins in mediating keratinocyte adhesion to the BM, and this adhesion assists in maintaining the long-term self-renewal capability of keratinocytes[135,136]. A reduction in either α6β4 integrin[16] or β1 integrins[16,137] was shown to trigger terminal differentiation in keratinocytes. The α6β4 integrin and β1 integrins activate the phosphatidylinositol 3-kinase (PI3K) and mitogen activated protein kinase (MAPK) pathways respectively to promote the proliferation of undifferentiated keratinocytes[16]. It is likely that signal transduction from the biochemical and biophysical interactions of α6β4 integrin and β1 integrins with their complementary ECM components is required for the maintenance of undifferentiated keratinocytes.

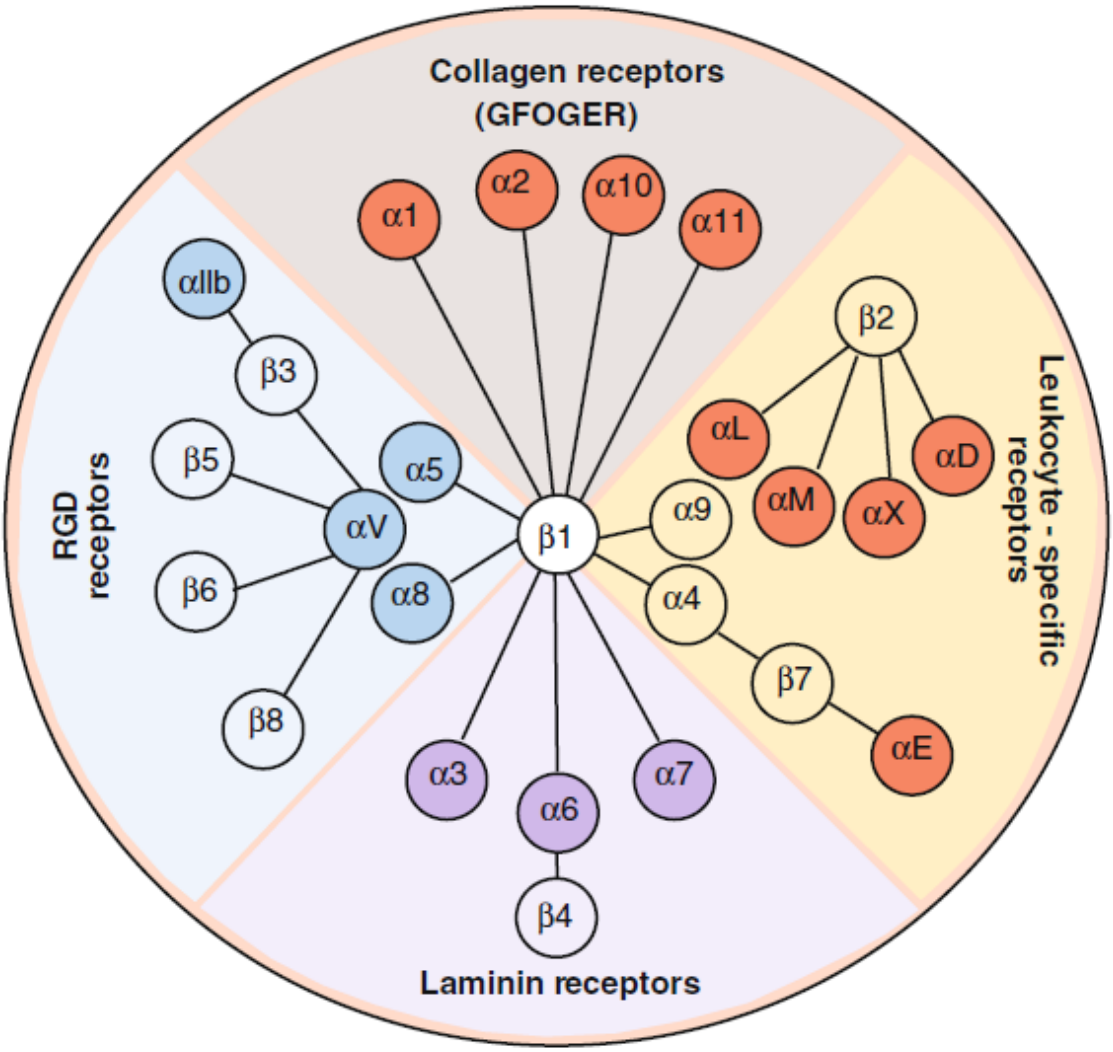

Figure 1.5: Representation of the integrin family. The integrin family contains 24 heterodimers, each with a unique extracellular domain that recognizes a distinct and overlapping collection of ECM proteins. These integrins bind laminins, collagens, fibronectin and other cell surface receptors.

1.4 Tissue Engineering of Skin

1.4.1 Current Progress

In normal circumstances, most wounds heal without any medical intervention. However, wounds that extend deep into the dermis usually require medical attention, as they heal poorly if there is an area of exposed dermis without keratinocytes[138]. Traditionally, the "gold standard" of treating such wounds has been a split-thickness skin autograft, comprising the epidermis and a small portion of the dermis. This is harvested from healthy donor tissue from a site on the same patient[139]. Although these autografts can cover the wound, they carry the risk and expense associated with surgery as well as the creation of a second wound. In the case of extensive third-degree burns, donor tissue sites are limited, and an extensive wound may be covered using either allografts or xenografts; these serve as a temporary cover, as allografts or xenografts typically get rejected by the immune system after a week[138,140], and the fact that xenografts cannot be permanently revascularized, leads to the loss of this tissue. Due to these challenges, other options are being investigated as alternatives to the use of skin autografts, allografts and xenografts for restoring skin barrier functions[141].

In 1975, Rheinwald and Green successfully developed a technique that permitted epidermal keratinocytes to be cultured *in vitro* from a skin biopsy[142]. This work pioneered skin tissue engineering. It allowed the production of cultured epidermal cells, which could be used as autografts to provide permanent wound coverage. Using this technique, there is less need for large donor sites, whilst enabling more rapid wound healing and yielding better functional and cosmetic results than if the wound was not grafted or was treated with a xenograft. However, it takes 2-3 weeks before a sufficient number of keratinocytes can be grown from a biopsy to provide wound coverage[143,144]. To overcome the delay, cultured epidermal allografts were developed to overcome the delay. These are derived from cadavers, unrelated adult donors and neonatal foreskins, which are grown and stockpiled in advance for treating burns and other chronic wounds such as chronic leg ulcers[143,145,146]. Although reasonable success is achieved with partial thickness burns, autografts and allografts failed to give satisfactory responses in deeper burns and other injuries involving the dermis. The primary reason is the unstable attachment of the cultured epidermal layer to the wound bed due to the absence of a dermal substrate[139]. The use of artificial dermal scaffolds

is now being investigated as a way of assisting the attachment of cultured epidermal grafts to the wounded area.

1.4.2 Current Challenges

1.4.2.1 Xenogeneic Contaminants

Our increased understanding of skin biology has led to a number of advancements in wound treatment. However, there has been a growing concern about the safety of these treatments. The method developed by Rheinwald and Green is still used clinically. Although this method is effective for culturing keratinocytes for transplantation purposes, it uses poorly defined animal-derived components and feeder cells, which present a risk because they expose patients to animal-derived components and cells that may contain animal pathogens and immunogenic molecules[141]. One such xenogeneic component is fetal bovine serum (FBS), which is commonly used for *in vitro* cell/tissue culture. While FBS contains essential growth factors and cytokines require for cell proliferation, it may also contain viruses, mycoplasma or prions. Although thorough screening minimises the risks, a study has shown the persistent presence of bovine serum protein within a skin graft that can cause graft rejection due to an immune reaction[147].

Lethally irradiated mouse 3T3 fibroblasts are commonly used as a feeder layer to assist keratinocyte growth. These feeder cells secrete ECM proteins and growth factors, which are essential for the attachment and the proliferation of keratinocytes[148]. A concern with the use of mouse feeder cells is the risk of disease transmission. In addition, mouse feeder cells can cause human cells to display xenogeneic antigens. For example, recent reports have shown in mouse-feeder dependent cell cultures, such as the culture of human ESC expresses the mouse xeno-antigen, Neu5Gc[149]. Another xenoantigen is the so-called Gal epitope, the oligosaccharide α-Gal, which can be transmitted through feeder cells and xenogeneic biological scaffolds used for wound treatments. This epitope is found in high densities on the cell surfaces of most species, with the exception of Old World monkeys and humans. Studies have shown that the Gal epitope can activate the human complement cascade, and so cause acute graft rejection[14,15,150]. To avoid the possible acquisition of xenoantigens by cultured keratinocytes, there has been a focus on eliminating the use of xenobiotic feeder cells

for culturing keratinocytes to be used in clinical treatments. Potentially, irradiated autologous or allogeneic human fibroblasts could replace the murine feeder cells. However, allogeneic fibroblasts have a potential risk of immunological rejection, and irradiated growth arrested feeder cells may potentially transmit damaged genetic material to the keratinocytes[148,151].

1.4.2.2 Serum-Free Culture

To address the potential risk of xenogeneic contamination from the Rheinwald and Green system, an *in vitro* culture system that omits both the feeder layer and serum was developed[152,153]. This system uses a defined serum-free media that contained the necessary growth factors and a collagen matrix to support keratinocyte attachment and growth[152,153]. While this *in vitro* culture system may meet regulatory approval, its ability to propagate keratinocytes still remained inferior compared to the Rheinwald and Green system. Keratinocytes grown in the serum-free culture system have a more limited lifespan, showing diminished self-renewal capacity and an increased commitment towards differentiation or senescence[153,154]. This suggests that a thorough understanding of the growth requirement for keratinocytes to grow under a defined serum-free conditions without a fibroblast feeder layer has yet to be established.

1.5 Extracellular Matrix for Tissue Engineering

As previously mentioned, the ECM has a profound influence on directing a cell's fate. Hence, ECMs are considered critical elements to be included in tissue engineering procedures. There have been many attempts to use synthetic matrices, or isolated ECM components such as collagen, fibrin or hyaluronan to recapitulate the ECM's function. However, these have failed to reproduce the molecular complexity or organisation of native tissue ECM[155,156]. As a consequence, the use of the native ECMs as biomaterials has expanded. Hence, there is considerable interest in the use of either tissue or cell-derived ECM (CDM), as a natural biomaterial. While tissue derived ECMs have been granted Food and Drug Administration approval and are widely used, clinical studies have suggested several disadvantages, which include: potential pathogen transfer, anti-host responses, uncontrolled degradation and other issues[156]. As an alternative, CDM has been examined as a replacement for the native tissue-derived ECM. These CDMs

are a complex and structured mixture of ECM proteins, which mimic certain aspects of the native tissue microenvironment. The generation of CDM involves three major considerations: cell source, culture condition and decellularisation method[155].

1.5.1 Cell Source

The primary determinant of CDM composition is dependent on the type of cells used[155]. This is illustrated by a study by Lu *et al.*[157], where they compared the CDM generated by fibroblasts, chondrocytes and MSC. All matrices contained common components such as type I collagen, type III collagen, fibronectin, vitronectin, laminin and decorin. However, fibroblast CDM lacked versican and aggrecan, whereas these components were detected in both chondrocyte and MSC CDM. These differences in ECM components can affect cell behaviour. This was demonstrated by Marinkovic *et al.*[158], as they showed tissue-derived ECM contains specific ECM components that are able to direct the MSC to a particular lineage; i.e, adipose-derived stromal cell matrix was better in promoting adipogenesis than bone marrow-derived stromal cell matrix. This demonstrates that careful considerations are required when choosing the CDM to be used.

One goal of this thesis was to create a CDM that mimics the skin dermis. Hence dermal fibroblasts were considered as a cell source. Current studies have suggested that there are different subsets of dermal fibroblasts located in the superficial papillary dermis and the deep reticular dermis. The papillary dermis is characterised by a relatively thin and poorly organised ECM and has a high cell density. In contrast, a dense network of ECM fibres and a low cell density was observed in the reticular dermis[159,160]. Furthermore, the composition of ECM proteins, cytokines and growth factors were observed to differ between these dermal compartments. For example, a higher ratio of type III to type I collagen, higher levels of decorin and a lower level versican were observed in the papillary dermis compared to the reticular dermis[113,161,162]. These differences between the dermal layers were also reflected at a cellular level. Site-matched papillary and reticular dermal fibroblasts were found to synthesise an ECM that differed in their protein compositions, according to whether the fibroblasts were from the papillary or reticular dermis. A summary of the differences between papillary and reticular dermis observed *in vivo* and *in vitro* studies are as presented in Table 1.2.

Differences in ECM composition and organisation found between papillary and reticular dermis seemed to influence the keratinocytes differently. In a skin equivalent model, papillary dermal fibroblasts were shown to better promote epidermal morphogenesis compared to reticular dermal fibroblasts, and reduced terminal differentiation was observed in skin equivalent models generated using reticular dermal fibroblasts. Reduced terminal differentiation was assessed by a decrease in the thickness of the cornified layer, through hematoxylin-eosin-saffron staining and immunohistological staining of filaggrin (a marker for terminally differentiated keratinocytes)[163-165]. In addition, as indicated by Ki67 staining, a significant reduction in proliferating basal keratinocytes was also observed when reticular dermal fibroblasts were used in the skin equivalent cultures[165]. These distinct differences were retained when the skin equivalent constructs were grafted onto nude mice indicating that the ECM produced seems to "set" the cultured keratinocytes down a particular path[164]. Interestingly, papillary and reticular dermal fibroblast perform different roles during wound healing. In wounded adult mouse skin, it was shown that dermal repair is mediated by the reticular dermal fibroblasts, whereas it was only during re-epithelialization that the papillary dermal fibroblasts were recruited[166]. Collectively, these data suggest that ECM generated by reticular dermal fibroblasts promotes cell migration of keratinocytes into the wounded area. Once within the wound, the keratinocytes are induced to proliferate and differentiate by the ECM produced by papillary dermal fibroblasts, to promote the re-epithelialization of the skin wound. Thus, the differences in the ECM produced by papillary and reticular dermal fibroblasts are reflected in the behaviour of the keratinocytes that interact with these matrices.

Table 1.2: Comparison of ECM composition of the papillary and reticular dermis.

ECM PROTEINS	PAPILLARY DERMIS	RETICULAR DERMIS
RATIO OF TYPE I: TYPE III COLLAGEN	Low	High
TYPE IV COLLAGEN	Positive	Negative
TYPE XII COLLAGEN	Positive	Negative
TYPE XIV COLLAGEN	Negative	Positive
TYPE XVI COLLAGEN	Positive	Negative
TENASCIN-C	Positive	Negative
TENASCIN-X	Weakly Positive	Positive
VERSICAN	Weakly Positive	Positive
DECORIN	Positive	Weakly Positive
MATRIX GLA PROTEIN (MGP)	Negative	Positive
FIBRONECTIN	Positive	Positive
HYALURONAN	Positive	Diffused

This table was adapted from Sorrell *et al.*[160]and Sriram *et al.*[159]

1.5.2 Culture Conditions: Macromolecular Crowding

While it is possible to generate an acellular ECM *in vitro*, the current *in vitro* culture conditions used to generate CDM have been described as "highly inefficient". The ECM deposited under standard culture conditions are said to be unstructured and lacking critical components. This means these matrices, do not replicate the *in vivo* microenvironment of the tissue from which the cells were obtained. Cells within an *in vivo* tissue microenvironment are surrounded by a high density of macromolecules (~20.6 – 80mg/ml), a situation which is generally not replicated *in vitro* cultures (1 - 10mg/ml)[167]. Recent evidence has revealed that the macromolecular density in the external environment is critical in enhancing the rate of a host of biochemical reactions like enzyme-substrate reactions[168]. This means that in cell cultures molecular interactions taking place outside of the cells may not be occurring at the rates that are required for the assembly of the organised structures that are seen *in vivo*. Hence, it is possible that the physiological differences in the macromolecular density between the *in vivo* microenvironment and it's *in vitro* counterpart may be the cause of the unstructured ECM that is typically observed in *in vitro* cultures[167,169] (Fig. 1.6A). To correct this problem, inert synthetic, or natural macromolecules termed macromolecular crowders (MMC) were added into *in vitro* cultures to mimic the crowded conditions that occur *in vivo*. These culture conditions were termed

macromolecular crowding[167]. Numerous reports have shown that the addition of MMC enhances the deposition and the formation of a structured ECM[169-176] (Fig. 1.6B). Hence, the addition of MMC to dermal fibroblast cultures may produce a matrix that best mimics the physiological dermal ECM.

1.5.3 Decellularisation

Decellularisation is a technique used in tissue engineering to remove cells from natural tissues and organs so that only the ECM remains. This ECM can then be used as a biological scaffold for regenerative medicine. The primary goal of decellularisation is the removal of cell components and antigens that may trigger an immunological response in the host following transplantation. However, the need to remove cells and antigens must be balanced with the preservation of the biological activity, and the mechanical integrity of the ECM[155,177]. A combination of physical, chemical or biological approaches, each having their merits, have been used to decellularize tissue matrices. Table 1.3 list some of the know decellularization methods.

1.5.3.1 Physical Methods

Physical methods, which include freezing, hydrostatic pressure, sonication and agitation have been used to facilitate the decellularization of tissues. One of the most frequently used physical techniques for decellularization is snap freezing. As a result of the rapid freezing of tissues, cells undergo lysis that is caused by the formation of intracellular ice crystals that disrupt the cell membrane. However, the rate of temperature change during snap freezing has to be monitored, to prevent the disruption of the ECM[177,178]. If performed correctly this method has been shown not to alter the mechanical properties of the ECM and only cause minor disruptions of the tissue architecture[178,179]. Hydrostatic pressure, sonication and agitation have been used for decellularization to accelerate, and improve, the efficiency of delivering a cell-lysis agent into the tissues. However, these methods have a tendency to disrupt the integrity of the ECM as well as reduce GAG content of the decellularised ECM[177,178].

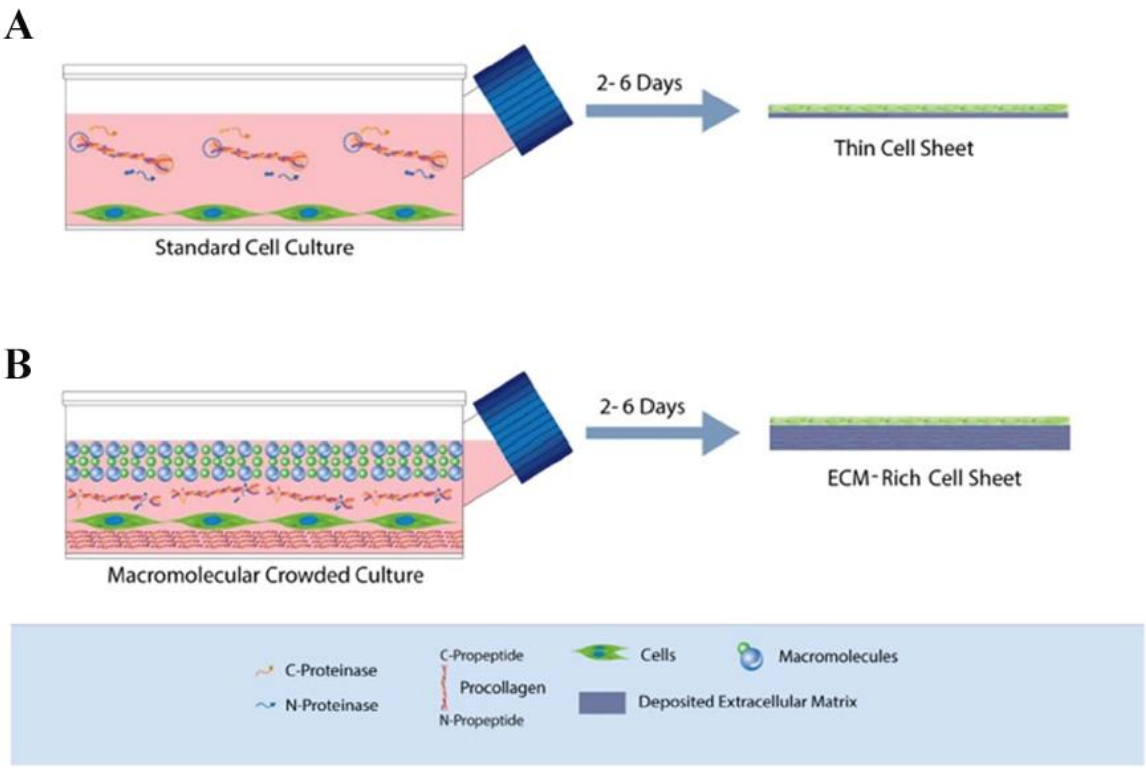

Figure 1.6: Schematic representation of the enhancement of ECM deposition through macromolecular crowding. A) The deposition of ECM in the standard cell culture system is inefficient because the culture medium lacks the density of macromolecules that is present in the tissues. B) The addition of macromolecular crowders to *in vitro* cultures creates an effective volume occupancy that was found to consequently increase the rate of ECM deposition. Adapted from Kumar *et al*.[174]

1.5.3.2 Chemical Methods

Chemical decellularization typically involved the use of alkaline or acid reagents and/or detergents to disrupt and solubilize the cell membranes[155,177]. Hydrochloric acid, ammonium hydroxide and acetic acid have been used to disrupt the cell membranes and release the intracellular components. Further study showed that these chemicals also caused the loss of important molecules, such as GAGs, from the ECM structure. Other commonly used chemicals for decellularization are detergents, as they will solubilize cell membranes. The detergents used for this purpose can be classified into three categories: non-ionic, ionic and zwitterionic[180]. Generally, non-ionic detergents such as Triton X-100 are preferred, as they remove cell components without impacting on the native ECM structure and its enzymatic activity. Zwitterionic detergents such as CHAPS also efficiently remove cell components with minimal ECM disruption in a similar manner as Triton X-100[180]. In contrast, while ionic detergents, such as sodium dodecyl sulphate (SDS) and sodium deoxycholate, are able to remove cell components from the tissues effectively, they tend to disrupt the native tissue structure[177].

1.5.3.3 Biological Methods

Enzymes are a frequently used biological approach for decellularization. The advantage of using enzymatic agents such as proteases (trypsin) esterases (phospholipase A_2) and nucleases (DNase, RNase) is their specificity for a particular biological substrate[178,180]. Trypsin is a serine protease that is commonly used because it can selectively cleave cell adhesion molecules to detach the cells from a tissue surface. While it has been shown to be effective for decellularization, it also specifically targets collagen, and collagen degradation could lead to a decrease in the mechanical strength in the ECM scaffold[181]. Nucleases such as DNase and RNase are used to break down nucleic acids within the tissue and so facilitate their removal. Typically, these enzymes are an integral part of the decellularization protocol, as they help in the removal of the nucleic acids after cell lysis by other decellularization agents[180].

Table 1.3: A summary of commonly used decellularization methods to obtain ECM.

Method	Mode of Action	Effects on ECM
Physical		
Snap freezing	Intracellular ice crystals disrupt cell membrane	ECM can be disrupted or fractured during rapid freezing
Mechanical force	Pressure can burst cells and tissue removal eliminates cells	Mechanical force can cause damage to ECM
Mechanical agitation	Can cause cell lysis, but more commonly used to facilitate chemical exposure and cellular material removal	Aggressive agitation or sonication can disrupt ECM as the cellular material is removed
Chemical		
Alkaline; acid	Solubilizes cytoplasmic components of cells; disrupts nucleic acids	Removes GAGs
Non-ionic detergents		
Triton X-100	Disrupts lipid–lipid and lipid–protein interactions, while leaving protein–protein interactions intact	Mixed results; efficiency dependent on tissue, removes GAGs
Ionic detergents		
Sodium dodecyl sulphate (SDS)	Solubilize cytoplasmic and nuclear cellular membranes; tend to denature proteins	Removes nuclear remnants and cytoplasmic proteins; tends to disrupt native tissue structure, remove GAGs and damage collagen
Sodium deoxycholate		More disruptive to tissue structure than SDS
Triton X-200		Yielded efficient cell removal when used with zwitterionic detergents
Zwitterionic detergents		
CHAPS	Exhibit properties of non-ionic and ionic detergents	Efficient cell removal with ECM disruption similar to that of Triton X-100
Enzymatic		
Trypsin	Cleaves peptide bonds on the C-side of Arg and Lys	Prolonged exposure can disrupt ECM structure, removes laminin, fibronectin, elastin, and GAGs
Endonucleases	Catalyse the hydrolysis of the interior bonds of ribonucleotide and deoxyribonucleotide chains	Difficult to remove from the tissue and could invoke an immune response
Exonucleases	Catalyse the hydrolysis of the terminal bonds of ribonucleotide and deoxyribonucleotide chains	

1.5.4 Cell-Derived Matrices as a Stem Cell Niche for Keratinocytes

Currently, the expansion of sensitive, primary keratinocytes *ex vivo*, remains a challenge as they undergo phenotypic changes during prolonged *in vitro* culture. Specifically, the cells lose function and undergo senescence and/or spontaneous differentiation[155]. An approach that was suggested to solve this problem was to recreate the microenvironmental niches within which these cells naturally reside[154]. Recently, CDMs have been used to provide a microenvironmental niche to sustain stem and progenitor cells. For example, MSC-derived matrices have been generated to replicate the *in vivo* microenvironment of the bone marrow[182,183]. Analysis of the MSC-derived matrix revealed that it had a similar ECM composition to that of the bone marrow matrix, from where MSCs are derived. This ECM was found to contain collagens, laminins, decorin, nidogen, thrombospondins, vitronectin and fibronectin[155,182,183]. When compared to tissue culture plastic (TCP) or fibronectin-coated TCP, the MSC-derived matrix was better able to support the growth of undifferentiated MSCs. Furthermore, MSCs grown on their own matrix have greater osteogenic and adipogenic differentiation efficiency than that found if the MSCs were grown on TCP[182,183]. Similarly, dermal fibroblast-derived matrix has been used to direct the differentiation of embryonic stem cells towards a keratinocyte lineage[184]. However, to our knowledge, dermal fibroblast matrix has yet to be utilised for the expansion of keratinocytes.

1.6 Scarless Wound Healing

Adult mammalian wound healing is a highly evolved process that involves a complex series of coordinated biological pathways and the crosstalk between multiple cell types. While it is highly efficient in repairing the injured site, it typically results in the formation of scars[185,186]. Each year, over 100 million people in the developed world acquire scars as a result of surgery or trauma. Burn injuries in particular can elicit a fibrotic response that results in the formation of hypertrophic scars. In the United States alone, treatment of hypertrophic and other problematic scars has been estimated to cost $4 billion annually[187].

Scarring has an enormous clinical impact, and its morbidity varies depending on the anatomical site that is affected. If the scarring occurs in the head and neck, it could

lead to hearing loss (from auditory canal structure), nasal stenosis, microstomia, lip or eyelid ectropion and the restriction of neck movements[188,189]. Further, if this occurs in a growing child and is left untreated, it could lead to severe contractures that can lead to facial skeletal abnormalities[185,190]. In addition, when scarring occurs in the extremities, it can severely limit the mobility of limbs and digits, which could have crippling results[185]. Currently, there is no adequate treatment that is available to remedy these issues, short of reconstructive surgery. While this procedure is helpful in alleviating the issues from scarring, it cannot eliminate the scars[185].

Interestingly, an early gestation foetus has a remarkable regenerative ability in that it is able to heal cutaneous wounds without the formation of scar tissues[191]. Numerous studies have demonstrated that this regenerative capability of early gestation foetus occurs in all mammalian species studied to date, which includes humans, mice, rats, sheep, rabbits and monkeys[70,192-196]. In each foetal model, the gestational age of the foetus is a determining factor in the transition between scarless wound healing or a more fibrotic wound healing process[191,196]. Earlier studies on the biology of foetal wound healing focused on the intrauterine environment, as it was believed that the sterile and nutrient-rich amniotic fluid might have a role in foetal wound repair[191,197,198]. However, numerous studies have indicated that the foetal regenerative repair is independent of the intrauterine environment. For example, ontological investigations of wound healing during marsupial development within the maternal pouch demonstrated that scarless wound healing occurs despite the absence of sterile amniotic fluids[199]. Furthermore, wounds created on human foetal skin xenografted onto nude adult mice have been shown to retain their ability for scarless wound healing[200]. These findings clearly suggest that scarless wound healing is an intrinsic property of foetal skin and is independent of the intrauterine environment. A thorough understanding of the biological basis of the foetal wound phenotype may lead to therapies that could be used to recapitulate scarless wound healing in adults.

1.6.1 Inflammatory Response

A unique characteristic of foetal wound healing is the attenuation of the inflammatory response. Typically, an early response to a postnatal injury is the infiltration of immune cells such as neutrophils and macrophages; however, this is greatly reduced during foetal wound healing[201,202]. Interestingly, numerous studies have demonstrated that

foetal immune cells are capable of responding to pro-inflammatory signals. Foetal polymorphonuclear leukocytes, macrophages and lymphocytes, can respond to chemoattractants[201] and can be recruited into a wound in the presence of irradiated bacteria[203] or an irritant such as a mixture of carrageenan and turpentine[204]. These data indicated that the attenuated inflammatory response is a result of decreased recruitment of immune cells and is not an intrinsic deficiency of these cells.

Reports have shown there is a low expression of proinflammatory cytokines such as interleukin-6 (IL-6)[205] and interleukin-8 (IL-8)[206] during scarless foetal wound healing. Another study showed that administration of IL-6 during wound healing on human foetal skin transplanted onto SCID mice resulted in scar formation, whereas the control that did not receive IL-6 healed without a scar as expected of human foetal skin[205]. These results of a correlation between IL-6 and IL-8 production during the inflammatory response of wound healing in the adult skin are consistent with these cytokines being involved in the formation of scars. During skin wound repair in the foetus, the anti-inflammatory cytokine IL-10 was shown to be highly expressed. IL-10 is known to be a major regulator in suppressing inflammatory responses because it regulates the expression of IL-6 and IL8. Studies with IL-10 knockout mice showed an elevated expression of IL-6 and IL-8 during wound healing and scar formation was observed at the gestational age, which typically heals without scarring. Other, studies have demonstrated that the foetal regenerative capability could be artificially recapitulated through the overexpression of IL-10 using viral vectors[207]. This demonstrates that the proinflammatory response may be a factor that hinders scarless wound healing.

1.6.2 Fibroblasts Behaviour

Foetal fibroblasts have been shown to play a critical role during scarless wound healing[208]. Numerous studies have described functional differences between foetal dermal fibroblasts and their adult counterparts. In vitro studies have shown that fibroblasts derived from the foetal dermis differ in their ability to synthesise and degrade ECM proteins, in comparison to that seen by adult dermal fibroblasts. Furthermore, foetal dermal fibroblasts were observed to have higher proliferative[209] and migratory[210] capabilities, which decrease with ageing. A factor that may be essential for scarless wound healing is the migratory capability of fibroblasts. A study

by Coolen *et al.*[211] showed that in a burn injury model, more fibroblasts reached the wound site in the foetus when compared to the fibroblasts in adult wound. Once within the wound, the foetal fibroblast simultaneously proliferates and synthesises collagen. In contrast, in an adult wound, there is a delay in collagen synthesis, as the adult fibroblasts need to proliferate prior to collagen secretion and deposition[159,212]. This delay in the migration of fibroblasts into the wound and the associated deposition of collagen may be factors contributing to scar formation[159].

Wound contraction is an important part of the healing of dermal wounds. However, aberrant or excessive contraction leads to distortion of surrounding tissue, which contributes to scar formation[213]. Myofibroblasts play an essential role in wound contraction during skin wound healing. The presence of myofibroblasts is detected by the appearance of alpha-smooth muscle actin within the wound. Interestingly, wounds that occur during early gestation were observed to contain virtually no myofibroblasts. In contrast, in an adult wound, high numbers of myofibroblasts are detected[214]. Furthermore, myofibroblasts residing in adult wound are progressively more active with increased age, and myofibroblast activity correlates with wound contraction and the degree of scarring[215].

1.6.3 Extracellular Matrix Composition

1.6.3.1 Collagen Composition

The ECM plays an important role during wound healing, as it provides biochemical and biophysical cues that affect cell behaviour. Foetal dermal fibroblasts have been shown to differ from their adult counterparts in their ability to synthesise and degrade the ECM[185,191]. This results in compositional differences between the ECMs of the adult and foetal dermis. The foetal dermis is known to contain a high proportion of type III collagen, whereas type I collagen is the predominant collagen within the adult dermis. As the foetus develops, there is a transition towards a collagen profile that resembles the adult phenotype and a lower type III to type I collagen ratio. This change in the collagen profile correlates with the transition from scarless wound healing to wound repair with scar formation[201,216,217]. The pattern of collagen deposition in a foetal wound is a reticular "basket-weave" pattern that is indistinguishable from that of unwounded foetal skin. This deposition pattern gives rise to the suppleness and

flexibility of normal unwounded skin. In contrast, collagen deposition within the adult wound results in a densely packed collagenous matrix and collagen fibrils in a parallel orientation. This gives rise to the rigid and inelastic properties found in scar tissues[185,218].

1.6.3.2 Proteoglycan Composition

Proteoglycans have been shown to affect collagen organisation and fibrillogenesis during wound healing. The expression profile of proteoglycans change as the skin ages, and this has been associated with the scarless wound healing phenotype. As the skin ages, there is a decrease in the level of versican and a concomitant increase in the expression of decorin[219,220]. Versican is a chondroitin sulphate proteoglycan: it has a core protein to which is attached with chondroitin sulphate chains. Versican plays an important role during embryonic development as it regulates cell adhesion, cell migration, cell proliferation and ECM assembly. Versican interacts with hyaluronan through the amino-terminal domain (G1) of its core protein[106], and this may generate a microenvironment that is suitable for scarless wound healing. Decorin is a member of the small-leucine rich proteoglycan family, and it plays a significant role in tissue development[116]. The production of decorin is known to increase by 72% during the transition from scarless healing towards a scar forming phenotype[221]. Decorin is known to bind to collagen and regulate the rate and degree of collagen fibrillogenesis. Decorin's contribution is believed to ensure the formation of uniform collagen fibrils with similar diameters[116]. This results in the organisation of an ECM with high tensile strength[117,118]. Possibly the high level of decorin during adult wound healing contributes to the formation of an ECM with the rigid and inelastic properties found in scar tissues.

1.6.3.3 Glycosaminoglycans Composition

Another distinct difference between adult and foetal skin is the abundance of GAGs within the foetal dermis and within a wound matrix[222]. Foetal wounds were observed to contain a high, and prolonged elevation, of hyaluronan levels when compared to their adult counterparts. Furthermore, studies in foetal lambs have shown that the deposition of hyaluronan within the foetal wound is more rapid than that seen in adults. Interestingly, as the gestational age of the foetus increases, a decrease in hyaluronan

content was detected. This coincided with the appearance of proteoglycans such as decorin and perlecan, and the onset of scar formation after wound healing. A study by Iocono *et al.*[223] found that the addition of hyaluronan during adult wound healing resulted in wound healing that recapitulates the foetal scarless phenotype. Possibly hyaluronan contributes to scarless wound healing by stimulating cell migration, proliferation and differentiation. Currently, topical applications of hyaluronan are being investigated in a clinical setting for their wound healing effects, with promising results[191].

1.7 Aim of this Project

The contribution of the ECM in the regulation of cell fate is not well understood. However, recent research has indicated that the ECM plays a major role in regulating cell growth and differentiation. This thesis aimed to investigate the contribution of ECM in regulating keratinocyte behaviours. The work was performed in a number of sections.

- The first step was to develop methods to generate an acellular xenogeneic-free dermal fibroblast-derived ECM

- The functional effects of the acellular xenogeneic-free dermal fibroblast-derived ECM on keratinocyte behaviour in serum-free culture were assessed

- The composition of adult and foetal dermal fibroblast generated matrices were compared and,

- Keratinocyte growth patterns and gene expression were determined when these cells were grown on either adult or foetal dermal fibroblast generated matrices

1.8 Hypotheses

- The dermal fibroblast-derived ECM contains biochemical and biophysical cues that modulate the growth and differentiation of keratinocytes.

- Differences in ECM composition in adult and foetal dermal fibroblast matrices regulate keratinocyte proliferation and differentiation.

Chapter II:

Materials and Methods

2.1 Tissue Culture

2.1.1 Cell Lines

Adult Human Dermal Fibroblast

The aHDF cell line (Adult Donor 1) was purchased from the American Type Culture Collection (ATCC), Cat# PCS-201-012, Lot#61447289. The dermal fibroblasts were extracted from samples collected from a 34 year old female Caucasian during abdominoplasty.

The EBL028 (Adult Donor 2) cell line was kindly provided by Prof. Birgit Lane of the Institute of Medical Biology, Singapore. The dermal fibroblasts were extracted from samples collected from a 23 year old male Ceylonese during abdominoplasty.

Foetal Human Dermal Fibroblast

The fHDF (WS-1; Foetal Donor 1) cell line was purchased from the ATCC, Cat#CRL-1502. These cells were extracted from the back of a terminated foetus at 12 weeks gestation.

The FS13 (Foetal Donor 2) cell line was kindly provided by Prof. Birgit Lane of the Institute of Medical Biology, Singapore. The fibroblasts were extracted from a skin biopsy was taken from the back of a terminated foetus at the 13 weeks gestation.

Human Neonatal Keratinocytes

Human neonatal keratinocytes were purchased from Thermo Fisher Scientific, Gibco (Cat#C0045C).

2.1.2 Tissue Culture Media, Buffers and Solutions

Basic Tissue Culture Media and Additives

Dulbecco's Minimum Essential Medium (DMEM), Ham's F12 Nutrient Mixture, 1M HEPES, 200mM L-glutamine, 100mM Sodium Pyruvate and Human Serum and Defined Keratinocyte Serum Free Media (DKSFM) were purchased from Gibco, Life Technology. Foetal Bovine Serum (FBS) was purchased from Serana Europe GmBH

Complete DMEM Media

Complete DMEM media was prepared by supplementing DMEM with 10mM HEPES, 2mM L glutamine, 1 mM sodium pyruvate and 10% FBS.

Keratinocyte Serum Free Maintenance Media

The base medium was composed of DMEM and Ham's F12 in a 3:1 ratio or MCDB153 (where indicated) supplemented with 10mM HEPES, 2mM L glutamine, and 1mM sodium pyruvate. The calcium concentration of the base medium is 0.2mM unless otherwise indicated. The base medium was further supplemented with 25ng/ml adenine (Sigma), 400ng/ml hydrocortisone (SOLU-CORTEF®, Pfizer), 0.12 IU/ml insulin (Humulin ®), 10ng/ml epidermal growth factor (BD Bioscience), 5µm Forskolin (Sigma), 5ng/ml keratinocyte growth factor (Peprotech), 0.1mM monothioglycerol (MTG; Sigma), 200nM triiodothyronine (Sigma), 5ng/ml transferrin (Sigma) and 30µg/ml ascorbic acid (Wako Chemicals).

0.05M Ethylenediaminetetraacetic acid (EDTA) Stock Solution

0.7306g of EDTA (Spectrum Chemical) was dissolved in 40ml of ddH_2O. 1M NaOH was added to dissolve EDTA and adjust the pH to 7.4. The final volume was made up to 50ml using ddH_2O.

Adhesion Assay Buffer

DMEM was supplemented 10mM HEPES, 2mM L glutamine, 1 mM sodium pyruvate, 0.2% (w/v) bovine serum albumin, 25µg/ml Adenine, 0.4µg/ml Hydrocortisone and 0.12IU/ml Insulin

CyQuant Assay Medium

The CyQuant Assay Medium was prepared from reagents of the CyQuant Cell Proliferation Assay Kit (Molecular Probes, Invitrogen). Prior to running the assay, the 20x concentrated cell-lysis buffer was diluted 20-fold using ddH_2O to produce a 1x lysis buffer. To prepare the working solution, the CyQuant GR dye was diluted 1:1000 into the 1x lysis buffer.

2.1.3 Cell Counting

All cell counts were performed using a hemocytometer. 10µl of harvested cells were transferred into a microcentrifuge tube and mixed with 10µl of 0.4% trypan blue . The resulting cell mixture was applied into the hemocytometer. Live, unstained cells were counted from all four corners and the middle of the hemocytometer grid (Fig. 2.1;

number 1-5). The formula used to calculate the number of viable cells/mL was Total Cell Count ÷ 5 × 10^4 × 2 fold dilution.

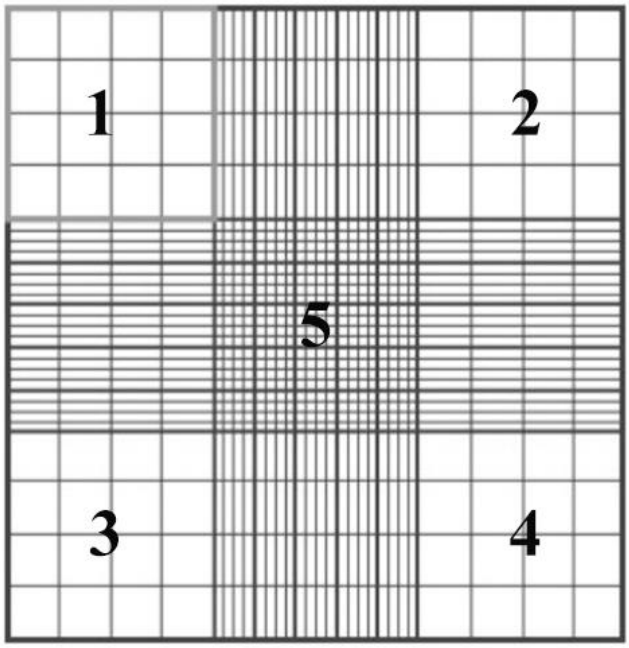

Figure 2.1: A representative diagram of a haemacytometer indicating one corner of the square that should be used for counting (Adapted from Abcam website)

2.1.4 Freezing and Thawing Cell Lines

Freezing Fibroblasts

The Fibroblast cells were harvested and resuspended in complete DMEM media. A cell count was conducted before being centrifuged at 1,100 RPM for 5 minutes. The media was carefully removed without disturbing the cell pellet. Freeze media (50% of complete tissue culture media, 40% FBS and 10% DMSO) was added to resuspend the cell pellet and 5 x 10^4 total cells were transferred into each cryovial. The cryovials were placed in a "Mr Frosty" freezing chamber (Nalgene Labware, Nalge Nunc International, Rochester, NY) and placed in a -80°C freezer before being transferred to liquid nitrogen storage.

Freezing Keratinocytes

Spent DKSFM media was recovered from keratinocyte culture, filtered with 0.25µm syringe filter unit before being used to make freezing media A (50% spent DKSFM/

50% fresh DKSFM) and freezing media B (40% spent DKSFM/ 40% fresh DKSFM/ 10%DMSO). The keratinocyte cells were harvested and resuspended in PBS/4% human serum/1mg/ml soybean trypsin inhibitor (Gibco, Thermo Fisher Scientific). A cell count was conducted before cells were centrifuged at 1,100 RPM for 5 minutes. The media was carefully removed without disturbing the cell pellet. Freezing media A was added to resuspend the cell pellet, followed by freezing media B and 5 x 10^4 total cells were transferred into cryovials. The cryovials were placed in a "Mr Frosty" freezing chamber (Nalgene Labware, Nalge Nunc International, Rochester, NY) and placed in a -80°C freezer before being transferred to liquid nitrogen storage.

Thawing Fibroblasts

Warmed complete DMEM media (3ml) was placed into a 25cm^2 tissue culture flask. Frozen cells in the cryovial were warmed quickly by immersing it in a 37°C water bath. The cell solution was transferred drop wise into the 25cm^2 tissue culture flask containing the warmed media. After the cells adhered (~1-2 hours), the media was replaced.

Thawing Keratinocytes

The 25cm^2 tissue culture flask was coated with 3ug/cm^2 of type I collagen (diluted in PBS), for 2 hours at 37°C, before the addition of warmed DKSFM. Frozen cells in the cryovial were warmed quickly by immersing it in a 37°C water bath. The cell solution was transferred drop wise into the 25cm^2 tissue culture flask containing the warmed DKSFM. After the cells adhered (~3-4 hours), the media was replaced.

2.1.5 Cell Culture and Maintenance

Fibroblasts

The fibroblast cell lines were cultured in complete DMEM medium and incubated in a humidified 37°C incubator equilibrated at 5% CO_2. When the adult or foetal fibroblasts reached 80-90% confluence and 70-80% confluence respectively, they were subcultured. Cells were used at less than 16 (adult) and 26 (foetal) passages for all experiments. To subculture the cells, the media was removed from the tissue culture flask and the growth surface was briefly rinsed with 5ml PBS before the addition of 500µl of 0.05% trypsin-EDTA (Life Technologies) and incubated for 5 min at 37°C. Cells were resuspended in 2.5mL of complete DMEM and transferred to a centrifuge

tube to be counted using a haemocytometer. The fibroblasts were seeded at 25 x 10^4 cells per T25 tissue culture flask for maintenance.

Keratinocytes

Keratinocytes were cultured in DKSFM media and incubated in a humidified 37°C incubator equilibrated at 5% CO_2. When keratinocytes reached 80% confluence, they were subcultured. Keratinocytes of passage 4 or 5 were used for all experiments. To subculture the cells, the media was removed from the T25 tissue culture flask, and the growth surface was briefly rinsed with 5ml PBS. Cells were then incubated with 4ml of 0.5mM EDTA/PBS RT for 5 min. The EDTA/PBS solution was then removed and replaced with 500µl of 0.05% trypsin-EDTA (Life Technologies) and incubated for 5 min at 37°C. Cells were resuspended in 5ml of PBS/4% human serum/1mg/ml soybean trypsin inhibitor and transfer to a centrifuge tube to be pelleted by centrifugation at 1000 rpm for 5 min. Keratinocytes were resuspended in DKSFM and counted using a haemocytometer. The keratinocytes were seeded at 20 x 10^4 cells per T25 tissue culture flask for maintenance.

2.1.6 Cell Adhesion Assay

Cell adhesion assays were performed in a 96 well tissue culture plate (NUNC). Quadruplicate wells either contained acellular fibroblast-derived matrix, type I collagen coating or uncoated tissue culture plastic. 100µl of 1% BSA in PBS was added into the well and incubated for 2 hours to block unreacted site on the plastic. The PBS/BSA was then removed, and the wells washed three times with PBS. Keratinocytes were harvest using 0.01% Trypsin-EDTA, washed once and then resuspended in adhesion assay buffer (section 2.1.2), at a concentration of 1 x 10^5 cells/ml. 100µl of this cell suspension (1 x 10^4 cells) was added into the wells and cells were left to adhere for 1 hours at 37°C. Any unbound cells were removed by washing the well gently twice with the adhesion assay buffer and once in PBS. The plate was left at -80°C overnight. The plate was brought up to RT before being quantified using the CyQuant cell proliferation assay kit (Molecular Probe, Invitrogen). 100µl of the CyQuant assay solution (Section 2.1.2) was then added to each well of the plate and then incubated at 37°C for 10 min. The fluorescence intensity was measured with a 485nm/535nm filter using an Enspire plate reader (Perkin Elmer). Results were

calculated as a percentage of a 100% control, which was prepared by pelleting 100µl of the original 1 x 10^5 cells/ml mixture, washing and storing the pellet at -80°C. The CyQuant cell proliferation kit fluorescently stains nuclear material to give an estimate of the relative cell number.

2.2 Immunofluorescence Staining

2.2.1 Solution, Buffers and Antibodies

4% Paraformaldehyde

4% paraformaldehyde (w/v; Sigma) was prepared by adding 2.4g of paraformaldehyde to 50ml PBS and heated at 60°C till the solution becomes clear. The solution was adjusted to pH 7.4 with 1M HCl and made up to 60ml with PBS, filtered and stored in the dark at 4°C for a maximum of 1 month. After this, the solution was discarded.

Etching Solution

15g of sodium hydroxide was dissolved in 60ml of ddH_2O and 90ml of absolute ethanol.

Phosphate Buffered Saline (PBS)

1 PBS tablet (Ameresco, Ohio, USA) was dissolved in 100ml of doubled distilled water (ddH_2O).

Blocking Solution

Blocking solution consisted of PBS supplemented with BSA and Goat Serum at 1% (v/v) and 10% (v/v), respectively.

Antibodies

Refer to Table 2.1, 2.2 and 2.3 for a list of primary, secondary and isotype control antibodies, respectively

Isotype Control Antibodies

Isotype control antibodies (Table 2.3) and secondary antibody only was utilized for respective antibodies to verify for the absence of non-specific staining.

2.2.2 Etched Glass Coverslip

Glass coverslips were treated with etching solution (Section 2.2.1) for 1 hour at RT. After treatment, coverslips were washed with ddH_2O several times before being dried overnight. The etched glass coverslips were cleaned with 70% ethanol and sterilized by UV-light before being used in experiments.

2.2.3 Basic Immunofluorescence Staining

Cells were seeded onto prepared etched glass coverslip. Once cells had adhered and spread, they were washed twice with PBS before being fixed with 4% paraformaldehyde in PBS for 15 minutes at room temperature. The cells were then washed twice with PBS before being blocked with 10% Goat Serum/1% BSA/PBS for 1 hour at room temperature. This was removed, and samples were incubated for 1 hour at room temperature with primary antibody (Table 2.1) prepared in 10% Goat Serum (Gibco)/1% BSA (Hyclone)/PBS at 1:200 dilution. Samples were washed 3 x 5 minutes with PBS before being incubated for 1 hour in the dark at room temperature with the appropriate secondary antibody (Table 2.2) prepared in 10% Goat Serum/1% BSA/PBS at 1:400 dilution. Samples were washed 3 x 5 minutes with PBS, then incubated in DAPI (1:2000 dilution in PBS) solution for 10 minutes. The coverslip was then mounted in Vectashield antifade mounting medium (Vector Laboratories) and sealed with nail varnish. Images were captured with Nikon A1+ Confocal Microscope (Nikon, Tokyo, Japan). Isotype control antibodies were used in place of primary antibodies to verify the specificity of staining.

2.2.4 Immunofluorescence Staining of Keratinocytes Phenotype Grown on Different Substrate.

The effect of different substrate on keratinocyte phenotype was investigated. Immunofluorescent staining of keratinocyte was done on etched glass coverslip placed into a 24 well plate. Wells either contains acellular fibroblast-derived matrix or Type I Collagen coating or uncoated etched glass coverslip. Keratinocytes were harvest, pelleted and then resuspended in DKSFM, at a concentration of 8 x 10^4cells/ml. 250µl of this cell suspension (2 x 10^4 cells) was added into the wells. At day 3, keratinocytes were fixed for 5 min with cold acetone: methanol (1:1). Cells were washed twice with PBS before being blocked with 10% Goat Serum/1% BSA/PBS for 1 hour at room

temperature. This was removed, and cells were incubated for 1 hour at room temperature with primary antibody prepared in 10% Goat Serum/1% BSA/PBS. Cells were washed 3 x 5 minutes with PBS before being incubated for 1 hour in the dark at room temperature with secondary antibodies prepared with 10% Goat Serum/1% BSA/PBS. Cells were washed 3 x 5 minutes with PBS and then incubated in DAPI (1:2000 dilution in PBS) solution for 10 minutes. The coverslip was then mounted in Vectashield antifade mounting medium (Vector Laboratories) and sealed with nail varnish. Images were captured with either Nikon A1+ Confocal Microscope or Carl Zeiss LSM510 Inverted Microscope.

Table 2.1 Primary Antibody

Antigen	Reacts Against	Clone	Species, Isotype	Application	Manufacturer or Provided By/ Catalogue No.
Alpha-smooth muscle actin	Mouse, Rat, Human	Monoclonal (1A4)	Mouse IgG2a	IHC, ICC and WB	Sigma (A2547)
Anti-Fibroblast Marker	Human	Monoclonal (TE7)	Mouse IgG1	ICC/IF, IHC-P and Flow Cytometer	Millipore (CBL271)
Chondroitin Sulphate	Mouse, Chicken, Cow, Human	Monoclonal (CS-56)	Mouse IgM	IHC, ICC and WB	Abcam (ab11570)
Fibronectin	Mouse, Rat, Dog, Human	Polyclonal	Rabbit IgG	IHC, ICC and WB	Abcam (ab2413)
Fibronectin	Mouse, Rat, and Human	Monoclonal (EP5)	Mouse IgG1	ELISA, ICC, IHC-P, IP, and WB	Santa Cruz (sc-8422)
Integrin Alpha-6	Mouse and Human	Monoclonal (GoH3)	Rat IgG2a	IP, ICC/IF, IHC-Fr, Flow Cytometry	Abcam (ab105669)
Integrin Beta-4	Human	Monoclonal (439-9B)	Rat IgG2b	WB, IHC-P, IHC-Fr,	Abcam (ab110167)

				Flow Cytometry	
Involucrin	Canine, Gorilla, Human and Porcine	Mouse, (SY5)	Mouse IgG1	ELISA, ICC, IF, IHC-Fr, IHC-P, IP, and WB	Sigma (I9018)
K10	Human	Monoclonal, (LH2)	Mouse IgG1	IHC, ICC and WB	Prof. Birgit Lane, A*STAR Institute of Medical Biology
K14	Mouse, Rat, Human, Pig	Monoclonal, (LL001)	Mouse IgG2a	IHC, ICC and WB	Prof. Birgit Lane, A*STAR Institute of Medical Biology
K16	Human,	Monoclonal, (LL025)	Mouse IgG1	IHC, ICC and WB	Prof. Birgit Lane, A*STAR Institute of Medical Biology
Ki67	Human	Monoclonal (MM1)	Mouse IgG1	ICC	Novacastra (NCL-L-Ki67-MM1)
Nidogen	Mouse, Rat, Human	Polyclonal	Rabbit IgG	ELISA, IHC-Fr, IHC-P, IP, and WB	Santa Cruz (sc-33141)
P63	Mouse, Rat, Dog, Human, Turtle	Monoclonal, (4A4)	Mouse IgG2a	ICC and IHC	Abcam (ab735)
Perlecan	Mouse, Rat, Human	Polyclonal	Rabbit IgG	IHC, ICC and WB	Prof. John Whitelock, University of NSW, Sydney
TAP63	Human	Polyclonal	Rabbit IgG	IHC and WB	BioLegend (618902)
Tenascin-C	Mouse and Human	Monoclonal (MTn-12)	Rat IgG1	ELISA, ICC/IF, IHC-Fr, IHC-P, IP, and WB	Abcam (ab6346)
Thy-1	Rhesus, Human, Pig	Monoclonal	Mouse IgG_1	IHC, ICC and Flow Cytometry	BD Bioscience (555593)

Type I Collagen	Mouse, Rat, Goat, Horse, Cow, Human, Pig	Polyclonal	Rabbit IgG	IHC, ICC and WB	Abcam (ab34710)
Type III Collagen	Mouse, Rat, Cow, Human	Polyclonal	Rabbit IgG	IHC, ICC and WB	Abcam (ab7778)
Type IV Collagen	Mouse, Rat, Dog, Human	Polyclonal	Rabbit IgG	IHC, ICC and WB	Abcam (ab6586)
Versican	Mouse, Rat, Human	Monoclonal (EPR12277)	Mouse IgG	IHC, ICC and WB	Abcam (ab177480)
Vimentin	Human, cow, dog, hamster,	Monoclonal (V9)	Mouse IgG1	IHC, ICC and WB	Dako (M0725)

Table 2.2 Secondary Antibody

Antibody Name	React Against	Conjugated	Application	Manufacturer/ Catalogue No.
Goat anti-mouse Ig	Mouse Ig, mainly IgG	HRP	WB	Dako (P0447)
Goat anti-rabbit Ig	Rabbit Ig, mainly IgG	HRP	WB	Dako (P0448)
Rabbit anti-rat Ig	Rat Ig, mainly IgG	HRP	WB	Dako (P0450)
Goat anti-rabbit IgG	Rabbit IgG (Fab)	Alexa-488	ICC	ThermoFisher Scientific (A11070)
Goat anti-rabbit IgG	Rabbit IgG	Alexa-546	ICC	ThermoFisher Scientific (A11035)
Goat anti-mouse IgG	Mouse IgG	Alexa-488	ICC	ThermoFisher Scientific (A11001)
Goat anti-Rat	Rat IgG	Alexa-488	ICC	ThermoFisher Scientific (A11006)
Goat anti-mouse IgG1	Mouse IgG1	Alexa-488	ICC	ThermoFisher Scientific (A21121)
Goat anti-mouse IgG1	Mouse IgG1	Alexa-546	ICC	ThermoFisher Scientific (A21123)
Goat anti-mouse IgG2a	Mouse IgG2a	Alexa-488	ICC	ThermoFisher Scientific (A21131)

Table 2.3 Isotype Control

Antibody Name	Application	Manufacturer/ Catalogue No.
Mouse IgG2a	ICC	Dako (X0943)
Mouse IgG1	ICC	Dako (X0931)
Rabbit IgG	ICC	Invitrogen (02-6102)

2.3 Development of Xenogeneic-Free Dermal Fibroblast Derived Extracellular Matrix (ECM).

2.3.1 Media, Buffer and Solutions

Normal ECM Deposition Media (NDM)

The basal medium for the NDM was composed DMEM mixed with Ham F12 at the ratio of 3:1. This was further supplemented with 2% human serum (Gibco, Thermo

Fisher Scientific) 10m HEPES, 2mM L glutamine, 1 mM sodium pyruvate and 30µg/ml ascorbic acid (Wako Chemicals)

Macromolecular Crowding ECM Deposition Media (MCDM)

The basal medium for the MCDM media was composed of 37.5mg/ml Ficol70 (Sigma) and 25mg/ml Ficol400 (Amersham) dissolved in DMEM: F12 (3:1). This was further supplemented to with 2% human serum (Invitrogen) 10m HEPES, 2mM L glutamine, 1 mM sodium pyruvate and 30µg/ml ascorbic acid (Wako Chemicals)

1M Tris Buffer (pH 7/8) Stock Solution

12.11g of Tris-base (Sigma) was dissolved in 90ml of ddH_2O. The pH was adjusted to either 7 or 8 using 1M HCl and volume was then adjusted to 100ml with ddH_2O.

5% Sodium Deoxycholate Stock Solution

5% (w/v) sodium deoxycholate (Sigma) was prepared by dissolving 1g of sodium deoxycholate in 20ml ddH_2O. This was filtered with 0.22µm syringe filter and stored at room temperature.

10x DNase I Reaction Buffer

The 10x DNase I Reaction consisted of 100mM Tris Buffer (pH 7), 25mM $MgCl_2$ (Sigma) and 5mM $CaCl_2$ (Sigma). This was filtered with 0.22µm syringe filter and stored at -20°C.

5x Phospholipase A_2 (PLA_2) Reaction Buffer

The 5x PLA_2 Reaction consisted of 250mM Tris Buffer (pH 8), 5mM $MgCl_2$ (Sigma) and 5mM $CaCl_2$ (Sigma). This was filtered with 0.22µm syringe filter and was stored at -20°C.

DNase I Working Solution

The DNase I working solution contained 0.02mg/ml DNase I (Amresco), 1X DNase I reaction buffer, and 0.16x EDTA-Free protease inhibitor (Roche). This was made fresh for each use.

Phospholipase A_2 Working Solution

The PLA_2 working solution consisted of 20U/ml of PLA_2 (Sigma), 1X PLA_2 reaction buffer, 0.5% sodium deoxycholate (Sigma) and 1x EDTA-Free protease inhibitor (Roche). This was made fresh for each use.

Ammonium Hydroxide Working Solution

The ammonium working solution consisted of 0.02M of ammonium hydroxide (Sigma), 0.5% Triton X-100 (Sigma) and 1x EDTA-Free protease inhibitor (Roche)

Urea Buffer

The urea buffer contained of 40mM Tris-Base (pH 7.5), 7M Urea, 2M Thio-Urea, 1% NP40 and 10mM DTT. The buffer was made fresh before use.

2.3.2 Immunofluorescence Staining for the Validation of Fibroblast Phenotype

This assay was performed to validate the identity of the fibroblast cell lines used to derive the ECM. The etched glass coverslips were placed in the wells of a 6 well plate and coated with 3µg/cm^2 of Type I Collagen for 2 hours at 37ºC. Excess collagen was removed, and the etched glass coverslip was washed twice with 500µl PBS before being overlaid with 250µl of the appropriate media. The aHDF cells were seeded at 10 x 10^4 cells into each well of a 6 well plate. The cells were cultured overnight to allow them to attach and spread. The coverslips were washed twice with PBS, and the cells were fixed with 4% paraformaldehyde/PBS for 15 minutes at room temperature. Cells were then washed twice with PBS before being permeabilized with cold 0.1% Triton X-100/PBS for 3 minutes. Following permeabilization, cells were washed twice with PBS before being blocked with 10% Goat Serum/1% BSA/PBS for 1 hour at RT. Blocking solution was removed, and cells were incubated for 1 hour at RT with primary antibody (vimentin, Thy-1 and TE-7) prepared in 10% Goat Serum/1% BSA/PBS. Cells were washed 3 x 5 minutes with PBS before being incubated for 1 hour in the dark at RT with secondary antibodies prepared with 10% Goat Serum/1% BSA/PBS. Cells were washed 3 x 5 minutes with PBS and then incubated in DAPI (1:2000 dilution in PBS) solution for 10 minutes. The coverslip was then mounted in Vectashield antifade mounting medium (Vector Laboratories) and sealed with nail

varnish. Images were captured with Zeiss Axioskop Fluorescent Microscope using Spot Advanced software.

Further validation of the dermal fibroblast was undertaken by confirming their ability to differentiate into myofibroblasts. The dermal fibroblasts were seeded at 3 x 10^4 cell/ well into the wells of a 24 well tissue culture plate containing etched glass coverslips. The dermal fibroblasts were induced to differentiate by adding 5ng/ml TGFβ1 (Peprotech) into the complete DMEM media and leaving them to grow for 3 days. Immunofluorescent staining was performed as described above to detect expression of alpha-smooth muscle actin.

Differentiation of the dermal fibroblast was also investigated under MMC condition. Following 7 days of ECM deposition, the fibroblasts were subjected to immunofluorescent staining to detect alpha-smooth muscle actin as described previously.

2.3.3 Proliferation of Fibroblasts under Macromolecular Crowding Condition

The effect of MMC on the proliferation of fibroblasts was investigated by determining the total number of cells at the end of ECM deposition. This was done in a 12 well tissue culture plate. Cells were seeded at 6 x 10^4 cells/well and cultured in either NDM or MCDM media for 7 days, with media changed every two days. At day 7, fibroblasts were fixed for 5 min with cold acetone: methanol (1:1). Cells were then blocked with PBS/1%BSA for 1 hour at RT before being incubated with 500µl of DAPI in PBS (1:1000) for 5 minutes. The fibroblasts were washed once with PBS and then left in 500µl of PBS. Nine sets of non-overlapping images were taken with the Olympus IX51 Inverted Microscope using a 4x objective lens. Cell numbers were determined by summing the number of nuclei in each field of view using Fiji-Image J software through its "Find Object" macro.

2.3.3 Immunofluorescent Staining for Extracellular Matrix Deposition under Macromolecular Crowding Condition

The production of extracellular matrix (ECM) by fibroblasts under normal or macromolecular crowding conditions was investigated. Immunofluorescent staining for ECM was done on etched glass coverslips placed into a 24 well plate. Cells were

seeded at 3 x 10^4 cells/well and cultured in either NDM or MCDM media for 7 days, with media changed every two days. The ECM produced was fixed with 4% paraformaldehyde in PBS for 15 min at RT. The ECM was washed twice with PBS before being blocked with 10% Goat Serum/1% BSA/PBS for 1h at RT. Blocking solution was removed, and cells were incubated for 1 hour at RT with primary antibody (recognizing ECM proteins) prepared in 10% Goat Serum/1% BSA/PBS. Cells were washed 3 x 5 minutes with PBS before being incubated for 1 hour in the dark at RT with secondary antibodies prepared 10% Goat Serum/1% BSA/PBS. The ECM was washed 3 x 5 minutes with PBS and then incubated in DAPI (1:2000 dilution in PBS) for 10 minutes. The coverslip was then mounted in Vectashield antifade mounting medium (Vector Laboratories) and sealed with nail varnish. Images were captured with Nikon A1+ Confocal Microscope (Nikon, Tokyo, Japan).

In order to generate a 3D representation of the matrix deposited, Z-stacked images of Type I Collagen were obtained using Nikon A1+ Confocal Microscope. Images were merged to generate a single image using the NIS-Elements AR analysis.

2.3.4 Decellularization of Fibroblast-Derived Matrix

2.3.4.1 Decellularization Methods

EDTA Method

At the end of Day 7 of ECM deposition, the cells were rinsed with PBS, followed by 2.5mM of EDTA in PBS. Cells were then incubated in 2.5mM of EDTA in PBS for 10 minutes at 37°C. Using a P1000 pipet, the cell monolayer was pipet sprayed off the surface. The surface was then washed once with PBS, followed by an incubation for 5 min at 37°C with 0.5% Triton X-100 in PBS. Finally, it was then washed thrice with PBS.

Ammonia Hydroxide (AH) Method

At the end of Day 7 of ECM deposition, the cells were rinsed twice with PBS, followed by incubation in ammonium hydroxide (Section 2.3.1) working solution at 37°C for 5 minutes. The remaining ECM was then washed with twice with PBS followed by incubation in DNase I working solution at 37°C for 30 minutes. Finally, it was then washed thrice with PBS.

Phospholipase A_2 (PLA_2) Method

At the end of Day 7 of ECM deposition, the cells were rinsed twice with PBS, followed by incubation in PLA_2 working solution (Section 2.3.1) at 37°C for 30 minutes. The remaining ECM was then washed with twice with PBS followed by incubation in DNase I working solution at 37°C for 30 minutes. Finally, it was then washed thrice with PBS

2.3.4.2 Determination of Decellularization Efficacy using Immunofluorescent Staining

The efficacy of three different decellularization method (EDTA, AH and PLA_2) was determined by its ability to remove cellular components (nuclear and cytoplasmic) while maintaining ECM integrity. Cells were seeded at 6 x 10^4 cells/well in a 12 well plate and cultured in MCDM media for 7 days, with media changed every two days. At the end of Day 7 of ECM deposition, the cells were removed using the decellularization method above and fixed with 4% paraformaldehyde in PBS for 15 min at RT before being washed twice with PBS.

The presence of DNA in decellularized ECM was determined by using DAPI (1µg/ml in PBS). Images were captured using a Zeiss LSM510 inverted fluorescent microscope.

The presence of membrane and cytoplasmic components in decellularized ECM was determined by immunofluorescence staining of actin (Phalloidin-TRICT), β4 integrin and α6 integrin. Images were captured using a Zeiss LSM510 inverted fluorescent microscope.

To determine ECM integrity after decellularization, Z-stacked images of Type I Collagen structures were obtained using Nikon A1+ Confocal Microscope. Images were merged to generate a single image using the NIS-Elements AR analysis. Further analysis of the integrity of ECM was performed via the quantification of ECM protein using fluorescence intensity. Decellularized ECM was immunostained for type I collagen or fibronectin and imaged using the Olympus IX51 Inverted Microscope. Fluorescence intensity per field of view was determined using FIJI Image J software.

2.3.4.3 Quantification of DNA Remaining After Decellularization

In addition to the visualization of DNA (as previously described), nucleic acids were also quantified using the CyQuant cell proliferation assay kit (Molecular Probe, Invitrogen). The CyQuant assay kit was used due to its propriety dye, which exhibits a strong fluorescence signal when bound to nucleic acids. Quadruplicate wells of a 96 well plate were used to quantify the residual nucleic acids for each decellularization method. Fibroblasts were harvested and seeded at 4.5 x 10^3 cells/well and cultured in MCDM media for 7 days, with media changed every two days. At the end of Day 7, the cells were removed using the different decellularization methods (Section 2.3.4.1). For the positive control, wells which still contain fibroblasts were used. Wells were washed twice before the plate was left in -80°C overnight. The plate was brought up to room temperature before being quantified using the CyQuant assay kit. 100µl of the CyQuant assay solution (Section 2.1.2) was then added to each well of the plate and then incubated at 37°C for 10 min. The fluorescence intensity was measured with a 485nm/535nm filter using an Enspire plate reader (Perkin Elmer). Results were calculated as a percentage of the control, which was calculated by the equation: Fluorescence Intensity of Decellularization/Fluorescence Intensity of Control x 100%.

2.3.5 Solubilisation of Decellularized Fibroblast-Derived ECM

Untreated or decellularized fibroblast-derived ECM on tissue culture plastic was treated with urea buffer and scraped before being transferred to a microcentrifuge tube. The solution was vortexed and incubated at RT for 30 min. After incubation, the sample was centrifuged at 14,000 RPM for 10 minutes. Without disturbing the pellet, the supernatant was transferred to a clean microcentrifuge tube and stored at -20°C. The protein concentration was determined using a filter paper based assay (Section 2.4.2)

2.4 Protein Analysis

2.4.1 Solution and Buffers

0.5% Coomassie Blue Staining Solution

The coomassie blue staining solution was prepared by dissolving 2.5g of Coomassie Brilliant Blue-R205 (Biorad) into a solution containing 35ml of glacial acetic acid and 465ml of ddH_2O. The solution was then filtered before used.

Coomassie Blue Destaining Solution

The coomassie blue destaining solution consisted of 40% methanol, 10% acetic acid and 50% ddH_2O. This was achieved by mixing 200ml of methanol, with 50ml of glacial acetic acid and 250ml of ddH_2O

Blocking Buffer (Western Blot)

5% (w/v) skim milk powder in PBS-T Buffer was prepared by dissolving 1g of skim milk powder (Diploma) in 20ml PBS-T. The buffer was made fresh for each use.

SDS PAGE Running Buffer

A 10x SDS PAGE running buffer was prepared. This buffer contained 250mM Tris-HCl, 2M glycine and 1%(v/v) SDS diluted in ddH_2O; the pH was adjusted to 8.3 using 1M NaOH. A 1x running buffer was prepared fresh for each run by diluting the solution with ddH_2O.

Sample Loading Buffer

Sample loading buffer (2x) consisted of 160mM Tris-HCL (pH 6.8), 4% (w/v) SDS, 20% (v/v) glycerol and 0.2% (v/v) bromophenol blue in ddH_2O.

Electro-Blotting Transfer Buffer

A 10x Blotting Transfer Buffer was prepared. This buffer contained 250mM Tris-HCl and 2M Glycine; the pH was adjusted to 8.3 using 1M NaOH. A 1x Blotting Transfer Buffer was prepared fresh for each electrotransfer run by adding 160mL of 10x stock was added to 1440 mL ddH_2O and 400 mL of methanol.

PBS-Tween (PBS-T) Buffer

0.1% (v/v) Tween-20 was added to 1x PBS.

2.4.2 Filter Paper-Based Protein Quantification Assay

This assay was developed by Minamide and Bamburg[224] as a means of quantifying proteins in the presence of reducing agent, detergents and other substances that interfere with current protein quantification assays. We have slightly modified the procedure of this assay. Bovine serum albumin (BSA; Thermo Scientific, Pierce) was used to generate a standard curve. The BSA was serially diluted to yield a

concentration range from 50µg/ml to 2000µg/ml. A volume of 8µl of protein samples were added onto a Whatman No.1 filter paper. The filter paper was left to air-dry before being rinsed with absolute methanol for 20 seconds. After being air-dried again, the filter paper was placed in 0.5% coomassie blue staining solution and incubated at RT for 30 minutes with gentle agitation on an orbital shaker. The filter paper was destained using Coomassie blue destaining solution for 2 hours with gentle agitation on an orbital shaker. The filter paper was left overnight to air-dry. A grayscale image of the filter paper was taken using the ChemiDoc XRS+ Imaging System (Biorad). Using image J, the pixel density of the samples were measured. The optical density was calculated by using this equation: Log_{10} (Max intensity/Mean intensity). The BSA standard curve was generated by plotting the mean absorbance of each BSA standard against its concentration in µg/ml. This standard curve was used to determine the protein concentration of the unknown samples.

2.4.3 SDS-PAGE Resolving and Stacking Gel

SDS-PAGE resolving gels were prepared by combining acrylamide/bis-acrylamide solution (29:1 ratio; Bio-Rad Laboratories) with 0.375 M Tris-HCl (pH 8), 0.1% SDS and ddH_2O. The acrylamide/bis-acrylamide was added in sufficient quantities to produce gel solution of 7.5 % or 10% acrylamide. Just prior to pouring, 0.1% (w/v) ammonium persulfate (Sigma) and 0.2% (v/v) TEMED (Sigma) were added into the gel mixture. The gel was then immediately poured between two glass plates (mini-gel) assembled in a gel caster (Hoefer, San Francisco, CA) leaving 2 cm space at the top of the glass plates for the stacking gel. The resolving gel was overlaid with ddH_2O and allowed to polymerize at room temperature (RT).

The stacking gels were prepared by combining 5% acrylamide/bis-acrylamide (29:1), 125mM Tris-HCl (pH 6.8), 0.1% (w/v) SDS and ddH_2O. Just prior to pouring, 0.1% v/v ammonium persulfate and 0.2% (v/v) TEMED were added to the gel mixture. This was then poured between the glass plates on top of the polymerized resolving gel, and the well casting comb was put in place. The stacking gel was left to polymerize at RT before removing the comb.

2.4.4 Protein Separation Using SDS-PAGE

Solubilized ECM extracts were separated by electrophoresis on a 7.5% SDS-PAGE under reducing conditions. Samples were prepared by adding 1 volume of SDS 2x loading buffer to 1 volume of protein sample in addition to 50mM of DTT and boiled for at 95°C for 5 min. This was loaded into the well of the SDS-PAGE gel, which was prepared and equipped onto the Mighty Small SE250 apparatus (Hoefer, Scientific Instruments, CA, USA). Precision Plus Kaleidoscope Prestained Protein Ladder (Biorad, California) was loaded onto each gel run. The proteins were separated using a constant current of 25 milliamps (mA) for 2 hours. Following protein separation, samples were transferred to a PVDF membrane via electroblotting.

2.4.5 Electro-Blotting Transfer

Following separation of protein through SDS-PAGE using electrophoresis, samples were transferred to an Immobilon-P PVDF membrane (Millipore, Bedford, MA, USA) using a wet blotting equipment. PVDF membrane was activated through methanol immersion and equilibrated in transfer buffer before use. Electroblotting was performed with 1x electroblotting buffer at 200 mAmp for 1 hour at RT. The membrane was blocked overnight at 4°C in blocking buffer

2.4.6 Western Blot

After overnight blocking, primary antibodies diluted in blocking buffer was added onto the membrane and incubated for 1h at RT. The membrane was washed 3 times using PBST before being incubated with the corresponding secondary antibodies conjugated with HRP for 1h at RT. The membrane was washed for 3 times using PBST before being incubated with Western Lightning Plus ECL substrate (Perkin Elmer, Waltham, MA) and protein bands were visualized with ChemiDoc^{TM} MP System (Bio-rad, California)

2.5 Quantitative Microscopic Techniques

2.5.1 Growth Curve

Growth curves were generated by monitoring cell growth in a 48 well tissue culture plate (NUNC) on a daily basis. Quadruplicate wells either contains acellular fibroblast-derived matrix or Type I Collagen coating or uncoated tissue culture plastic. Keratinocytes were harvest, pelleted and then resuspended in DKSFM, at a

concentration of 1 x 10^5 cells/ml. 100µl of this cell suspension (1 x 10^4 cells) was added into the wells. At each 24-hour interval, for 6 days, the wells containing keratinocytes were fixed for 5 min with cold acetone: methanol (1:1) and then kept in PBS at 4°C until the end of the growth curve. The keratinocytes were blocked with PBS/1%BSA for 1 hour at RT before being incubated with 300µl of 1:500 DAPI for 10 minutes. The keratinocytes were washed once with PBS and the left in 500µl of PBS. Images were taken on the Olympus IX-81 high content screening inverted microscope. Using a 10x objective lens, 7 x 11 non-overlapping quadrants were taken, to produce a 0.5cm^2 area image containing nuclei. Cell numbers were determined by summing the number of nuclei using Fiji-Image J software through its "Find Object" macro. A growth curve of cell numbers were plotted against time in hours.

2.5.2 Keratinocyte Cell Size

Keratinocyte cell size was determined in a 48 well tissue culture plate (NUNC). Quadruplicate wells contained either acellular fibroblast-derived matrix, type I collagen coating or uncoated tissue culture plastic. Keratinocytes were harvested, pelleted and then resuspended in DKSFM, at a concentration of 1 x 10^5 cells/ml. 100µl of this cell suspension (1 x 10^4 cells) was added into the wells. At day 3, keratinocytes were fixed for 15 min with 4% paraformaldehyde/PBS. The keratinocytes were washed twice with PBS, blocked with PBS/1%BSA for 1 hour at RT and incubated with 300µl of 1:200 Phalloidin-Alexa488 (Thermo Fisher Scientific) for 1h at RT. Keratinocytes were washed twice with PBS before being incubated for 10 min with 300µl of DAPI (1:500 in PBS), washed with PBS again and then left in 500µl of PBS Images were taken on the Olympus IX-81 high content screening inverted microscope. Using a 20x objective lens, 8 x 8 non-overlapping quadrants were imaged. Cell size was determined using the Cell Profiler software. A frequency plot was used to show the difference in cell size by cell area (small<medium<large=2000µm^2<4000µm^2<6000µm^2).

2.5.3 Quantification of Ki67 Positive Keratinocyte

Ki67 positive keratinocytes were determined in a 48 well tissue culture plate (NUNC). Quadruplicate wells contained either acellular fibroblast-derived matrix, type I collagen coating or uncoated tissue culture plastic. Keratinocytes were harvested,

pelleted and resuspended in DKSFM, at a concentration of 1 x 10^5 cells/ml. 100µl of this cell suspension (1 x 10^4 cells) was added into the wells. At day 3, keratinocytes were fixed for 5 min with cold acetone: methanol (1:1). The keratinocytes were blocked with PBS/1%BSA for 1 hour at RT before being incubated with 150µl of 1:100 mouse anti-Ki67 antibody for 1 hour at RT. Keratinocytes were washed 3 x 5 minutes with PBS before being incubated for 1 hour in the dark at room temperature with secondary antibodies prepared in 1%BSA/PBS. Keratinocytes were washed 3 x 5 minutes with PBS before being incubated for 10 min with 300µl of 1:500 DAPI. The keratinocytes were washed once with PBS and the left in 500µl of PBS. Images were taken on the Olympus IX-81 high content screening inverted microscope. Using a 10x objective lens, 7 x 11 non-overlapping quadrants were imaged. The percentage of keratinocytes positive for Ki67 was determined using the Cell Profiler software.

2.5.4 Quantification of p63 Positive Keratinocyte

P63 positive keratinocytes were determined in a 24 well tissue culture plate (NUNC). Quadruplicate wells either contains acellular fibroblast-derived matrix, type I collagen coating or uncoated tissue culture plastic. Keratinocytes were harvested, pelleted and then resuspended in DKSFM, at a concentration of 8 x 10^4 cells/ml. 250µl of this cell suspension (2 x 10^4 cells) was added into the wells. At day 3, keratinocytes were fixed for 15 min with 4% paraformaldehyde/PBS. Cells were then washed twice with PBS before being permeabilized for 3 minutes with cold 0.1% Triton X-100(Sigma)/PBS. The keratinocytes were blocked with 10% Goat Serum/1% BSA/PBS for 1 hour at RT before being incubated with 200µl of 1:100 mouse anti-p63 antibody for 1 hour at RT. Keratinocytes were washed 3 x 5 minutes with PBS before being incubated for 1 hour in the dark at room temperature with 200µl of secondary antibodies prepared with 10% Goat Serum/1% BSA/PBS. Keratinocytes were washed 3 x 5 minutes with PBS before being incubated for 10 min with 500µl of 1:2000 DAPI. The keratinocytes were washed once with PBS and the left in 500µl of PBS. Nine sets of images were taken on the Nikon A1+ Confocal Microscope using a 10x objective lens. The percentage of keratinocytes positive for p63 was determined using the Cell Profiler software.

2.5.5 Live Imaging of Keratinocytes Movement

Keratinocyte movement was observed in a 48 well tissue culture plate (NUNC). Quadruplicate wells either contains acellular fibroblast-derived matrix or Type I Collagen coating or uncoated tissue culture plastic. Keratinocytes were harvest, pelleted and then resuspended in DKSFM, at a concentration of 1×10^5 cells/ml. 100µl of this cell suspension (1×10^4 cells) was added into the wells. Live imaging was taken using Olympus IX-81 high content screening inverted microscope. The time-lapse images over 2 days were taken at 15-minute interval using a 10x objective lens.

2.6 Statistical Analysis

Data presented has quadruple replicates, which is either shown as representative of at least 3 independent experiments or a sum of 3 independent experiments. Statistical analysis was done with SPSS statistic software V22.0 (IBM corporation, NY). Data were tested for normality of distribution and homogeneity of variance. If the data were normally distributed and homogeneous in variance, a parametric test was conducted; if not, a non-parametric test was conducted. P-value ($p<0.05$) was considered statistically significant.

For normally distributed data, experiments containing two sets of condition were tested with a t-test. For experiments containing 3 conditions or more, one-way analysis of variance (ANOVA) was conducted followed by Tukey's posthoc test.

Non-normally distributed data were analysed using the Kruskal-Wallis one way analysis of variance followed by Wilcoxon's signed-ranked test was performed.

Chapter III:

Development of Acellular Xenogeneic-Free Dermal Fibroblast-Derived Extracellular Matrix

3.1 Introduction

The cellular niche has a profound influence on directing a cell's fate. A critical component of the cellular niche is the extracellular matrix (ECM), a highly complex and specialised three-dimensional structure. It is composed of collagens, elastin, proteoglycans and noncollagenous glycoproteins, which vary in composition in different type of tissues[68,225]. The different matrix components bind together to form a complex network, providing biophysical and biochemical cues that regulate cell functions, such as survival, proliferation, migration and differentiation[69]. Due to their ability to direct cell behaviour, ECMs are considered critical elements to be included in tissue engineering procedures. As a consequence, there have been many attempts to use synthetic matrices, or isolated ECM components such as collagen, fibrin or hyaluronan to recapitulate the ECM function. However, these have failed to reproduce the molecular complexity or organisation of native tissue ECM[155,156]. As a consequence, the use of native ECMs as biomaterials has expanded. Hence, there is considerable interest in the use of either tissue or cell-derived ECM (CDM) as a natural biomaterial. While tissue-derived ECMs have been granted Food and Drug Administration approval and are widely used, clinical studies have suggested several disadvantages, which include potential pathogen transfer, anti-host responses, uncontrolled degradation and other issues[156].

As an alternative, CDM has been examined as a replacement for the native tissue-derived ECM. This material is a complex and structured mixture of ECM proteins, which mimics some aspects of the native tissue microenvironment. The primary determinant of CDM composition is the type of cells used[155]. This is illustrated in a study by Lu *et al.*[157], where they compared the CDM generated by fibroblasts, chondrocytes and mesenchymal stem cells (MSC). All matrices contain common components such as type I collagen, type III collagen, fibronectin, vitronectin, laminin and decorin. However, fibroblast CDM lacked versican and aggrecan, which were detected in both chondrocyte and MSC CDM. This demonstrates that careful consideration is required when choosing the CDM to be used. As the primary goal of this project was to create a CDM matrix that mimics the skin dermis, dermal fibroblasts were considered as a cell source.

While it is possible to generate an acellular ECM *in vitro*, current *in vitro* culture methods generally give rise to an unstructured ECM that lacks critical components[167]. It is possible that differences between the *in vitro* and *in vivo* microenvironments are contributing to the unstructured ECM that is produced. Cells in culture are in a dilute solution of macromolecules of around 1-10mg/ml, which is several-folds lower than the normal physiological environment that can range from 20.6mg/ml to 80mg/ml[168]. This means that in cell culture, molecular interactions taking place outside of cells may not be occurring at rates required for the assembly of an ECM which resembles that seen *in vivo*. To mitigate this problem, the addition of large inert macromolecules such as Ficoll (a massive uncharged, highly branched polysaccharide made by GE Healthcare) to cultures to increase the concentration of macromolecules has been investigated. Molecules like Ficoll, when used in this context, have been called "macromolecular crowders" (MMC) and the process of mimicking the *in vivo* concentration of macromolecules in this way is called "macromolecular crowding". The addition of Ficoll to cell cultures was found to accelerate biochemical reactions and supramolecular assembly, and macromolecular crowding was observed to affect the deposition and architecture of the ECM[167].

If the CDM is then to be used as a growth substrate for other experimental cell, the deposited ECM will next need to be stripped of the cells that produced it, i.e "decellularised". The primary goal of decellularisation is the removal of cellular components and antigens that may trigger a pro-inflammatory response of the host. This is a required in preparation for ultimate clinical applications in which the CDM is to be transplanted onto a patient. However, the decellularisation process must be balanced with the preservation of the biological activity and mechanical integrity of the ECM[155,177]. A number of physical, chemical or biological approaches, have been used to decellularize tissue matrices, each having their merits. While these processing methods have been demonstrated on tissues, their effectiveness on cultured CDM is less clear.

This chapter describes the development of a method to obtain a highly enriched, structured and well-preserved acellular ECM that is generated using a xenogeneic free culture system. This acellular ECM would be used later in the study to investigate the role of ECM proteins in modulating keratinocyte behaviour (Chapter IV). To enhance

the deposition and the assembly of a more structured ECM, MMC has been used. Here, three decellularisation methods (EDTA-Triton, ammonia hydroxide and phospholipase A_2) were compared for their ability to effectively remove the cell components from the matrix, whilst maintaining an intact ECM architecture.

3.2 Supplementary Materials & Methods

3.2.1 Buffers and Antibodies

Primary Antibodies Used

Antigen	Clone	Species, Isotype	Antibody Working Concentration
Alpha-smooth muscle actin	Monoclonal (1A4)	Mouse IgG2a	0.5µg/ml (ICC)
Anti-Fibroblast Marker	Monoclonal (TE7)	Mouse IgG1	0.5µg/ml (ICC)
Fibronectin	Polyclonal	Rabbit IgG	5µg/ml (ICC)
Fibronectin	Monoclonal (EP5)	Mouse IgG1	0.2µg/ml (WB)
Integrin Alpha-6	Monoclonal (GoH3)	Rat IgG2a	2.5µg/ml (ICC)
Integrin Beta-4	Monoclonal (439-9B)	Rat IgG2b	2.5µg/ml (ICC)
Perlecan	Polyclonal	Rabbit IgG	1:200 (ICC), 1:1000(WB)
Thy-1	Monoclonal	Mouse IgG1	2.5µg/ml (ICC)
Type I Collagen	Polyclonal	Rabbit IgG	5µg/ml (ICC), 1µg/ml (WB)
Type I Collagen	Monoclonal (COL-1)	Mouse IgG1	7.5µg/ml (ICC)
Type IV Collagen	Polyclonal	Rabbit IgG	5µg/ml (ICC)
Vimentin	Monoclonal (V9)	Mouse IgG1	2.5µg/ml (ICC)

ICC - Immunocytochemistry; WB – Western Blot

Acetic Acid Buffer

The acetic acid buffer consists of 0.1M acetic acid and 20mM of EDTA.

SDS Buffer

SDS buffer comprises 250mM of Tris-HCl (pH 6.8) and 5% SDS (w/v).

Radioimmunoprecipitation Assay (RIPA) Buffer

RIPA buffer is 50mM of Tris-HCL (pH 8.0), 1% (v/v) TritonX-100, 0.5% (w/v) sodium deoxycholate, 0.1%(w/v) SDS and 150mM NaCl.

Urea Buffer

Urea buffer consists of 40mM Tris-Base (pH 7.5), 7M Urea, 2M Thio-Urea, 1% NP40 and 10mM DTT. The buffer was freshly made immediately before use.

3.2.2 Solubilisation of Extracellular Matrix for Western Blotting

Acetic Acid Buffer & RIPA Buffer Solubilisation

Decellularised ECM generated with MMC in a 12-well plate was solubilized by adding 200µl of acetic acid buffer, or RIPA buffer and incubating at RT for 4 hours with rocking. Then the matrix was scraped off the plate, transferred to a microcentrifuge tube and centrifuged at 12,000 rpm for 20min at 4°C. The supernatant was carefully removed without disturbing the insoluble pellet and transferred to another tube for storage at 4°C.

SDS Buffer Solubilisation

SDS buffer (200µl) was added to a decellularised ECM layers generated with MMC in a 12-well plate. The matrix was scraped off the surface of the 12-well plate and transferred to a microcentrifuge to be boiled at 95°C for 5 minutes. The sample was centrifuged at 12,000 rpm for 20min before the supernatant was carefully removed without disturbing the insoluble pellet and transferred to another tube for storage at 4°C.

Tri-reagent Solubilisation

Decellularised ECM layers were generated with MMC in a 12-well plate. This material was solubilized using Tri-Reagent® (Sigma Aldrich) following the manufacturer's protocol. Briefly, 500µl of Tri Reagent® was added to the ECM layer and incubated for 5 minutes at RT. The Tri-reagent mixture was transferred into a microcentrifuge tube, and 100µl of chloroform was added. It was vortexed and left to incubate at RT for 5 minutes. The sample mixture was centrifuged at 14,000 RPM, 4°C for 20 minutes. 300µl of the phenol phase (red layer) was transferred to a new tube and 900µl of isopropanol was added. It was vortexed and left to be incubated at RT for 10 minutes. The samples were then centrifuged at 14,000 RPM, 4°C for 10 minutes to pellet the precipitated proteins. The pellet was washed three times with 1ml of 0.3M guanidine hydrochloride/95% ethanol solution by repeated resuspension and centrifuging at 14,000 RPM for 20 minutes at RT. After the third centrifugation, the

pellet was dried under vacuum for 5 minutes before being dissolved in 1% SDS and stored at 4°C.

Urea Buffer Solubilisation

Decellularised ECM generated with MMC in a 12-well plate was solubilized with urea buffer and scraped off the plate before being transferred to a microcentrifuge tube. It was vortexed and incubated at room temperature for 30 minutes. After incubation, the sample was centrifuged at 14,000 RPM for 10 minutes. Without disturbing the pellet, the supernatant was transferred to a clean microcentrifuge tube and stored at 4°C.

3.2.3 Microscopy

A number of different microscopes were used for the work described in this chapter:
-Phase contrast images were obtained using Zeiss Axiovert bright field inverted microscope (Zeiss, Oberkochen, Germany) or an Olympus IX-51 inverted microscope (Olympus, Tokyo, Japan).

-Immunofluorescence images were captured using either a Zeiss Axioskop upright microscope (Zeiss, Oberkochen, Germany), Nikon A1+ confocal microscope (Nikon, Tokyo, Japan) or Zeiss LSM510 confocal microscope (Zeiss, Oberkochen, Germany)

3.3 Results

3.3.1 Characterisation of the Adult Dermal Fibroblasts Used for Matrix Production

3.3.1.1 Cell Cultures without Macromolecular Crowding

During cell culture, the adult human dermal fibroblast (aHDF) cells had a uniform, spindle-like morphology, which is typical of fibroblasts. To determine whether the aHDFs expressed fibroblast markers, they were stained with antibodies recognising either Thy-1[226] or vimentin[227]. They were also stained with the TE-7 monoclonal antibody (mAb), which has been described to be specific for fibroblasts. All cells were positive for these fibroblast markers (Fig. 3.1A).

Myofibroblasts are associated with scarring and fibrosis[228]. To determine if the aHDF cells had myofibroblast characteristics, they were stained with an antibody recognising

alpha-smooth muscle actin (α-SMA). Subconfluent aHDF cultures failed to stain with this antibody (Fig.3.1B). To determine whether these aHDF cells were capable of differentiating into myofibroblasts, they were treated with TGFβ (See section 2.3.2). Such a treatment is known to induce myofibroblast differentiation[229]. After TGFβ treatment, the cells bound the mAb recognising α-SMA to reveal prominent stress fibres, which were indicative of stress fibres in myofibroblasts (Fig.3.1B).

3.3.1.2 Macromolecular Crowding Culture for Extracellular Matrix Deposition

This study's objective was to develop a method for producing a xenogeneic-free cell-derived matrix, hence the FBS in the culture medium was replaced with 2% human serum, and this medium was used for ECM deposition by dermal fibroblasts. A medium using human serum (See section 2.3.1), which was capable of sustaining fibroblast growth, had already been optimised by Prof. Coombe's lab (data not shown).

In an attempt to enhance the efficiency of ECM deposition and assembly, the "Ficol 70&400" mixture was added to the medium containing human serum to act as MMCs (See section 2.3.1). The possibility that the addition of the Ficol cocktail to the medium alters fibroblast behaviour was investigated. Phase contrast images at one-day post seeding did not show a change in fibroblast morphology, as the aHDFs retained their uniform spindle-like morphology (Fig. 3.2A). However, differences in fibroblast morphology could be observed from day four onwards after seeding. In the absence of MMC, the fibroblasts retained a spindle-like morphology but lost contact inhibition and began to grow on top of each other upon reaching confluence. By day seven, they formed weave-like patterns. However, with MMC, the fibroblasts appeared larger and flatter and remained as a contact-inhibited monolayer at day seven. The fibroblasts were also observed to align themselves to resemble a reticular pattern (Fig. 3.2A).

It was possible that the morphological changes observed in fibroblasts cultured with MMC may have indicated that they were differentiating into myofibroblasts. To check if differentiation had occurred, the fibroblasts were immunostained for α-SMA at day seven. Positive α-SMA staining was observed in these fibroblasts regardless of the presence or absence of MMCs, but cell cultured without MMC demonstrated prominent α-SMA positive stress fibres; whereas fibroblast cultured with MMC showed diffuse α-SMA staining (Fig. 3.2B). These data suggest that fibroblasts

cultured to confluence without MMC have progressed further towards a myofibroblast phenotype than fibroblasts cultured with MMC over the same time period. As medium-containing MMC appeared to alter the differentiation potential of the aHDFs, the possibility that MMC affect cell proliferation was examined. Cultures were stained with DAPI and cell counts were obtained at day seven according to the method described in section 2.3.3. Fibroblasts cultured with MMC showed a significant ($p \leq 0.01$) decrease in cell number compared to those that were grown without MMC (Fig. 3.2C).

3.3.2 Macromolecular Crowding and aHDF Extracellular Matrix Deposition

The appearance of the matrix produced by aHDFs grown with or without MMC was examined. Immunostaining of the matrix deposited when aHDFs were cultured with MMC revealed an increase in the staining intensity of type I collagen, type IV collagen, fibronectin and perlecan (Fig. 3.3A). To examine this further cells and ECM were solubilised by a number of different methods and the mixture resolved via 7.5% SDS-PAGE and analysed using Western blotting to detect fibronectin. As the majority of ECM proteins are cross-linked, they are frequently difficult to solubilise[230]; hence, four different solubilization methods were tested: RIPA buffer, acetic acid buffer, SDS buffer and Tri Reagent®. Only ECM solubilized with SDS buffer enabled fibronectin to be detected (Table 3.1). SDS buffer and urea buffer were then compared to assess their ability to solubilize the ECM by comparing the amount of type I collagen present using Western blotting. Type I collagen was detected in extracts obtained with both buffers, but band density was greater when urea buffer was used (Table 3.1). Given this finding, urea was used to investigate whether MMC altered the amount of ECM deposited. A slight increase in band intensity was observed for perlecan, when the ECM deposited without MMC was compared to ECM deposited with MMC (Fig. 3.3B&C). However, no differences in band intensity was observed for type I collagen.

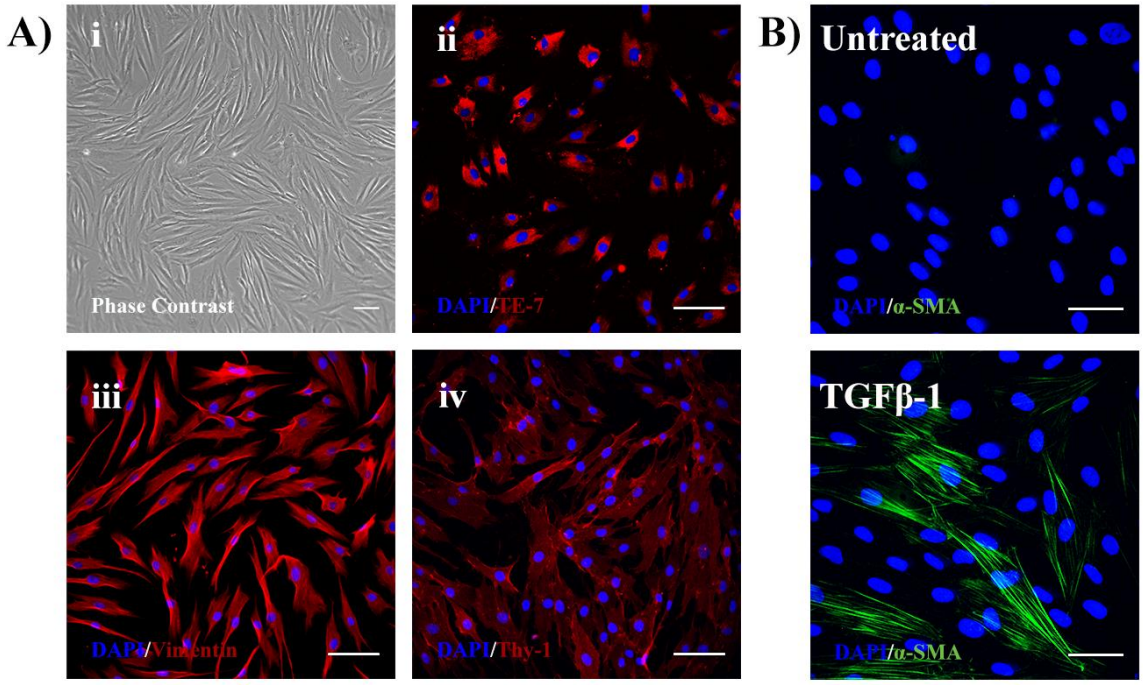

Figure 3.1: Characterization of human dermal fibroblast.

A) aHDF (10 x 10^4 cells) were seeded into a 6-well plate containing etched glass coverslips coated with type I collagen and cultured overnight. Cell morphology is seen in the phase contrast image **(i)**. aHDFs fixed with 4% paraformaldehyde were stained with antibodies recognising TE-7 **(ii)**, vimentin **(iii)** or Thy-1 **(iv)**. The secondary antibody was an anti-mouse IgG1 Alexa Fluor® 546-conjugated antibody. Nuclei were stained with DAPI (blue). Scale bars are 100µm.

B) aHDFs differentiation into myofibroblasts following TGFβ-1 stimulation. aHDF (3 x 10^4 cells) were seeded into wells of a 24-well plate containing etched glass coverslips. 5ng/ml TGFβ-1 was added, and after three days, cells were fixed with 4% paraformaldehyde and stained for alpha-smooth muscle actin. The secondary antibody was an anti-mouse IgG_{2a} Alexa Fluor® 488-conjugated antibody. Nuclei were stained using DAPI (blue). Scale bars are 50µm.

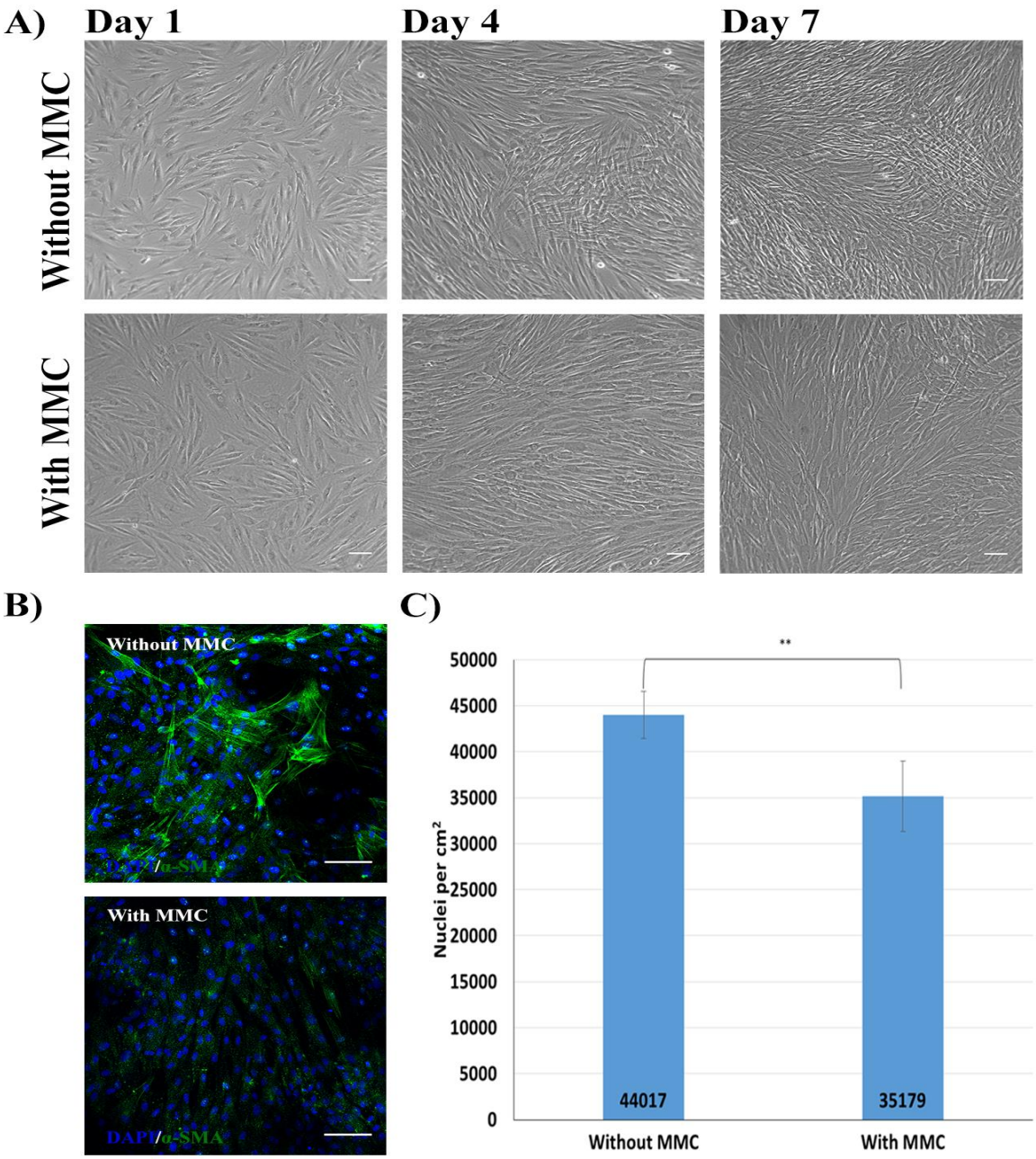

Figure 3.2: The effect of MMC on fibroblast behaviour.

A) Phase contrast images of aHDF cultured with or without MMC. Scale bars are 100µm.

B) Myofibroblast differentiation with and without MMC. aHDFs were grown under the two conditions for seven days. The cells were fixed with 4% paraformaldehyde, stained for α-SMA and imaged using a confocal microscope. The secondary antibody was an anti-mouse IgG_{2a} Alexa Fluor® 488-conjugated antibody. Nuclei were stained using DAPI (Blue). Scales bars are 100µm.

C) The number of aHDFs after culturing with or without MMC for seven days. Cell nuclei were visualised with DAPI and nuclei in nine non-overlapping fields of view were counted. Data are expressed as mean ± SD. The figure is a representative of triplicate experiments. **P<0.01.

Table 3.1 Summary of ECM solubilization methods analysed by western blotting.

ECM Protein	Method of Solubilisation				
	RIPA Buffer	Acetic Acid Buffer	Tri-reagent	SDS Buffer	Urea Buffer
Fibronectin	✖	✖	✖	✓	NT
Type I Collagen	NT	NT	NT	✓	✓✓

"✖" indicates - not detected; "✓" indicates – detected; "✓✓" indicates - detected with visually darker bands; "NT" indicates - not tested

To visualise the location of the fibroblasts with respect to the ECM, aHDF cultures generated with and without MMC were immunostained for type I collagen and the nuclei were stained with DAPI. A three-dimensional (3D) construct was generated using confocal microscopy to view the position of the cells and the ECM. Without MMC, type I collagen was located between the cells (Fig. 3.4i), whereas MMC caused the deposition of a dense layer of type I collagen on top of the fibroblasts (Fig. 3.4ii).

The matrix produced by aHDFs grown with or without MMC was also examined after the cells were removed. The fibroblasts were removed using phospholipase A_2 (PLA_2; see section 2.3.4.1) and type I collagen and fibronectin in the acellular matrix were examined by immunostaining. Analyses of the relative fluorescence intensities of type I collagen and fibronectin indicated a significant ($p \leq 0.05$) increase in type I collagen staining in cultures containing MMC. However, no differences in the intensity of fibronectin staining were detected (Fig. 3.5B). To further investigate the type I collagen that was deposited. ECM from cultures decellularised with PLA_2 was solubilized with urea buffer, resolved by 7.5% SDS-PAGE and analysed by Western blotting. These results from these experiments suggested slightly more type I collagen was present when MMC was omitted (Fig. 3.5C). To determine the total concentration of ECM protein remaining after decellularisation, protein concentration was determined using a filter paper-based protein quantification assay originally developed by Minamide and Bamburg[224]. This assay enables the determination of the protein level in the presence of reducing agent, detergents and other substances that interfere with other protein quantification assays. By this method, no difference in total protein concentration was detected in extracts of ECM generated with or without MMC (Fig. 3.5D).

To ensure that the similarity of fluorescence intensity of fibronectin staining between non-MMC and MMC cultures is not a result of signal saturation, the antibody recognising fibronectin was titrated. As revealed in figure 3.6, no differences in the intensity of fibronectin staining was observed, despite an increase in the antibody used. This suggests that there was no change in fibronectin deposited between culture with or without MMC.

As MMC has been shown to facilitate the supramolecular assembly of type I collagen to produced a more fibrillar structure[231], it was possible that different epitopes may be exposed following macromolecular crowding, and if so another type I collagen antibody may give different immunostaining outcomes compared to that of the polyclonal antibody used in Figure 3.3-3.5. Hence, the staining pattern of the monoclonal antibody (COL-I) recognising type I collagen was explored. As revealed in Figure 3.7, the resulting immunofluorescence staining pattern obtained using the monoclonal antibody COL-I was the opposite to that seen with the polyclonal antibody (Fig. 3.7). That is, there was a more intense stain with the COL-I mAb in ECM from culture without MMC. These data suggest that the polyclonal antibody recognises a conformational epitope in type I collagen that is generated or exposed by macromolecular crowding, whilst the monoclonal epitope is lost or sequestered in the compact MMC-generated matrix.

3.3.3 Decellularisation Methods For Generating Acellular Extracellular Matrices

As macromolecular crowding enabled a more structured and even deposition of ECM, and no myofibroblast differentiation was detected when aHDFs were grown under MMC conditions, MMC was used to generate the ECM from herein. To determine which decellularisation methods were most effective in removing the cells, whilst preserving the ECM proteins and structure, three different decellularisation protocols were compared using EDTA, ammonium hydroxide (AH) and phospholipase A_2 (PLA_2).

3.3.3.1 Removal of Cell Components

Phase contrast images revealed that all three decellularisation protocols removed the fibroblasts. Fibril-like structures were observed with AH and PLA_2 treatments.

However, they were absent when the EDTA decellularisation method was used (Fig. 3.8). The efficiency of each decellularisation protocol in removing nuclear components was examined by staining the decellularised material with DAPI to detect DNA and RNA. Before the decellularisation treatments, clear oval-shaped blue nuclei were observed. After decellularisation, DAPI staining was visibly absence for both EDTA and PLA_2 treatments. However, blue-stained fragments were observed after AH treatment (Fig. 3.9A). In order to better compare the amount of nucleic acids remaining, a CyQuant assay was used. The CyQuant assay kit was originally designed to quantify cell proliferation through the measurement of DNA content. This kit contains a proprietary dye that only exhibits strong fluorescence when bound to nucleic acid. This assay revealed that both EDTA and PLA_2 were significantly ($p \leq 0.01$) better than AH at removing the nucleic acid components (Fig. 3.9B), which was consistent with the observation from DAPI staining.

To determine whether the cytoplasmic components of the aHDFs were removed after the decellularisation treatments, phalloidin-TRITC staining was used to detect actin filaments. As shown in Figure 3.10A, actin filament fragments were detected following AH treatment, but no staining was apparent when EDTA and PLA_2 treatments were used.

Collectively, these data suggested PLA_2 treatment was the best of these methods to generate an acellular fibroblast-derived ECM. This method was also used to examine the retention of membrane-bound proteins remained in the matrix. Following PLA_2 treatment the ECM was immunostained for β4 and α6 integrin. The lack of staining indicated that these membrane-bound proteins were removed (Fig. 3.10B).

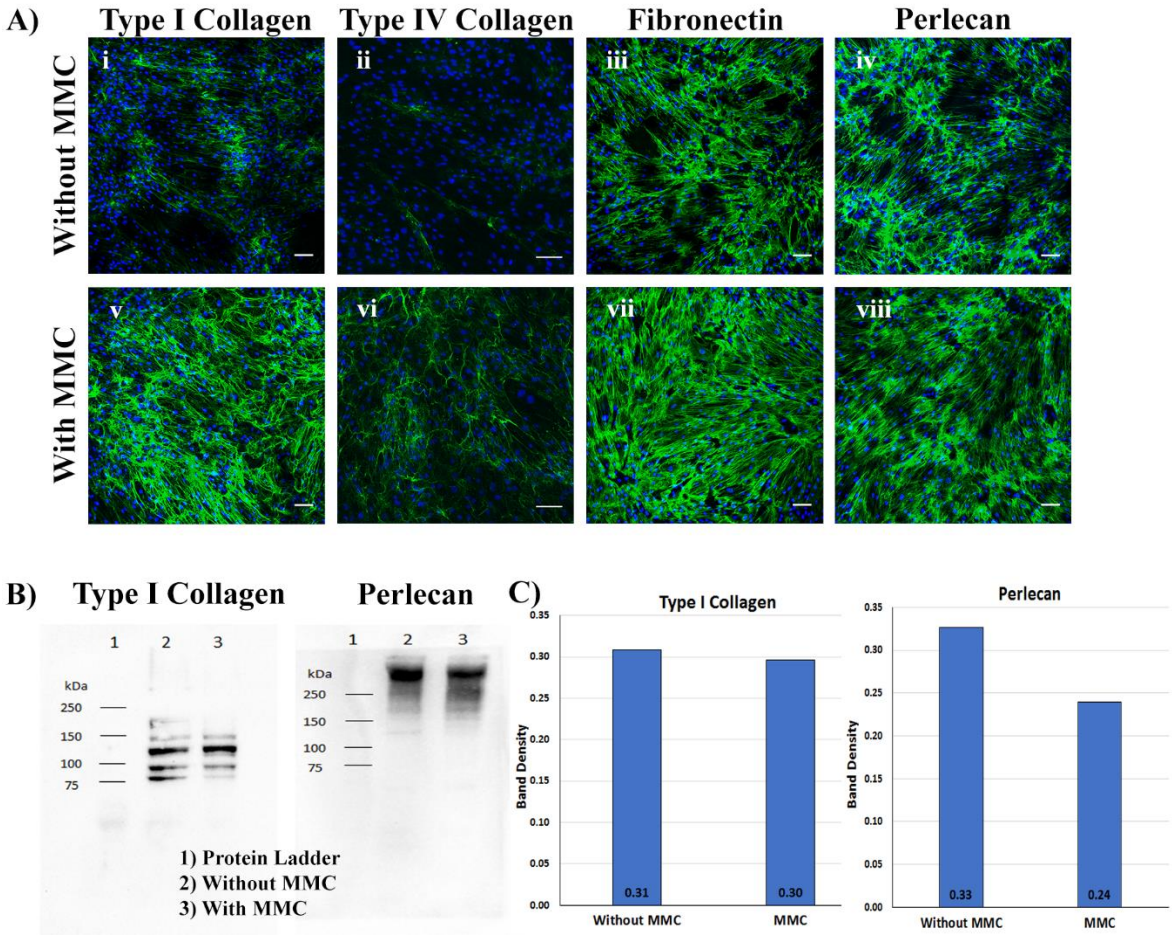

Figure 3.3: The effect of MMC on aHDF ECM deposition.

A) aHDFs were grown with or without MMC for seven days. The cells and matrix were fixed with 4% paraformaldehyde and immunostained for type I collagen (i, v), type IV collagen (ii, vi), fibronectin (iii, vii) and perlecan (iv, viii). Images were obtained using a confocal microscopy. The secondary antibody was an anti-rabbit IgG Alexa Fluor® 488-conjugated antibody. Nuclei were stained with DAPI (Blue). Scales bars are 100µm.

B) Western blot of aHDFs following seven days of culture with or without MMC. The cell and matrix layer were solubilized with Urea buffer and resolved in 7.5% SDS-PAGE and visualised by Western blotting with ECL detection using antibodies recognising type I collagen and perlecan.

C) Quantification of band density on western blot for type I collagen and perlecan

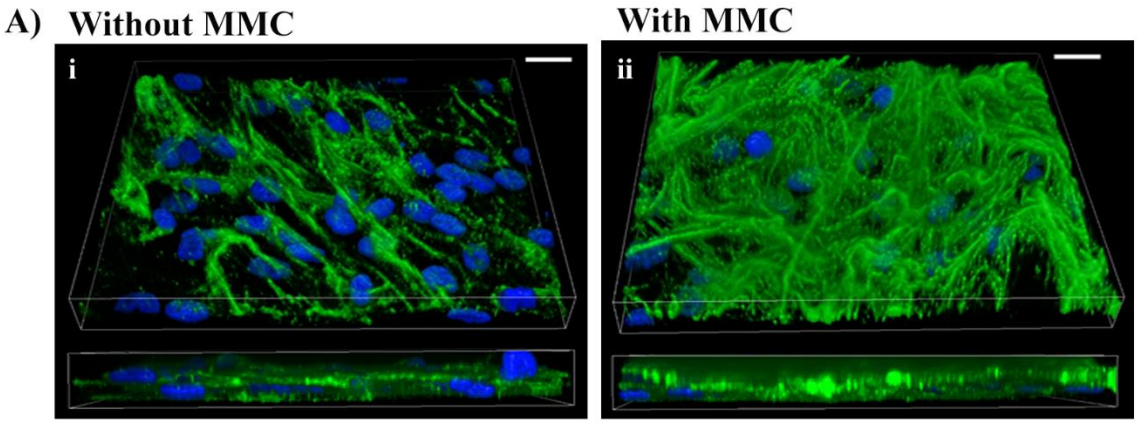

Figure 3.4: The effect of MMC on the 3D architecture of the ECM deposited by aHDF. A 3D Z-stacked confocal image of Type I Collagen deposited by aHDFs grown without (i) or with MMC (ii) for seven days. Cells and matrix were fixed with 4% paraformaldehyde and immunostained for Type I Collagen using an anti-collagen, rabbit IgG polyclonal antibody. The secondary antibody was an anti-rabbit IgG Alexa Fluor® 488-conjugated antibody. Nuclei were stained with DAPI (Blue). Scale bars are 10μm.

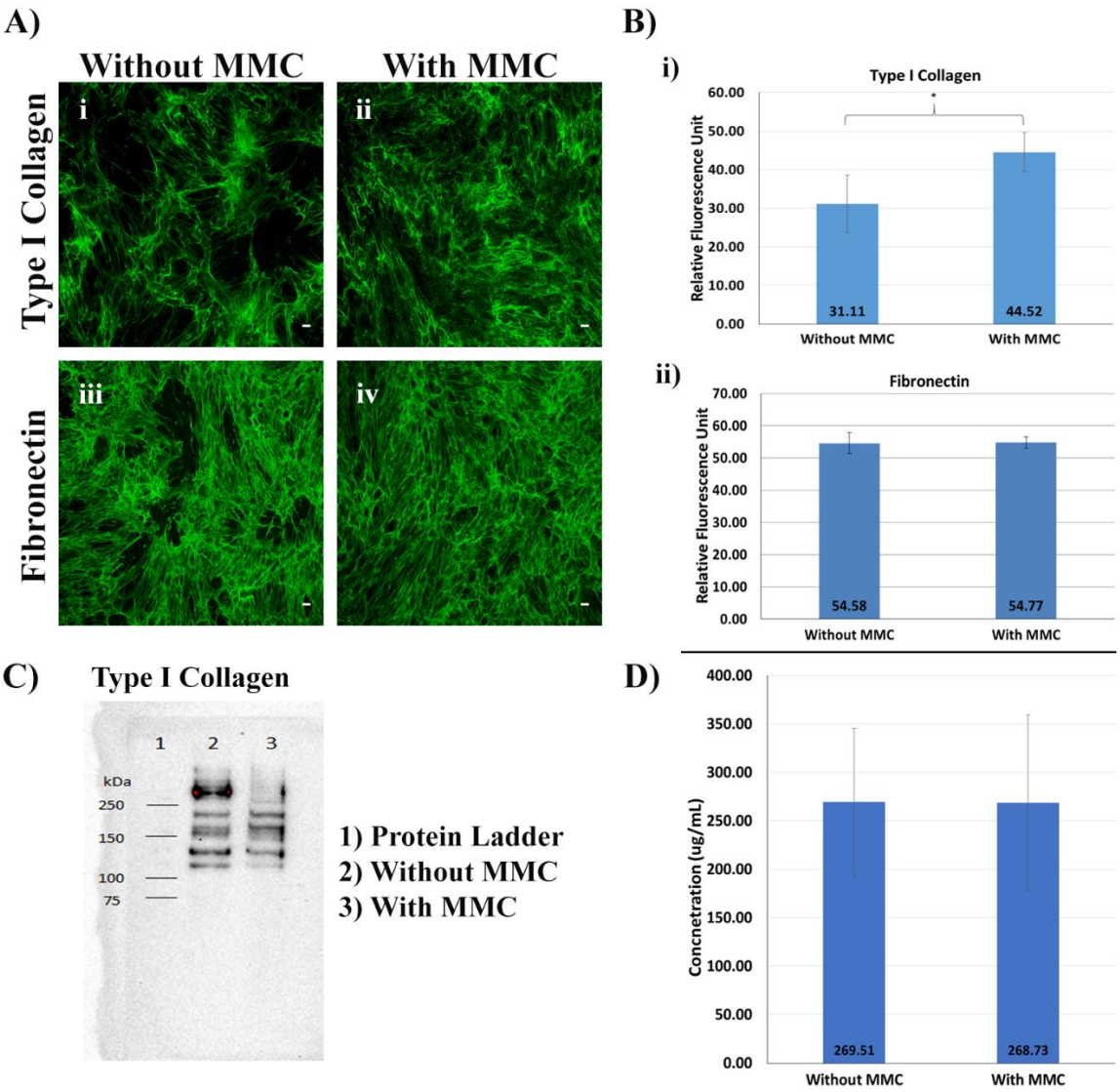

Figure 3.5: The effect of MMC on ECM deposition. The aHDF cells were grown with or without MMC until day seven. The fibroblasts were removed using PLA_2 decellularisation

A) Representative images of ECM generated with or without MMC and immunostained for Type I Collagen or Fibronectin. Scale bars are 100µm.

B) Quantification of fluorescence intensity of antibody staining of Type I Collagen (i) or Fibronectin (ii) deposited with or without MMC. *P<0.05. Data are expressed as mean ± SD and n=2 experiments

C) Western blot of type I collagen generated with or without MMC. The cells were removed with PLA_2 before the ECM was solubilized with urea buffer and resolved in a 7.5% SDS-PAGE. Proteins were visualised by Western blotting using an antibody recognising type I collagen with ECL detection.

D) Protein concentration of ECM after seven days of culture with or without MMC. Cells were removed using PLA_2 and the matrix solubilized with urea buffer. Protein concentrations were determined using a filter paper based protein quantification assay. Data are expressed as mean ± SD and n=2 experiments.

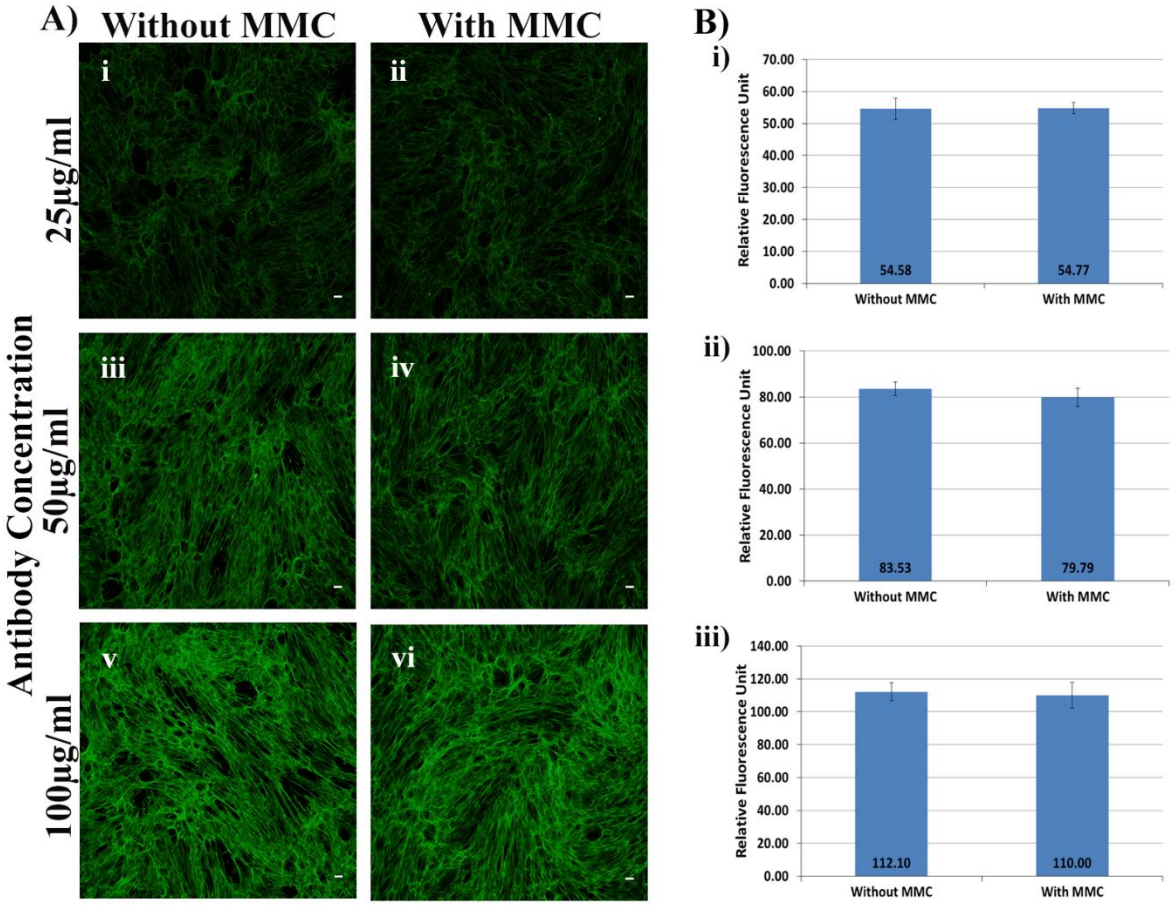

Figure 3.6: Anti-fibronectin antibody staining of ECM. The aHDF cells were grown with or without MMC until day seven. The fibroblasts were removed using PLA_2 decellularisation

A) Representative images of ECM generated with or without MMC and immunostained with antibody recognising fibronectin at 25µg/ml (i-ii), 50µg/ml (iii-iv) and 100µg/ml (v-vi). Scale bars are 100µm.

B) Quantification of fluorescence intensity of antibody staining of fibronectin with 25µg/ml (i), 50µg/ml (ii) and 100µg/ml (iii) for ECM deposited with or without MMC with nine set of images each. Data are expressed as mean ± SD.

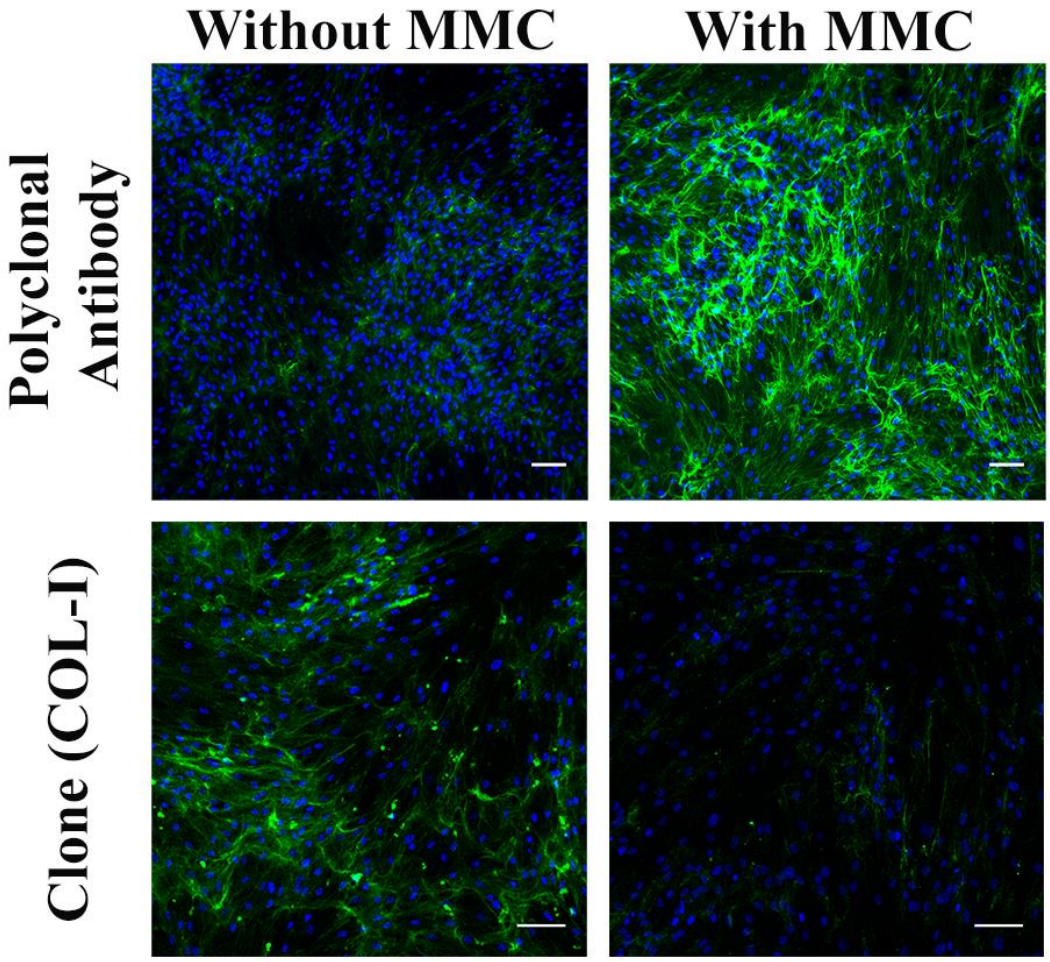

Figure 3.7: Type I Collagen staining of fibroblast-derived ECM generated with or without MMC using two different antibodies. aHDFs were grown with or without MMC for seven days. The cultures were fixed with 4% paraformaldehyde and immunostained for Type I Collagen with two different anti-type I collagen (ABCAM, ab34710 [polyclonal] and ab6308 [monoclonal: COL-I]) antibodies. Images were taken using confocal microscopy. The secondary antibodies were an anti-rabbit IgG Alexa Fluor® 488-conjugated antibody for the polyclonal antibody, and anti-mouse IgG Alexa Fluor® 488-conjugated antibody for the mAb. Nuclei were stained using DAPI (Blue). Scales bars are 100µm.

3.3.3.2 Preservation of ECM Structure and Retention of ECM Proteins

To determine whether the decellularisation treatments disrupted the structure of the ECM, 3D Z-stacked confocal images were taken for the differentially decellularised ECMs following type I collagen immunostaining. Fibrillar structures of type I collagen resembling the non-decellularised control were clearly visible following AH and PLA_2 treatments. However, the EDTA treatment disrupted the structure of the type I collagen filaments (Fig. 3.11). The thickness of the ECM was measured by determining the depth of type I collagen staining. In the absence of the decellularisation treatments, the ECM was found to have a thickness of 9µm. After decellularisation using AH or PLA_2 protocols, the thickness of the ECM shrank to around 6µm, whereas, following EDTA treatment, the ECM thickness was about 3µm (Fig. 3.12).

To examine whether ECM proteins remained following decellularisation, the fluorescence intensity of type I collagen and fibronectin were quantified. From the data in Figure 3.13, it is clear a significant reduction in the fluorescence intensities of both type I collagen and fibronectin staining were observed after EDTA treatment. In contrast, both AH and PLA_2 treatments were shown to preserve both type I collagen and fibronectin immunostaining.

3.3.4 Proteomic Analysis of PLA_2-derived Acellular Extracellular Matrix

Collectively the data demonstrated that the PLA_2 decellularisation protocol produced an intact ECM that was devoid of most cell components, hence this method was used to generate acellular matrices for further analysis. To determine the composition of the ECM from two different dermal fibroblast donors, mass spectrometry (MS)-based proteomic was used. MS analysis identified 539/953 and 632/775 proteins from ECM-derived from aHDF (Fib-Matrix Donor 1) and the primary cells, EBL028 (Fib-Matrix Donor 2). Two separate MS analyses were performed on the ECM samples. A thorough examination of the data set revealed the majority of the proteins identified were intracellular/cell surface proteins (Appendix A). As MS-based proteomics is a sensitive technique, it was more able to detect these cell components than immunofluorescence staining. In order to curate the ECM proteins, both MS analyses were combined and categorised using the human matrisome database (MatrisomeDB, http://matrisomeproject.mit.edu/). This database categorises the ECM proteins into "core matrisome" (ECM glycoproteins, collagens and proteoglycans) and "matrisome-

associated proteins" (ECM-affiliated proteins, ECM regulators and secreted factors)[230]. Amongst the protein identified, 103 and 99 were determined to be ECM proteins from aHDF and EBL028 respectively, and 87 of these proteins were expressed by both dermal fibroblast donors. It was also revealed that 16 and 12 proteins were specific for aHDF or EBL028 respectively. A closer examination indicates that the majority of the proteins unique to either aHDFs or EBL028 were in the "matrisome-associated protein" category (Fig. 3.14).

The primary goal of this chapter was the development of an acellular matrix that mimics the skin dermal ECM. To investigate how closely the ECM produced by the dermal fibroblasts *in vitro* matched skin dermal ECM, a database containing the ECM signature of the skin dermis was compared to our proteomic analysis. A tissue-based map of the human proteome was recently generated by Uhlén M and his colleagues[232]. They determined the protein expression patterns specific for each organs using RNA sequencing and they verified their results using microarray-based immunohistochemistry. This led to the development of an online resource, which is called the "Human Protein Atlas" database (http://www.proteinatlas.org/). This database was used as a basis to curate for ECM specific proteins of the skin dermis using "MatrisomeDB". A number of core ECM proteins such as collagen III alpha 1 (COL3A1) and laminin alpha-4 (LAMA4), which are known to be present in the skin dermis, were not found in the "Human Protein Atlas" database. Hence, to ensure a more comprehensive list of ECM proteins of the dermis, the proteomic dataset of the skin prepared from studies by Bliss E. *et al.*[233] was used to supplement the "Human Protein Atlas" database. A close examination revealed that a majority of the core matrisome proteins expressed in the skin dermis were also found in the dermal fibroblast-derived ECM that I prepared (Fig.3.15). However, the majority of the matrisome-associated proteins are absent in the dermal fibroblast-derived ECM (Fig. 3.16-3.17).

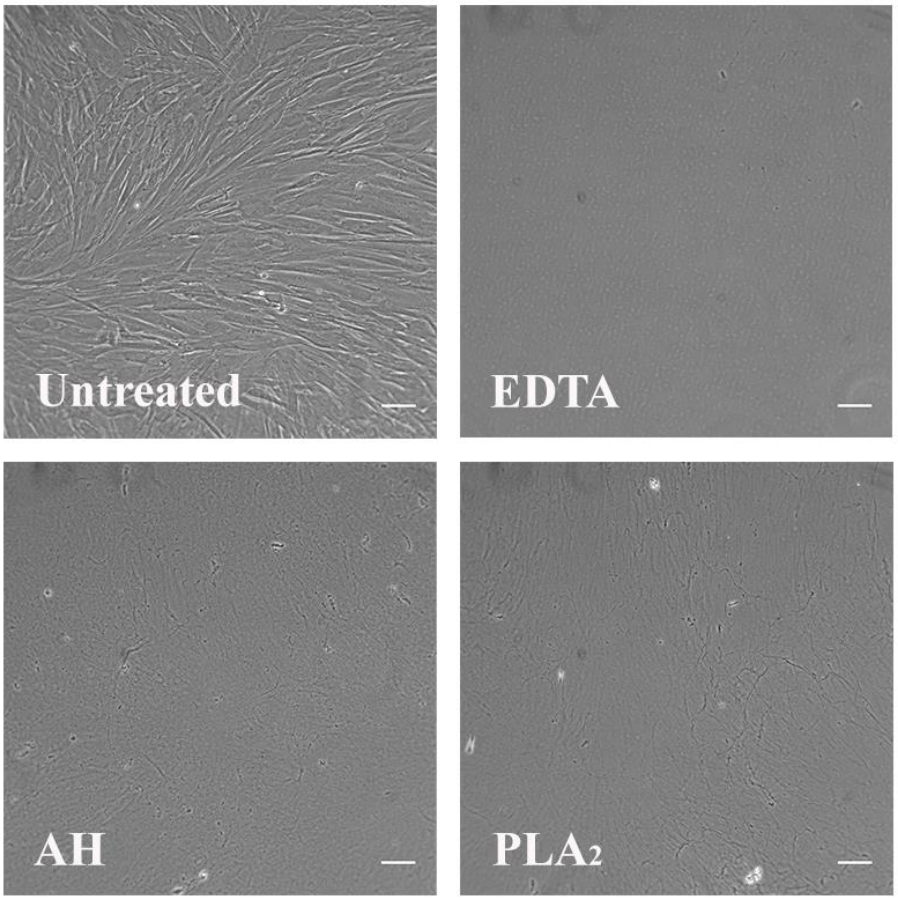

Figure 3.8: Phase contrast images of decellularised dermal fibroblast-derived ECM prepared using EDTA, ammonia hydroxide (AH) or phospholipase A_2 (PLA_2). The untreated control shows a confluent cell layer before decellularisation. The aHDF cells were grown with MMC until day seven and decellularised as indicated. Scale bars are 100µm.

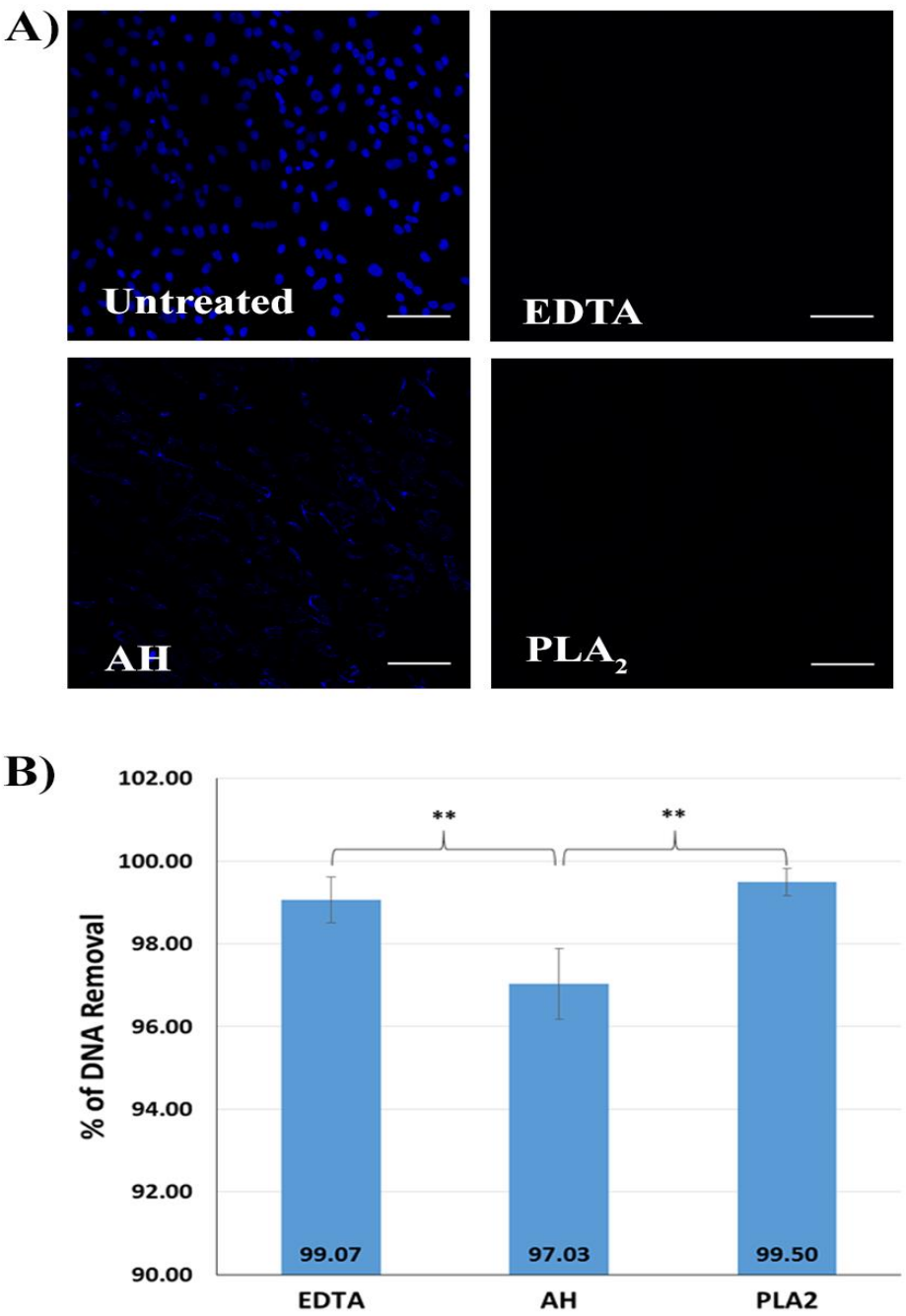

Figure 3.9: Efficacy of different decellularisation treatments for removing nuclear components. The aHDF cells were grown with MMC until day seven. The cell layer was decellularised using EDTA, ammonia hydroxide (AH) or phospholipase A_2 (PLA_2).

A) DAPI staining of the decellularised ECM and untreated control. Scale bars are 100µm.

B) Quantification of the percent of DNA removed after decellularisation. The CyQuant dye was used to determine the DNA present. **$p<0.01$. n=3 experiments.

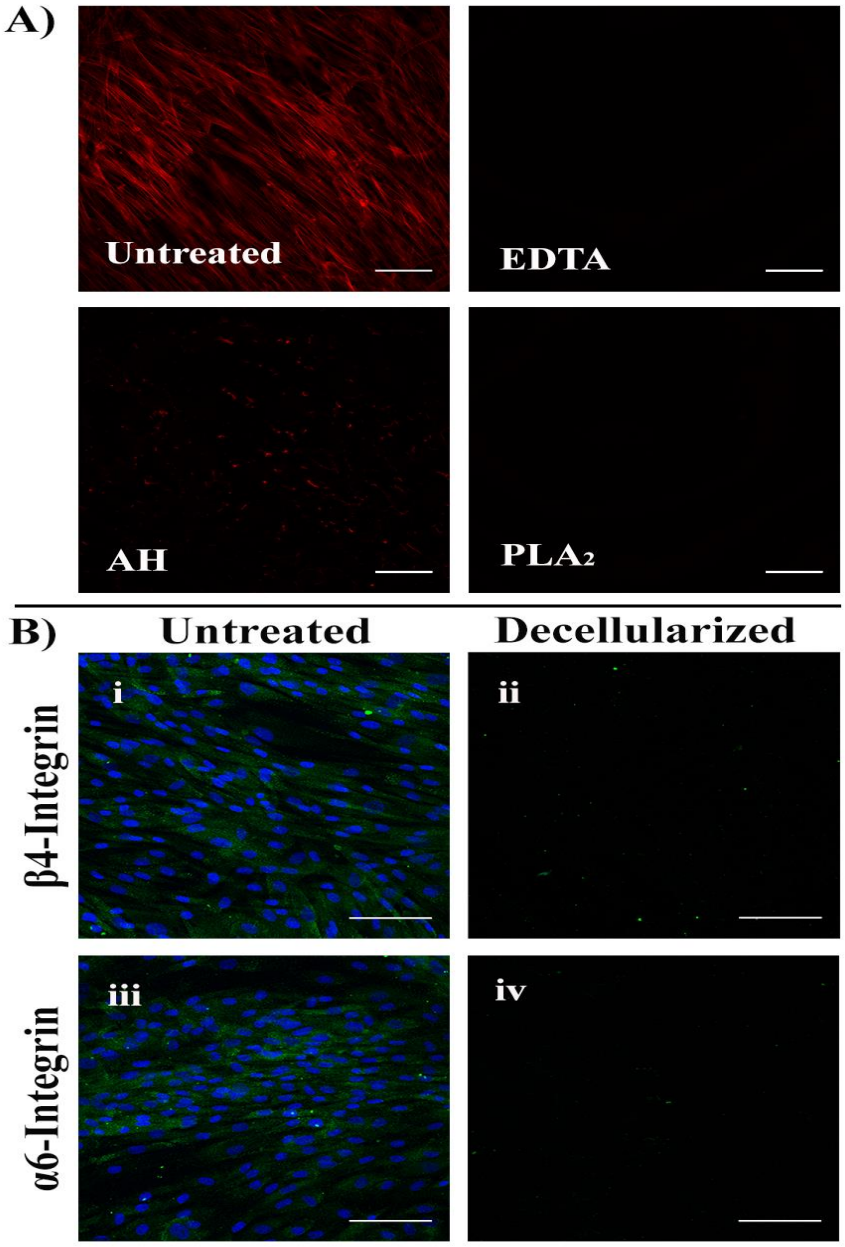

Figure 3.10: Efficacy of different decellularisation treatments for removing cell components. The aHDF cells were grown with MMC until day seven. The cell layer was decellularised using EDTA-Triton (ET), Ammonia-Triton (AT) or Phospholipase A_2 (PLA_2).

A) Phalloidin staining of decellularised ECM and untreated control aHDF monolayer for polymerised actin. This is to detect any remaining cell fragments. Scale bars are 100µm.

B) Immunofluorescence staining of PLA_2 decellularised ECM and untreated control aHDF monolayer for β4 (i, ii) & α6 (iii, iv) integrins. The secondary antibody was an anti-rat IgG Alexa Fluor® 488-conjugated antibody (Green). Nuclei were stained with DAPI (Blue). Scales bars are 100µm.

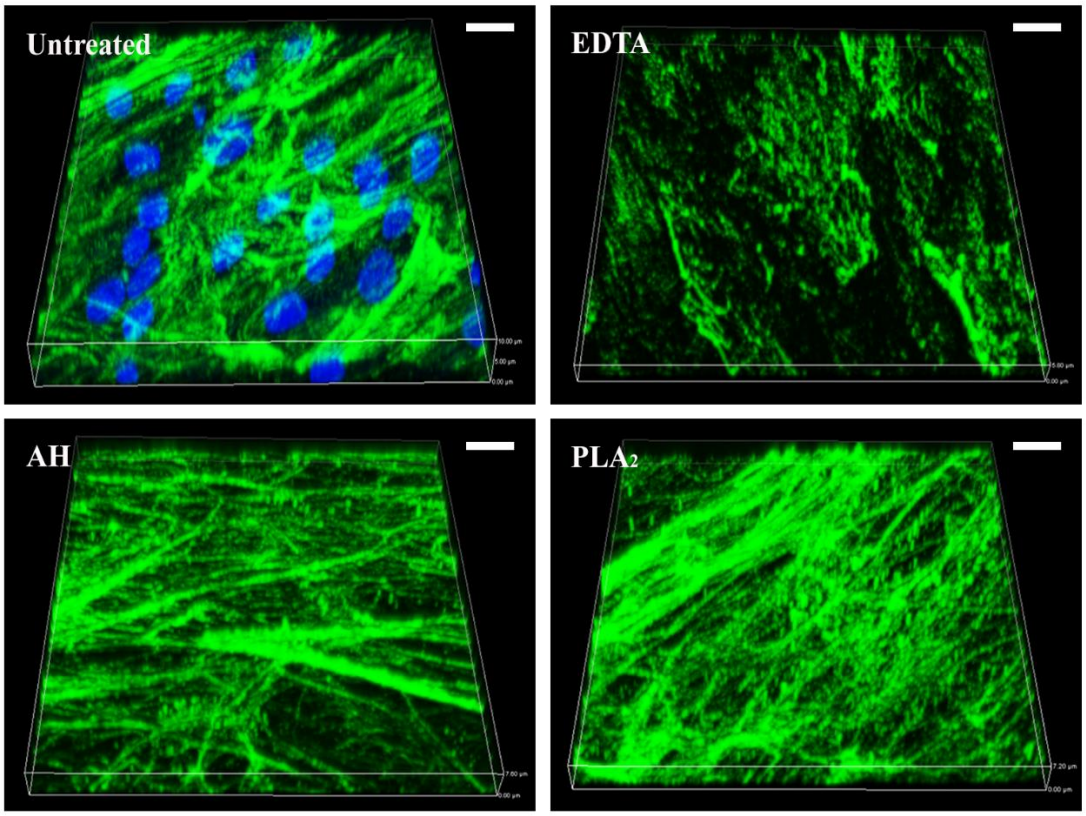

Figure 3.11: The 3D architecture of the ECM deposited by human dermal fibroblast. The aHDF cells were grown with MMC until day seven. The cell layer was decellularised using EDTA, ammonia hydroxide (AH) or phospholipase A_2 (PLA_2). The ECM was fixed with 4% paraformaldehyde and immunostained for type I collagen. 3D z-stacked confocal images were taken using Nikon A1+ Confocal Microscope. The secondary antibody was an anti-rabbit IgG Alexa Fluor® 488-conjugated antibody (Green). Nuclei were stained using DAPI (Blue). Scales bars are 10µm.

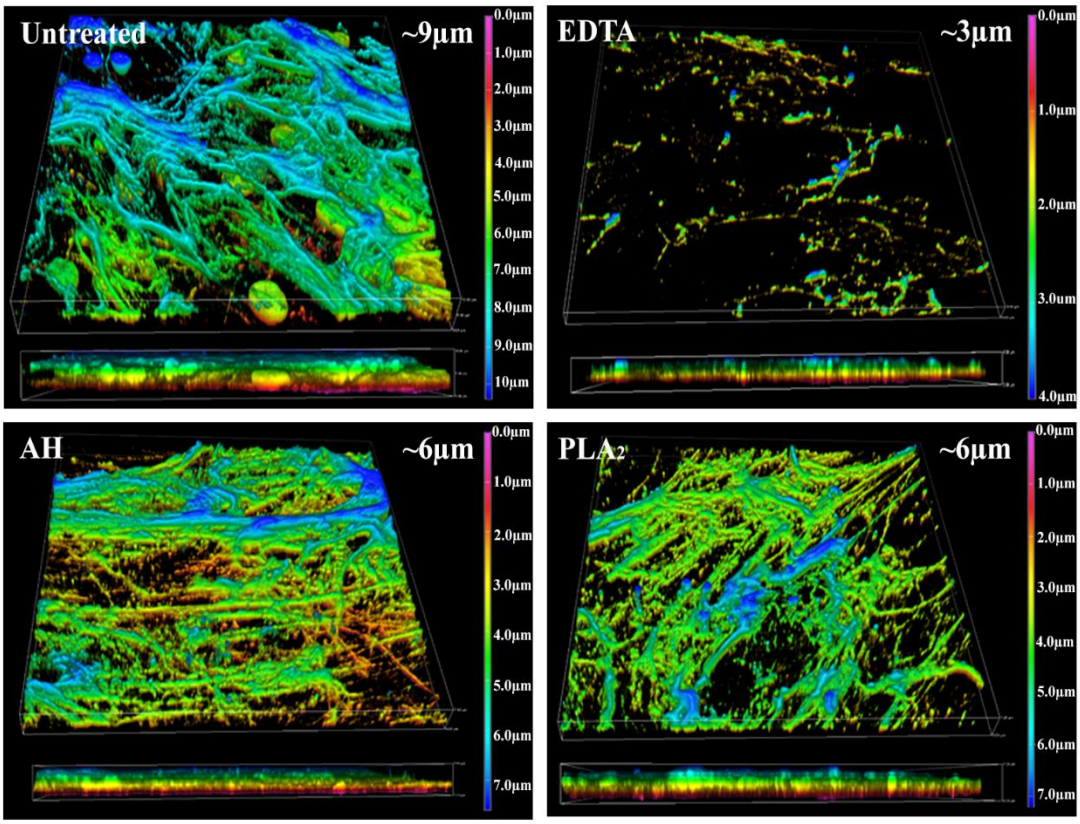

Figure 3.12: The thickness of the ECM after decellularisation. The aHDF cells were grown with MMC until day seven. The cell layers were decellularised using EDTA, ammonia hydroxide (AH) or phospholipase A_2 (PLA_2). The ECM was fixed with 4% paraformaldehyde and immunostained for type I collagen. 3D z-stacked confocal images were taken using Nikon A1+ Confocal Microscope. The colour coding represents the Z-depth location within the 3D image.

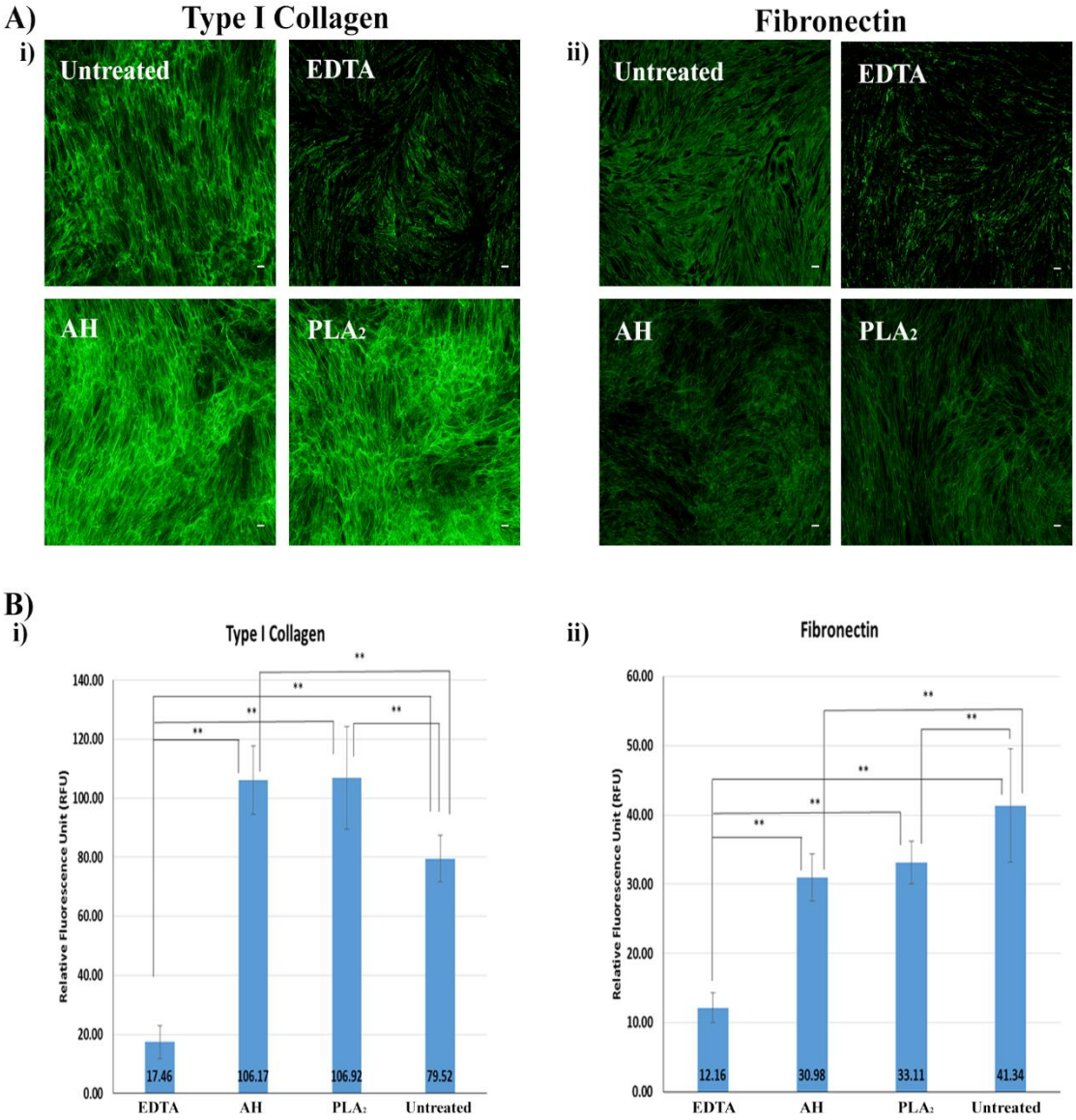

Figure 3.13: Quantification of the ECM deposition after decellularisation treatments. The aHDF cells were grown with MMC until day seven.

A) Representative images of ECM obtained using different decellularisation treatments: EDTA, ammonia hydroxide (AH) & phospholipase A_2 (PLA_2). The acellular ECM was immunostained for type I collagen or fibronectin. Scale bars are 100µm.

B) Quantification of fluorescence intensity of type I collagen (i) and fibronectin (ii) immunostaining after decellularisation. *P<0.05. Data are expressed as mean ± SD. The figure is a combination of 2 independent experiments.

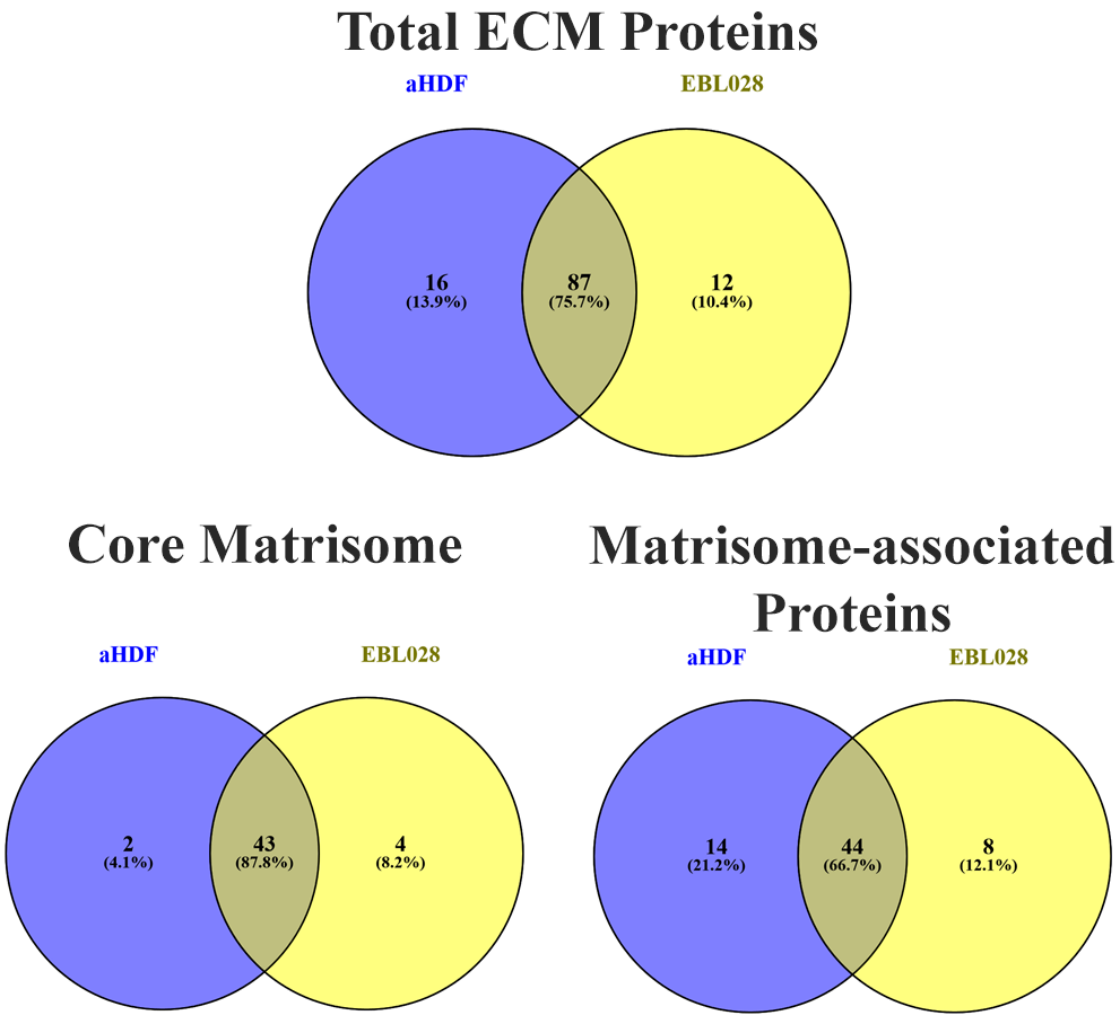

Fig 3.14: A comparison of the matrisome of aHDF and EBL028 dermal fibroblast.

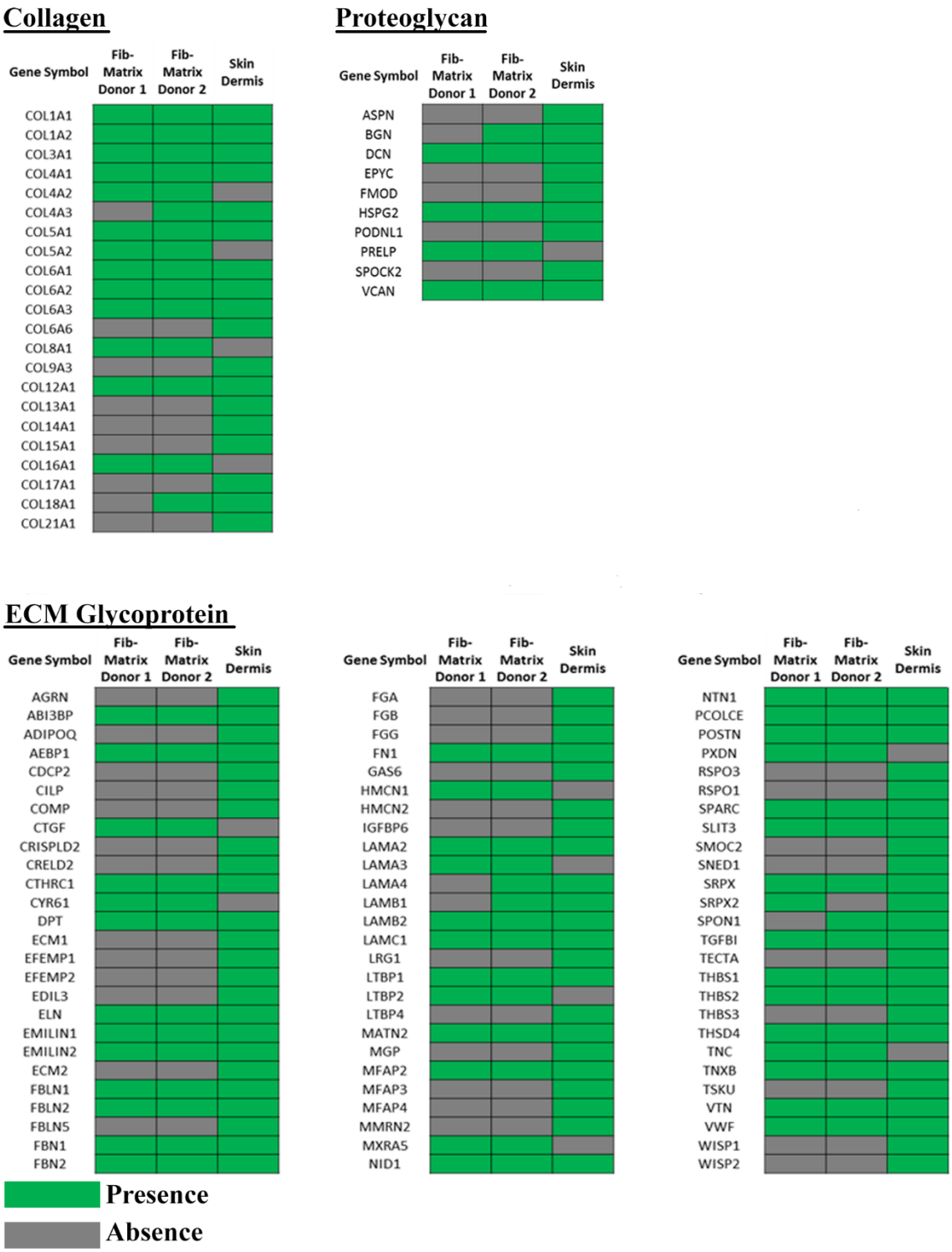

Figure 3.15: Comparison of core matrisome between fibroblast-derived extracellular matrix (Fib-Matrix) and the skin dermis. Colour code represents the presence and absence of proteins. Fib-Matrix Donor 1 is aHDF cells and Fib-Matrix Donor 2 is EBL028 cells.

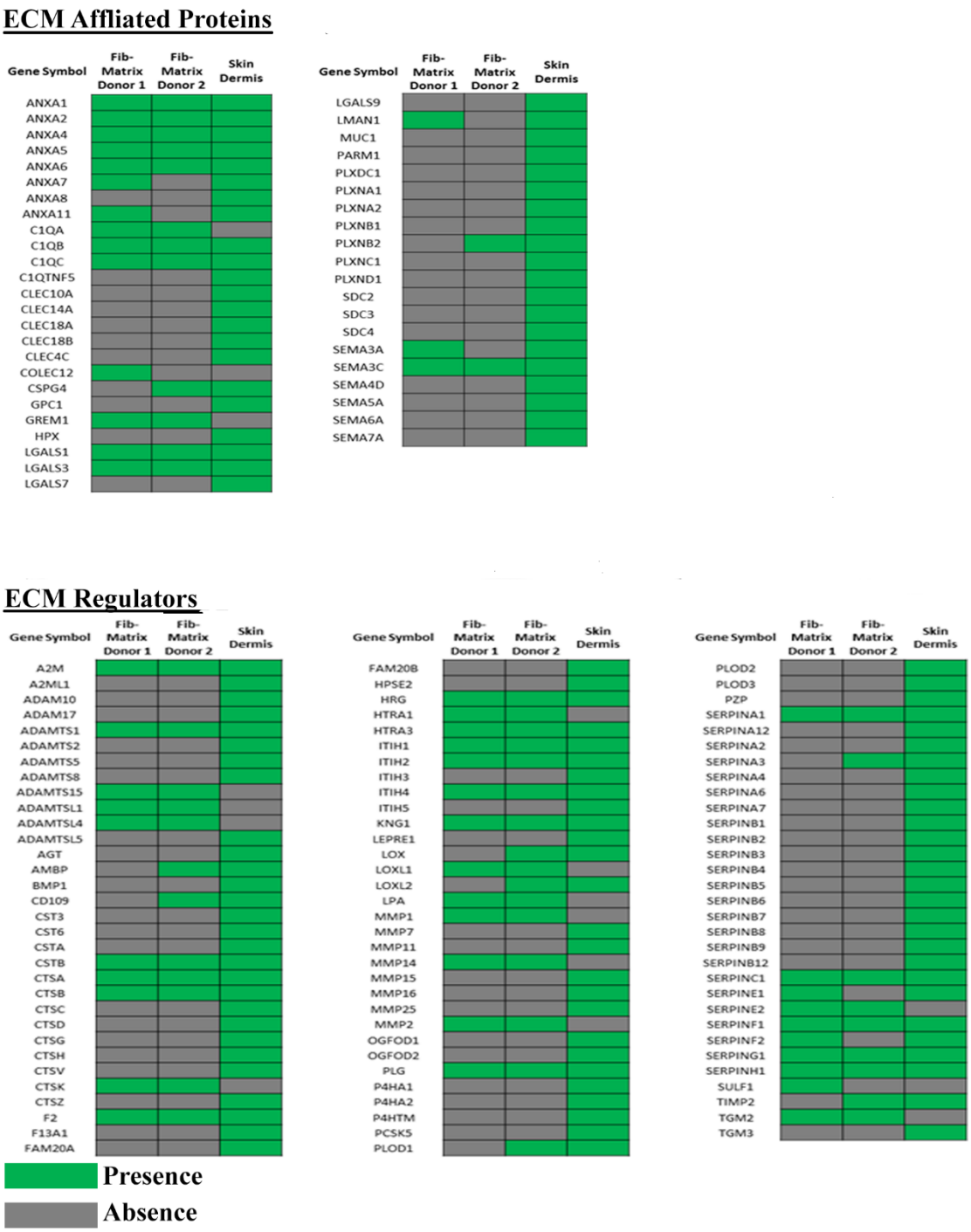

Figure 3.16: Comparison of matrisome-associated proteins between fibroblast-derived extracellular matrix (Fib-Mat) and the skin dermis. Colour code represents the presence and absence of proteins. Fib-Matrix Donor 1 is aHDF cell and Fib-Matrix Donor 2 is EBL028 cell.

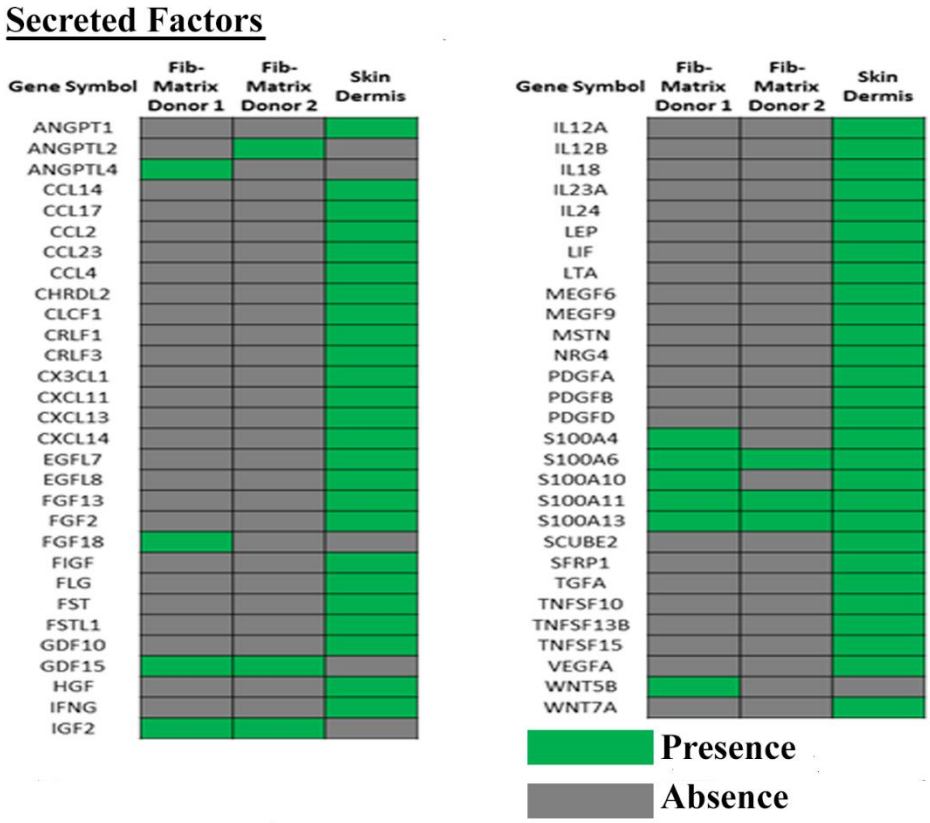

Figure 3.17: Comparison of secreted factors between fibroblast-derived extracellular matrix (Fib-Mat) and the skin dermis. Colour code represents the presence and absence of proteins. Fib-Matrix Donor 1 is aHDF cell and Fib-Matrix Donor 2 is EBL028 cell.

3.4 Discussion

This chapter describes the development of a xenogeneic-free dermal fibroblast-derived ECM. Using macromolecular crowding, a well-assembled fibroblast derived-ECM could be attained. Three decellularization methods were investigated, and of these methods, the PLA_2 method was able to achieve a fine balance between the removals of the cells and cellular components and the preservation of ECM components.

3.4.1 Characterisation of Human Dermal Fibroblasts

The use of CDM has been attracting interest for recapitulating the tissue microenvironmental niche in which stem cells reside. A major consideration in generating CDM is the cell source, as it would be the main determinant of the composition of the ECM that is produced. Typically, cells will produce matrices that will mimic the composition of the native tissue from which they were derived[155]. The goal of this present work was to generate a CDM that mimics an *in vivo* dermal microenvironment. As the main contributors to the dermal ECM are fibroblasts, we acquired primary adult dermal fibroblasts (aHDF) from the ATCC. Previous studies have shown that within the dermis, fibroblasts are heterogeneous, with subpopulations of fibroblasts producing ECM of different compositions and organisation[160]. Hence, to ensure reproducibility of the dermal fibroblast-derived ECM in our study, it was essential to investigate the phenotype of the aHDF used.

Under the normal cell culture conditions used in this study, phase contrast microscopy revealed that the aHDFs have a uniform spindle-like shaped morphology that is typical of fibroblasts. These cells also exhibited the positive staining with the fibroblast markers TE-7, Thy-1 and vimentin, which indicated that they were fibroblasts (Fig. 3.1A). However, these markers are unable to differentiate between papillary and reticular dermal fibroblasts. Until recently, the distinction between papillary and reticular dermal fibroblasts was based on their *in vitro* phenotypic differences. However, the recent global gene expression analysis by Janson *et al.*[234] revealed that up to 116 genes are differentially expressed by papillary and reticular dermal fibroblasts. Although, out of the 30 genes that they found to differentiate between papillary and reticular dermal fibroblast, only matrix GLA protein (MGP), an ECM protein, was a reliable marker for reticular dermal fibroblasts. Driskell *et al.*[166] further showed that CD26 and Dlk1 were differentially expressed by cells of the papillary and

reticular dermis respectively, indicating that different cell types are found in the papillary and reticular dermis. The ECM profile of the aHDF CDM that was generated (Fig. 3.15-3.17) was similar to the reported papillary dermis ECM[159,160]. In this matrix, the presence of type IV, XII and XVI collagen as well as versican, decorin and tenascin-c were detected, but MGP and type XIV collagen were not (Fig. 3.15). These data suggest it is very likely that our aHDFs are papillary dermal fibroblasts.

In this study, MMC was used for ECM deposition. Numerous reports had indicated no change in cell behaviour when cells were cultured with MMC[167,174,176]. However, distinct phenotypic changes in cell morphology and growth characteristics were observed when aHDFs were cultured with MMC. With MMC, at culture confluence (Day 7), our dermal fibroblasts retained contact inhibition and did not form multilayer mounds. In contrast, without MMC multilayer mounding occurred (Fig. 3.2A). There was also a decrease in cell proliferation with MMC (Fig. 3.2C).

In response to tissue injury, fibroblasts may differentiate into myofibroblasts (under the influence of TGF- β1), and so play a major role in wound healing, promoting wound closure and matrix deposition. Typically, after wound closure, myofibroblasts undergo apoptosis and disappear. However, their persistence after healing is the embodiment of active fibrosis and scaring[228,235,236]. The ECM produced by myofibroblasts differs from the original dermal ECM, in composition and organisation and myofibroblast ECM is reported not to support the proliferation and differentiation of keratinocytes to the same extent as a normal skin dermis[160,237]. Hence, the presence of myofibroblasts within our fibroblast population was undesirable, as the goal was to generate CDM for keratinocyte growth (Chapter IV). It has been reported that during culture, a percentage of fibroblast will differentiate into myofibroblast[228], but in this present study, this was not observed, and the absence of α-SMA staining suggested myofibroblasts did not develop during culture expansion. Myofibroblasts were observed however, upon the addition of TGF-β1 (Fig.3.1B) or when grown to confluence without MMC (Fig. 3.2B). Under these conditions, the cells formed prominent stress fibres that stained for α-SMA as described by others[238,239]. This did not happen when cells were cultured with MMC, suggesting that MMC suppresses myofibroblast differentiation through an unknown mechanism.

3.4.2 Macromolecular Crowding and Extracellular Matrix Deposition

Numerous reports by others have indicated that the addition of MMC enhances the deposition and the formation of a more structured ECM[169-176]. In this study, a Ficoll cocktail of MMC was used to assist the deposition of ECM by aHDF. Immunofluorescence staining suggested an increase in the deposition of ECM proteins when MMC was used, as reported by the other studies (Fig. 3.3A). However, further investigations of the aHDF ECM using different assays did not yield the same conclusion. Instead, no difference in type I collagen or more perlecan were detected by Western blotting, when aHDFs were cultured without MMC (Fig. 3.3B) rather than the reverse. Furthermore, total protein concentration quantification of acellular matrix revealed no differences in ECM deposition with or without MMC (Fig. 3.4D). Based on these data, it was possible that the difference of results from the two assays may have been due to the cells masking areas of ECM from antibody penetration and hence causing a reduced fluorescence signal. As the cell numbers were higher in cultures without MMC (Fig. 3.2C), this effect would be more pronounced. In addition, as the Western blots were performed with proteins solubilized from samples that contained both cells and ECM, the higher fibroblast number in cultures without MMC (Fig. 3.2C) may have contributed to the different results.

Results from 3D constructs of the aHDFs and their ECM using confocal microscopy to view the position of ECM in relation to the cells, seem to support the explanation of cells masking the ECM. Without MMC, a layer of type I collagen was observed to be located between the cells. In contrast, a dense layer of type I collagen was observed on top of the cells when fibroblasts were grown with MMC (Fig. 3.4). Thus the presence of the fibroblasts may have resulted in lower ECM proteins being detected by immunofluorescence in non-MMC cultures. To test if this was the case, the cells were removed by decellularisation using PLA_2 and stained for type I collagen. However, after the cells were removed, the data from immunofluorescence staining still suggested higher deposition of type I collagen when cultures were subjected to MMC (Fig. 3.5Bi). Interestingly, no differences in the deposition of fibronectin with or without MMC were detected by immunofluorescence staining (Fig. 3.5Bii). In contrast, Western blotting of the decellularised ECM samples showed a slightly higher type I collagen deposition without MMC (Fig. 3.5C).

A further explanation for differences in the results from the immunofluorescence staining and the Western blots may lie with the fact that proteins are detected in their native state when cultures are subjected to immunofluorescence staining, whereas in the blotting experiments, the 3D-structure of the matrix has been lost. This it was possible that the epitope on type I collagen that is recognised by the antibody in the immunofluorescence experiment may be more exposed with MMC culture. However, in Western blot assay, the proteins are denatured, and so any differences in protein conformation as a result of MMC are not an issue. Based on this assumption, a different antibody recognising a different epitope of type I collagen was obtained for immunofluorescence. Interestingly, using the new antibody, there was more staining of type I collagen in cultures without MMC (Fig. 3.7). As macromolecular crowding had been shown to affect collagen fibrillogenesis and so give rise to a different structural configuration of collagen fibres[231,240], it is likely this is the explanation for the current data.

Our data is consistent with that of Prewitz *et al.*[241], who also saw a higher deposition of collagen in cultures without MMC. Furthermore, they also showed no difference in fibronectin deposition between non-MMC and MMC cultures, which is similar to our observation. Most of the studies[167,172,174-176] that have reported more ECM is deposited by cells cultured with MMC have relied on assessing ECM deposition from a visual interpretation of immunofluorescence staining. This method is subjective and depends on the investigators and the antibodies used, as shown above. For example, Kumar *et al.*[174] initially reported no difference in fibronectin deposited, with or with MMC (Ficoll mixture). However, their proteomic quantification revealed a high deposition of fibronectin, when MMC (Ficoll mixture) was used. Subsequently, they validated their proteomic data through complementary fluorescence intensity data, which confirmed higher deposition of fibronectin under macromolecular crowding conditions. It is uncertain why there is discrepancy within this study. Clearly, it is not appropriate to only use immunofluorescence data derived from the staining pattern of a single antibody as evidence for differences in the amount of ECM proteins deposited with or without MMC. Our data have indicated that differences in the conformations of the deposited ECM proteins can vary with MMC and this should be considered when choosing the assay to assess the relative amount of ECM proteins deposited.

All fibrillar collagens are initially synthesised as soluble precursor molecule called procollagen. The cleavage of procollagens by BMP1/procollagen C-proteinase (PCP) to collagens is a necessary process in assembling the major fibrous components of ECM[242]. This process has been proposed to be part of the rate-limiting step in the deposition and supramolecular assembly of collagen in standard culture condition[167]. The activity of PCP was reported to be lower in standard culture, resulting in only a small amount of collagen matrix being formed, while procollagen was removed during culture media change. Using MMC, an increase of PCP activity was observed, resulting in an enhanced procollagen conversion to collagen[171,243]. Interestingly, ascorbic acid (AA) was shown to also able to augment the activity of PCP[244]. Furthermore, an increase in collagen synthesis as well was observed with the addition of AA[245,246]. Hence, if the culture system was supplemented with an optimal amount of AA, the addition of MMC may not result in an increase in collagen deposition. This was evidenced through Prewitz *et al*.[241] study, whereby they saw higher collagen deposition with MMC, only in the absence of ascorbic acid. Hence, it is likely that an optimal amount of AA has been supplement into our culture system, resulting in no further increase in collagen deposition.

3.4.3 Characterization of Decellularisation Methods to Generate Acellular Extracellular Matrix

The main goal of decellularization is to efficiently remove any cellular and nuclear components that could potentially induce an immunological response after transplantation[177,247]. However, this goal needs to be balanced with the preservation of the biological and mechanical properties of the ECM. We compared three different decellularisation methods and found that PLA_2 most efficiently removed cellular and nuclear components while preserving the ECM integrity.

Initially, whether DNA remained after decellularisation was tested by staining the ECM layer with DAPI. Both EDTA and PLA_2 methods were more efficient in removing DNA as compared to the AH method, in which distinct nuclear fragments were observed (Fig. 3.8A). Further quantification of DNA removal similarly revealed that the EDTA and PLA_2 methods were effective in removing 99% of the DNA (Fig. 3.8B). While AH method only removed up to 96% of the DNA, which is similar to other reported work[248,249]. In contrast, the efficiency of PLA_2 reported in other

studies[250,251] was lower than that shown here. However, these studies used PLA_2 to decellularize complex organ structures as opposed to a cell layer, which may be the reason for the lower efficiency.

The removal of cell components such as cell membrane associated- and intracellular proteins would help to minimise the host's immunological response to a biological scaffold[252] if the ECM was to be grafted in a clinical application. Hence, after decellularisation, the ECM was stained with phalloidin-TRITC, to detect F-actin, an intracellular cytoskeletal protein. It was observed that both the EDTA and the PLA_2 method were effective in removing F-actin. However, with the AH method, distinct F-actin fragments were still present (Fig. 3.9A). The cumulative data, therefore, suggested that PLA_2 was the best candidate to use to obtain an acellular CDM. Further investigation of PLA_2 decellularized matrices revealed a huge reduction in the cell-membrane proteins β4 & α6 integrin (Fig. 3.9B). These data indicated that the efficiency of PLA_2 in removing cellular components was consistent with what has previously been reported for the decellularization of mouse skeletal muscle[251].

As well as effectively removing cellular and nuclear components, an ideal decellularization method should have minimal impact on the ECM content and ultrastructure[247]. Both type I collagen and fibronectin are important ECM components of skin. The tensile strength of the skin is predominantly due to the type I collagen as it is the major collagen present and fibronectin has a major role in promoting cell adhesion, migration and differentiation[86]. Of the three decellularisation methods, PLA_2 and the AH method preserved both type I collagen and fibronectin and both methods also preserved the ultrastructure of type I collagen. In contrast, the EDTA method did not preserve the content of the ultrastructure of the ECM (Fig. 3.10-3.12). The ability of PLA_2 on retaining ECM integrity is also consistent with the study by Chaturvedi *et al.*[251] on mouse skeletal muscle.

Recent evidence indicates that ECMs are tissue-specific, in that the ECM from one tissue best maintains cells from the same tissue. For example, Marinkovic *et al.*[158] showed that the proliferation of bone marrow mesenchymal stem cells and adipose mesenchymal stem cells was better sustained when these cells were cultured on their own corresponding tissue-derived ECM. Similarly, Sellaro *et al.*[253] reported that ECM

derived from liver is more able to sustain the phenotype of hepatic sinusoidal endothelial cells during *in vitro* culture compared to ECM derived from urinary bladder, or from the small intestinal submucosa. To assess whether our acellular CDM generated through PLA_2, still retained ECM proteins, which were similar to those of the dermal ECM, mass spectrometry proteomic analysis was conducted. These data indicated that most of the ECM components are still present, although, some of the expected growth factors were missing. Mass spectrometry, however, has limited a capacity for detecting low abundance proteins, which may explain why many of the secreted factors were not detected. In addition, it is known that keratinocytes can regulate the gene expression of fibroblasts. For example, when cocultured with keratinocytes, fibroblasts upregulate their expression of fibromodulin (FMOD) and vascular endothelial growth factor A (VEGFA)[254]. This may explain the absence of these proteins in the mass spectrometry data obtained from aHDFs cultured alone.

The basement membrane (BM) is a highly specialised ECM that separates the epidermal and dermal compartments of the skin. Its unique composition provides both structural support and biochemical cues that influences cell behaviour. The BM is composed of four major components, type IV collagen, a laminin family member, nidogen, and perlecan[11]. The overall structure of the BM is the result of both laminin and type IV collagen self-assembling into independent networks. Nidogen and perlecan then link the laminin and type IV collagen networks by binding both proteins, increasing the stability and structural integrity of the BM[11-13]. These molecules are also shown to be crucial for the maintenance of basal keratinocyte's stem-cell-like characteristics in adults, as the anchoring of keratinocytes to the BM modulates their differentiation[16-18]. The proteomic data indicate that type I collagen, laminins, nidogen as well as perlecan are well preserved in the PLA_2 generated CDM, and so it is possible the CDM would provide an appropriate microenvironment for the growth of undifferentiated keratinocytes.

The proteomic analysis also revealed the presence of proteoglycans such as decorin, perlecan and versican in the PLA_2 generated CDM. These proteoglycans have been shown to be present within the skin dermal ECM. Perlecan has been shown to act as a co-receptor for FGF, participating in the cell signalling to promote cell proliferation[104]. Furthermore, disruption of perlecan expression in keratinocytes

resulted in the formation of a poorly organised epidermis as a result of premature apoptosis and the failure to undergo normal epidermal stratification[17]. Another proteoglycan that is present within the CDM is decorin, which interacts with type I collagen, fibronectin, TGF-β and thrombospondin. Decorin knockout mice studies revealed its role during collagen fibrillogenesis as the loss decorin resulted in abnormally large and irregular collagen fibrils. This indicates decorin to be crucial for the formation of uniform correctly sized collagen fibrils[116,117]. Decorin has also been shown to bind to TGF-β, and so inhibit its activity. Matsumoto *et al*[255] reported that TGF-β stimulation inhibited keratinocyte growth. Importantly, the inhibition of keratinocyte proliferation closely correlates with the progression of keratinocytes to terminal differentiation. Using involucrin as a keratinocyte differentiation marker, Matsumoto *et al*[255] demonstrated an increase in involucrin expression upon TGF-β stimulation, indicating an increase in keratinocyte differentiation. These data highlight the importance of TGF-β signalling in keratinocyte differentiation. Hence, it is likely that the inhibition of TGF-β activity by decorin will only modulate the growth and differentiation of keratinocytes[255]. Versican has also been observed in the generated CDM as well. Zimmermann *et al.*[113] showed that versican is located within the proliferative zone in the epidermis, suggesting a general function of versican in cell proliferation.

Collectively these studies outline the roles played by some of the ECM molecules detected in the aHDF derived ECM in the maintenance of keratinocytes proliferation. These studies also highlight the importance of the preserving these molecules in a CDM that is to be used to support keratinocyte growth.

3.5 Conclusions

The main objective of this chapter was to generate an acellular CDM that mimics the skin dermal microenvironment. This matrix was to be used in chapter IV to study keratinocyte behaviour when they were cultured on this substrate. The data presented suggest the CDM generated has characteristics that resemble the skin dermal microenvironment.

Macromolecular crowding was reported to enhance the deposition and supramolecular assembly of ECM. However, in this study, we reported a higher deposition of type I collagen when aHDFs were cultured without MMC. Nevertheless, a uniform deposition and assembly of ECM was observed with MMC.

Effective decellularisation methods should efficiently remove cellular and nuclear components while preserving the ECM integrity. Out of the three methods that were tested, PLA_2 was shown to be most effective in removing both cellular and nuclear components, while preserving the ECM components and ECM ultrastructure.

3.6 Future Direction

In this study, we determined the deposition of type I collagen through immunofluorescence staining and Western blot. However, both assays yielded opposing results. The data showed that immunofluorescence levels could be affected by changes in the morphology of the ECM upon macromolecular crowding. For this reason using a biochemical assay such as Sircol™ Collagen Assay Kit (Biocolor) to quantify the amount of collagen may be more appropriate. In addition, the ECM could also be stained with Sirius red, to visualise the total collagen.

Sulphated glycosaminoglycans (GAGs) play an important role in ECM signalling; they can directly modulate cytokine/growth factor interaction with their cell surface receptor, and they can sequester cytokines/growth factors to ECM and indirectly affect cell signalling. It has been shown by Prewitz *et al.*[241] that there is a decrease in GAGs in the ECM generated by mesenchymal stem cells when cultured with MMC. It will be useful to investigate whether there is a decrease in GAGs when our fibroblasts were cultured with MMC. To quantify the amounts of GAGs, the Blyscan™ GAGs Assay kit could be used.

3.7 Acknowledgments

I would like to thank Ms Catherine Legrand for her help in determining the protein concentration of the solubilized ECM.

Chapter IV:

Keratinocyte Growth and Behaviour on Fibroblast-Derived Extracellular Matrix

4.1 Introduction

The skin is an indispensable barrier that safeguards the body from the external environment. To sustain its effectiveness, it possesses the ability to self-renew, which enables the replacement of dead cells and wound repair[1]. In normal circumstances, most cutaneous wounds heal without medical intervention. However, if the wound is extensive and extends down into the dermis, medical attention may be required[138]. Traditionally, the therapeutic strategy in treating large deep wounds has been to use split-thickness skin autografts. However, this treatment approach is not viable in the case of extensive burn injury, as patients tend to lack any healthy donor sites[140].

Due to the limitations of skin autografts, the grafting of cultured keratinocytes is an alternative treatment to assist in the repair of damaged skin. This method uses a technique developed by Rheinwald and Green[142] to expand keratinocytes *in vitro* from a skin biopsy taken from the patient. The expansion of keratinocytes is achieved using an irradiated mouse fibroblast feeder layer and medium containing foetal bovine serum (FBS). While this method is effective in rapidly expanding keratinocytes for transplantation purposes, the reliance on xenogeneic components carries a potential risk of exposing the patients to animal pathogens and immunogenic molecules[141]. To address these concerns, *in vitro* culture systems that omit both the feeder layer and serum were developed. This system uses a defined serum-free medium that contains the necessary growth factors and a collagen matrix to support keratinocyte attachment and growth[152,153].

While this defined culture system may meet regulatory approval, its ability to propagate keratinocytes is inferior to the Rheinwald and Green system. Keratinocytes grown in the defined serum-free system have a more limited lifespan; they have a diminished self-renewal capacity and an increased commitment towards differentiation or senescence[153,154]. This suggests that the defined serum-free system does not fully meet the requirements of keratinocytes to grow these conditions without a fibroblast feeder layer. It is possible that crucial elements required to sustain the long-term maintenance of keratinocytes might reside in the fibroblast feeders used in the Rheindwald and Green system. Fibroblasts are known to secrete cytokines, growth factors and extracellular matrix (ECM). Generally, the focus for defined culture

systems has been on cytokines and growth factors synthesised by fibroblasts[255,256], but it is possible the ECM is a crucial requirement that has been overlooked.

The ECM is complex meshwork of macromolecules, comprising fibrous structure proteins (e.g. collagen, fibronectin, laminin and elastin), specialised proteins (e.g. growth factors) and proteoglycans (e.g. perlecan). It was previously thought to be an inert structure that provided a platform for cell adhesion, but it is now known that the ECM provides both biochemical and biomechanical cues that regulate cell behaviours like adhesion, migration, proliferation and differentiation[66,67]. Currently, there is considerable interest in utilising cell-derived matrices to reproduce the cells' microenvironment as it is found in tissues. Numerous studies have shown that acellular ECM assists in maintaining the stem cell phenotype and their self-renewal ability during in vitro expansion[257-260]. However, to my knowledge, no other studies have been reported on keratinocyte expansion on a dermal cell-derived matrix.

This chapter describes the functional characterization of the fibroblast-derived extracellular matrix (Fib-Mat) that was developed in Chapter 3. We hypothesised that Fib-Mat could serve as a native microenvironment to enable the growth of undifferentiated keratinocytes. Hence, in this study, the effect of Fib-Mat on regulating keratinocyte proliferation and differentiation was investigated.

4.2 Supplementary Materials & Methods

4.2.1 Antibodies

Primary antibodies used

Antigen	Clone	Species, Isotype	Antibody Working Dilution
Involucrin	Monoclonal, (SY5)	Mouse IgG1	2.5µg/ml (ICC)
K10	Monoclonal, (LH2)	Mouse IgG1	Neat
K14	Monoclonal, (LL001)	Mouse IgG2a	Neat
K16	Monoclonal, (LL025)	Mouse IgG1	Neat
Ki67	Monoclonal (MM1)	Mouse IgG1	5µg/ml (ICC)
p63	Monoclonal, (4A4)	Mouse IgG2a	2.5µg/ml (ICC)
TAp63	Polyclonal	Rabbit IgG	2µg/ml (ICC)

ICC - Immunocytochemistry

4.2.2 Microscopy

A number of different microscopes were used for the work described in this chapter:

- Phase contrast images were obtained using Zeiss Axiovert Bright Field Inverted Microscope (Zeiss, Oberkochen, Germany)

- Immunofluorescence images were captured using either a Zeiss Axioskop Upright Microscope (Zeiss, Oberkochen, Germany), an Olympus IX-51 Inverted Microscope (Olympus, Tokyo, Japan) or a Nikon A1+ Confocal Microscope (Nikon, Tokyo, Japan).

4.3 Results

4.3.1. Keratinocyte Growth on Different Substrates

The ability of Fib-Mat, type I collagen and tissue culture plastic (TCP) to support keratinocyte proliferation in our keratinocyte maintenance medium (KMM; section 2.1.2) was investigated. After three days of culture on the Fib-Mat, a homogenous population of keratinocytes presenting a small cobblestone-like morphology was observed. In contrast, when grown on either type I collagen or TCP, a proportion of keratinocytes were observed to have a large, flat cell morphology (Fig. 4.1A).

The effect of Fib-Mat, type I collagen and TCP on keratinocyte differentiation status were examined next. Keratinocytes were grown on these three different substrates in KMM for three days before being immunostained for involucrin, an early marker of keratinocyte terminal differentiation[261]. Immunofluorescence images revealed high involucrin expression, regardless of which substrate the keratinocytes were growing on (Fig. 4.1B).

4.3.2 Optimisation of Keratinocyte Maintenance Medium

We hypothesised that KMM could have caused the keratinocyte differentiation observed on all substrates (Fig 4.1B). From the literature, two components were identified within the KMM as potentially responsible for keratinocyte differentiation: serum[262,263] and the calcium concentration[263]. Table 4.1 summarises the optimisation of the KMM components.

4.3.2.1 Human Serum

To examine the effect of human serum on keratinocyte differentiation, cells were cultured on Fib-Mat for three days. They were grown in KMM with/without human serum being present. Based on involucrin staining, a reduction in keratinocyte differentiation was observed when human serum was absent from KMM (Fig. 4.2). This suggested that human serum was contributing to keratinocyte differentiation. Hence it was removed from the KMM.

4.3.2.2 Calcium Concentration

The effect of varying calcium concentrations on keratinocyte differentiation was investigated. Keratinocytes were cultured for three days on Fib-Mat in KMM containing different calcium concentrations. As observed in Figure 4.3, a reduction of involucrin expression was observed when the cells were grown in lower calcium concentrations. This suggested that calcium-induced keratinocyte differentiation in a dose-dependent manner, which is consistent with the literature[263].

4.3.2.3 Culture density

The density of keratinocyte cultures may also be a differentiation trigger factor as Poumay and Pittelkow[264] have shown it to be a strong inducer of keratinocyte terminal

differentiation. To determine if this was the case in my system, keratinocytes were plated at either low or high cell densities and grown in modified KMM for three days. To make modified KMM, the base medium of DMEM/F12 (3:1), was substituted with MCDB153, a low calcium medium that has been shown to support keratinocyte proliferation. At a low seeding density, 70-80% confluence was reached by day 3. In contrast, at higher cell seeding density, a confluence cell monolayer was achieved by day 3. A reduction in keratinocyte differentiation, as demonstrated by involucrin expression, was observed when keratinocytes were grown at a lower cell density (Fig. 4.4).

4.3.3 Keratinocyte Growth on Different Substrates in Defined-Keratinocyte Serum Free Medium

A comparison of our KMM (developed "in-house) with defined keratinocyte serum-free media (DKSFM) from Gibco showed they were very similar[255,256], although the concentrations of the individual components were not identical (Table 4.2). Nevertheless, substituting our KMM with the well accepted DKSFM (Gibco) seemed appropriate, and so all further keratinocyte cultures were done in DKFSM.

4.3.3.1 Proliferation of Keratinocytes on Different Substrates

Using DKSFM, the ability of Fib-Mat, type I collagen and TCP to support the adhesion and proliferation of keratinocytes were investigated. Keratinocytes were observed to adhere well to both Fib-Mat and type I collagen but poorly on TCP. While keratinocytes proliferated on all three substrates, their behaviour differed on each substrate. On Fib-Mat, keratinocytes grew as colonies with distinct boundaries, and cells within the colonies had a small cobblestone morphology, which persisted until day 6 whereupon the cells reached a near confluent monolayer. Whilst a similar behaviour was also observed on TCP, keratinocytes appeared to consist of a heterogeneous population of cells with differing cell sizes. In contrast, keratinocytes on type I collagen seemed to grow as single cells and comprised of a mixed population of differing cell sizes. Also, on type I collagen cell confluence was reached at day 4 as opposed to day 6 on Fib-Mat and TCP (Fig. 4.5).

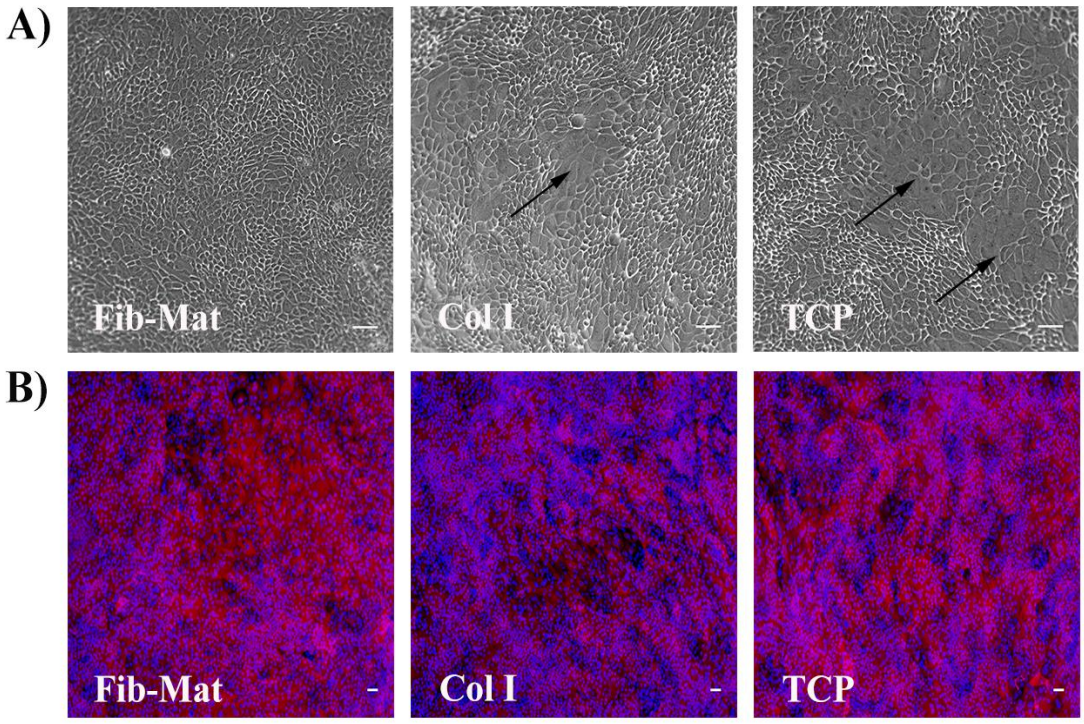

Figure 4.1: Keratinocytes growing on different substrates in keratinocyte maintenance media

A) Cell morphology of keratinocytes cultured on the Fib-Mat, type I collagen (Col I), and TCP for three days in KMM as seen by phase contrast microscopy. Scale bars are 100µm. Arrows indicate areas of increased keratinocyte cell size.

B) Keratinocyte differentiation status. Keratinocytes were grown on Fib-Mat, Col I and TCP for 3 days in KMM. Keratinocytes were fixed with cold acetone: methanol (1:1) and stained with an anti-involucrin mAb (Clone: SY5). The secondary antibody was an anti-mouse IgG_1 Alexa Fluor® 546-conjugated antibody (Red). Nuclei were stained with DAPI (Blue). Scales bars are 100µm.

Table 4.1: Optimisation of keratinocyte maintenance medium. Red indicates the component investigated for optimisation. Green indicates changes made resulting from prior optimisation.

	Fig. 4.1	Fig. 4.2	Fig. 4.3	Fig. 4.4
Components	Final Concentration			
DMEM:F12 (3:1) Base Media	✓	✓	✓	-
MCDB 153 Base Media	-	-	-	✓
Human Serum	2%	+/- 2%	×	×
L-Glutamine	2mM	2mM	2mM	2mM
HEPES	10mM	10mM	10mM	10mM
Sodium Pyruvate	1mM	1mM	1mM	1mM
Calcium Chloride	1.42 mM	1.42 mM	*	0.2mM
Adenine	25ng/ml	25ng/ml	25ng/ml	25ng/ml
Hydrocortisone	400ng/ml	400ng/ml	400ng/ml	400ng/ml
Insulin	0.12 IU/ml	0.12 IU/ml	0.12 IU/ml	0.12 IU/ml
Forskolin	5µM	5µM	5µM	5µM
Keratinocyte Growth Factor (KGF)	5ng/ml	5ng/ml	5ng/ml	5ng/ml
Epidermal Growth Factor (EGF)	10ng/ml	10ng/ml	10ng/ml	10ng/ml
Transferin	5ng/ml	5ng/ml	5ng/ml	5ng/ml
Triiodothyronine	200nM	200nM	200nM	200nM
Monothioglycerol	0.1mM	0.1mM	0.1mM	0.1mM
Ascorbic acid	30µg/ml	30µg/ml	30µg/ml	30µg/ml

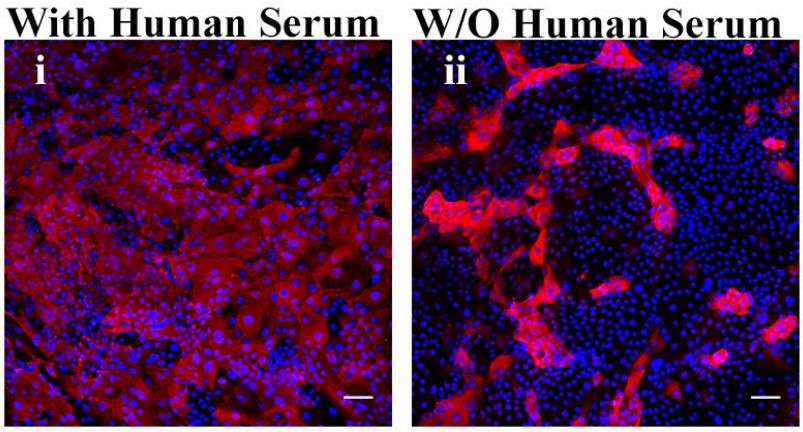

Figure 4.2: The effect of human serum on keratinocyte differentiation.
Keratinocytes were grown on Fib-Mat for 3 days in KMM with or without 2% human serum. Keratinocytes were fixed with cold acetone: methanol (1:1) and stained for involucrin as described in Figure 4.1. Nuclei were stained with DAPI (Blue). Scales bars are 100µm.

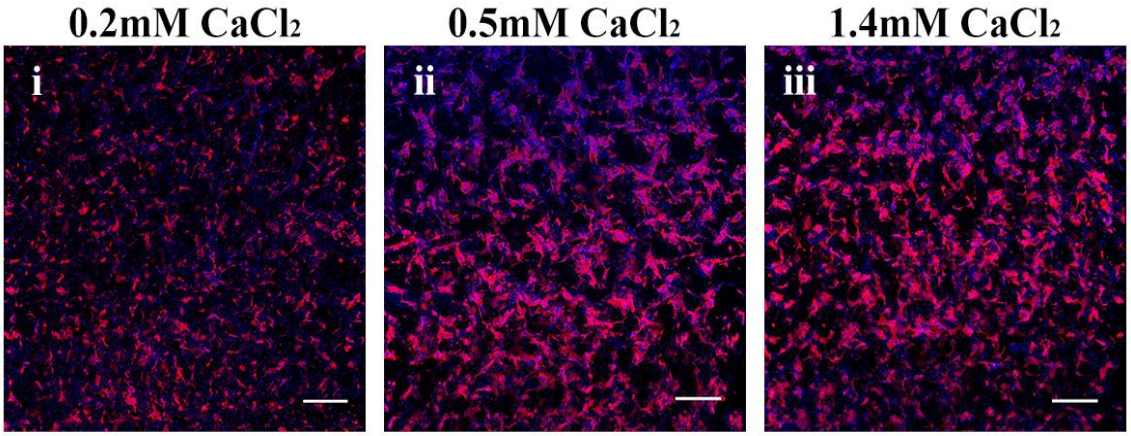

Figure 4.3: The effect of different calcium concentrations on keratinocyte differentiation.
Keratinocytes were grown on Fib-Mat for 3 days in KMM containing 0.2µM (i), 0.5µM (ii) and 1.4µM (iii) calcium chloride. Keratinocytes were fixed with cold acetone: methanol (1:1) and stained for involucrin as described in Figure 4.1. A total of 36 images were taken with 6 x 6 grid pattern and stitched together using Nikon A1+ Inverted Confocal Microscope. Nuclei were stained with DAPI (Blue). Scales bars are 1000µm.

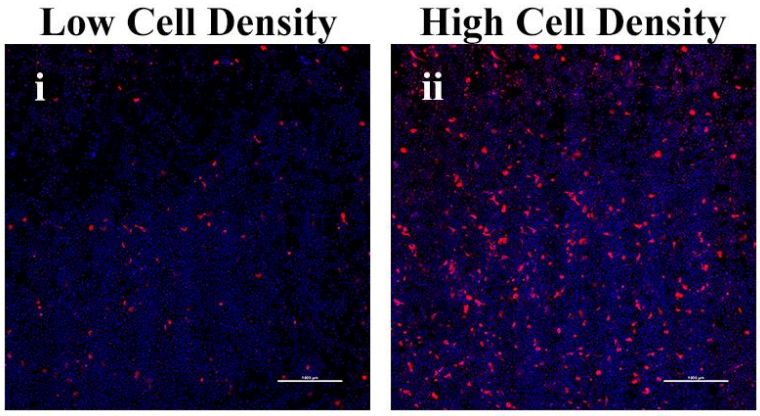

Figure 4.4: The effect of cell density on keratinocyte differentiation.
Keratinocytes at low (7.5 x 10^3 cell/cm^2) and high (15 x 10^3 cell/cm^2) seeding densities were grown on the Fib-Mat for 3 days in KMM. Keratinocytes were fixed with cold acetone: methanol (1:1) and stained for involucrin as described in Figure 4.1. A total of 36 images were taken with 4 x 4 of grid pattern and stitched together using Nikon A1+ Inverted Confocal Microscope. Nuclei were stained with DAPI (Blue). Scale bars are 1000µm.

Table 4.2: Comparison of keratinocyte maintenance medium (KMM) and defined keratinocyte serum-free medium (DKSFM) composition.

	KMM	DKSFM
COMPONENTS	**Final Concentration**	
MCDB 153 BASE MEDIA	✓	✓
L-GLUTAMINE	2mM	7mM
HEPES	10mM	14mM
SODIUM PYRUVATE	1mM	0.5mM
CALCIUM CHLORIDE	0.2mM	0.1 mM
ADENINE	25ng/ml	24ng/ml
HYDROCORTISONE	400ng/ml	500ng/ml
INSULIN	0.12 IU/ml	0.14 IU/ml
FORSKOLIN	5µM	5µM
KERATINOCYTE GROWTH FACTOR (KGF)	5ng/ml	10ng/ml
EPIDERMAL GROWTH FACTOR (EGF)	10ng/ml	10ng/ml
TRANSFERIN	5ng/ml	11ng/ml
TRIIODOTHYRONINE	200nM	10µM
MONOTHIOGLYCEROL	0.1mM	-
ASCORBIC ACID	30µg/ml	100µg/ml
ETHANOLAMINE	-	0.1mM
PHOSPHOETHANOLAMINE	-	0.1mM

To determine the ability of the different substrates to support cell adhesion, the percent of keratinocytes that adhered was determined. Keratinocytes were seeded onto either Fib-Mat, type I collagen or TCP and incubated for 1 hour at 37°C before being washed with PBS to remove non-adherent cells. The percentage of adhering cells was calculated using the CyQuant assay (Section 2.5.2). A statistically significant difference in keratinocyte adhesion was observed across all three substrates ($p<0.01$). A higher proportion of keratinocytes was found attached to Fib-Mat (84%), than to type I collagen (77%) or TCP (56%; Fig. 4.6). This was consistent with the observation of the cultures by phase contrast microscopy (Fig. 4.5).

Next, the potential of the different substrates for supporting keratinocyte proliferation was examined. The CyQuant assay was used to measure cell number. This assay uses a dye that fluoresces after binding to nucleic acid and so can be used in association with the standard curve to determine cell number. However, initial attempts to generate a keratinocyte growth curve were unsuccessful. The data obtained were very variable resulting in high standard deviations (data not shown). To resolve this issue, the total number of cell nuclei were determined. Keratinocytes were seeded at low density (1×10^4 cells) on the different substrates and grown for 6 days in DKSFM. The cells were fixed before being stained with DAPI, and the total number of nuclei determined. Interestingly, keratinocytes were found to proliferate at a different rate on Fib-Mat, type I collagen or TCP. On Fib-Mat, keratinocytes initially proliferated more slowly than keratinocytes on type I collagen but reached a similar cell number by day 3. Thereafter, an exponential rate of proliferation was observed on Fib-Mat, which was higher than that which occurred on type I collagen. On TCP, keratinocytes proliferated the slowest and the rate plateaued by day 4 (Fig. 4.7). While the cell numbers differed, the shape of the growth curves of type I collagen and TCP were similar.

From the growth curve data (Fig. 4.7), it appeared that Fib-Mat best-promoted keratinocyte proliferation. To test this hypothesis, the expression of Ki67, a marker for proliferation was examined (Section 2.5.3). Keratinocyte expression of Ki67 was determined on day 3, as the growth curve (Fig. 4.7) indicated a change in proliferation behaviour on each of the substrates at this point. As displayed in Figure 4.8A, higher Ki67 expression was observed on Fib-Mat, as compared to type I collagen and TCP. Further quantification of Ki67 expressing cells confirmed this observation. A

significantly higher number of keratinocytes expressed Ki67 ($p<0.01$) when they were cultured on Fib-Mat (Fig. 4.8B). A similar trend was also observed when the numbers of Ki67 expressing cells were determined on day 4 and 5 (data not shown).

4.3.3.2 Characterisation of Keratinocyte Differentiation Status on Different Substrates

To determine the keratinocyte differentiation status on each substrate, cultures were stained with markers such as cytokeratin 14 (K14), cytokeratin 10 (K10) and involucrin. K14 is a marker of basal keratinocytes, while K10 and involucrin are early markers of terminal differentiation. To acquire better image resolution at high magnification, etched glass coverslips (EGC) were used. However, to check if a change in the growth surface affected keratinocyte behaviour, keratinocytes were grown on either TCP or EGC, which were coated with either Fib-Mat, type I collagen or were uncoated. Cells were grown for 3 days in DKSFM before being fixed and stained for K14. As can be seen in Figure 4.9, keratinocytes grown on all surfaces were positive for K14. No marked differences were observed between the cells on these surfaces except the comparison of TCP and EGC coated with type I collagen. On EGC coated with type I collagen, keratinocytes grew as colonies. Whereas, keratinocytes grew as single cells on TCP coated with type I collagen. As this appeared to be only a minor behavioural change, staining of K14, K10 and involucrin were done on EGC coated with either Fib-Mat, type I collagen or left uncoated. The expression of K14 was observed in keratinocytes on all three substrates, indicating the presence of basal keratinocytes. However, a small population of keratinocytes on uncoated EGC appeared to have lost K14 expression (Fig. 4.10). A higher proportion of keratinocytes grown on type I collagen and TCP compared to keratinocytes grown on Fib-Mat were observed to express keratin 16 (K16;Fig. 4.10), an indicator of physiological and cellular stress[265,266]. While the expression of K10 was not observed in keratinocytes on any substrate, involucrin expression was detected in cells on all substrates. However, a higher proportion of keratinocytes were positive for involucrin when grown on uncoated EGC, as compared to keratinocytes on Fib-Mat or type I collagen (Fig. 4.10).

4.3.3.3 The p63 Expression in Keratinocytes Grown on Different Substrates

The p63 protein has been described as a potential marker for keratinocyte stem cells[267]. Accordingly, keratinocytes on each of the substrates were examined for p63 expression. Keratinocytes were grown on Fib-Mat, type I collagen and TCP for 3 days in DKSFM before being immunostained with an antibody recognising p63. As seen in Figure 4.11A, while p63 expression was detected in keratinocytes on all three substrates, the number of cells expressing p63 differed. Quantification of the number of p63 expressing cells (Section 2.5.4) showed a significantly ($p<0.01$) higher number of p63 positive cells on Fib-Mat and type I collagen when compared to TCP. It was interesting that the percentage of p63 positive cells was similar on both Fib-Mat and type I collagen substrate (Fig. 4.11B).

Current reports indicate that p63 exists in two different isoforms, which are ΔNp63 and TAp63. Studies by Koh *et al.* [35] suggest that the expression of TAp63 is critical for activating late keratinocyte differentiation genes. To investigate the proportion of cells that were positive for TAp63, keratinocytes were immunostained with the polyclonal antibody that is specific for this isoform. Interestingly no TAp63 was detected in any of the keratinocytes, regardless of the substrates on which they were growing (Fig. 4.12).

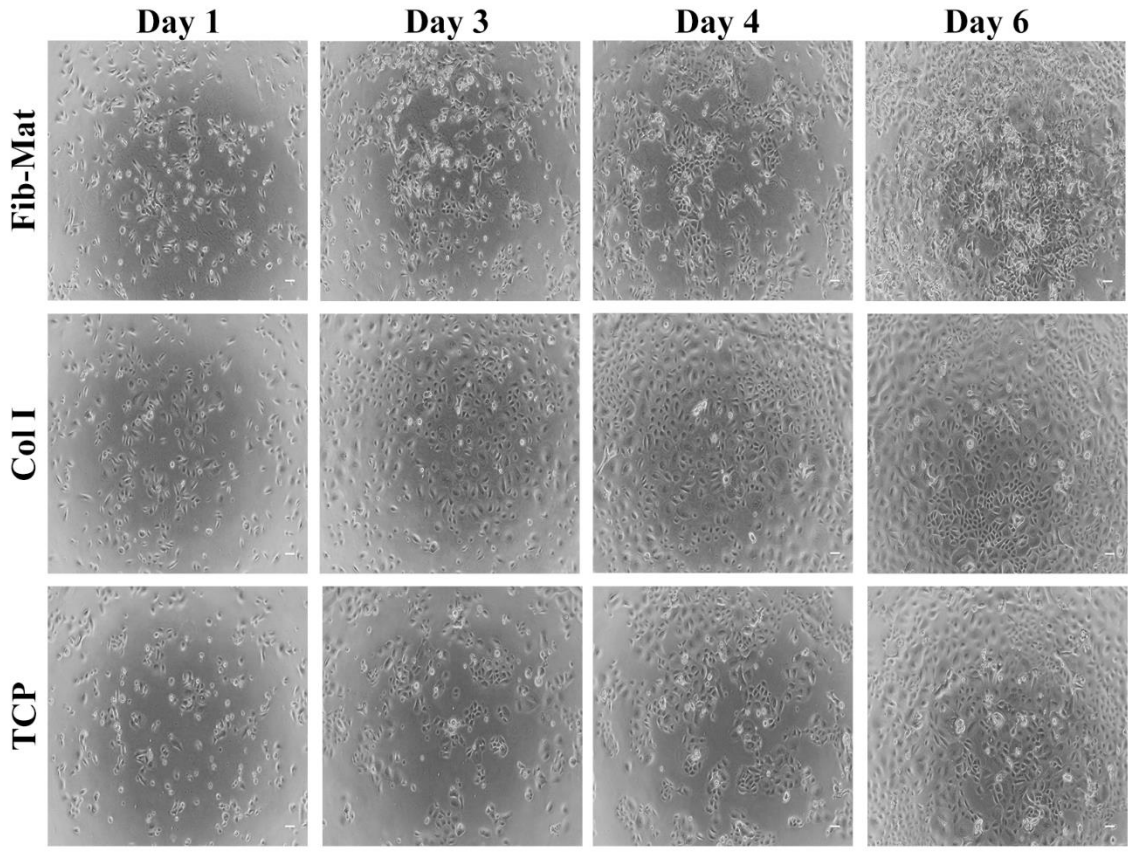

Figure 4.5: Cell morphology of keratinocytes growing on different substrates in DFSM as captured by phase contrast microscopy.
Keratinocytes (2 x 10^4 cells) were seeded into wells of a 24-well plate that either contained fibroblast-derived matrix (Fib-Mat), type I collagen coating (Col I; 3ug/cm^2) or uncoated TCP and cultured for 6 days in DKSFM. Scale bars are 100µm.

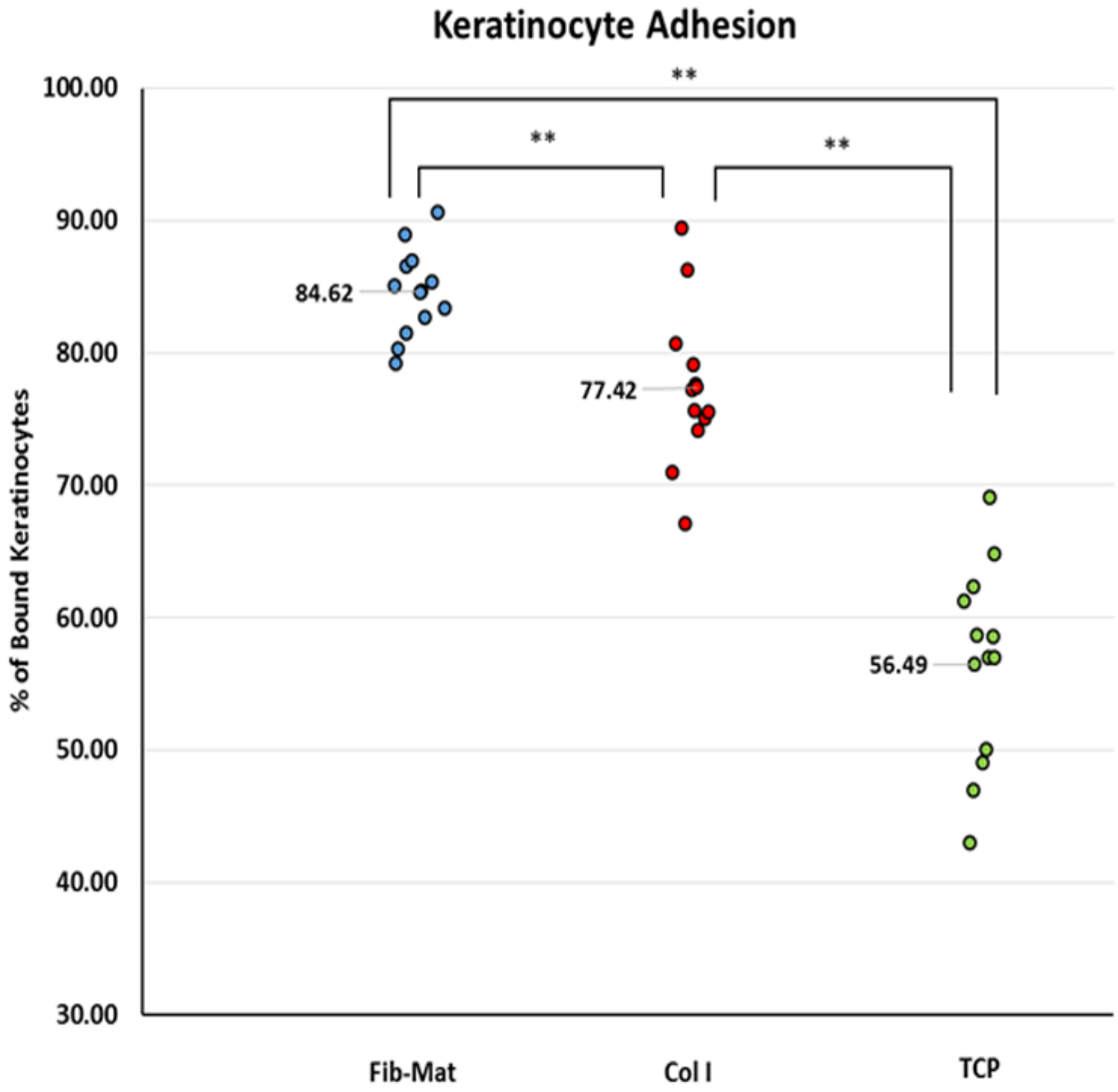

Figure 4.6: The ability of different substrates to support keratinocyte adhesion. Keratinocytes (1 x 10^4 cells) were seeded into wells of a 24-well plate that either contained Fib-Mat, type I collagen coating (Col I; 3ug/cm^2) or uncoated TCP. Keratinocytes adhered for one hour at 37°C in adhesion buffer and cell adhesion was determined using the CyQuant assay and represented as a percentage of the total cells seeded. The value shown is the mean percentage of bound keratinocytes. Shown are pooled data from three separate experiments. Statistical analysis using ANOVA followed by Tukey's test was conducted. **$p<0.01$

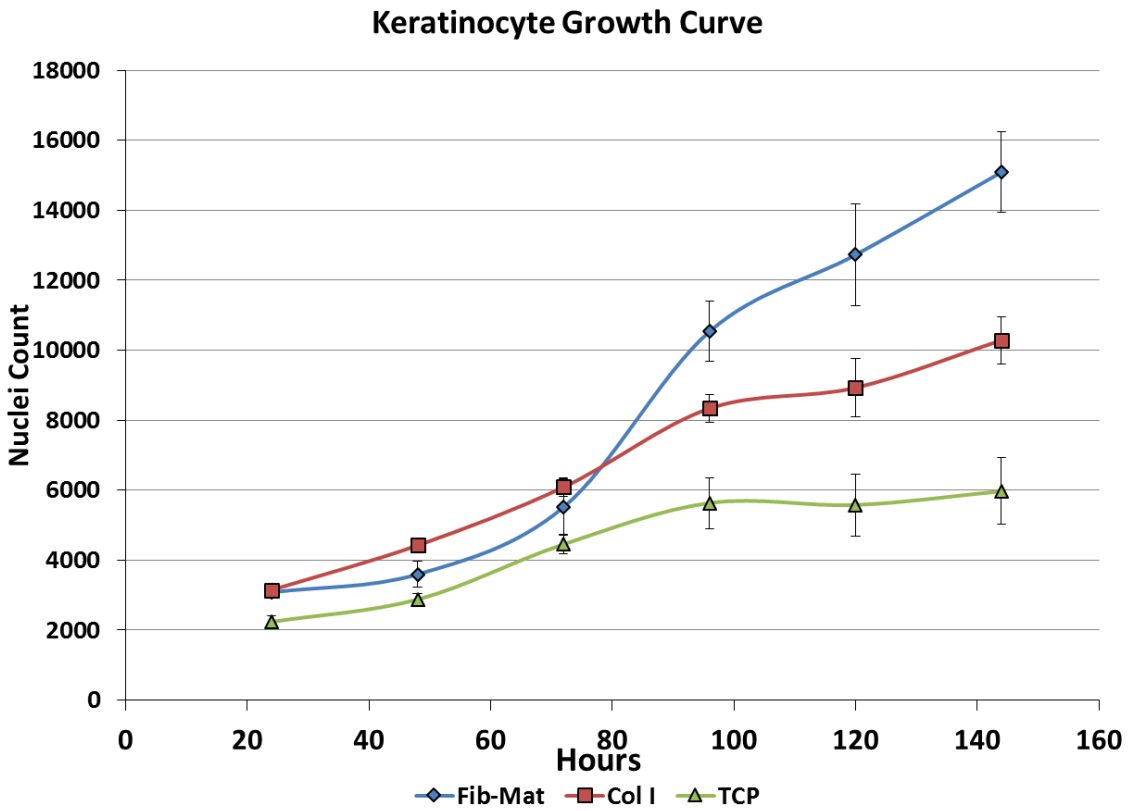

Figure 4.7: Growth curve of keratinocytes growing on different substrates
Keratinocytes (1 x 10^4 cells) were seeded into wells of a 48-well plate that either contained fibroblast-derived matrix (Fib-Mat), type I collagen coating (Col I; 3ug/cm^2) or uncoated TCP and cultured for 6 days in DKSFM. At 24-hour intervals, keratinocytes were fixed with cold acetone: methanol (1:1), stained with DAPI and total nuclei were counted. The data shown are the mean ± standard deviation obtained from 4 replicate wells. A representative of three separate experiments is shown.

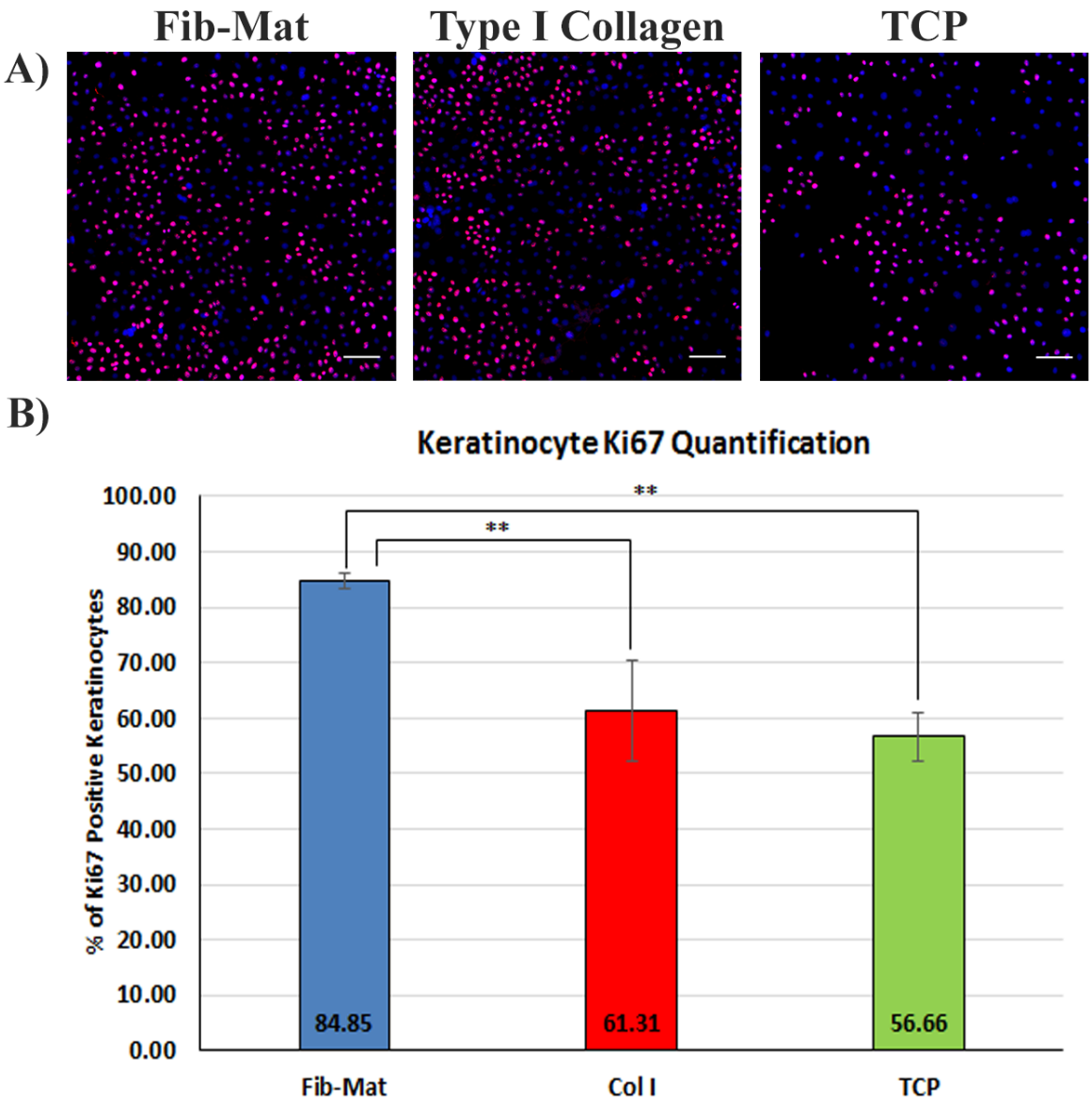

Figure 4.8: Quantification of Ki67 staining in keratinocytes grown on different substrates.

Keratinocytes (1 x 10^4 cells) were seeded into wells of a 48-well plate that either contained fibroblast-derived matrix (Fib-Mat), type I collagen coating (Col I; 3ug/cm^2) or plain tissue culture plastic (TCP) and cultured for **3 days** in DKSM. Keratinocytes were fixed with cold acetone: methanol (1:1) then stained for Ki67, a biomarker of actively-dividing cells. Nuclei were stained with DAPI (Blue).

A) A representative image of keratinocytes immunostained for Ki67. Scale bars are 100µm.

B) Quantification of keratinocytes positive for Ki67 expression. The data shown are the mean percent of Ki67 positive keratinocytes ± standard deviation. The data shown is a representative of three separate experiments. Statistical analysis using ANOVA followed by Tukey's test was conducted. **$p<0.01$

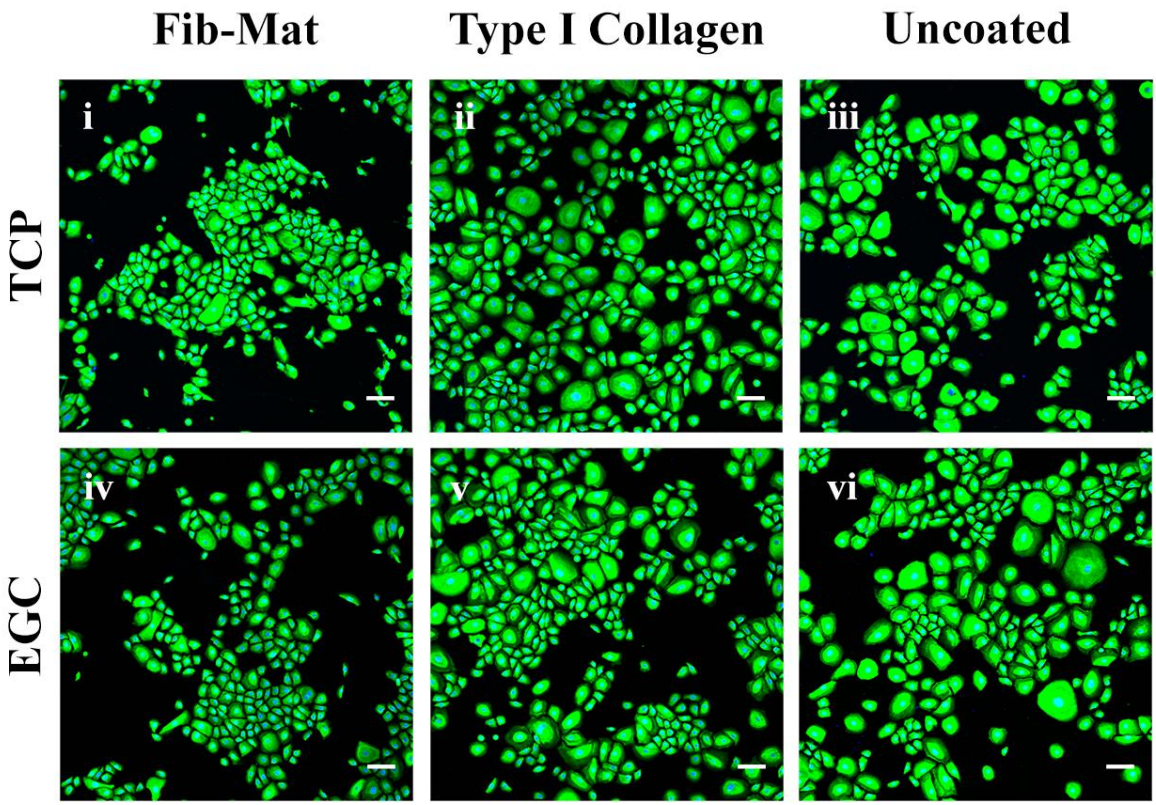

Figure 4.9: Comparison of tissue culture plastic (TCP) and etched glass coverslips (EGC) as a platform for keratinocyte growth.
Keratinocytes ($2x10^4$ cells) were seeded into wells of a 24-well plate that either contained TCP (i-iii) or EGC (iv-vi). The EGC or TCP was coated with either fibroblast-derived matrix (Fib-Mat; i,iv), type I collagen ($3ug/cm^2$; ii,iv) or were uncoated (plain; iii, vi). Keratinocytes were cultured for 3 days in DKSFM then fixed with cold acetone: methanol (1:1) and stained for cytokeratin 14 (K14). The secondary antibody was an anti-mouse IgG Alexa Fluor® 488-conjugated antibody (Green). Nuclei were stained with DAPI (Blue). Scales bars are 100µm.

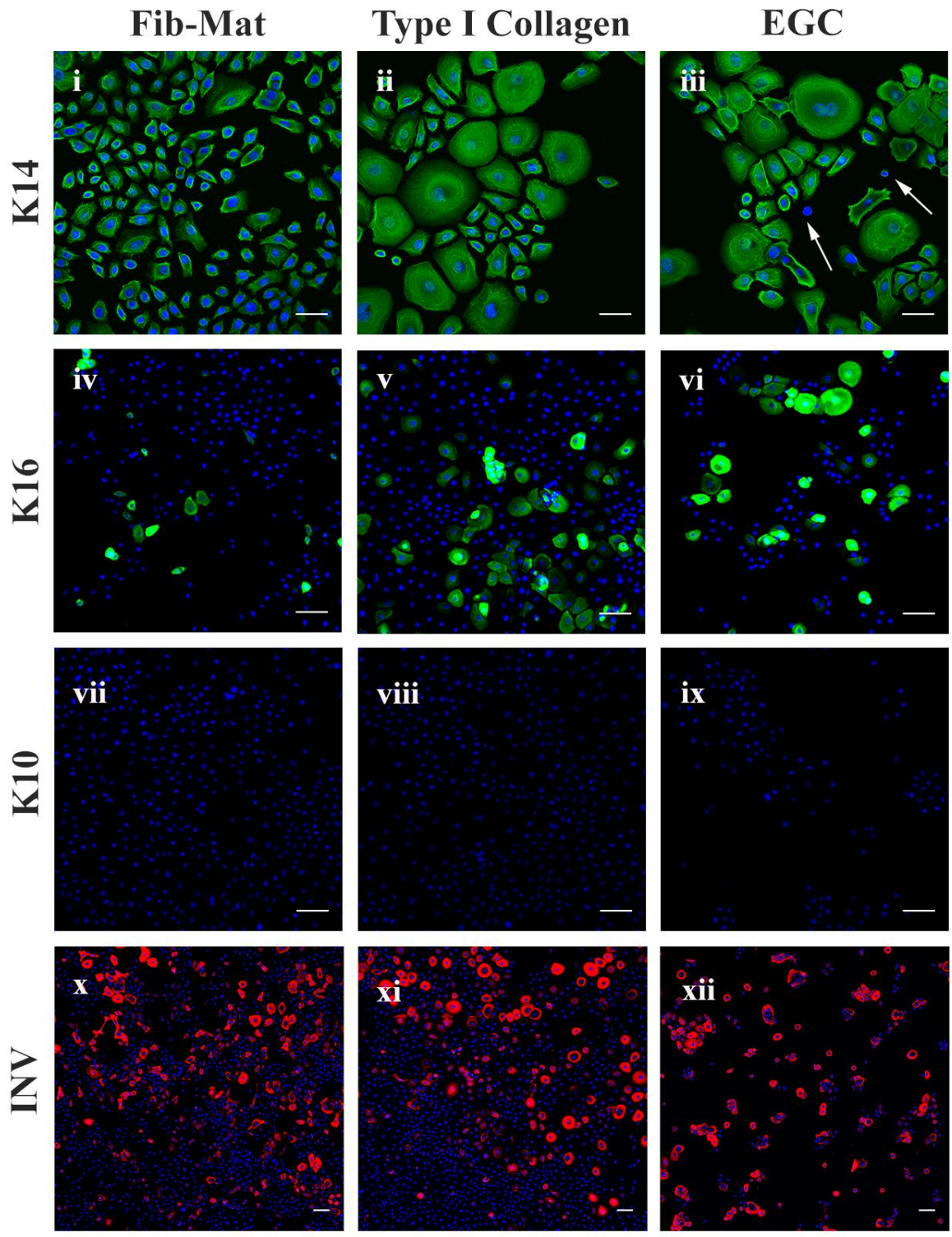

Figure 4.10: The expression of K10, K14, K16 and involucrin on keratinocytes grown on fibroblast-derived ECM (Fib-Mat), type I collagen and etched glass coverslips (ECG). Keratinocytes ($2x10^4$ cells) were cultured for 3 days in DKSFM on different substrates. Keratinocytes were fixed with cold acetone: methanol (1:1) and stained with antibodies recognising cytokeratin 14 (K14; i-iii), cytokeratin 16 (K16; iv-vi) cytokeratin 10 (K10; vii-ix) or involucrin (INV; x-xii). Nuclei were stained using DAPI (Blue). Scales bars are 50µm for K14 and 100µm for K10, K16 and involucrin. Arrows indicate keratinocytes with no K14 expression.

4.3.3.4 Keratinocyte Cell Size on Different Substrates

Keratinocytes grown on Fib-Mat were observed to have a small cell size as compared to cells cultured on type I collagen and TCP (Fig. 4.13A). To determine and quantify keratinocyte cell size, an assay was established based on the Haase *et al.* [268] study that determined the cell size by the area that was covered by the cell (Section 2.5.2). Keratinocytes were grown on Fib-Mat, type I collagen and TCP for 3 days in DKSFM before being fixed and stained for polymerised actin using phalloidin-Alexa Fluor® 488 (Fig. 4.13B). Using the Olympus IX-81 high content screening inverted microscope, 64 non-overlapping images were taken. Cell Profiler® software was used to determine the cell size based on cell area. A threshold of approximately 4000 individual keratinocytes were analysed from each substrate, as it was the minimum number of cells measured in TCP. Cell size was determined and categorised into small, medium and large. The measurement of cell area for each category is as follow: small<medium<large = $<2000\mu m^2<4000\mu m^2<6000\mu m^2$. Analysis of the size of individual keratinocytes revealed a statistically significant difference ($p \leq 0.05$) in cell size between cells grown on Fib-Mat or type I collagen. The majority of keratinocytes residing on Fib-Mat were of a smaller cell size. This was not the case for cells on type I collagen. Indeed, the large flat keratinocytes were most common on type I collagen (Fig. 4.13C). While there were differences in cell size between cells on Fib-Mat and TCP, the differences were not statistically significant.

4.3.3.5 Movement of Keratinocytes on Different Substrates

To observe how keratinocytes moved on each substrate, a time-lapse microscopy system was used. Cells were seeded onto Fib-Mat, type I collagen or TCP and left overnight to adhere before time-lapse images over 2 days were taken at 15-minute intervals. Distinct keratinocyte colonies were only seen when cells were on TCP. Instead, pseudo-colonies were observed for cells on Fib-Mat and type I collagen, where the keratinocytes would migrate collectively, before dispersing or combining with other colonies. The majority of keratinocytes grown Fib-Mat were highly motile over the 2 day period. A similar cell behaviour was observed for cells on type I collagen, however, as time progressed, a proportion of the keratinocytes became less motile, and reduced motility was accompanied by an increase in cell size. Keratinocytes on TCP were the least motile, and an increase in cell size was also observed as time progressed (Links to videos are in the Appendix B).

Cell motility is highly linked to the organisation of the actin cytoskeleton. To examine the arrangement of filamentous actin (F-actin) in the keratinocytes, the cells were grown on Fib-Mat, type I collagen or EGC for 3 days before being stained with phalloidin-Alexa Fluor® 488. On type I collagen and EGC, well-developed actin stress fibres were observed at the keratinocyte circumference. This was more prominent with keratinocytes that were of a larger size. In contrast, on Fib-Mat, pronounced stress fibres at the keratinocyte circumference were less visible (Fig. 4.14).

4.4 Discussion

The regenerative ability of keratinocyte stem cells has been well described in numerous studies[269-273]. However, the potential of *in vitro* expanded keratinocytes has been limited by the current culture system. This is because it does not meet the regulatory standards of being xenogeneic free, as murine feeders and FBS are used. Another system has been used to expand keratinocytes; this system uses a defined serum-free medium, and a collagen matrix to support cell attachment and growth[152,153,274]. Prolonged culture of keratinocytes under the latter system induces drastic phenotypic changes, specifically a diminished capacity for self-renewal and an increased commitment towards differentiation or senescence[49,153,275]. A critical factor that has been described to enable the long-term expansion of keratinocyte stem cells is by recreating the microenvironmental niche in which they naturally reside in[154]. A key component of the microenvironmental niche that is lacking in the current *in vitro* culture system is a native ECM. In an effort to recapitulate the dermal niche that the keratinocytes inhabit *in vivo*, we have used a dermal fibroblast-derived ECM (Fib-Mat), the development of which is described in Chapter III. In this current chapter, the Fib-Mat was shown to better support the proliferation of undifferentiated keratinocytes, when compared to type I collagen or tissue culture plastic (TCP).

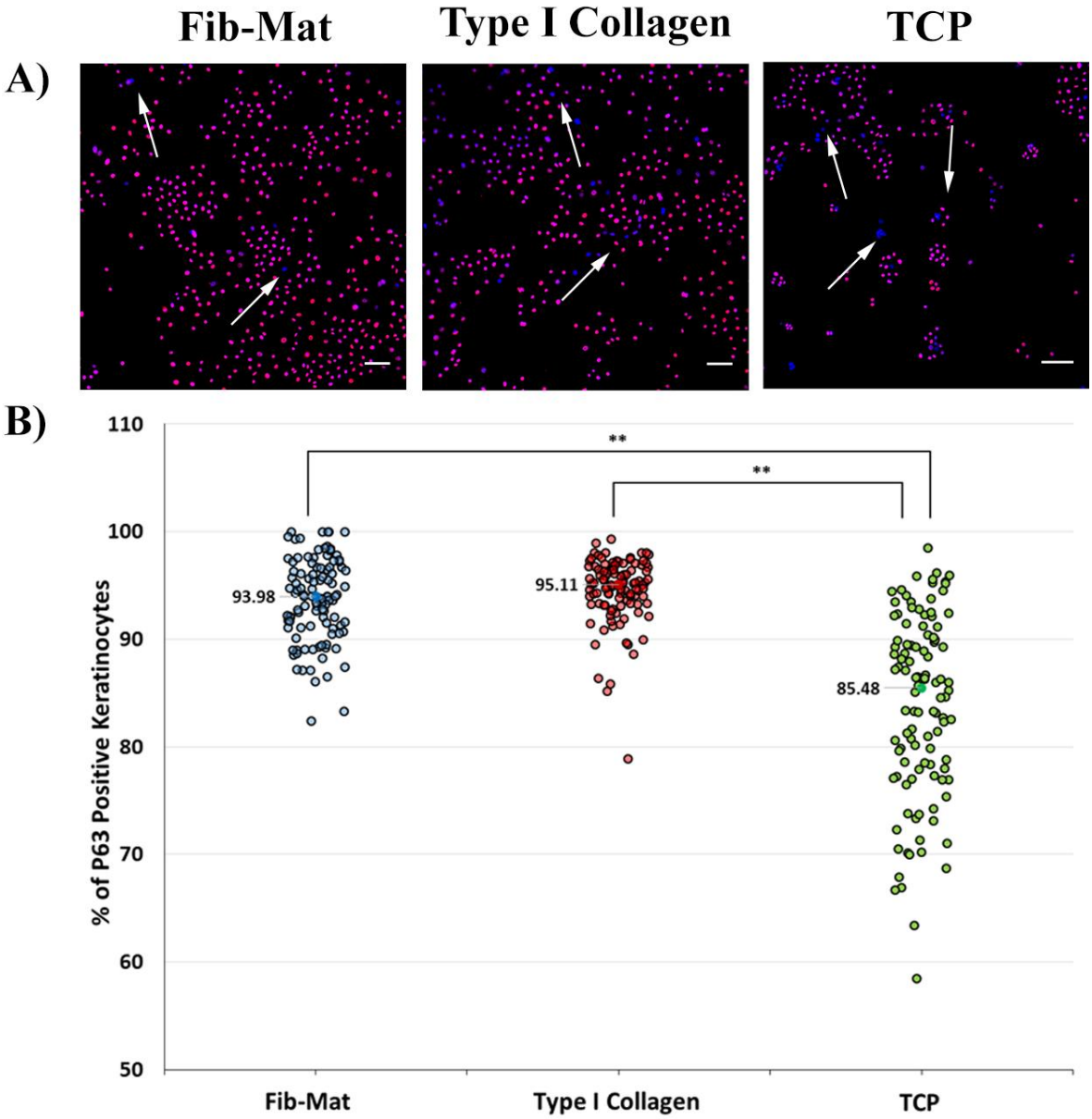

Figure 4.11: Quantification of p63 expression by keratinocytes grown on different substrates. Keratinocytes (2 x 10^4 cells) were seeded into wells of a 24-well plate that either contained Fib-Mat, type I collagen coating (Col I; 3ug/cm^2) or uncoated TCP and cultured for **3 days** in DKSFM. Keratinocytes were fixed with 4% paraformaldehyde then stained for p63. Nuclei were stained using DAPI (Blue).
A) Representative image of keratinocyte immunostained for p63. Arrows indicate the area of p63 negative keratinocytes. Scale bars are 100 µm.
B) Quantification of keratinocytes positive for p63. The data shown is a representative of three separate experiments. Statistical analyses were a Kruskal-Wallis test followed by a Mann-Whitney test. **p<0.01

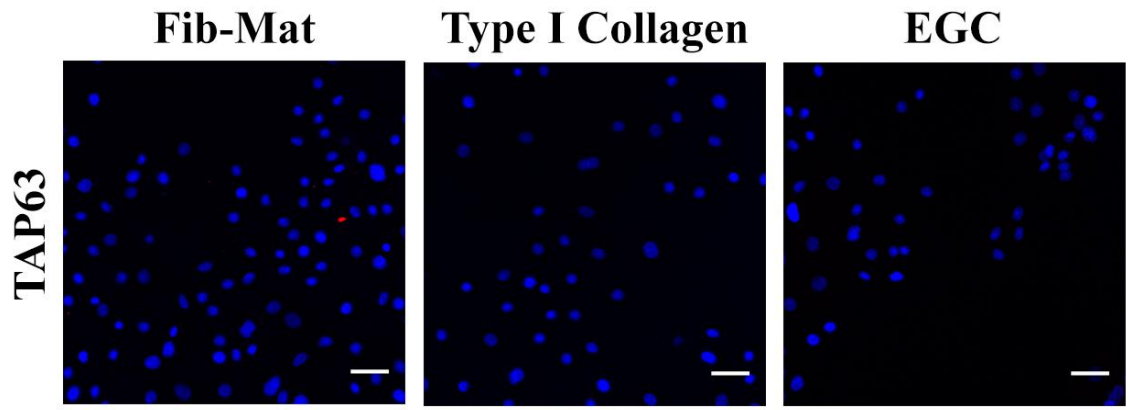

Figure 4.12: Expression of TAp63 by keratinocytes grown on different substrates. Keratinocytes ($2x10^4$ cells) were seeded into wells of a 24-well plate that either contained ECG coated with Fib-Mat, type I collagen ($3ug/cm^2$) or were uncoated (ECG). The keratinocytes were cultured for 3 days in DKSFM before being fixed with cold acetone: methanol (1:1) and stained for TAp63. Nuclei were stained using DAPI (Blue). Scale bars are 100µm.

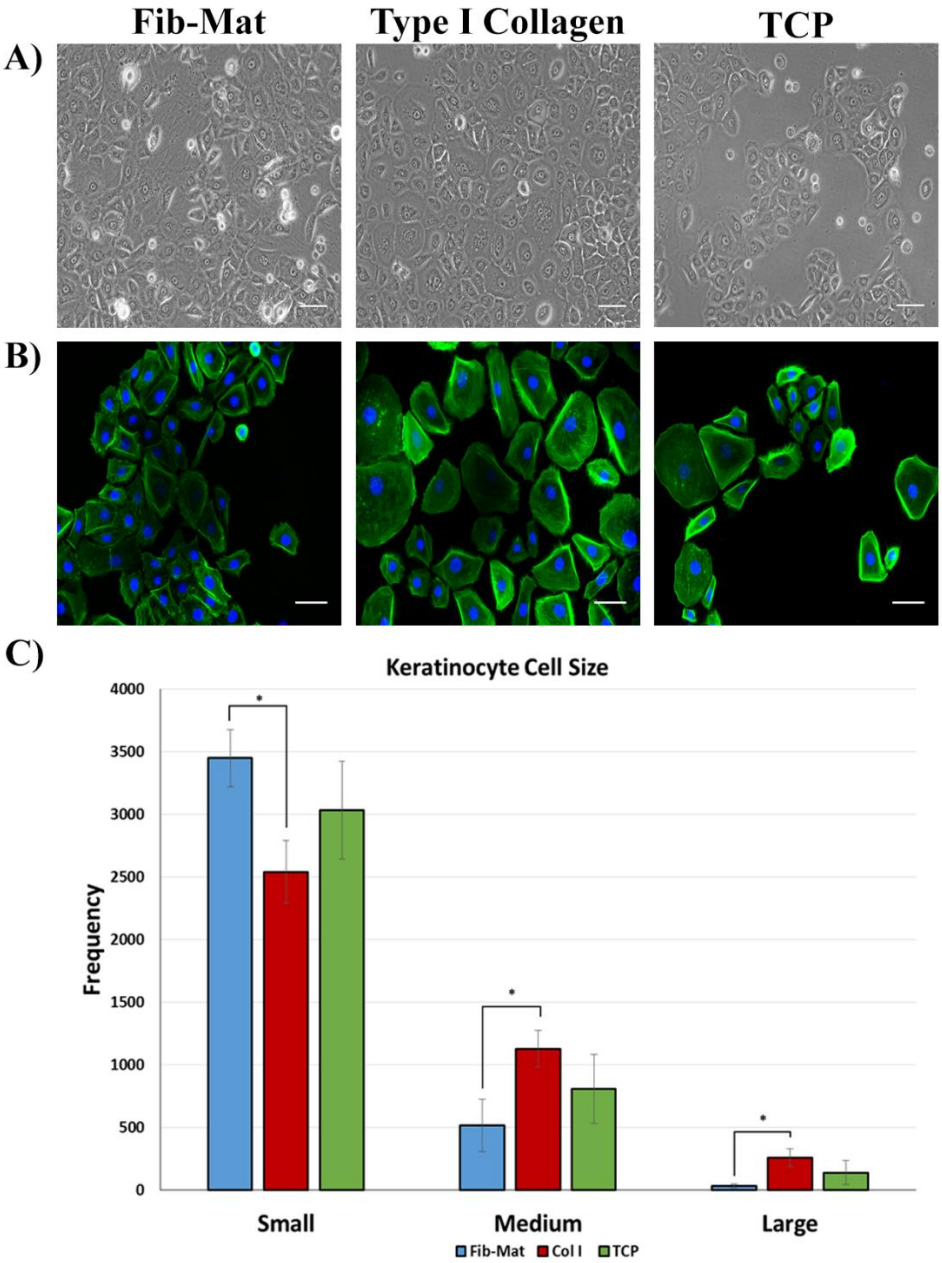

Figure 4.13: The cell size of keratinocytes grown on different substrates.
Keratinocytes (1 x 10^4 cells) were seeded into wells of a 48-well plate that contained either Fib-Mat, type I collagen coating (Col I; 3ug/cm^2) or uncoated TCP and cultured for **3 days** in DKSFM. Keratinocytes were fixed with 4% paraformaldehyde before being stained with phalloidin-Alexa Fluor® 488 (Green). Nuclei were stained with DAPI (Blue).
A) Representative phase contrast images of keratinocytes grown on Fib-Mat, Col I and uncoated TCP. Scale bars are 100 µm.
B) Representative images of keratinocyte stained with phalloidin-Alexa Fluor® 488. Scale bars are 50 µm.
C) Frequency of keratinocytes of differing cell size. Cell size was categorised as small, medium or large based on cell area **within the image** (small<medium<large = <2000µm^2<4000µm^2<6000µm^2). The data shown are the mean frequency ± standard deviation. Pooled data from three separate experiments are shown. Statistical analyses using ANOVA followed by Tukey's test were conducted. *p≤0.05

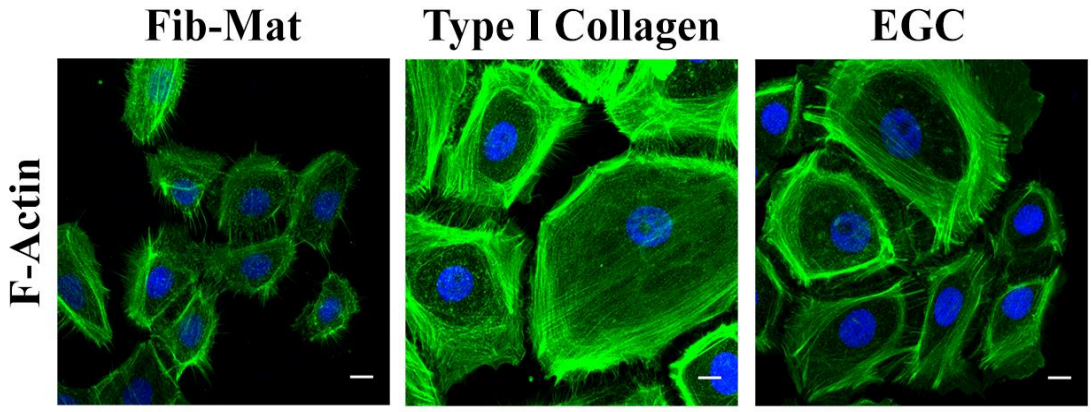

Figure 4.14: Arrangement of F-actin in keratinocytes grown on different substrates

Keratinocytes ($2x10^4$ cells) were seeded into wells of a 24-well plate that contained EGC. These had either Fib-Mat, type I collagen ($3ug/cm^2$) or uncoated EGC. Keratinocytes were cultured for three days in DKSFM before being fixed with 4% paraformaldehyde and stained for F-actin using phalloidin-Alexa Fluor® 488 (green). Images were taken using a confocal microscope. Nuclei were stained with DAPI (Blue). Scales bars are 10µm

The ability of the Fib-Mat to sustain the proliferation of undifferentiated keratinocytes in a serum-free medium was assessed. Type I collagen was used as a positive control, as it is generally used with KSFM to propagate keratinocytes[152,153]. Tissue culture plastic served as a negative control, as it does not contain any biological substrate. A significant increase in keratinocyte adhesion to Fib-Mat was found compared to the adhesion on type I collagen and TCP (Fig. 4.6). Furthermore, higher cell proliferation was observed on Fib-Mat, as assessed by growth curves, and Ki67 expression experiments (Fig. 4.7-4.8). These data are in agreement with other studies, which reported corresponding "tissue-specific" cell-derived matrix better supported the attachment and proliferation of cells such as mesenchymal stem cells[183,276,277] and synovium-derived stem cells[278,279]. In this study, an initial lag phase was observed in the proliferation of keratinocytes grown on Fib-Mat, before an exponential increase in proliferation was observed (Fig. 4.7). As Fib-Mat is a more complex biological substrate compared to type I collagen, the acclimatisation of keratinocytes towards this platform may explain the initial slower proliferation.

Keratins are cytoplasmic intermediate filaments that are expressed by keratinocytes in a site-specific and differentiation-dependent manner. Keratin 14 (K14) is normally expressed in keratinocytes in the basal layer of the epidermis. However, as keratinocytes differentiate and migrate towards the surface of the epidermis, the K14 expression is downregulated[280,281]. Studies assessing the *in vitro* culture of keratinocytes in which K14 has been knocked down, have suggested an involvement of K14 in cell proliferation and differentiation, with decrease in K14 expression associated with a reduction in cell proliferation and an increase in differentiation markers such as K10 and involucrin[282,283]. In this present study, immunofluorescence analysis revealed that K14 was expressed in keratinocytes grown on all three substrates, as expected. It was noted that there was a small proportion of keratinocytes grown on EGC that appear to have lost their expression of K14. However, these cells were not stratified. Neither was K10 expression observed regardless of the substrate the keratinocytes were cultured on. However, involucrin expression was observed in keratinocytes grown on all three substrates, with a higher proportion of keratinocytes being involucrin-positive on EGC. The changes in K14 and involucrin expression coincided with a decrease in keratinocyte proliferation when grown on TCP/EGC. These data suggest that keratinocytes on TCP/EGC are more prone to initiating

differentiation even when the cells are not yet stratified. The maintenance of K14 expression by keratinocytes residing on Fib-Mat is consistent with their preserved growth potential. However, there was no apparent decrease in K14 expression, despite a reduction in keratinocyte proliferation on type I collagen. However, it is likely that a different conclusion for keratinocytes grown on type I collagen from that observed using immunofluorescence would occur if the assessment of K14 expression was done through quantitative RT-PCR.

Expression of the transcription factor, p63 has been described as an indicator of keratinocyte stem cells and keratinocyte progenitor cells. A functional link between p63 expression with the maintenance of keratinocyte stem cells has been shown by both Mills *et al.*[22] and Yang *et al.*[23] using a p63-/- mouse. Further studies by Parsa *et al.*[284] showed that p63 expression is restricted to keratinocytes with high proliferative potential that reside within the basal layer of the skin. They also revealed that p63 is absent from keratinocytes that were undergoing terminal differentiation. Currently, our study demonstrated that there is a high level of p63 expression in keratinocytes grown on Fib-Mat or type I collagen, whereas, fewer keratinocytes expressed p63 when cultured on TCP (Fig. 4.11). Interestingly, the expression of p63 expression coincided with a decline in growth potential (Fig. 4.7-4.8) and an increase in involucrin expression (Fig. 4.10). This inability of TCP to support the growth of undifferentiated keratinocytes is consistent with data reported by Coolen *et al.*[152].

Previous reports have indicated that serial *in vitro* culture of keratinocyte on type I collagen causes them to undergo terminal differentiation and senescence[153,275]. For this reason, it was expected that the expression of p63 by keratinocytes grown on type I collagen would be lower. Intriguingly, a high level of p63 expression was observed, which was similar to that of cells grown on Fib-Mat. Youn *et al.*[275] reported no change in p63 expression, even when keratinocytes were repeatedly passaged on type I collagen, which may explain what was observed for keratinocytes grown on type I collagen in this study. Recently, p63 has been reported to have a dual role in keratinocyte stem cell maintenance and differentiation. It exerts this different function through its two isoforms, TAp63 and ΔNp63. During late keratinocyte differentiation, TAp63 expression was shown to be upregulated[35], whereas the expression of the ΔNp63 isoform decreased[285]. As the antibody first used in this study was a pan-p63

antibody (4A4), it could not differentiate between the two isoforms. Hence, an antibody recognising TAp63 was acquired to investigate Tap63 expression in keratinocytes grown on the different substrates. Surprisingly, no expression of TAp63 in keratinocytes grown on either Fib-Mat, type I collagen or TCP was detected (Fig. 4.12). However, due to the lack of a positive control cell line for TAp63, it is uncertain whether the keratinocytes grown on these different substrates really do not express TAp63. Although, to my knowledge, the antibody recognising TAp63 that I have used was only shown to detect exogenous overexpression of TAp63 and not its endogenously expressed counterpart. The endogenous expression of TAp63 may be very low and hence may not have been detected by the immunofluorescence staining technique used here. A different approach would be to assess the mRNA expression of TAp63 through qRT-PCR.

During physiological in vivo differentiation and epithelial maturation, an increase in the size of keratinocytes has been reported. The increase in keratinocyte cell size has been suggested to be a reliable indicator of keratinocytes undergoing terminal differentiation. Studies reported an enlargement of keratinocyte cell size during differentiation, which was typically accompanied by the expression of involucrin, a marker for terminal differentiation[261,286]. Other studies have established that keratinocytes of a small cell size are undifferentiated and retain a high proliferative capability[287-289]. Based on these observations, numerous investigators have described cell size as a criteria to distinguished between keratinocyte stem cells and keratinocytes committed towards differentiation[154,288,289]. Notably, by phase contrast microscopy, it was found that keratinocytes grown on Fib-Mat had a smaller cell size when compared to keratinocytes grown on type I collagen and TCP (Fig. 4.5). Quantification of cell size indicated that there was a higher proportion of keratinocytes with a small cell size when they were grown on Fib-Mat. In contrast, keratinocytes became larger when they were cultured on type I collagen (Fig.4.13). These data were consistent with what Esteban-Vives *et al.*[153] had reported. Similarly, an increase in cell size was observed for keratinocytes grown on TCP, although this increased size was not statistically significantly different from keratinocytes grown on Fib-Mat.

A recent report by Nanba *et al.*[290] indicated that cell motility is an attribute that could be used to identify undifferentiated keratinocytes. They indicated that keratinocyte

colonies presenting with a high rotational movement and in which individual cell displayed high motility was a good indicator that these colonies contained undifferentiated keratinocytes with a high proliferative capability. In this study, keratinocytes grown on Fib-Mat appear to be highly motile (See video in Appendix B). Distinct keratinocytes colonies were not observed on Fib-Mat or type I collagen, but keratinocyte colonies did form on TCP. Rather pseudo-colonies formed on both Fib-Mat and type I collagen, whereby keratinocytes would collectively migrate together before dispersing and forming new pseudo-colonies. The majority of keratinocytes grown on Fib-Mat were observed to be highly motile at all times. In contrast, less cell motility was observed for keratinocyte cultured on type I collagen and TCP and this was particularly evident when the time in culture was extended. The reduction in cell motility of individual keratinocytes was accompanied by an increase in the size of these keratinocytes. Changes in cell size, with cell motility during keratinocyte differentiation has been previously reported by Sun *et al.*[286]. These data are further evidence that keratinocytes grown on type I collagen and TCP were undergoing differentiation.

Actin filament reorganisation is the primary mechanism for changes in cell shape and cell motility, and it has been shown to have an impact on the proliferation and differentiation of keratinocytes[127,291,292]. In the present study, it was found that keratinocytes residing on type I collagen or EGC without a matrix protein coating (a TCP equivalent: refer section 4.2.3.2) had developed a circumferential actin network, similar to that reported by Nanba *et al.*[292] and described to be indicative of reduced cell movement and imminent differentiation. In contrast, keratinocytes grown on Fib-Mat presented with short actin bundles that were distributed radially. This arrangement of actin was said to be an indicator of proliferative, undifferentiated keratinocytes[292](Fig. 4.14). Rho-associated kinase (ROCK) has been reported to play a role during keratinocyte differentiation, inducing changes in the thickness and density of actin fibre structures[47,292]. Its activity has been shown to correlate with substrate stiffness, with stiffer substrates leading to ROCK activation[293]. While the stiffness of the substrates was not measured, rigid surfaces such as TCP/EGC and type I collagen-coated TCP/EGC have been reported by others to be stiffer (>1GPa) than cell-derived matrices (200-600Pa) [294,295]. It is likely that our Fib-Mat provides a more physiologically compliant stiffness that assisted in suppressing or down regulating

keratinocyte differentiation rather more than TCP/EGC or type I collagen-coated TCP/EGC.

Collectively the data described here indicate that keratinocytes grown on Fib-Mat are less differentiated than keratinocytes cultured on TCP, which show signs of undergoing early commitment to terminal differentiation. Whereas, despite exhibiting cell size, cell motility and actin reorganisation characteristics that are indicative of terminal differentiation, keratinocytes grown on type I collagen still expressed markers (K14 and p63) of undifferentiated keratinocytes. Others have also found that keratinocytes may retain some markers characteristic of undifferentiated cells during the early stages of differentiation. For example, Webb *et al*. [296] found that keratinocytes residing on the basal layer of the epidermis do not switch off the expression of keratin 15 (a marker of keratinocyte quiescence, and in some circumstances of stem cells) even during the differentiation process. Furthermore, Esteban-Vives *et al*[153], observed that keratinocytes grown on type I collagen still retained K15 expression despite showing signs of differentiation. Hence, it is likely that on type I collagen, the keratinocytes are in the early stages of terminal differentiation, even though some markers of undifferentiated cells are still expressed.

Cell-ECM interactions are known to play a major role in modulating cellular behaviour. For example, it has been reported that cell-ECM interactions preserve the self-renewal ability of stem cells by preventing differentiation processes. However, our data and other reports have shown that the use of single ECM molecules does not sustain the long-term growth of undifferentiated stem cells. In this very reductionist approach, the cross-talk of signalling pathways between matrix molecules and growth factors within the tissue microenvironment are overlooked. Numerous reports[297-299] have shown the synergistic impact of several matrix molecules better sustain, potentiate or negate the signalling pathways that influence cellular behaviour. For example, Flaim *et al.* [297] showed that during embryonic stem (ES) cell differentiation towards a liver progenitor lineage, the combination of type I collagen with laminin and type III collagen with laminin, have a positive effect on the differentiation of the ES cells towards a liver progenitor lineage, even though previously they have shown to have a negative effect on differentiation individually. Furthermore, Watt *et al.*[87] showed that the combination of laminin, type IV collagen and fibronectin inhibited the

differentiation of keratinocytes during *in vitro* culture. Our Fib-Mat contains numerous ECM proteins, including laminin, type IV collagen and fibronectin, the combination of signals from which may help to suppress or restrain keratinocyte differentiation.

Recently, Chacón-Martínez et al. have described an advanced *in vitro* culture system that allowed the enrichment of multipotent mouse hair follicle stem cells (HFSC) and their long-term maintenance. This system utilises Matrigel to provide the extracellular matrix environment for the defined medium that they developed. The composition of this medium includes FGF2, VEGF-A and the ROCK inhibitor Y27632. Although this system may be effective for the expansion of HFSC, Matrigel is derived from Engelbreth-Holm-Swarm mouse sarcoma, which would introduce an undesirable xenogeneic component, and could make this system unsuitable for clinical applications. In my study, I have demonstrated that Fib-Mat provides a suitable xenogeneic-free matrix microenvironment for the proliferation of undifferentiated keratinocytes. It would be interesting to test the Fib-Mat that I have developed with the defined medium developed by Chacón-Martínez et al. to see if together the combination better enriches for undifferentiated keratinocytes. However, defined culture medium described by Chacón-Martínez et al[300] was designed for hair follicle stem cells (HFSC). While HFSC and interfollicular epidermal stem cells (IFESC; are the type of stem cells contained in the populations of neonatal keratinocytes which were used for this thesis) may be collectively called keratinocyte stem cells in the literature, they do have distinct transcriptional profiles[301]. Furthermore, Chebotaev et al[302] have demonstrated that HFSC and IFESC respond differently when treated with glucocorticoid. Hence, while the culture medium described by Chacon-Martinez et al[300] may be suitable for HFSC, it is unknown whether or not it is similarly suitable for culturing the IFESC that were used in this thesis without further optimisation. Nevertheless, it would be interesting to see if this defined medium when used with my Fib-Mat could enrich for undifferentiated keratinocytes and so ensure even better long-term expansion that has been achieved in this present study.

4.5 Conclusions

In summary, our results demonstrated that the Fib-Mat (developed in Chapter III) was able to support the proliferation of undifferentiated keratinocytes, in a serum-free culture system. Furthermore, our data indicated that this Fib-Mat provides a microenvironment that is capable of decreasing keratinocyte differentiation far more than that seen when type I collagen or TCP are used in the same culture system. Hence, it is anticipated that the culture system using Fib-Mat described in this chapter will enable the preparation of more undifferentiated keratinocytes than has previously been possible, whilst maintaining xenogeneic free conditions that meet the requirements of the regulatory authorities for the development of cells to be used for therapeutic purposes.

4.6 Further Direction

Barrandon *et al*. [303] has described the use of colony forming assays as an invaluable tool for determining the presence of stem cells within a keratinocyte population. The use of this assay would enable us to verify that Fib-Mat does indeed better retain a keratinocyte stem cell population compared to type I collagen and TCP. Currently, this assay is being optimised for use. Additionally, keratinocyte stem cell markers such as K15[304], K19[305] and ABCG2[306] could be used.

The ability of keratinocytes to form a mature stratified epidermis is essential if they are to be used to reconstitute patient skin. Recently, Lamb and Ambler[307] showed that keratinocytes propagated in serum-free and feeder-free culture conditions were unable to form stratified epidermis. It will be important to determine whether keratinocytes grown on Fib-Mat can form a fully mature stratified epidermis in a skin equivalent model. Benny *et al*.[308] reported a technique for generating a skin equivalent construct with enriched basement membrane that is physiologically mimic an intact human skin. This technique will be used to generate the skin equivalent model.

The studies in this chapter were performed using keratinocytes that have been subcultured till passage 3 before being used; it will be interesting to culture freshly isolated keratinocytes using the Fib-Mat and serum free medium to determine the long-term effectiveness of this system for expanding and maintaining undifferentiated keratinocyte progeny. In addition, while the Rheinwald and Green culture system

contains xenogeneic components, it is still considered to be a reliable system to expand keratinocytes[154]. Hence, a long-term comparison between our keratinocyte culture system with the Rheinwald and Green culture system should be conducted in the future. This would be a very interesting study and should involve a careful comparison between the extent of keratinocyte differentiation, rates of proliferation and calculations of the number of rounds of cell division possible in each culture system. It is envisaged that such a study would be required before my culture system could be recommended for clinical use.

Chapter V:

Foetal and Adult Dermal-Fibroblast Extracellular Matrix Differentially Influence Keratinocyte Behaviour

5.1 Introduction

Scar formation is a major clinical problem that has a significant economic and social impact. Each year, in just the first world countries alone, over 100 million people acquire scars, which are a result of either trauma or surgery. Currently, there are no adequate remedies for the treatment of scarring. Hence, an effective therapy that is capable of restoring the skin to its original state would be highly valued[185,191]

The foetal skin has an intrinsic regenerative capability that can restore the architecture, organisation and function of an injured site. This ability is preserved until the start of the third trimester, where skin wound healing transitions to a repair response, and scar formation[196,309]. While the mechanism of scarless wound healing remains elusive, it is known that the response of foetal and adult skin during wound healing have their distinct characteristics. These differences range from the inflammatory response, cytokine profiles and the composition of the ECM[186,196]. In adult skin, the inflammatory response marks the earliest reaction towards an injury. In contrast, the inflammatory response is lower in foetal skin, owing to the absence of a fully developed immune system in the foetus. This led to the hypothesis that inflammation may restrict regeneration and promote fibrosis and scar formation. This idea was examined in studies with immunodeficient adult mice that lacked a lymphocyte-mediated inflammatory response; in these mice, wounds healed without scar formation[310-312]. However, a transplantation study in which skin from adult sheep was transplanted onto the back of foetal sheep, and then the transplanted skin was subjected to an incisional wound, showed that this wound healed with the formation of a scar[195]. This result suggested that there may be intrinsic factors within foetal skin besides the foetal inflammatory response, which are responsible for the regenerative capability of foetal skin.

Numerous studies have reported that the ECM composition of the foetal dermis is different from that of the adult dermis. Principle components within both foetal and adult dermis are type I collagen and type III collagen, but compared to adult dermis, foetal dermis has a higher ratio of type III to type I collagen[201,216]. As foetal development progresses, the ratio of type III to type I collagen changes so that eventually type I collagen predominates. This shift was observed to correlate with

changes in the healing response, specifically the switch from a scarless repair to scar formation[313]. Another distinguishing feature of the foetal dermis is the abundance of GAGs, specifically chondroitin sulfate[192,314] and hyaluronic acid[222,315]. Both of these GAGs have been shown to play important roles in ECM structure as well as in influencing cell behaviour such as proliferation and migration[316,317]. Additionally, ECM glycoproteins such as fibronectin[314] and proteoglycans such as decorin[220] and versican[219] have also been shown to be differentially expressed between adult and foetal skin dermis. Such differences in the ECM composition may be the key to understanding the process of scarless wound healing. Although limited comparisons of ECM composition between the adult and foetal dermis have been conducted, to our knowledge, a complete evaluation of the ECM components has yet to be conducted. As fibroblasts are major contributors of both foetal and adult dermis, determination of the differences in the ECM proteins secreted by adult and foetal dermal fibroblasts may provide an understanding of the mechanism responsible for scarless wound healing.

Despite having some knowledge of the differences in the ECM microenvironment between adult and foetal skin, it is not known how these differences will affect keratinocyte behaviour. Hence understanding the responses of keratinocytes to matrices deposited by foetal and adult dermal fibroblasts may provide clues as to the signals that control the regenerative repair processes of foetal skin. This knowledge can then be used to transfer a foetal healing response onto the adult wound.

This chapter describes the characterization of the ECM profile between foetal- and adult dermal fibroblast derived-ECM using quantitative proteomics. Also, the influence of these matrices on keratinocyte cell behaviour was investigated by assessing gene expression using microarray.

5.2 Materials & Methods

5.2.1 Primary Antibodies Used

Antigen	Clone	Species, Isotype	Antibody Working Dilution
Alpha-smooth muscle actin	Monoclonal (1A4)	Mouse IgG2a	0.5µg/ml (ICC)
Anti-Fibroblast Marker	Monoclonal (TE7)	Mouse IgG1	0.5µg/ml (ICC)
Chondroitin Sulphate	Monoclonal (CS-56)	Mouse IgM	5µg/ml (ICC)
Fibronectin	Polyclonal	Rabbit IgG	5µg/ml (ICC)
Nidogen	Polyclonal	Rabbit IgG	1µg/ml (ICC)
Tenascin-C	Monoclonal (MTn-12)	Rat IgG1	5µg/ml (ICC)
Thy-1	Monoclonal	Mouse IgG1	2.5µg/ml (ICC)
Type I Collagen	Polyclonal	Rabbit IgG	5µg/ml (ICC), 1µg/ml (WB)
Type III Collagen	Polyclonal	Rabbit IgG	5µg/ml (ICC)
Type IV Collagen	Polyclonal	Rabbit IgG	5µg/ml (ICC), 1µg/ml (WB)
Versican	Monoclonal (EPR12277)	Mouse IgG	5µg/ml (ICC)
Vimentin	Monoclonal (V9)	Mouse IgG1	2.5µg/ml (ICC)

5.2.2 Microscopy

A number of different microscopes were used for the work described in this chapter:

-Phase contrast images were obtained using Zeiss Axiovert Bright Field Inverted Microscope (Zeiss, Oberkochen, Germany) or an Olympus IX-51 Inverted Microscope (Olympus, Tokyo, Japan).

-Immunofluorescence images were captured using either a Zeiss Axioskop Upright Microscope (Zeiss, Oberkochen, Germany), a Nikon A1+ Confocal Microscope (Nikon, Tokyo, Japan) or a Zeiss LSM510 Confocal Microscope (Zeiss, Oberkochen, Germany)

5.2.3 RNA Extraction and Microarray Analysis

5.2.3.1 RNA Extraction

Total RNA was extracted from neonatal keratinocytes grown on a 10cm^2 tissue culture dish coated with foetal dermal fibroblast derived-matrix, adult dermal fibroblast derived-matrix or type I collagen. After three days of culture, the cells were washed twice with PBS and 2ml of TRIzol® (ThermoFisher, Massachusetts, USA) was added and incubated for 5 minutes at RT. The TRIzol® mixture was transferred into two separate microcentrifuge tubes, 1 ml in each tube. To each sample, 200µl of chloroform was added, vortexed and left to stand for 5 minutes. The samples were then centrifuged at 14,000 RPM, at 4°C for 20 minutes. 500µl of the aqueous phase (top translucent layer) was transferred to a new microcentrifuge tube, mixed with 500µl of isopropanol and left to stand for 5 minutes. The mixture was then centrifuged at 14,000 RPM, at 4°C for 20 minutes. The supernatant was removed, and 1ml of 70% ethanol was added to the pellet. This mixture was centrifuged at 14,000 RPM, RT for 10 minutes. The supernatant was poured away, and any remaining supernatant was pipetted out. The pellet was placed into a heating block for 10 minutes at 37°C, and after 85µl of RNase-free water was added, it was left at 4°C to dissolve overnight.

5.2.3.2 RNA Purification

The dissolved RNA was treated with 80ul of 3 Kunitz unit of RNase-free DNase I (Qiagen) for 30 minutes at 37°C. The treated RNA was further purified using an RNeasy Mini Kit (Qiagen). The sample was mixed with 350µl of RLT buffer (a guanidine-thiocyanate–containing lysis buffer) and left to stand for 1 min. After the addition of 250µl of 100% ethanol, the samples were transferred to a spin column and centrifuged at 14,000 RPM, at RT for 1 min. The filtrates were discarded, and 500µl of RPE buffer (wash buffer) was added to each spin column, which were then centrifuged at 14,000 RPM, at RT for 2 minutes. The filtrate was discarded, and another 500µl of RPE was added to the spin columns, which were centrifuged again at 14,000 RPM, at RT for 2 minutes. A final spin at 14,000 RPM at RT for 2 minutes was done to remove any remaining liquid in the spin columns. 50µl of RNase-free water was added to the membrane in the spin column and left to stand for 10 minutes. The spin column were placed into new microcentrifuge collection tube and was centrifuged at 14,000 RPM, at RT for 5 minutes to elute the RNA. The RNA concentration was quantified using a NanoDrop ND-1000 (Thermo Fisher Scientific).

5.2.3.3 Microarray Analysis

The extracted and purified RNA samples were sent to A*STAR Biopolis Shared Facility, Microarray Facility, Singapore. Before the samples were analysed by microarray, the quality of the RNA was checked using Agilent 2100 Bioanalyzer. Microarray analyses of the samples were performed using an Affymetrix HuGene 2.0 ST Chipset. The data generated were passed to Dr Simon Lieven from the Epithelial Biology Lab, Institute of Medical Biology, Singapore for further analysis. The data were background corrected, normalised and analysed with R package "Limma" and "Oligo". "Oligo" is a package that allows the users to pre-process the microarray data while "Limma" enables the expression of many genes to be analysed simultaneously. The data were then analysed with Tibco® Spotfire software. The processed data were sent back to Curtin University, School of Biomedical Sciences, where they were further curated to determine which genes were differentially expressed with a fold change of more than 1.5 and with adjusted p-values of ≤ 0.05.

5.2.4 Proteomics

5.2.4.1 Extracellular Matrix Solubilisation and Digestion

Adult or foetal fibroblast-derived ECMs were generated by seeding 90 x 10^4 cells into a 100mm cell culture dish and culturing up to 7 days in MCDM (section 2.3.1). The resulting fibroblast-derived ECMs were decellularized using PLA_2 (section 2.3.4.1). To solubilize the acellular ECM, 600µl of 8M Urea/50mM Tris-HCl pH8 was added before scraping the matrix off the plastic surface and transferring it to a microtube. The matrix mixture was incubated in 50µl of 10mM DTT and 50µl of 55mM Iodoacetamide for 1 hour at RT. The matrix proteins were digested with sequencing grade endoproteinase Lys-C (Promega) at a ratio of 1:100 (Lys-C: expected protein amount) for 4 hours at RT. The digested matrix was then diluted with ddH_2O to adjust the Urea to a concentration of less than 1M before being further digested with sequencing grade-modified trypsin (Promega) at a ratio of 1:100 (Trypsin: expected protein amount) overnight at RT. Samples were acidified by adding 200µl of 10% trifluoroacetic acid to ensure binding of samples to the C-18 column. The Sep-Pac C-18 column cartridge (Waters, Milford MA) was washed three times with 1ml of 100% acetonitrile and then primed by washing a further three times with 0.1% trifluoroacetate acid. Each sample was run through separate C-18 column cartridges.

The column cartridges were then washed three times with 0.1% trifluoroacetate acid before being eluted with 1ml of 0.1% formic acid.

5.2.4.2 TMT10plex Isobaric Labelling and Mass Spectrometry (MS)

The peptide concentration of each samples was estimated using UV absorbance at 214nm. Then 20ug sample of peptide was added to 25µl of 100mM triethylammonium bicarbonate (TEAB) for labelling with 10µl of TMT10plex isobaric tags (Thermoscientific) for 1 hour at RT. Labelling was quenched with 10ul of 1M Tris pH7.5. The samples were cleaned and desalted by using Sep-Pac C-18 column cartridges, which were washed three times with 0.1% trifluoroacetate acid before being eluted with 10mM Ammonia Formate. The total amount of each eluted samples was injected and analysed on a Dionex 3000 Ultimate nanoflow HPLC system (Thermo Fisher Scientific) coupled to Thermo Scientific ™ Orbitrap Fusion ™ Tribrid ™ Mass Spectrometer (MS). An in-house column packed with 75µm silica beads with 2.5µm Reposile beads was used for reverse –phase separation. The peptides were separated using a 60min gradient of 5% to 50% acetonitrile in 0.1% formic acid before being run into the MS. The data generated were analysed using Proteome Discoverer (Version 1.4.0.288. Thermo Fisher Scientific). The MS/MS spectra were searched with the Mascot 2.5.1 search algorithm using the Human UniProt Database and a list of matching proteins for the peptides detected in each sample were generated.

5.3 Results

5.3.1 Characterisation of Adult and Foetal Dermal Fibroblasts

Morphological differences were observed between adult and foetal dermal fibroblasts during *in vitro* culture. Adult dermal fibroblasts exhibited a uniform, thick, spindle-like morphology, which is a typical fibroblast phenotype. In contrast, foetal fibroblasts had a thin stellate-shaped morphology (Fig. 5.1). Both adult and foetal dermal fibroblasts were observed to stain positively for the fibroblast markers Thy-1 and vimentin (Fig. 5.2i-viii). Although, Thy-1 expression was noted to be lower in foetal dermal fibroblasts than in the adult cells.

The possibility that there may be a myofibroblast subpopulation within the adult and foetal dermal fibroblast was investigated. To distinguish the myofibroblast

subpopulation, an antibody recognising alpha-smooth muscle actin (α-SMA) was used as a marker. Although α-SMA staining was observed in both adult and foetal fibroblasts the staining patterns differed. A small number of foetal dermal fibroblasts were observed to have prominent α-SMA positive stress fibres, whereas adult dermal fibroblasts showed a diffuse α-SMA staining (Fig. 5.2ix-xii).

5.3.2 Proteomic Analysis of ECM derived from Adult and Foetal Dermal Fibroblasts.

The compositional differences between ECM derived from adult and foetal dermal fibroblast were investigated using quantitative proteomics. Figure 5.3 shows a schematic diagram of the quantitative proteomics. The ECM from two different donors of adult (aHDF: Adult Donor 1; EBL028: Adult Donor 2) and foetal dermal fibroblast (fHDF: Foetal Donor 1; FS13: Foetal Donor 2) were compared. The fibroblasts were cultured as described (section 5.2.2.1) and after ECM deposition, the bulk of the cellular components were removed through decellularisation using PLA_2 (section 2.3.4.1) to allow better detection of low abundance ECM proteins, which could be masked due to the presence of the cells. The ECM was extracted by solubilizing it in 8M Urea before it was digested into peptides. An equal amount of peptides from each sample were labelled with a tandem mass tag (TMT) reagent (TMTplex10), to allow for multiplexed relative quantification of proteins between the multiple samples. TMTs are isobaric labels that have the same total molecular weight. Hence, peptides derived from different samples that were labelled with different tags remain indistinguishable during HPLC separation and peptide-precursor ion mass measurement by MS. However, upon fragmentation in the MS/MS sequencing analysis, the TMTplex tags generate low molecular mass reporter ions with different distinct masses. The reporter-intensity ratios were then used for relative quantification of each peptide allowing it to be traced back to its original sample[318,319].

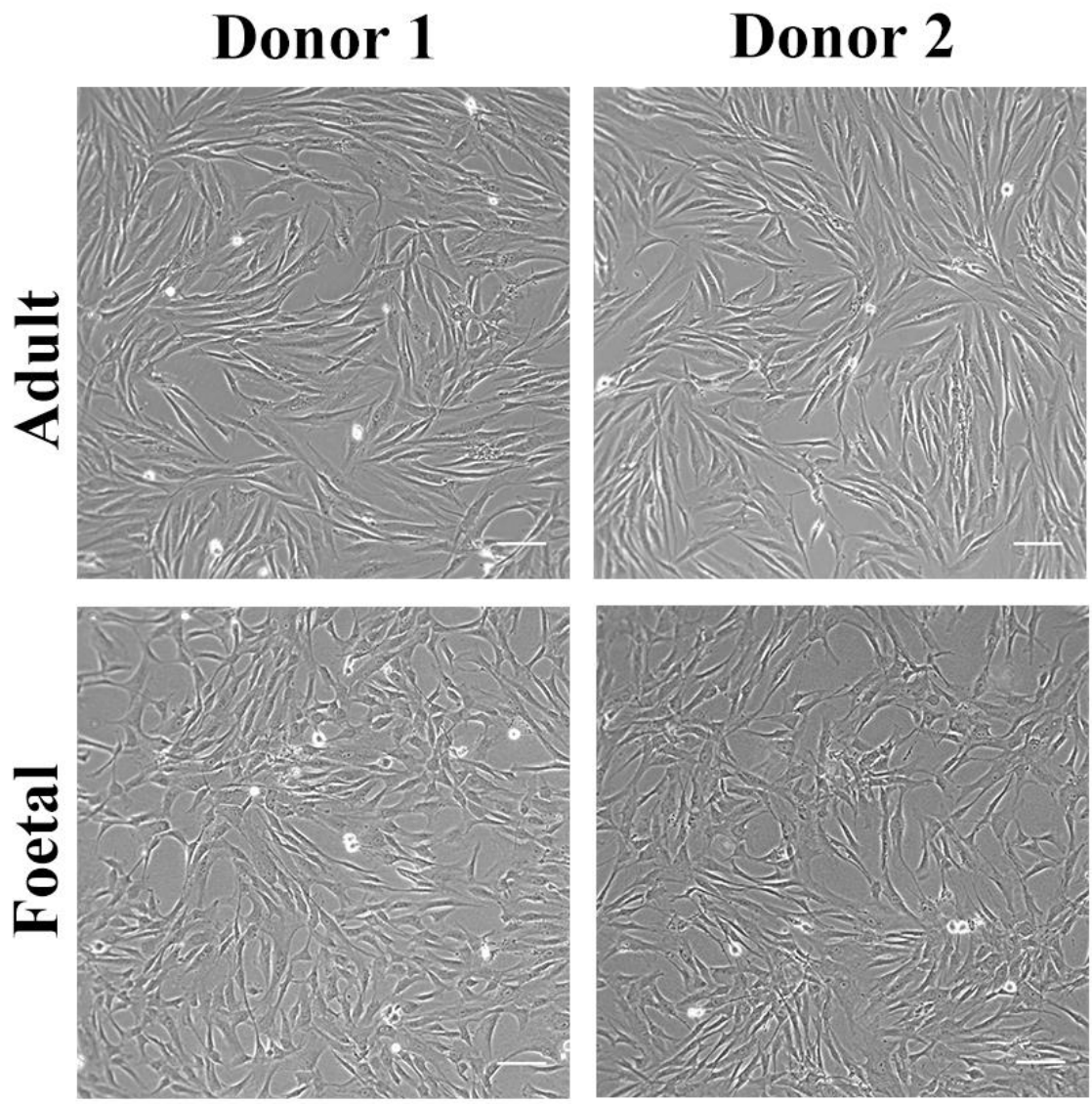

Figure 5.1: Phase contrast images of adult and foetal dermal fibroblasts. Cell morphology of dermal fibroblasts during culture as seen by phase contrast microscopy. Scale bars are 100μm.

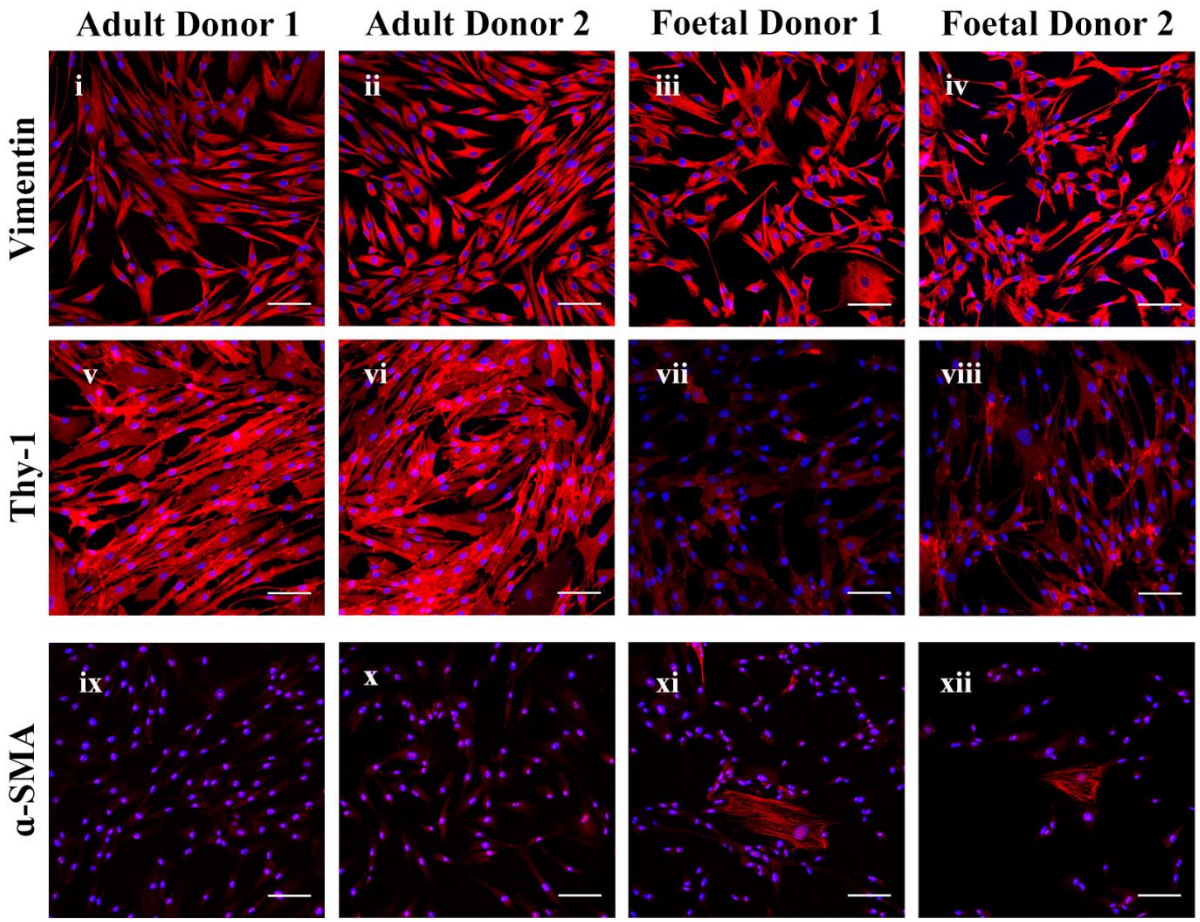

Figure 5.2: Characterization of adult and foetal dermal fibroblasts. Adult and foetal dermal fibroblasts (2 x 10^4 cells) were seeded into a 24-well plate containing etched glass coverslips and cultured until day two. The cells were fixed with 4% paraformaldehyde and stained with antibodies recognising vimentin **(i-iv)**, Thy-1 **(v-viii)** or α-SMA **(ix-xii)**. The secondary antibody was an anti-mouse IgG1 Alexa Fluor® 546-conjugated antibody. Nuclei were stained with DAPI (blue). Scale bars are 100µm.

The proteomic dataset was curated for ECM proteins using the human matrisome database (MatrisomeDB, http://matrisomeproject.mit.edu/), which categorises the ECM proteins into "core matrisome" (ECM glycoproteins, collagens and proteoglycans) and matrisome-associated proteins" (ECM-affiliated proteins, ECM regulators and secreted factors) [230]. Figures 5.4-5.7 display quantitative heatmaps of the expression intensities of ECM glycoproteins, collagens, proteoglycans, ECM-affiliated proteins, ECM regulators and secreted factors from adult and foetal donor samples. The heatmap depicts the relative concentration of the same protein from the different samples. Among the core matrisome proteins, the presence of the basement membrane components, laminin chains: LAMA4, LAMB1, LAMB2 & LAMC1, type IV collagens, nidogens: NID1 & NID2, and perlecan (HSPG) were detected. An abundance of laminin chains and a lower level of type IV collagen were apparent within the adult dermal ECM in comparison to the foetal dermal ECM. No differences were detected in the levels of NID1, NID2 and HSPG between the adult and foetal matrices. An abundance of ECM regulators were apparent in adult dermal ECM; these included ADAMTS1, ADAMTS2 AMBP, CD109, F2, HRG, HTRA1, HTRA3, ITIH1, ITIH2, ITIH4, KNG1, LOXL1 and SERPIN proteins. Interestingly, TIMP2 (tissue inhibitor of matrix metalloproteinase-2) was more abundant in foetal ECM, suggesting this regulator was required to inhibit matrix degrading enzymes. These and the other ECM proteins shown in Figure 5.4 to 5.7 indicate the differences in the ECM compositions of adult and foetal dermal fibroblast matrices.

5.3.3 Immunofluorescence Staining of Extracellular Matrix Proteins.

To independently evaluate if there were differences in the abundance of ECM proteins between adult and foetal dermal fibroblast ECM, immunofluorescence staining was conducted. Both adult and foetal dermal fibroblasts were cultured on EGC for 7 days in MMC media before being decellularized with PLA_2. The resulting ECM layer was immunostained with antibodies that recognised the major ECM components (i.e., type I collagen, type III collagen, type IV collagen, fibronectin, versican and nidogen) that were shown to be present at different levels in adult and foetal dermal ECMs by quantitative proteomics. The immunofluorescence images obtained (Fig. 5.8 - 5.9) were consistent with the quantitative proteomic data, as they showed a higher abundance of type I collagen, type III collagen, type IV collagen, fibronectin and versican in the foetal dermal ECM relative to the adult dermal ECM. However, no

difference in the abundance of nidogen between the foetal and adult dermal ECM was observed. Interestingly, differences in the structure of the ECM between adult and foetal samples were apparent. A more compact deposition of type I collagen, type III collagen, type IV collagen and fibronectin was observed in the foetal dermal fibroblast ECM compared to the adult counterpart. Also, the fibril structures of these ECM proteins appeared to be thinner in the foetal matrices.

Coolen *et al*. [314] reported that were higher levels of chondroitin sulphate in the foetal dermis compared to that of the adult. To determine whether this was true for our adult and foetal dermal derived-ECM, they were stained with an antibody recognising chondroitin sulphate. This antibody stained the foetal dermal derived-ECM more strongly than the adult derived-ECM (Fig. 5.10).

To better visualise the deposition ECM proteins by adult and foetal dermal fibroblasts, a 3D construct of the immunostained ECM layer at higher magnification was generated using confocal microscopy. In foetal dermal fibroblast ECM, a fine reticular/basket-weaved pattern was observed for both type I collagen and type IV collagen. In contrast, thick and dense parallel bundles of type I collagen and type IV collagen were seen in the adult dermal fibroblast ECM (Fig. 5.11).

5.3.4 Western Blot of Extracellular Matrix Proteins.

To further assess the differences in ECM protein abundance between adult and foetal dermal fibroblast ECM, Western blotting was performed. PLA_2 decellularised ECM from adult and foetal dermal fibroblast cultures solubilized in urea buffer, and the same amount of total protein was loaded into wells of a 7.5% polyacrylamide gel and the proteins were resolved by SDS-PAGE. Antibodies recognising type I collagen and type IV collagen were used for the Western blots. These data indicated that foetal dermal fibroblast deposited more type I collagen and type IV collagen than adult fibroblasts (Fig. 5.12). These data were consistent with the data obtained by quantitative proteomics and by immunofluorescence staining. The higher molecular weight of type I and type IV collagen are collagen chains formed as a collagen complex. The absence of this complex in the adult matrix suggests a lower level of expression that was not detectable by western blotting.

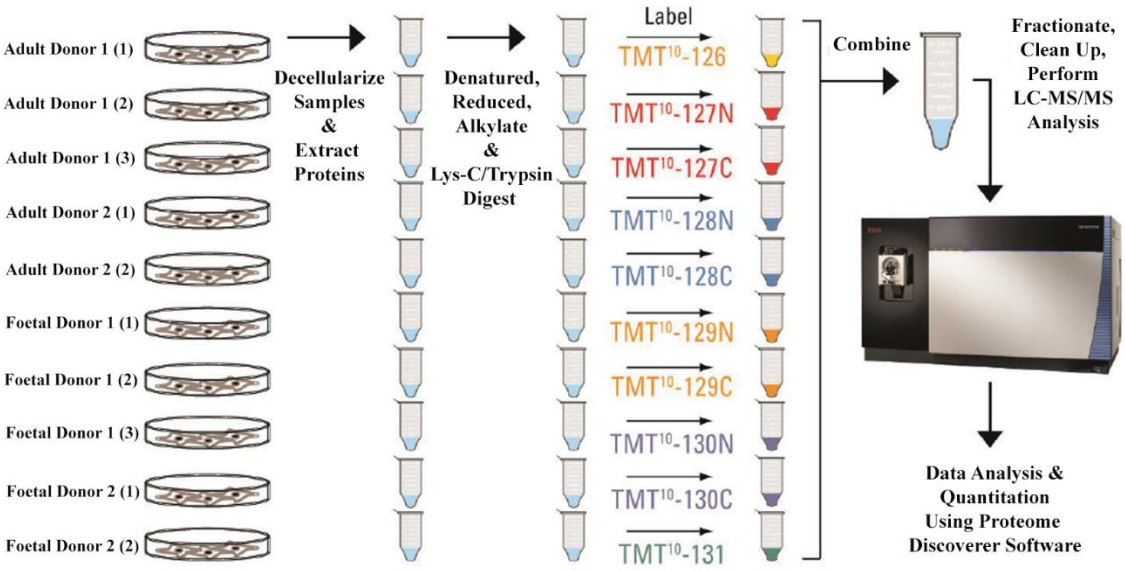

Figure 5.3: A schematic diagram of quantitative proteomic analysis of the ECM from adult and foetal dermal fibroblasts. Adult and foetal dermal fibroblasts were cultured for seven days with MMC. After 7 days, the cell layer was removed using PLA_2. The ECM proteins were solubilised and digested to peptides before being labelled with TMTplex10. The peptides were then analysed with a mass spectrometer. The data obtained were analysed using Proteome Discoverer software. Both adult and foetal donor 1 had three biological replicates while adult and foetal donor 2 had two biological replicates.

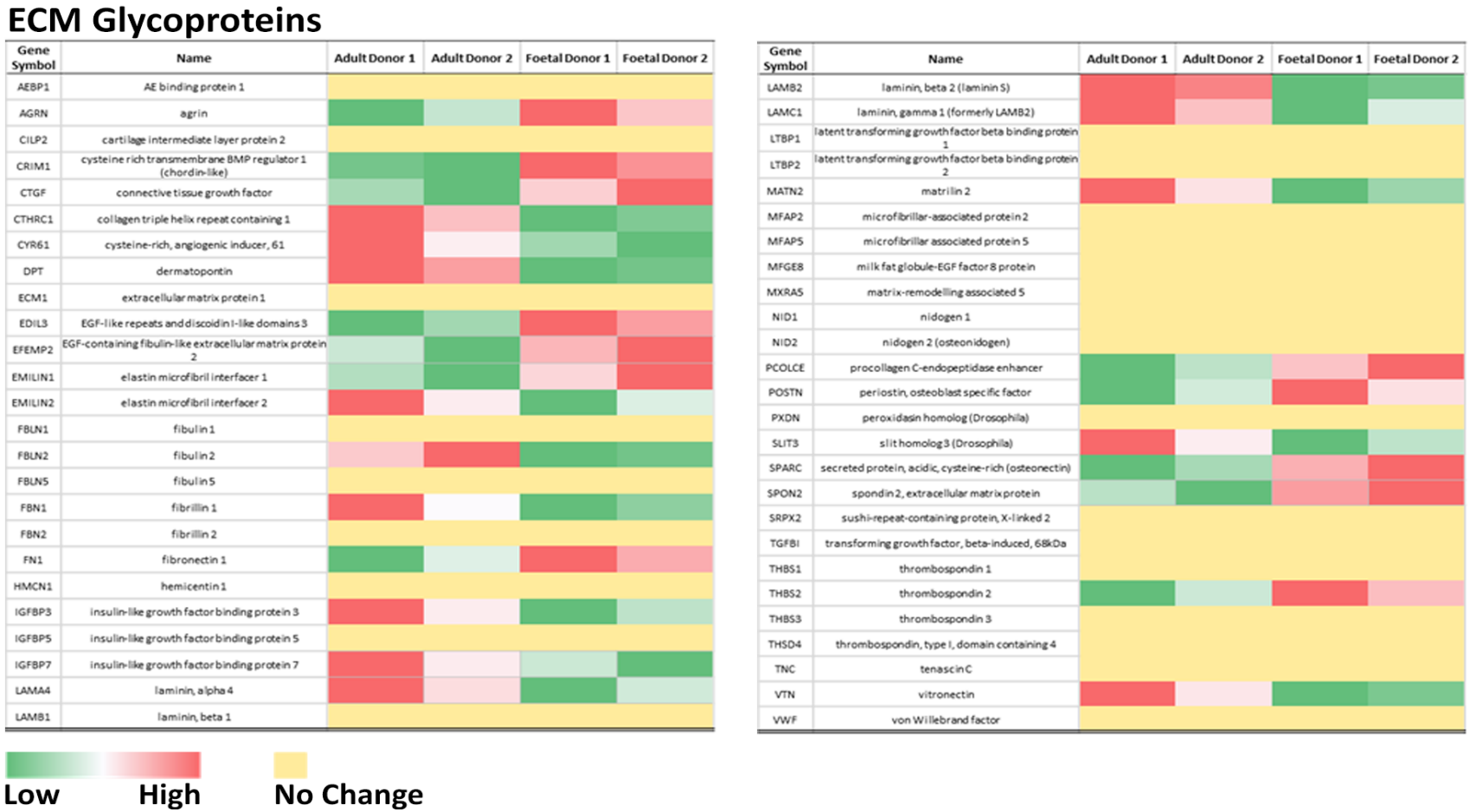

Figure 5.4: Heatmap of the quantitative expression of ECM glycoproteins deposited by adult- and foetal-dermal fibroblasts. The adult and foetal dermal fibroblasts were grown with MMC until day seven. The cell layer was removed using PLA_2. The ECM proteins were solubilised and digested to peptides before being labelled with TMTplex10. The peptides were then analysed by mass spectrometry. Green = low expression, red = high expression for each donor sample compared for that particular ECM glycoprotein. Yellow = no change for that particular protein between adult and foetal samples.

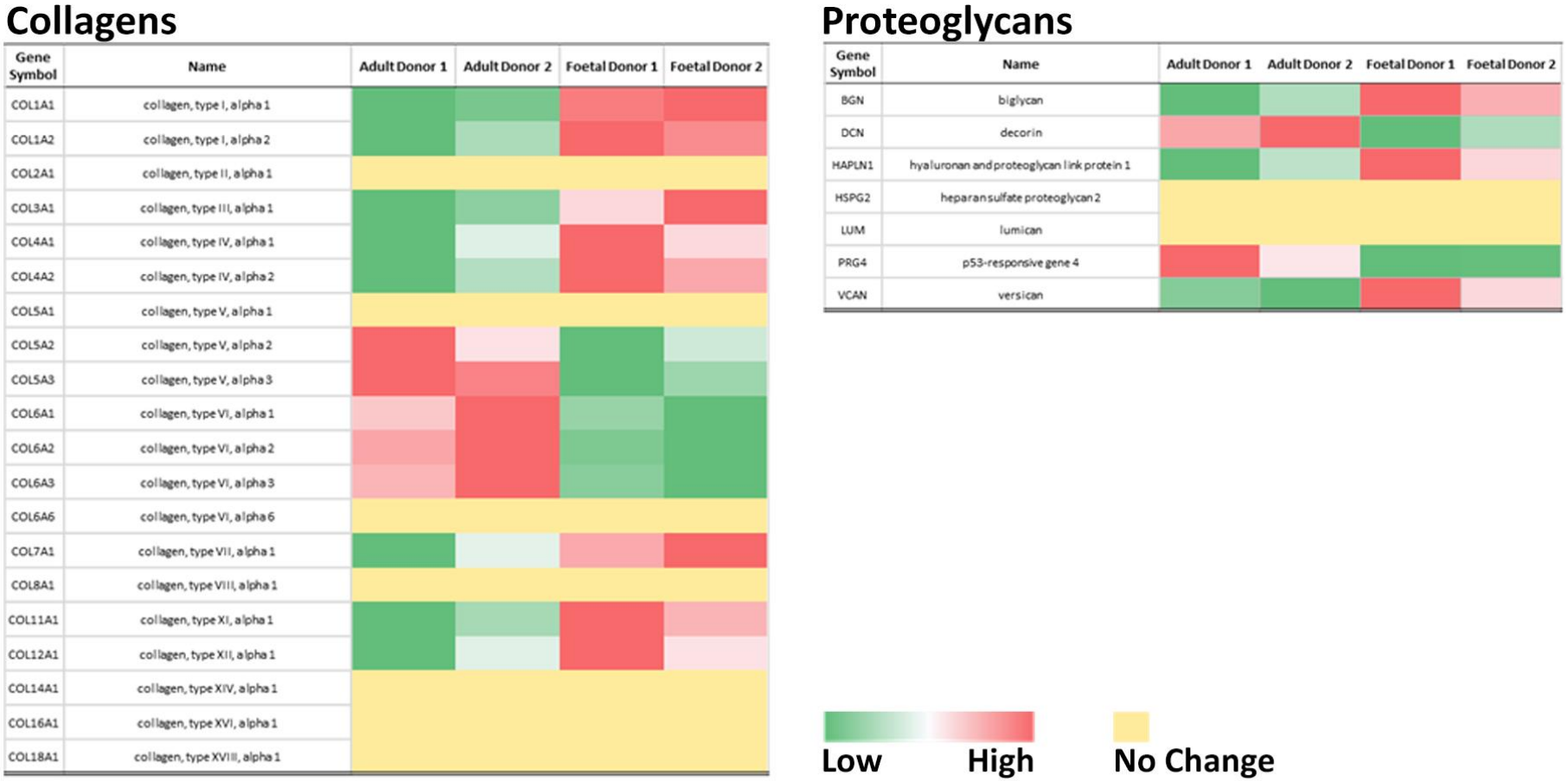

Figure 5.5: Heatmap of the quantitative expression of collagens and proteoglycans deposited by adult- and foetal-dermal fibroblast. The adult and foetal dermal fibroblasts were grown with MMC until day seven. The cell layer was removed using PLA_2. The ECM proteins were solubilised and digested to peptides before being labelled with TMTplex10. The peptides were then analysed by mass spectrometry. Green = low expression, red = high expression for each donor sample compared for that particular ECM glycoprotein. Yellow = no change for that particular protein between adult and foetal samples.

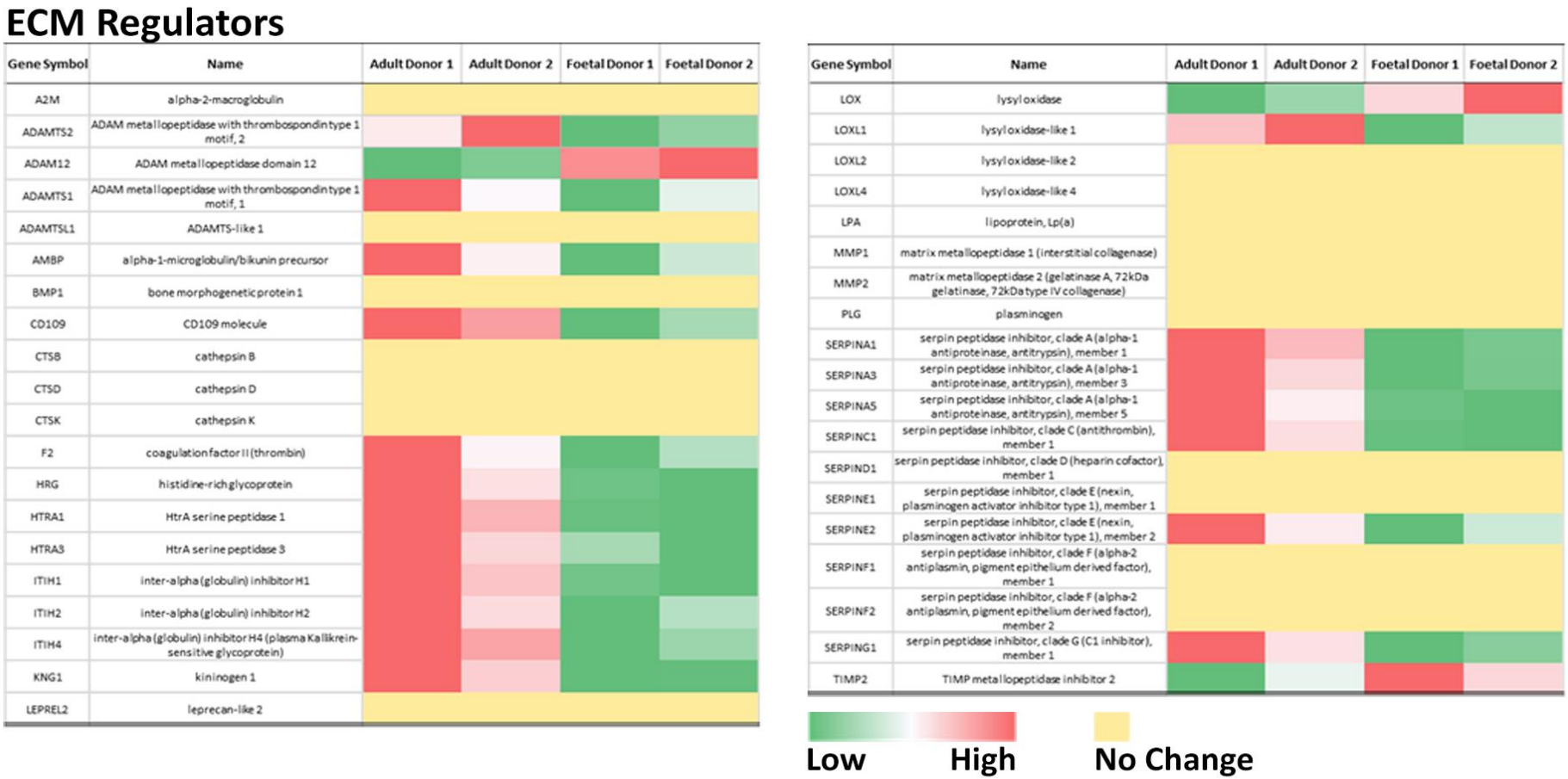

Figure 5.6: Heatmap of the quantitative expression of ECM regulators deposited by adult- and foetal-dermal fibroblast. The adult and foetal dermal fibroblasts were grown with MMC until day seven. The cell layer was removed using PLA_2. The ECM proteins were solubilised and digested to peptides before being labelled with TMTplex10. The peptides were then analysed by mass spectrometry. Green = low expression, red = high expression for each donor sample compared for that particular ECM glycoprotein. Yellow = no change for that particular protein between adult and foetal samples.

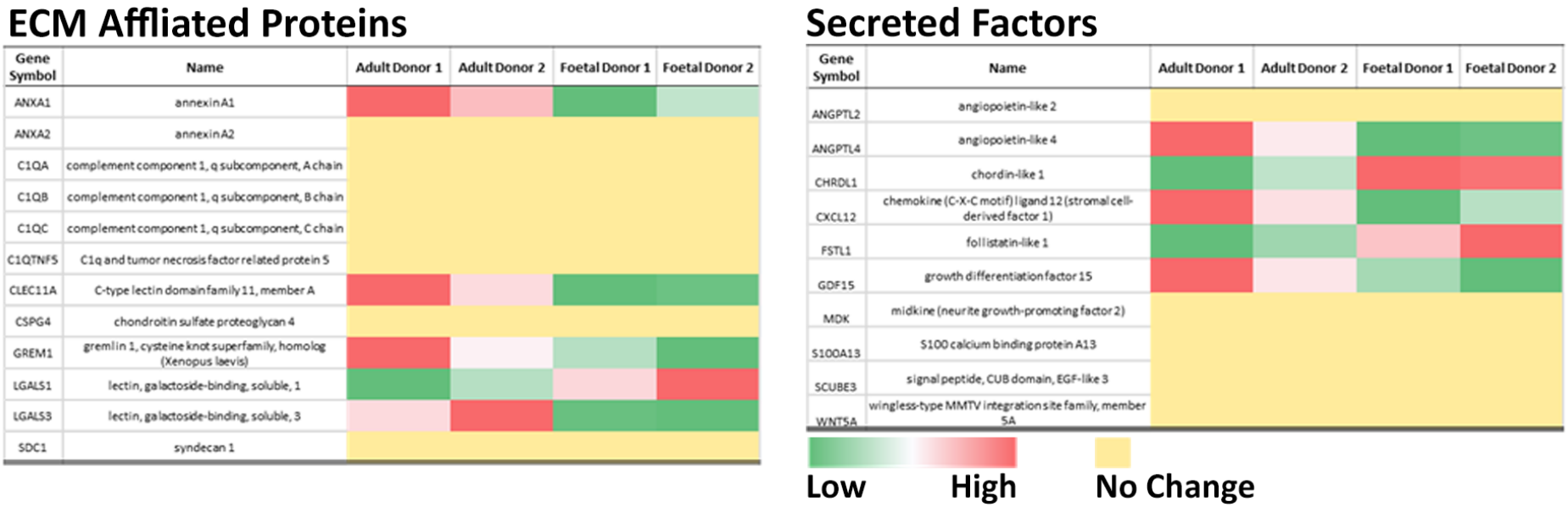

Figure 5.7: Heatmap of the quantitative expression of ECM-affiliated proteins and secreted factors deposited by adult- and foetal-dermal fibroblast. The adult and foetal dermal fibroblasts were grown with MMC until day seven. The cell layer was removed using PLA_2. The ECM proteins were solubilised and digested to peptides before being labelled with TMTplex10. The peptides were then analysed by mass spectrometry. Green = low expression, red = high expression for each donor sample compared for that particular ECM glycoprotein. Yellow = no change for that particular protein between adult and foetal samples.

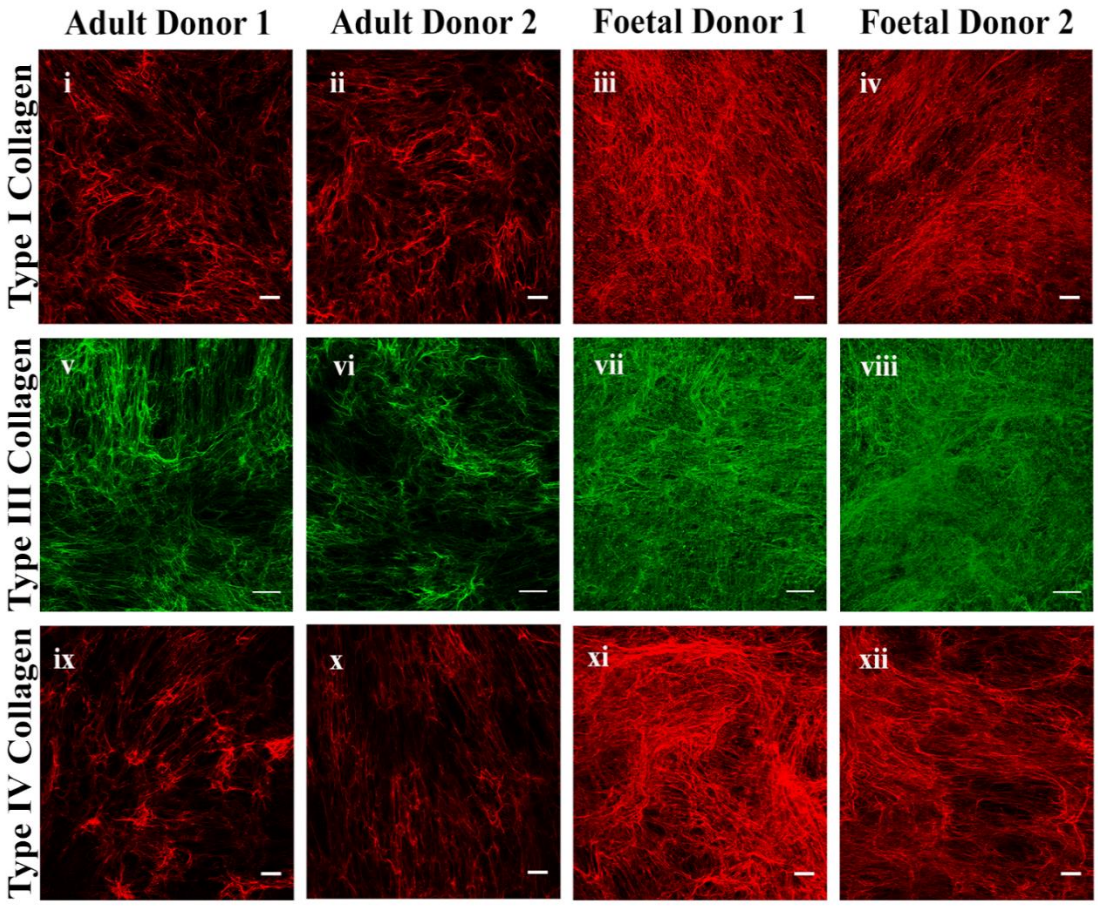

Figure 5.8: Deposition of collagens by adult or foetal dermal fibroblasts. Adult and foetal dermal fibroblasts were cultured for seven days with MMC. After seven days, the cells were removed using PLA_2, and the ECM was fixed with 4% paraformaldehyde and stained with antibodies recognising type I (i-iv), type III (v-vii), or type IV (ix-xii) collagen. Images were taken using either Nikon A1+ Confocal Inverted Microscope (i-iv & ix-xii) or Zeiss LSM510 Confocal Inverted Microscope (v-vii). Scale bars are 100µm.

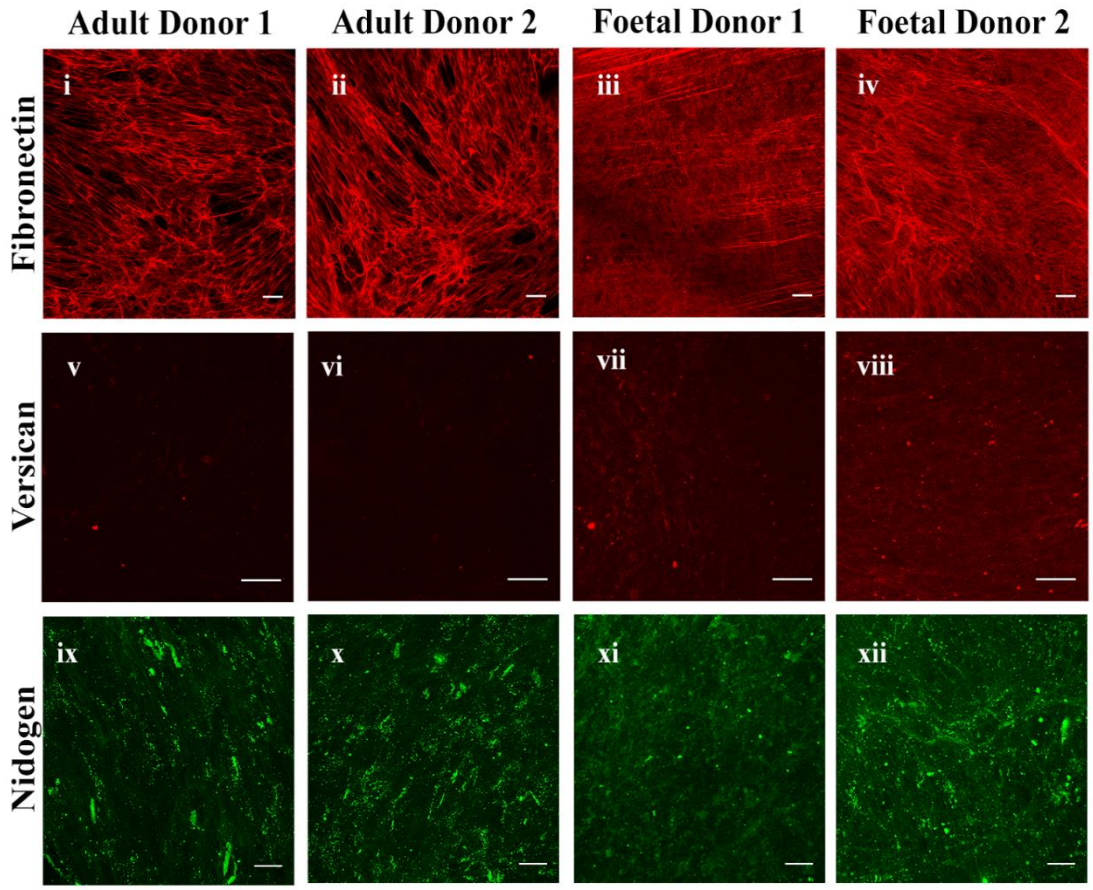

Figure 5.9: Deposition of fibronectin, versican and nidogen by adult or foetal dermal fibroblasts. Adult and foetal dermal fibroblasts were cultured for seven days with MMC. After 7 days, the cells were removed using PLA_2, and the ECM was fixed with 4% paraformaldehyde and stained with antibodies recognising fibronectin (i-iv), versican (v-vii) or nidogen (ix-xii). Images were taken using Nikon A1+ Confocal Inverted Microscope. Scale bars for fibronectin are 100μm and for versican & nidogen are 50μm.

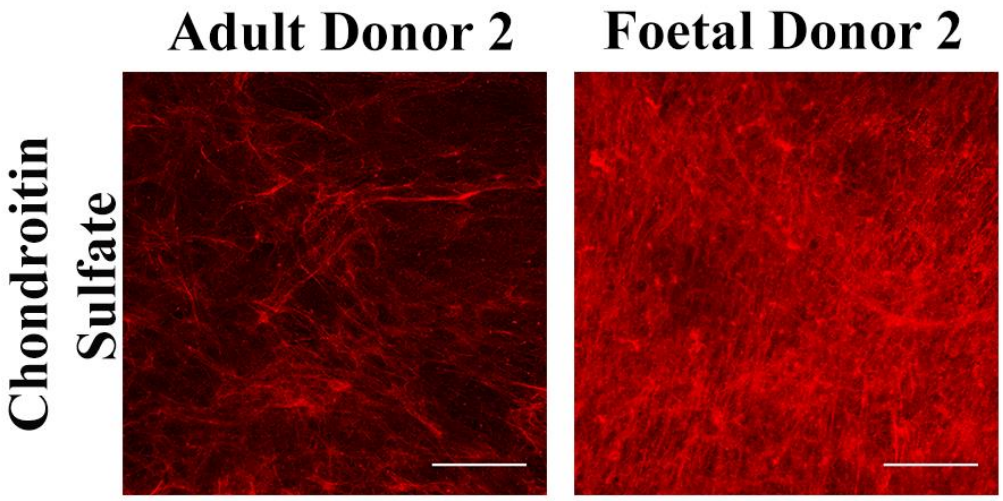

Figure 5.10: Deposition of chondroitin sulphate by adult or foetal dermal fibroblasts Adult and foetal dermal fibroblasts were cultured for seven days with MMC. After 7 days, the cells were removed using PLA_2, and the ECM was fixed with 4% paraformaldehyde and stained with an antibody recognising chondroitin sulphate. Images were taken using Nikon A1+ Confocal Inverted Microscope. Scale bars are 100μm.

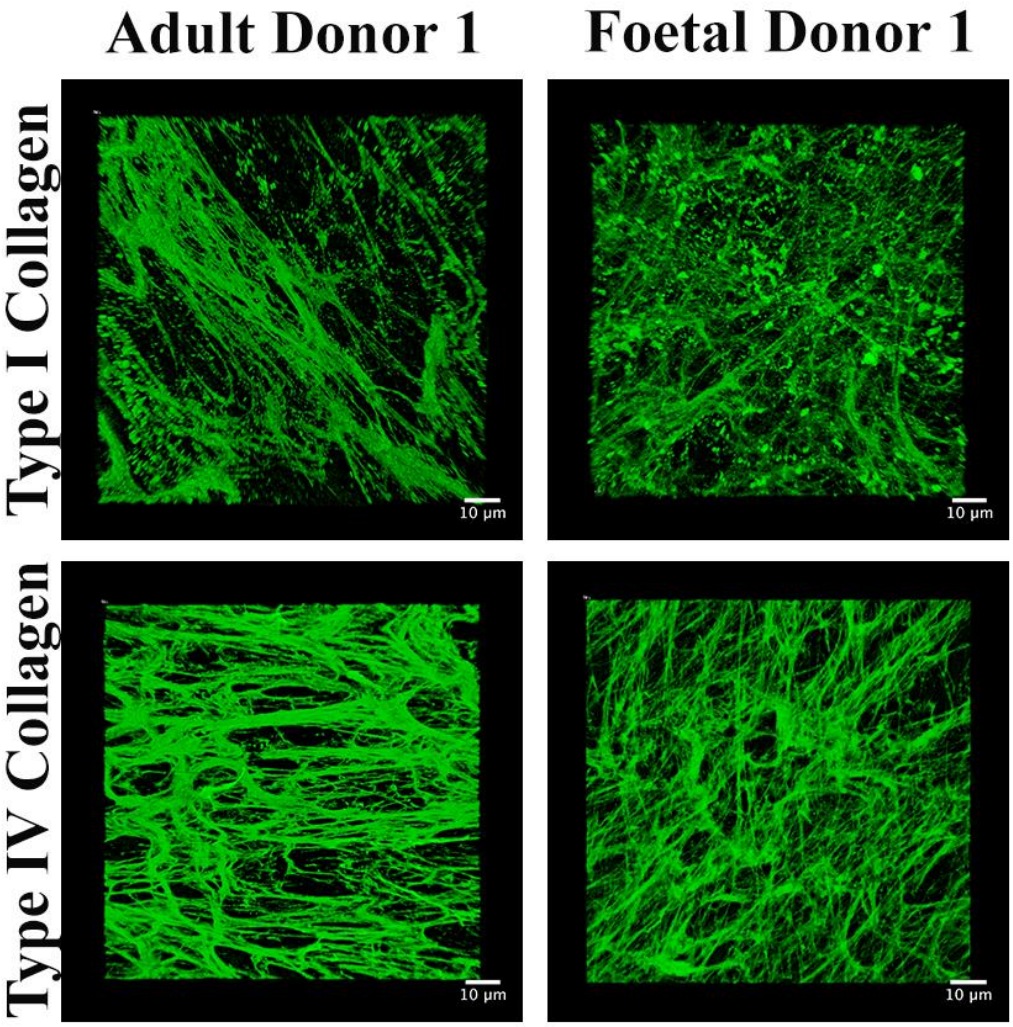

Figure 5.11: Differences in type I collagen and type IV collagen ultrastructure between adult and foetal dermal fibroblast-derived matrices. Adult and foetal dermal fibroblasts were cultured for seven days with MMC. After 7 days, the cells were removed using PLA_2, and the ECM was fixed with 4% paraformaldehyde and stained with antibodies recognising type I collagen and type IV collagen. Z-stacked images were taken using a Nikon A1+ confocal microscope. Represented is a compressed Z-stacked image generated using Fiji Image J program. Scale bars are 10µm.

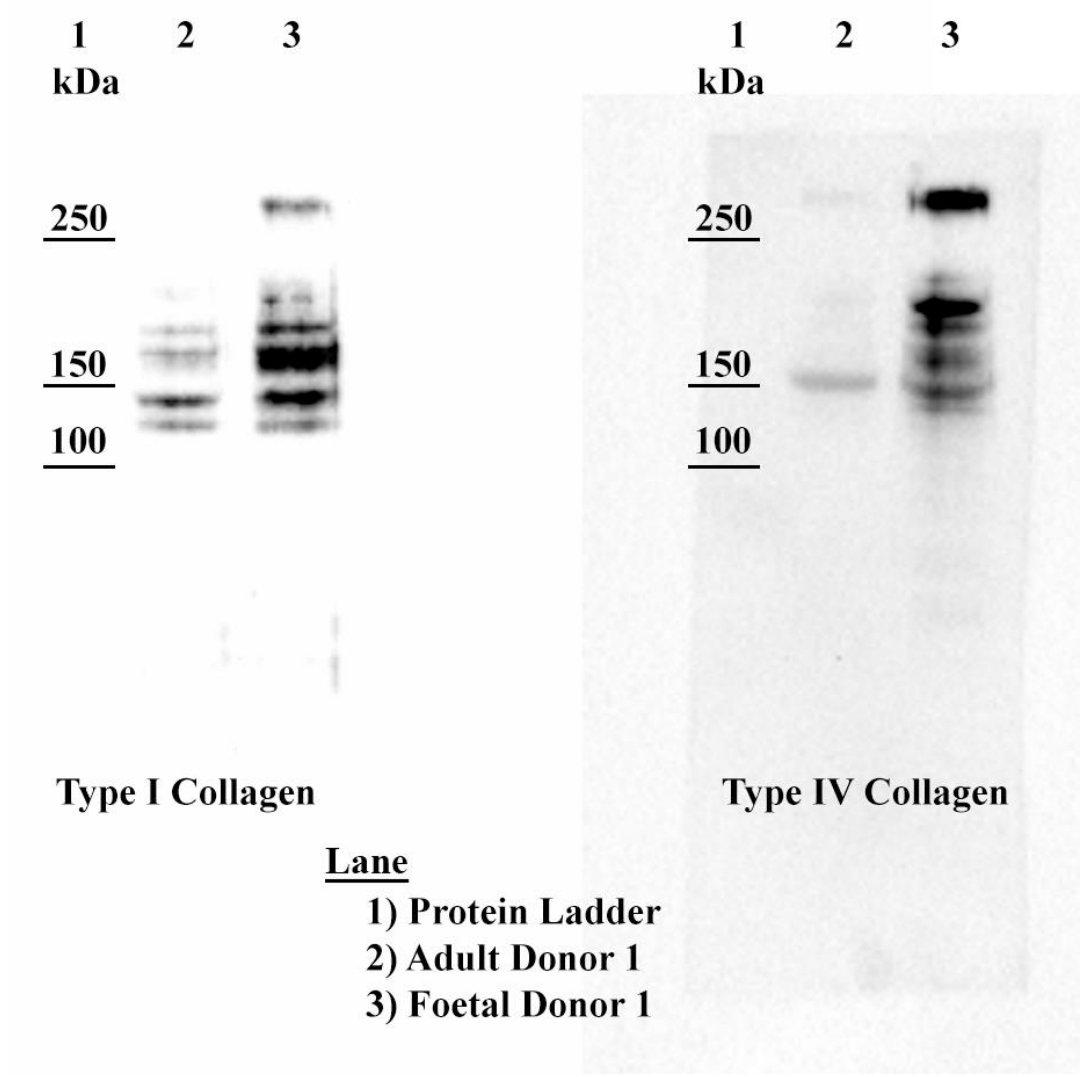

Figure 5.12: Western blots of type I collagen and type IV collagen deposited by adult or foetal dermal fibroblasts. The adult and foetal dermal fibroblasts were grown with MMC for seven days. The fibroblasts were removed using PLA_2 before the ECM was solubilized in urea buffer and the proteins separated by SDS-PAGE using 7.5% gel. Proteins were transferred to a PVDF membrane. Western blotting with ECL detection was conducted using antibodies recognising type I collagen and type IV collagen

5.3.5 Quantification of the ECM deposited.

Brink *et al.*[320] reported that foetal dermal fibroblasts secrete a higher quantity of total ECM protein compared to that secreted by adult dermal fibroblasts. To investigate whether this was the case with our ECM samples, the total quantity of ECM protein produced by foetal and adult dermal fibroblasts was assessed. Both adult and foetal dermal fibroblasts were cultured for 7 days in MMC media before being decellularized with PLA_2 and solubilized with urea buffer. The protein concentration was determined using a filter paper-based protein quantification assay that was developed by Minamide and Bamburg[224] (section 2.4.2). This assay enables determination of the protein concentration in the presence of reducing agents, detergents and other substances that interfere with other protein quantification assays. Using this assay a significantly higher amount of ECM protein was found to be deposited by foetal dermal fibroblasts compared to that deposited by their adult counterparts. No significant difference in total protein was observed between the two adult and the two foetal donors (Fig. 5.13).

5.3.6 Proliferation of Keratinocytes on Adult or Foetal Dermal Fibroblast Matrices

The ability of adult dermal fibroblast-derived matrices (AD-MAT) and foetal dermal fibroblast-derived matrices (FT-MAT) to support the proliferation of keratinocytes was investigated. Keratinocytes were observed to adhere and proliferate well on both AD-MAT and FT-MAT. A uniform population of cells having small cobblestone morphology was observed for keratinocytes grown on both AD-MAT and FT-MAT (Fig. 5.14). Cell proliferation was quantified after culturing the keratinocytes on either AD-MAT or FT-MAT in DKSFM for three days. The cells were fixed before being stained with DAPI, and the number of nuclei was determined. A significantly higher number of nuclei indicating a higher proliferative response ($p \leq 0.05$) was observed in keratinocytes that were grown on the FT-MAT as compared to cells grown on the AD-MAT (Fig. 5.15).

5.3.7 Keratinocyte Cell Size on Adult or Foetal Dermal Fibroblast Matrices

In chapter IV, it was shown that a higher proportion of keratinocytes grown on aHDF (adult donor 1) derived ECM were of a smaller cell size compared to those cultured

on type I collagen. Accordingly, the effect of matrix on keratinocyte size was determined for keratinocytes grown on adult dermal fibroblast-derived ECM (adult donor 2) and foetal dermal fibroblast-derived ECM (foetal donor 1 & 2). Type I collagen-coated TCP was used as a control. Keratinocytes were grown on the different substrates for three days in DKSFM before being fixed and stained with phalloidin-Alexa Fluor® 488. Using an Olympus IX-81 high content screening inverted microscope, 64 non-overlapping images were taken (Fig. 5.16). Cell Profiler® software was used to determine the cell size based on cell area as indicated by the actin staining. The measurements of cell area from the images were categorised as follows: small<medium<large = $<2000\mu m^2<4000\mu m^2<6000\mu m^2$ and the number of cells in each category were determined. A significantly higher proportion of keratinocytes growing on AD-MAT or FT-MAT were found to fit into the smallest cell size category, compared to that observed for keratinocytes growing on type I collagen. No significant difference in cell size was observed between keratinocytes on AD-MAT or FT-MAT (Fig. 5.17).

5.3.8 Microarray Analysis of Keratinocytes Grown on Adult or Foetal Dermal Fibroblast Derived-ECM

To investigate how differences in the proteins in adult and foetal ECM affected the gene expression of keratinocytes grown on these matrices, a microarray analysis of gene expression was performed. Figure 5.18 is a schematic diagram of the microarray analysis used for keratinocytes grown on either adult or foetal dermal fibroblast-derived matrices. Type I collagen-coated TCP was used as a control, as it is typically the substrate used for keratinocyte culture. Briefly, keratinocytes were cultured on these three different substrates in DKSFM for three days before total RNA was extracted and used for the microarray analysis using the Affymetrix HuGene 2.0 ST Chipset. To ensure the quality and integrity of the microarray data, principal component analysis (PCA) and hierarchal dendrogram clustering were conducted. PCA is a technique used to emphasise on the variation while portraying the strong patterns of sample treatments from the dataset. This allows PCA to display distinct population based on the sample treatments. Hierarchal dendrogram clustering is used to visualise the similarity between sample clusters. If samples that have been obtained from the same treatment group do not cluster, it is likely that the microarray data

quality and integrity is low[321]. In the present study, both analyses: the PCA and the hierarchical dendrogram clustering showed that the samples clustered according to the substrate on which the keratinocytes were grown. Thus, regardless of the donor, the gene expression patterns of keratinocytes grown on FT-MAT were more similar then the gene expression patterns of keratinocytes grown on AD-MAT or type I collagen (Fig. 5.19).

Gene Ontology (GO) analysis of upregulated genes within the microarray dataset revealed biological processes representing functions related to cell division when keratinocytes were grown on FT-MAT (Fig. 5.20). In contrast, when keratinocytes were cultured on AD-MAT, biological processes indicative of keratinocyte differentiation was observed (Fig. 5.21). Transcriptomic heatmap profiles revealed major differences in gene expression when keratinocytes were grown on the different substrates. Genes associated with cell cycle, DNA repair and DNA double-stranded break repair were observed to be highly upregulated when keratinocytes were cultured on FT-MAT. In contrast, these genes were downregulated when keratinocytes were grown on type I collagen (Fig. 5.22). Genes associated with epidermal development and lipid metabolic processes were highly upregulated when keratinocytes were cultured on AD-MAT and type I collagen. However, when keratinocytes were grown on either FT-MAT, only a small proportion of genes associated with epidermal development and lipid metabolic processes were upregulated (Fig. 5.23). A further functional analysis using the STRING protein interaction database[322] revealed that FT-MAT contained a microenvironment that promotes BMP4 signalling (Fig. 5.24).

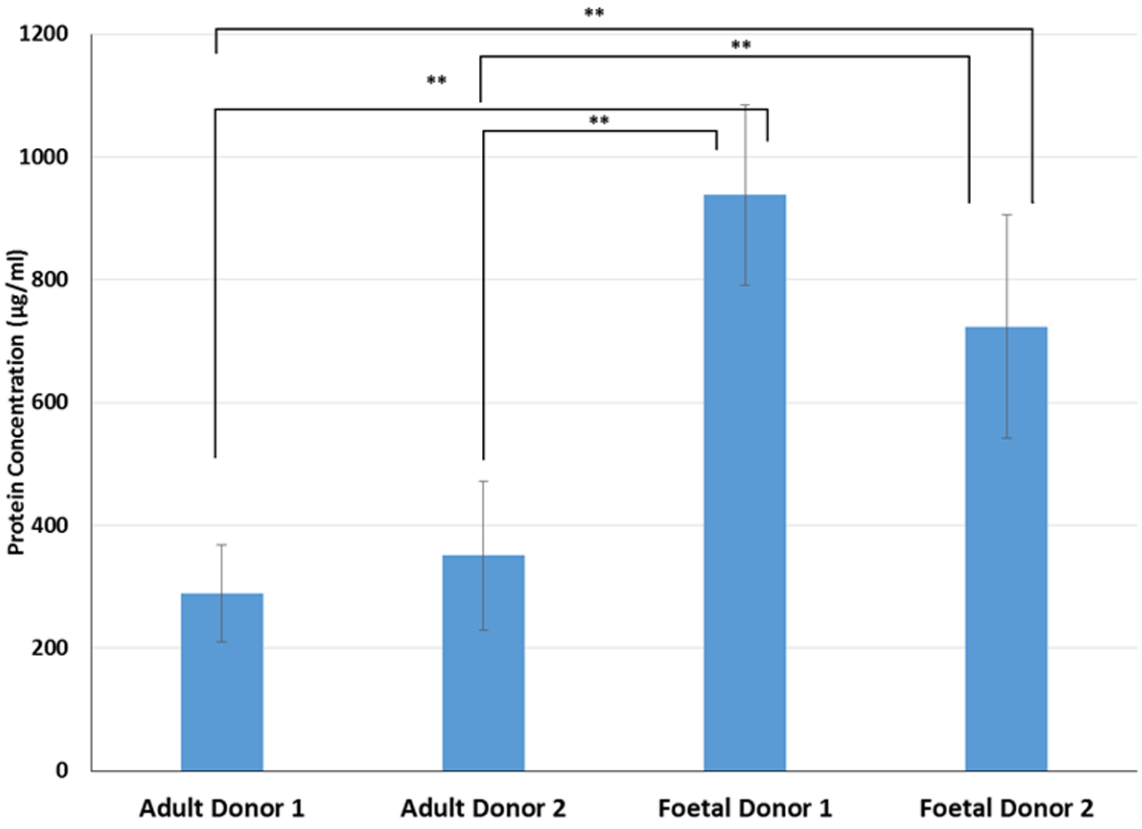

Figure 5.13: Quantification of the ECM secreted and deposited by adult and foetal dermal fibroblasts. Adult and foetal dermal fibroblasts were cultured for seven days with MMC. After 7 days, the cells were removed using PLA_2, the ECM was extracted, and the protein concentration was determined (section 2.4.2).Data are expressed as mean ± SD. Statistical analysis using ANOVA followed by Tukey's test was conducted. **P<0.01

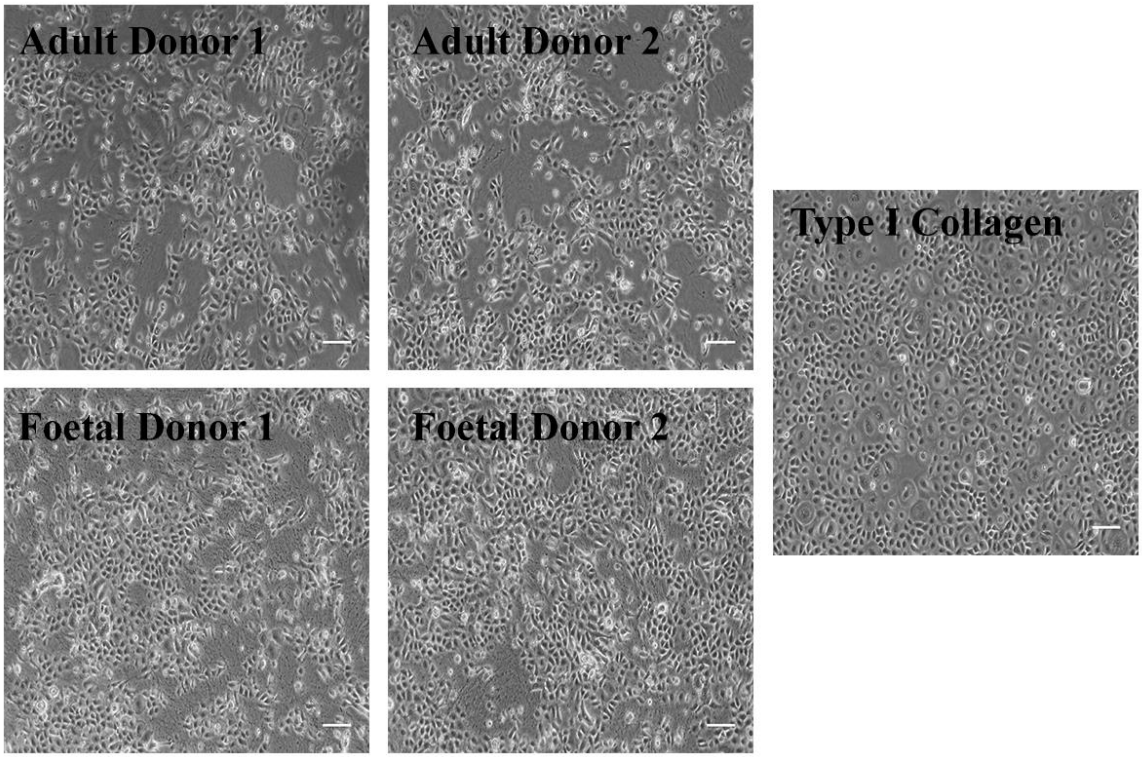

Figure 5.14: Phase contrast images of keratinocytes growing on adult or foetal dermal fibroblast matrices, or type I collagen-coated tissue culture plastic. Keratinocytes (2 x 10^4 cells) were seeded into wells of a 24-well plate that contain different growth substrates and were cultured in defined keratinocyte serum-free media for three days. Images were taken using Olympus IX-51 Inverted Microscope. Scale bars are 200µm.

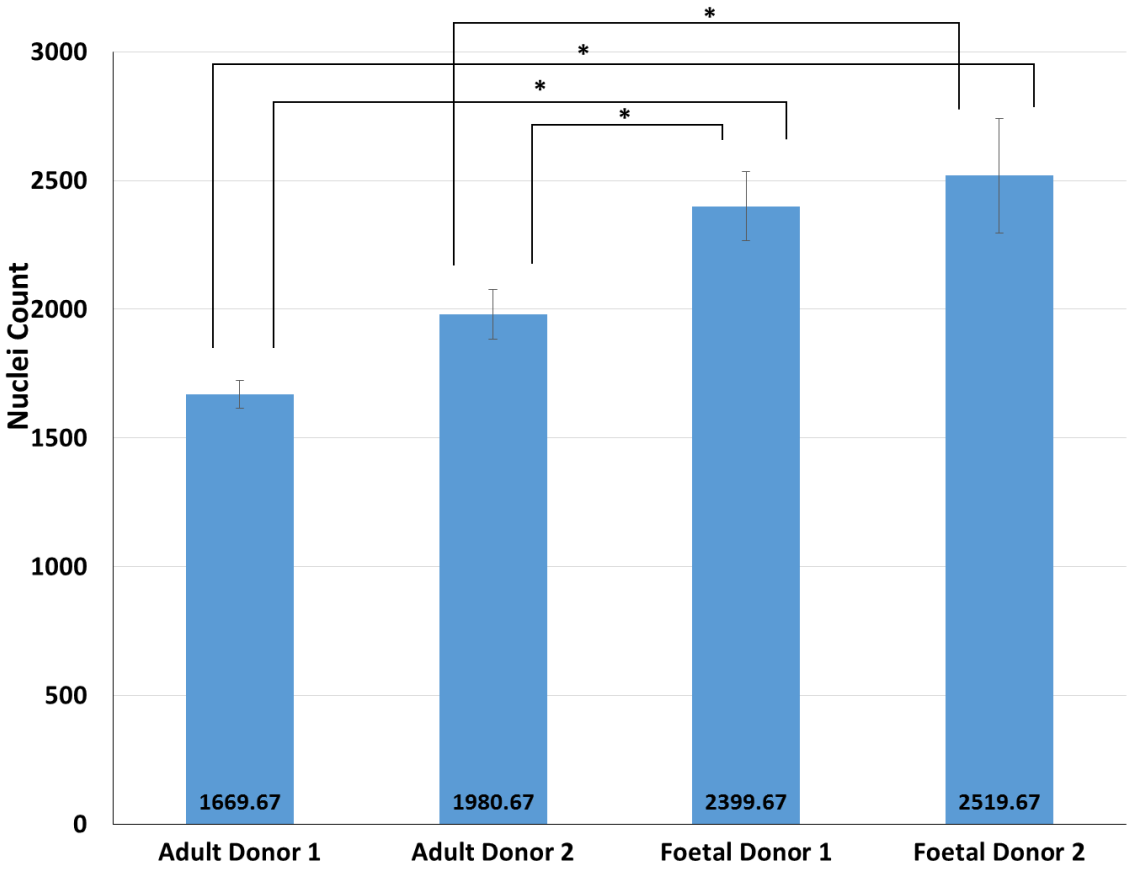

Figure 5.15: Growth of keratinocytes on adult or foetal dermal fibroblast matrices. Keratinocytes (1 x 10^4 cells) were seeded into wells of a 48-well plate that contained either adult fibroblast-derived matrix or foetal fibroblast-derived matrix and were cultured in DKSFM for three days. The keratinocytes were fixed with 4% paraformaldehyde. After being stained with DAPI, nuclei from a set of nine images per samples were counted. The data shown are the mean nuclei count ± standard deviation. The data shown are representative of two experiments. Statistical analysis using ANOVA followed by a Tukey's test was conducted. *P<0.05

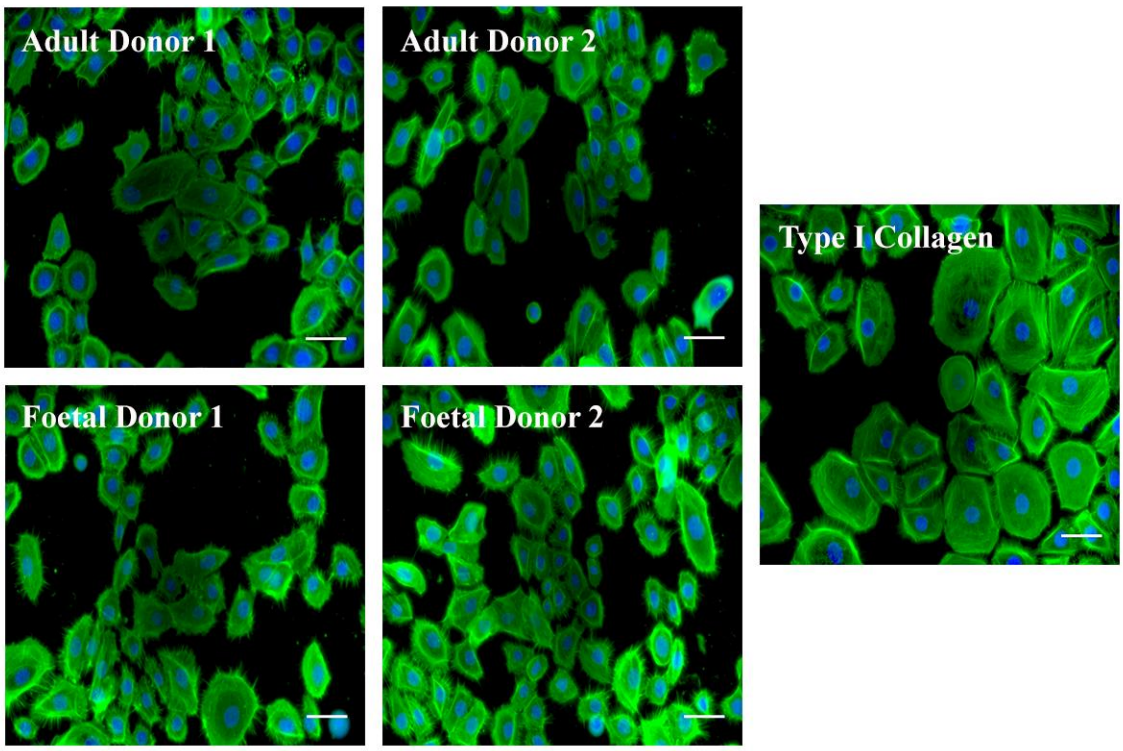

Figure 5.16: Representative images of immunofluorescence staining for F-actin of keratinocytes grown on different substrates. Keratinocytes (1 x 10^4 cells) were seeded into wells of a 48-well plate that either contained adult dermal fibroblast-derived matrix (Adult Donor 1 & 2), foetal dermal fibroblast-derived matrix (Foetal Donor 1 & 2) or a type I collagen coating (3ug/cm^2). They were cultured for **three days** in DKSFM, then fixed with 4% paraformaldehyde and stained with phalloidin-Alexa Fluor® 488 (Green). Nuclei were stained with DAPI (Blue).

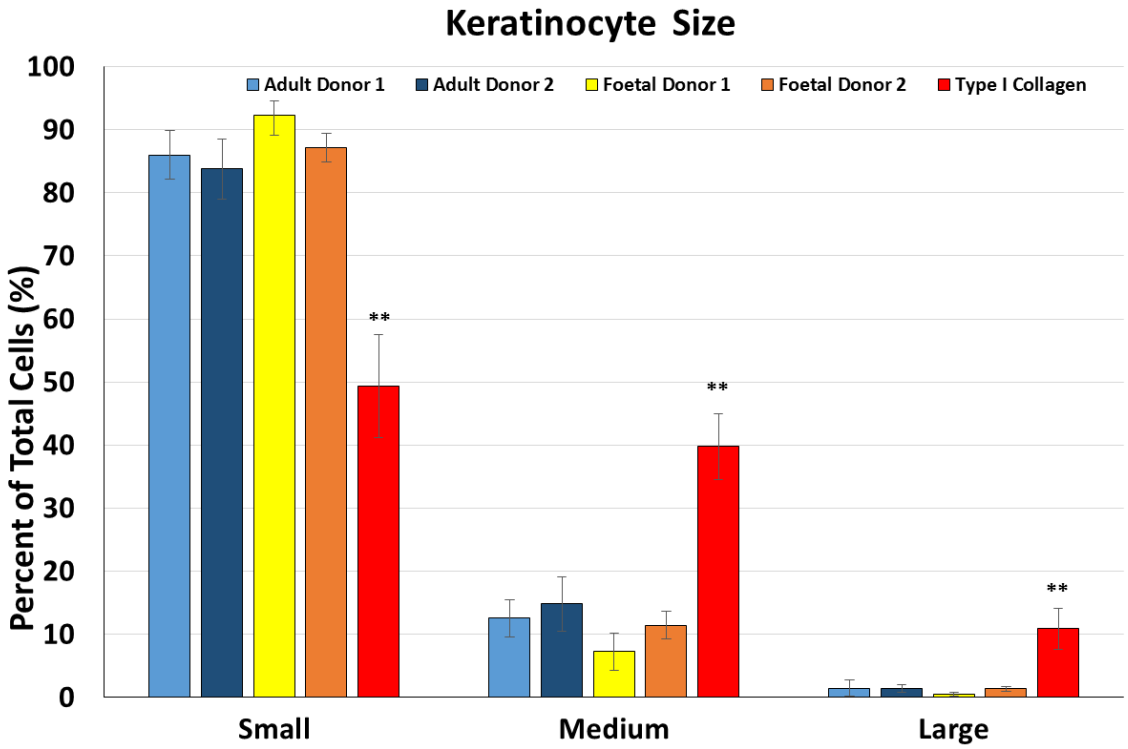

Figure 5.17: The size of keratinocytes grown on different substrates. The percent of keratinocytes in each size category is shown. Cell size was categorised as small, medium and large based on cell area (small<medium<large = <2000µm^2<4000µm^2<6000µm^2). Data are expressed as mean ± SD. Statistical analysis using ANOVA followed by a Tukey's test was conducted. **P<0.01. The data shown are representative of two experiments.

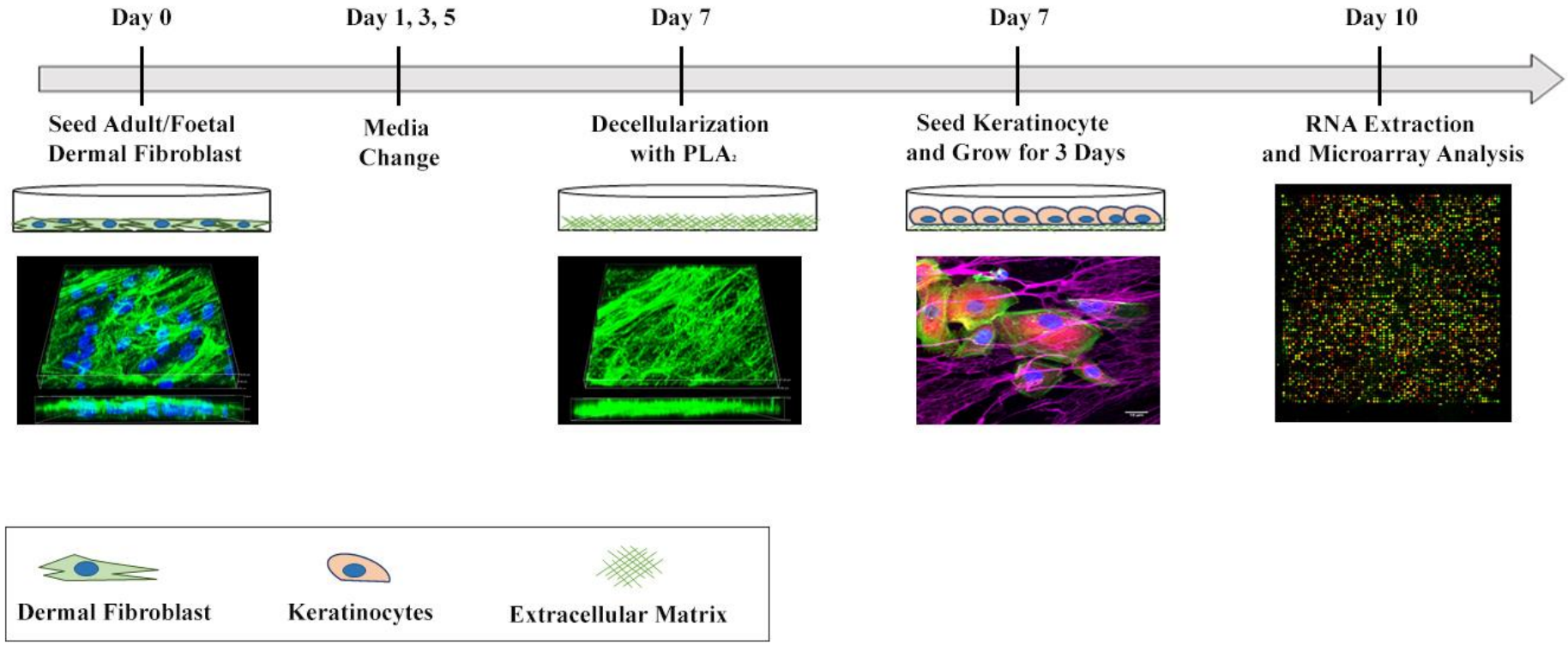

Figure 5.18: Schematic diagram of the microarray analysis of keratinocytes grown on either adult or foetal dermal fibroblast-derived matrices. Adult and foetal dermal fibroblasts were cultured for seven days with MMC. After 7 days, the cells were stripped using PLA_2, and the ECM seeded with keratinocytes. The cells were grown for three days before total RNA was extracted. Microarray analyses of the samples were processed using Affymetrix HuGene 2.0 ST Chipset. The data were curated to retain gene expression differences with a statistical significance of equal to or less than 0.05.

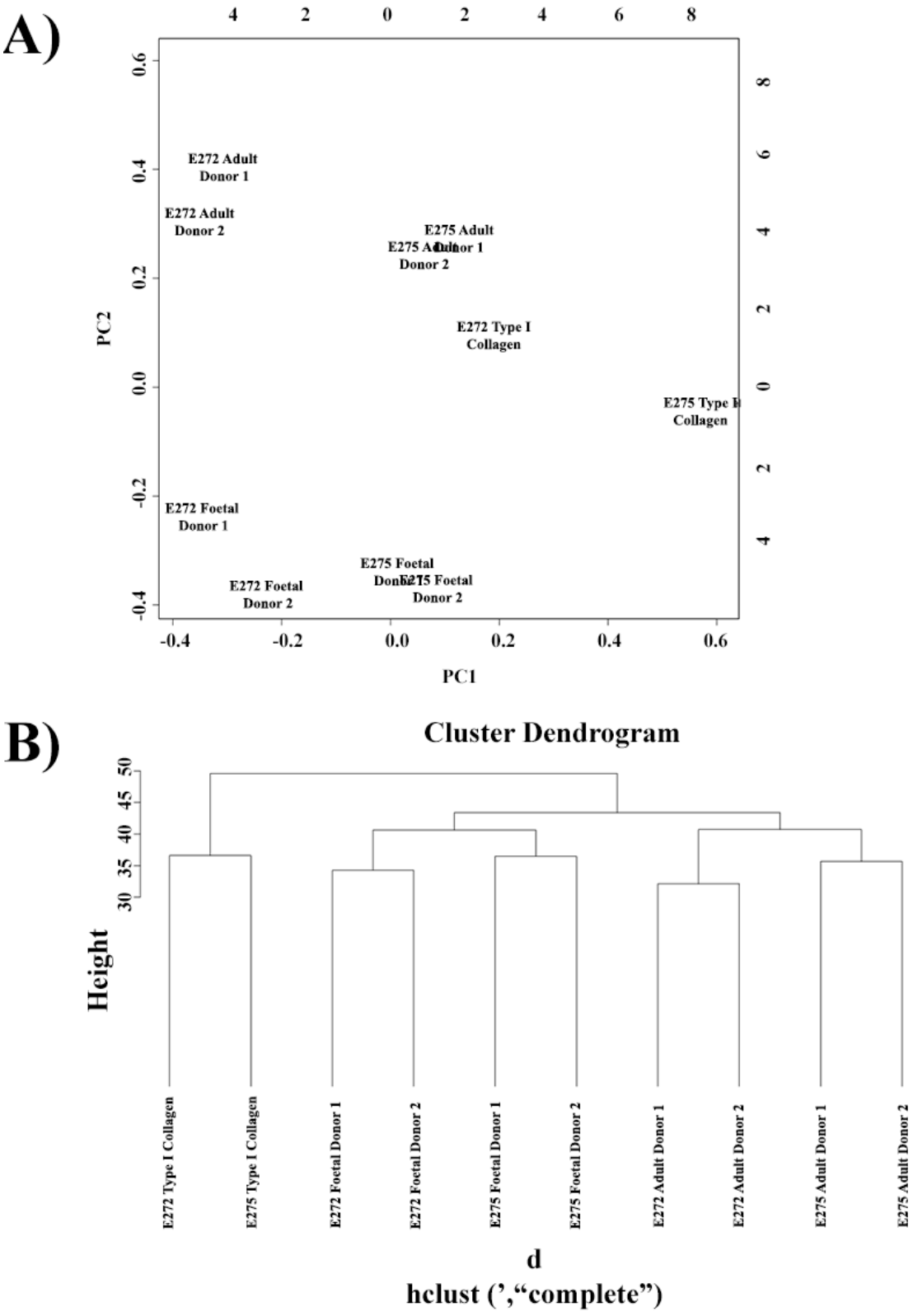

Figure 5.19: Microarray data cluster analysis

A) Principal component analysis (PCA)

B) Dendrogram Hierarchal Clustering

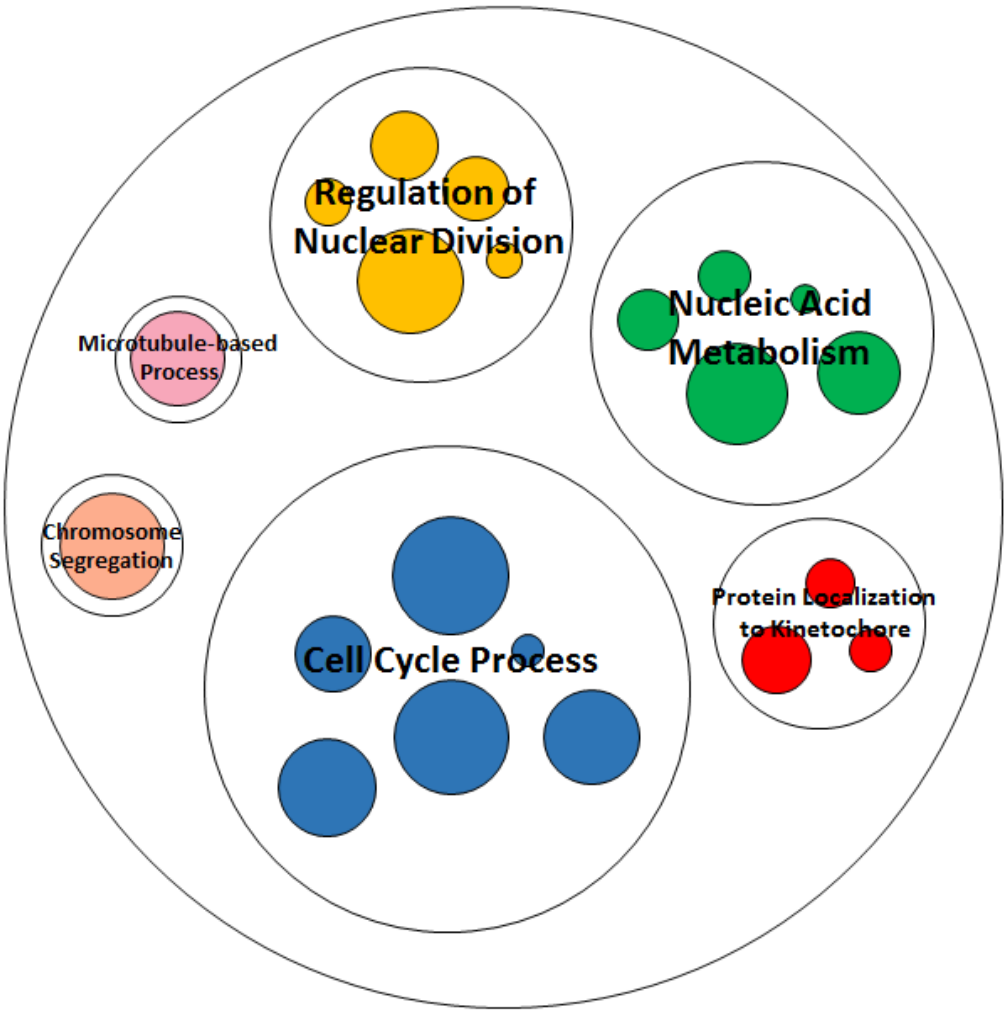

Figure 5.20: TreeMap of the gene ontology analysis of genes upregulated in keratinocytes grown on the foetal dermal fibroblast derived-matrix. Gene expression values with more than a two-fold change and adjusted p-value of ≤0.05 were used for gene ontology (GO) analyses. The dataset was analysed with the Gene Ontology Enrichment Analysis and Visualization (GORILLA) tool, to generate enriched GO terms. The output was further analysed with Reduce + Visualise Gene Ontology (REVIGO) tool, to summarise and collate the GO terms into representative biological processes. The resulting REVIGO output was visualised using Drastic Treemap software. The size of the circles is inversely correlated with the adjusted p-value (i.e., larger size indicates a smaller p-value). Gene ontology terms and their categorization of the representative biological processes used to generate this treemap are shown in Appendix C.

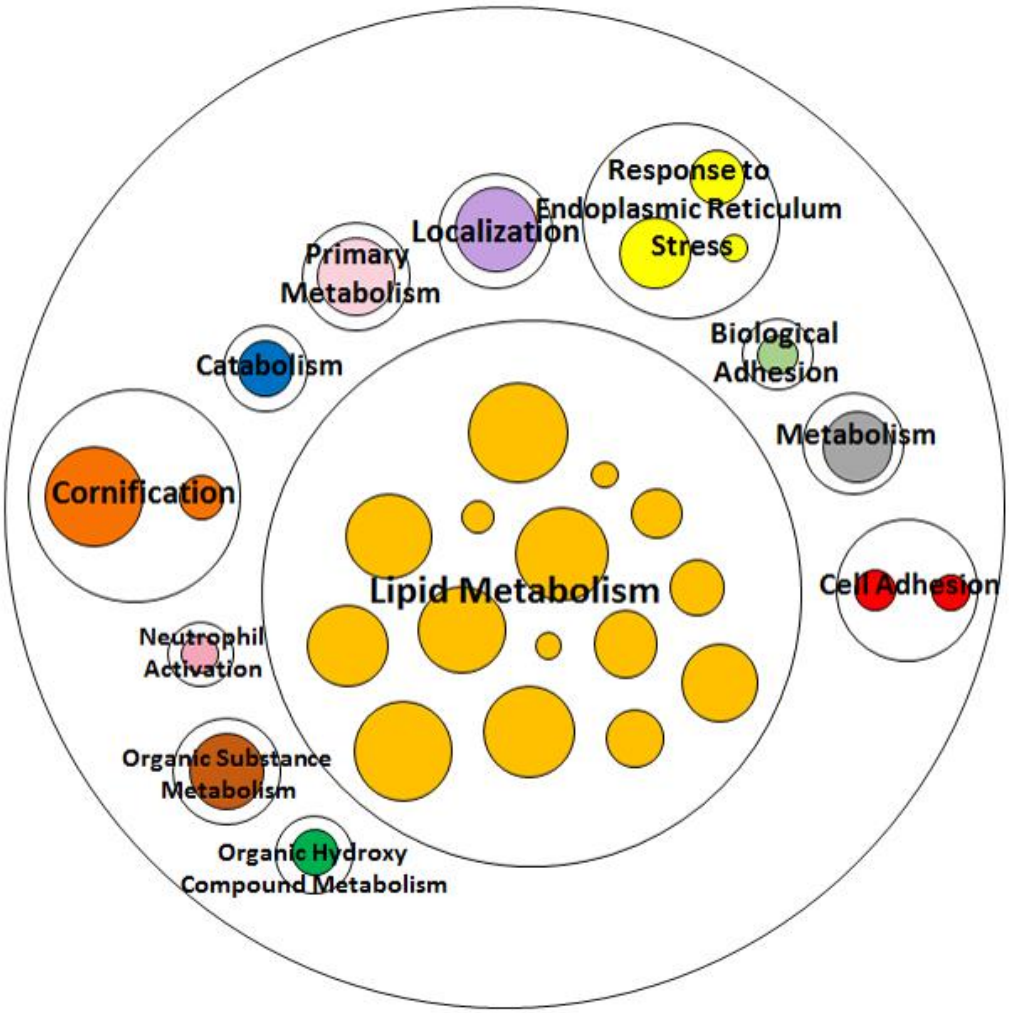

Figure 5.21: TreeMap of the gene ontology analysis of genes upregulated in keratinocytes grown on adult dermal fibroblast derived-matrix. Gene expression values with more than a two-fold change and adjusted p-value of ≤0.05 were used for gene ontology (GO) analyses. The dataset was analysed with the Gene Ontology Enrichment Analysis and Visualization (GORILLA) tool, to generate enriched GO terms. The output was further analysed with Reduce + Visualise Gene Ontology (REVIGO) tool, to summarise and collate the GO terms into representative biological processes. The resulting REVIGO output was visualised using Drastic Treemap software. The size of the circles is inversely correlated with the adjusted p-value (i.e., larger size indicates a smaller p-value). Gene ontology terms and their categorisation of the representative biological processes used to generate this treemap are shown in Appendix C.

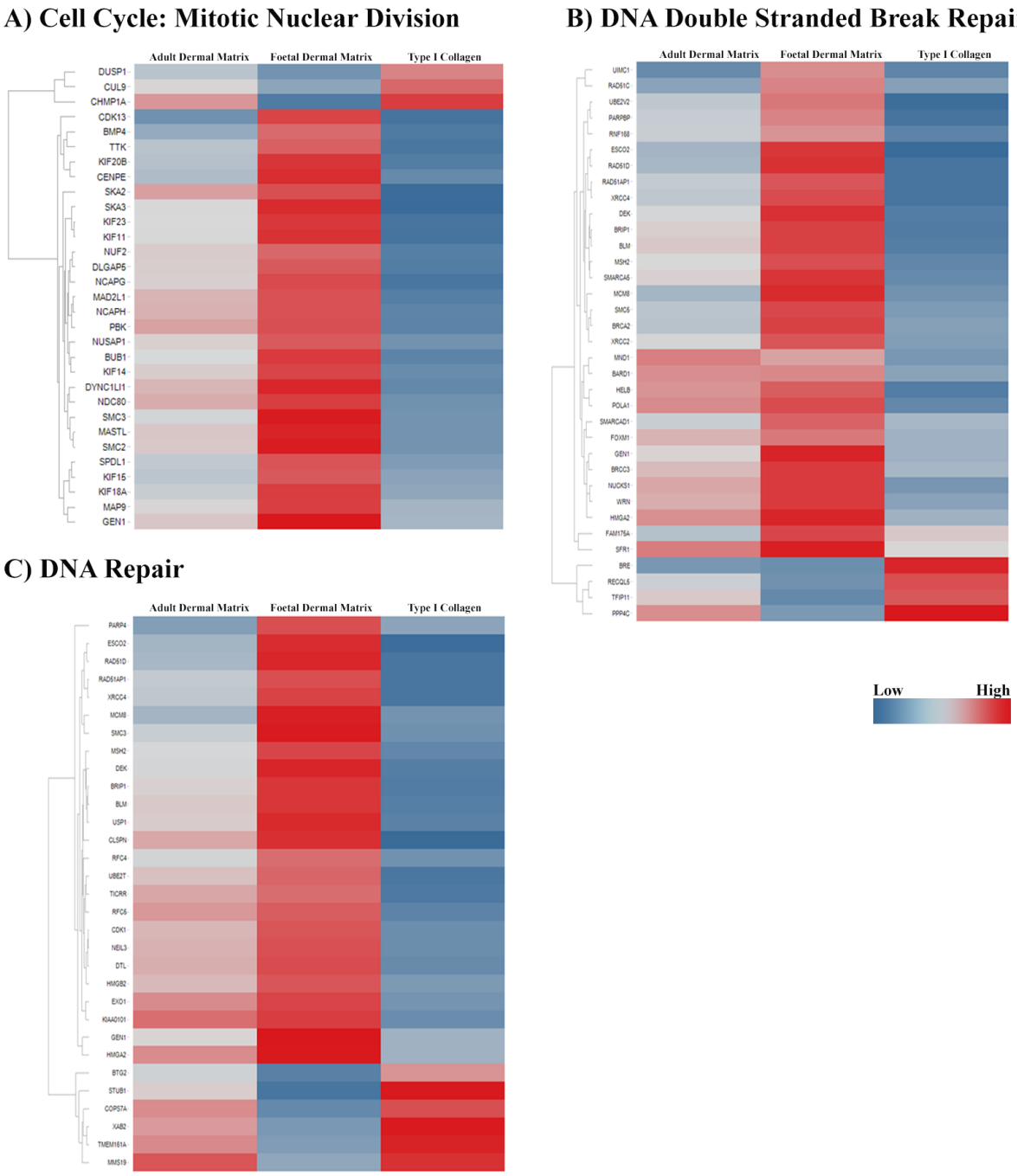

Figure 5.22: Transcriptome heatmap profiles of cell cycle, DNA repair and DNA double-stranded break repair genes for keratinocytes grown on different substrates. Microarray analysis of the genes expressed differentially by keratinocytes grown on either adult dermal fibroblast derived-matrix, foetal dermal fibroblast derived-matrix or type I collagen-coated TCP. Tibco® Spotfire software was used to analyse and display the microarray dataset to show the hierarchal cluster with average linkage analysis of normalised gene expression (adjusted p-value of <0.05). Differentially overexpressed (Red) and underexpressed (Blue) genes were observed in keratinocytes grown on the three different substrates for A) cell cycle, B) DNA double-stranded break repair, and C) DNA repair.

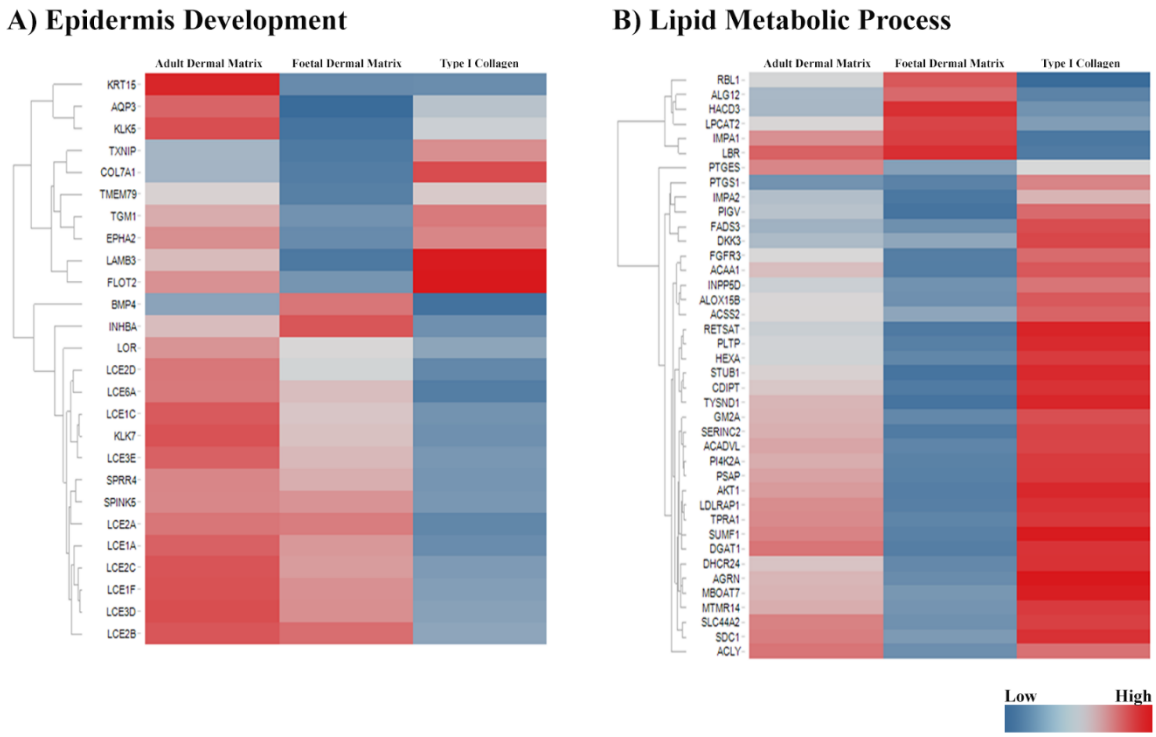

Figure 5.23: Transcriptome heatmap profiles of epidermis development and lipid metabolic processes genes for keratinocytes grown on different substrates. Microarray analysis of the genes expressed differentially by keratinocytes grown on either adult dermal fibroblast derived-matrix, foetal dermal fibroblast derived-matrix or type I collagen-coated TCP. Tibco® Spotfire software was used to analyse and display the microarray dataset to show the hierarchal cluster with average linkage analysis of normalised gene expression (adjusted p-value of <0.05). Differentially overexpressed (Red) and underexpressed (Blue) genes were observed in keratinocytes grown on the three different substrates for A) epidermis development and B) lipid metabolism.

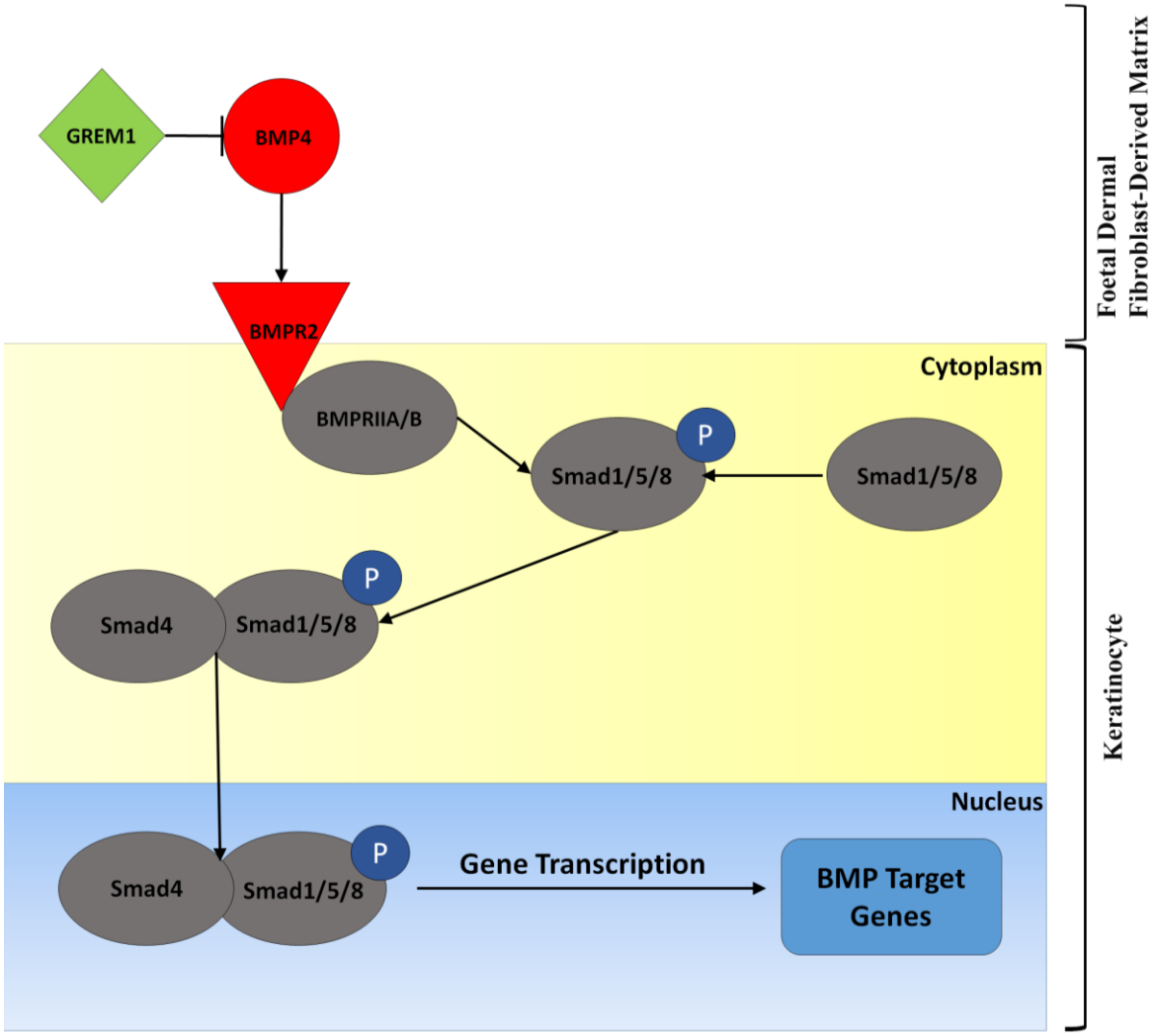

Figure 5.24: A Schematic of the BMP4 signalling pathway for keratinocytes grown on foetal dermal fibroblast-derived matrix. The pathway was created using STRING analysis. The colour of each node either indicates upregulation (red), downregulation (green) or no change (grey) in gene expression. GREM1 is a BMP4 antagonist. BMP4 binds to its receptor BMPR2 to trigger signalling and phosphorylation of Smad1/5/8. The phosphorylated Smad1/5/8 then form a complex with Smad4 and is transported into the nucleus to mediate BMP-dependent gene transcription.

5.4 Discussion

During early and mid-gestation of the foetus, skin injuries heal without the formation of scars. Foetal dermal fibroblasts are thought to be the main effector of the scarless wound healing process. Two aspects in which foetal fibroblasts differ from adult fibroblasts and which may modulate wound healing, is their deposition of ECM proteins and the growth factors they secrete[208,309,323]. To investigate these differences we acquired dermal fibroblasts from two adult donors and two foetal donors. Differences in the composition of ECM proteins deposited by adult and foetal dermal fibroblasts were detected by both immunofluorescent staining and proteomic analyses. When keratinocytes were grown on matrices generated by either adult or foetal dermal fibroblasts, dramatic differences in the gene expression profiles of these keratinocytes were observed. Keratinocytes grown on the two different substrates also differed in their proliferation rates. Collectively, these data indicate that the ECM has a profound influence on the rate of keratinocyte differentiation.

5.4.1 Characterisation of the Adult and Foetal Dermal Fibroblast Phenotype

Differences in the morphology of cultured adult and foetal dermal fibroblasts were observed. Adult dermal fibroblasts from both donors had a spindle-shaped morphology, which is a typical phenotype of fibroblasts. In contrast, a stellate-like morphology was observed for the foetal dermal fibroblasts (Fig. 5.1). Despite this difference in morphology, dermal fibroblasts from both the adult and foetal donors were positive for the fibroblast markers vimentin[227] and Thy-1[226] (Fig. 5.2). However, a lower expression level of Thy-1 was apparent in the foetal fibroblasts regardless of donor. To our knowledge, this study is the first to report a difference in Thy-1 expression between adult and foetal dermal fibroblasts.

Thy-1 is a glycosylphosphatidyl-anchored protein and a member of the immunoglobulin superfamily. It has been shown to play a role in directing the differentiation of dermal fibroblasts, as the loss of Thy-1 prevents the differentiation of fibroblasts into myofibroblasts following TGFβ1 stimulation[226,324]. In this study, staining with an α-SMA antibody revealed a small population of myofibroblasts within the foetal dermal fibroblasts (Fig. 5.2ix-xii). This is consistent with the findings of Walraven *et al.*[325], as they similarly reported myofibroblasts within their *in vitro*

cultured foetal dermal fibroblasts. An apparent contradiction is that foetal dermal fibroblasts have been reported to lack a response to TGFβ1 stimulation, resulting in the absence of myofibroblast differentiation[326]. In my cultures, it is possible that either the low expression of Thy-1 by the foetal fibroblasts prevented myofibroblast differentiation occurring following TGFβ1 stimulation, or the levels of TGFβ1 expressed by these fibroblasts were low, or a combination of these possibilities gave rise to only a few myofibroblasts.

5.4.2 Proteomic Analysis of the Extracellular Matrices Produced by Adult and Foetal Dermal Fibroblasts

One of the distinguishing features between the scarless wound healing of the foetus and the scarring skin repair of an adult is the composition of the dermal ECM. Therefore, knowledge of the components within the foetal dermal ECM may contribute to an understanding of the mechanism of scarless wound healing. Here, differences in the ECM deposited by adult and foetal dermal fibroblasts were investigated by quantitative proteomics. Tandem mass tag isobaric labelling was used in the quantitative proteomic analysis due to its compatibility with performing high-throughput quantification and sample multiplexing. This method allowed the four matrix samples to be combined within an experimental run thereby eliminating any run-to-run variation that may occur and isobaric labelling has been reported to have greater reproducibility and quantification precision than metabolic labelling. It is also ideal for quantifying both high- and low-abundance proteins because it has a wide dynamic range[327].

The quantitative proteomic analysis revealed striking differences in the expression patterns of ECM proteins between the foetal and adult matrices. Consistent with other reported literature, higher levels of type I collagen, type III collagen, type IV collagen, fibronectin, versican, and biglycan were observed in the foetal dermal fibroblast matrices compared to the adult matrices[192,216,219,220,313,314,328]. In contrast, adult dermal fibroblast matrices showed a higher amount of decorin and type VI collagen than in the foetal matrices, which is similarly in agreement with the literature[221,329]. Interestingly, while it has been reported that foetal dermal fibroblasts produce more type V collagen than their adult counterparts[201], in this current study, higher levels of

the type V collagen chains (COL5A2 & COL5A3) were found in the adult dermal fibroblast matrices, whereas there was no change in the level of another type V collagen chain, COL5A1. It has been reported that during skin development, there is a transition from type V collagen α_1 chain to α_2 chain[330], which could explain the higher COL5A2 levels observed in the adult dermal matrices. Furthermore, Wenstrup *et al*.[331] showed that type V collagen is essential for initiating and regulating collagen fibril assembly. The increase in COL5A2 and COL5A3 in adult matrices in this study may have contributed to the different structure of the collagen fibrils seen in these matrices compared to that seen in the foetal matrices (Fig. 5.11).

Amongst the ECM components identified, a greater abundance of type IV collagen and agrin was detected in the foetal dermal fibroblast matrices compared to the adult matrices. Both of these ECM proteins participate in BM assembly[9,11] and type IV collagen is also crucial for the maintenance of the stem cell-like characteristics of basal keratinocytes[16,88,332-334]. Agrin is an accessory ECM proteoglycan within BMs. Interestingly, Gaetani *et al*. [335] also reported a higher abundance of agrin within a foetal dermal matrix compared to an adult matrix. While little is known about agrin's function within the skin, it is said to be an important proteoglycan for the organisation of cellular networks and functionality of tissues during early development[335,336]. Within the brain, agrin is known to be involved in synaptogenesis of the entire nervous system, regulating the formation of synaptic junctions. Agrin is also known to stabilize the BM structure within the microvasculature of the brain, which contributes to the blood-brain barrier[336]. It is likely agrin may play a role in stabilising the BM of the skin, as well as helping in the formation of neuronal synapses within the dermis. Interestingly, agrin has been shown to bind to $\alpha V\beta 1$ integrin[337] and low-density lipoprotein receptor-related protein 4 (LPR4)[338]. Watt *et al.*[339] have reported that the activation of $\alpha V\beta 1$ integrin is essential in preventing terminal differentiation in keratinocytes. Furthermore, LPR4 activation has been shown to be essential in hair follicle development and other skin appendages[340]. It is likely that agrin may participate in the development of the skin and its appendages while maintaining undifferentiated keratinocyte population within the basal layer.

Laminins are a family of trimeric multidomain glycoproteins that are involved in BM formation. They are composed of an α-chain, β-chain and γ-chain. Each laminin

glycoprotein is named according to its subunit composition[76,77]. In this study, the proteomic data revealed the presence of laminin subunits α4, β1, β2 and γ1, which make up laminin-411 and laminin-421 (Fig. 5.4). It is probable that there was less laminin-421 in the FT-MATs as these matrices had lower levels of laminin β2 chains, whilst it is likely that there was no change in the level of laminin-411 because the laminin β1 subunit levels were similar in both AD-MAT and FT-MAT. Laminin-411 and laminin-421 are known to localise in the BM of blood vessels and neuromuscular junctions respectively[341,342]. Ishikawa *et al.* [343] demonstrated that both laminin-411 and laminin-421 bound to the integrin α6β1, and as a consequence promoted the adhesion and migration of tumour cells originating from melanoma, glioma and carcinoma. Currently, the details of laminin-421 functions within the skin are not understood.

The dynamic remodelling of the ECM is mediated by ECM regulators (proteinases and their corresponding proteinase inhibitors), and this remodelling is crucial for embryonic development, morphogenesis, tissue remodelling and wound healing. The major proteinases involved in ECM remodelling are the matrix metalloproteinases (MMPs), the ADAMs (a disintegrin and metalloproteinase), ADAMTS (a disintegrin and metalloproteinase with thrombospondin domains) and their corresponding inhibitors[196,344]. In this study, the proteomic data showed no difference in the MMP-1 and MMP-2 levels between AD-MAT and FT-MAT, however an increase in TIMP2 was observed in FT-MAT. This is in contrast to a study by Chen *et al.* [345], who reported a lower expression of MMP-2 and TIMP2 in the foetal skin. TIMP2 is an inhibitor of MMPs, and it preferentially inactivates MMP-2[346]. From my data although there may not be a difference in MMP-2 levels in the two matrices, it appears that the effect of MMP-2 will be less in FT-MAT because of the increased levels of TIMP2. In this study, in comparison to the AD-MATs, FT-MATs were shown to contain a higher level of ADAM12 but a lower level of ADAMTS1 and ADAMTS2. The ADAMs and ADAMTS proteases are key remodelling enzymes that are involved in procollagen processing as well as the cleavage of proteoglycans like versican and aggrecan{Porter:2005tf}. The dynamic remodelling of the ECM by these proteinases and their corresponding inhibitors may be one of the factors contributing to scarless wound healing.

Periostin is another ECM protein that was present at a higher level in FT-MATs than in AD-MATs. Periostin is a 90kDA ECM protein that is mainly expressed in the BM at dermal-epidermal junctions during early development. As the gestational stage progresses, periostin expression diminishes and it becomes localised around the hair follicles[347,348]. Interestingly, in a mouse knockout which lacked periostin, there were no apparent defects in the epidermis of both adults and the developing embryo, suggesting that periostin may have a limited role in skin homeostasis and development[349]. In contrast, recent studies suggest periostin contributes to dermal regeneration, as it has been shown to localise to the ECM compartment during tissue remodelling in wound healing[350,351]. Further investigations showed that periostin-deficient adult mice had reduced wound healing abilities, due to a delay in re-epithelization[350]. Furthermore, periostin has also been shown to facilitate the regenerative repair of skeletal muscle[352] and heart muscle[353] after injury. Curiously, periostin has been reported to be abundant in both keloid and hypertrophic scars[354] and other studies have implicated periostin in fibrosis and in the induction of myofibroblasts[355]. This suggests that periostin could also be contributing to the formation of myofibroblasts in the foetal fibroblast cultures described here.

Growth factors are secreted morphogenic proteins that direct cell behaviour and guide tissue repair and renewal[356]. Several growth factors such as transforming growth factor β (TGFβ), platelet-derived growth factor (PDGF) and fibroblast growth factors 2 (FGF2) have been shown to be differentially expressed between adult and foetal skin during wound healing. Whitby and Ferguson[357] reported that both TGFβ and FGF2 were only detected in adult skin wounds, while PDGF was detected in both adult and foetal skin wounds. Further studies by Broker *et al.* [358]showed that TGFβ and FGF2 were highly expressed by adult dermal fibroblasts. However, our proteomic data did not reveal any differences in TGFβ levels between AD-MATs and FT-MATs, and PDGF and FGF2 were not detected in either type of matrix. As mass spectrometry has limited capacity for detecting proteins present at low concentrations, PDGF and FGF2 may not have been detected due to their low abundance. Of the growth factors that were detected, chordin-like 1 and follistatin-like 1 were found to be highly expressed in FT-MATs. Both proteins are known to antagonise bone morphogenetic proteins (BMP), and both were shown to be essential during embryonic skin development[359].

5.4.3 The Influence of Adult and Foetal Dermal Fibroblast Matrices on Keratinocyte Behaviour

In this study, the influence of AD-MAT and FT-MAT on keratinocyte behaviour was investigated. Initially, the ability of AD-MAT and FT-MAT to support the adhesion and proliferation of keratinocytes was assessed microscopically. Phase-contrast microscopy revealed that keratinocytes adhered, proliferated and maintained a small cobblestone morphology on both AD-MATs and FT-MATs (Fig. 5.14). Quantification of cell numbers three days after seeding revealed more proliferation of keratinocytes grown on FT-MATs (Fig. 5.15). This was consistent with other studies, which have shown that foetal derived matrices are more conducive to the expansion of adult cells than their adult matrix counterparts[259,360-362].

Cell size has been reported to be a good indicator of proliferating undifferentiated keratinocytes. A number of authors have reported that small keratinocytes are undifferentiated and retain a higher proliferative capability[287-289]. In this present study, quantification of keratinocyte size revealed no significant differences between keratinocytes grown on AD-MAT and FT-MAT. However, a significantly higher proportion of keratinocytes were observed to have a larger cell size when cultured on type I collagen (Fig. 5.17). This is consistent with data in chapter IV as well as with what was reported by Esteban-Vives *et al.*[153]. Collectively, these data indicate that both AD-MATs and FT-MATs are capable of maintaining more apparently undifferentiated keratinocytes as indicated by their small size than the case when keratinocytes were seeded on type I collagen.

Comparative gene expression analysis using microarray showed that AD-MAT and FT-MAT exert different influences on keratinocytes behaviour. When keratinocytes were grown on AD-MAT, gene ontology analyses revealed genes related to keratinocyte differentiation were upregulated (Fig. 5.21). In contrast, when keratinocytes were cultured on FT-MAT, gene ontology analyses revealed the upregulation of genes related to cell division (Fig. 5.20). The upregulated expression of cell division related genes on FT-MAT is consistent with the increase in cell proliferation that was observed (Fig. 5.15). These data support the notion that the differences in ECM composition that were detected between adult and foetal dermal matrices have an effect on the keratinocyte gene expression. The changes in

keratinocyte gene expression observed seem to reflect the role these matrices play during epidermal development. During the initial stages of epidermal development, cell division occurs in both basal and suprabasal layers, as a means of rapidly expanding the epidermis during foetal growth[363]. It is highly likely that the FT-MATs have an ECM composition that is permissive for cell division. Upon reaching maturity, the epidermis undergoes homeostatic regulation such that epidermal renewal occurs by balancing terminal differentiation with cell division[363]. It is likely the AD-MATs have an ECM composition that is appropriate for the homeostatic regulation of keratinocyte growth and differentiation as the microarray data showed the expression of genes for both cell proliferation and differentiation in keratinocytes that were grown on this substrate. Curiously, gene ontology analysis indicates aberrant gene expression with no significant biological role, when keratinocytes were grown on type I collagen were compared to those grown on a native ECMs (Data not shown). This may indicate that single ECM molecule may not be sufficient to elicit corresponding signalling pathways require to regulate cell fate.

The maintenance of genomic stability during cell division is crucial for normal development, cell homoeostasis and tumour suppression. The DNA repair mechanisms prevent the accumulation of DNA damage in cells and so prevent the genomic integrity being compromised[364]. Failure of DNA repair mechanisms could result in mutations or chromosomal aberrations, which could lead to cells undergoing malignant transformation and cancerous growth[365]. The microarray data indicated that both AD-MATs and FT-MATs contained ECM signals to initiate DNA repair mechanisms. In contrast, the genes responsible for DNA repair were downregulated by the type I collagen substrate, indicating that this substrate does not provide an ideal microenvironment for keratinocyte expansion.

GREM1 is an antagonist of the growth factors, BMP2 and BMP4, and acts to inhibit their signalling pathways. Our proteomic data indicated that less GREM1 was expressed within the FT-MATs (Fig. 5.7). This suggests that there may be an increase in BMP2 and BMP4 signalling in keratinocytes grown on the FT-Mats (Fig. 5.24). Further examination of our microarray data from keratinocytes grown on FT-MATs, revealed that there was an increase in the expression of both BMP4 and its

corresponding transmembrane receptor, BMPR2. BMP4 is known to bind to BMPR2 to form a complex that then binds to the BMP type II receptor chain (BMPRII), and so triggers the phosphorylation of a set of Smad proteins called receptor Smad (R-Smad1/5/8) [366]. Phosphorylated receptor Smads will bind to the nuclear Smad (Smad4), which is then transported into the nucleus to be recruited into the transcriptional complexes which mediate BMP-dependent gene transcription[366]. Interestingly, Hayashi *et al.* [367] demonstrated that the BMP-SMAD-ID pathway suppresses p16/INK4A-mediated cell senescence. Furthermore, BMP4 is known to support embryonic stem cell self-renewal by inhibiting the p38 mitogen-activated pathways (MAPK)[368]. Hence, it is likely that the FT-MATs provided a microenvironment that promoted BMP4 signalling and so contributed to the enhanced keratinocyte proliferation and prevention of cell senescence that was observed when keratinocytes were cultured on this substrate.

Nishiyama *et al.*[350] reported the presences of periostin in the ECM to be important for stimulating keratinocyte proliferation. Our proteomic data revealed a higher level of periostin within the FT-MATs (Fig. 5.7). Furthermore, our microarray data showed an increase in periostin expression when keratinocytes were grown on FT-MATs, indicating that there may be a positive-feedback loop. Hence, periostin may be another ECM component involved in promoting keratinocyte proliferation. In addition, periostin may promote keratinocyte proliferation through a different signalling pathway than BMP4. Periostin is known to be a ligand of αvβ3 and αvβ5 integrins[369]. In ovarian cancer, the activation of either αvβ3 or αvβ5 integrin has been shown to enhance cell proliferation via integrin-linked kinases. The integrin-linked kinases phosphorylate Akt (protein kinases B) to promote cell growth and survival through the Akt signalling pathway[370]. It is plausible that both the Akt and BMP4 signalling pathway may act synergistically to promote both cell growth and survival when keratinocytes are cultured on FT-MATs.

Key cellular events such as proliferation, migration and differentiation are controlled by the reciprocal interaction between intrinsic transcriptional regulation and extrinsic signals[133,371]. This study highlights the strong influence that the extrinsic signals generated by ECM composition have on keratinocyte gene expression (Fig. 5.22-5.23). The different transcriptional profiles also indicate the importance of cell-matrix

interactions in controlling cell behaviour. Cells predominantly respond to the ECM cues through their integrin transmembrane receptors. Dynamic transcriptional regulation of integrin expression by cells modulates the cells' affinity for specific ECM components, which in turn regulates the cells' responsiveness towards the surrounding matrix. This in turn determines the downstream signalling events that will influence cell behaviour and cell fate[133]. Marinkovic *et al*.[158] and Ang *et al*.[372] reported that placing MSCs in an ECM with a pro-adipogenic composition resulted in more efficient differentiation towards the adipocyte lineage compared to that which could be achieved using an ECM of a different composition. Hence, both the literature data and my microarray data indicate that the precise control of a cell's fate can best be achieved by placing the cells in an appropriate ECM microenvironment.

5.5 Conclusions

In the present study, the data clearly indicate there is a compositional difference in the ECM produced by adult and foetal dermal fibroblasts. Furthermore, this difference in ECM composition between AD-MAT and FT-MAT differently influence keratinocyte behaviour. Keratinocytes grown on AD-MAT were observed to undergo both differentiation and cell proliferation. In contrast, on FT-MAT, keratinocytes were observed to have a higher proliferative capacity. This indicates that FT-MAT may contain an ECM composition that is more permissive to cell division, and may result in scarless wounds. A closer examination of the ECM components within the FT-MAT may uncover the mechanism behind the unique scarless wound healing of the foetus.

5.6 Future Directions

In this study, the compositional differences of ECM proteins between AD-MAT and FT-MAT have been shown through proteomic analysis. Furthermore, microarray analysis revealed that these differences do influence keratinocytes behaviour. Hence, it will be interesting to explore the role of each of the ECM proteins that are highly expressed in FT-MAT for their influence on keratinocytes behaviour. This could be achieved by knocking out the candidate ECM proteins in the foetal fibroblasts using the CRISPR-Cas9 system and generating a matrix to be used as a substrate for growth. Understanding the role of the candidate ECM proteins in FT-MAT may uncover new approaches for modulating tissue regeneration. Furthermore, the microarray data have indicate the FT-MAT may provide a microenvironment for BMP4 signalling, which may promote the self-renewal of keratinocytes. Further investigation on BMP4 signalling pathways will be investigated, to determine whether it is activated when keratinocytes are cultured on FT-MAT.

5.7 Acknowledgments

I would like to thank Ms Catherine Legrand for her help in determining the protein concentration of the solubilized ECM. I would like to also thank some of my collaborators, who have been essential in completing experiments that are critical to this study. Dr Simon Lieven (Birgitte Lane's Lab) in the analysis the microarray data. Dr Radoslaw Mikolaj (A*STAR Institute of Molecular Cell Biology) and Dr Rajkumar Ramalingam (Brian Burke's Lab, A*STAR Institute of Medical Science) for performing the proteomic analysis.

Chapter VI:

General Conclusions and Future Perspective

6.0 Conclusions and Future Perspective

The results presented in this study highlight the importance of cell-ECM interactions in supporting the proliferation of undifferentiated keratinocytes. The data indicated that a native ECM generated from dermal fibroblasts was able to recapitulate the dermal microenvironmental niche sufficiently to support the growth of undifferentiated keratinocytes, whereas type I collagen was less effective in this regard. Furthermore, differences in the ECM composition between matrices from adult or foetal dermal fibroblasts were reflected in the markedly different gene expression patterns of keratinocytes grown on these matrices.

Methods for generating CDMs have been published previously, as have studies reporting the use of these matrices to support the proliferation of undifferentiated stem cells[155,156,247,258,260,373]. Currently, this study (**Chapter III**) describes a novel method to generate a xenogeneic-free dermal fibroblast-derived matrix (Fib-Mat) using macromolecular crowding tissue culture conditions during the deposition of the ECM, and PLA_2 for decellularisation. Our data indicated that a well assembled ECM that completely covered the culture surface was generated under macromolecular crowding. The PLA_2 decellularisation protocol used to generate the acellular Fib-Mat, produced matrices that were free of nuclear and cell components that could potentially induce an immunological response if the matrices were used *in vivo*. Furthermore, according to our analyses this decellularisation protocol had minimal impact on the ECM content and ultrastructure. Importantly, the resulting Fib-Mat contained an ECM composition that was similar to that reported for the skin dermis[159,160].

Barrandon *et al*.[154] suggested that the critical factor for enabling the *in vitro* long-term expansion of keratinocyte stem cells is the recreation of the microenvironmental niche that they reside in. A key component of the microenvironmental niche is the native dermal ECM. This is lacking in the commonly used keratinocyte serum free culture system, which consists of keratinocyte serum free media and a substrate of type I collagen. In **Chapter IV**, the Fib-Mat, developed in **Chapter III,** was examined to determine whether this matrix was a better replacement for the dermal microenvironmental niche than type I collagen. Our data showed that Fib-Mat better supported the adhesion and proliferation of keratinocytes in the serum free system, than type I collagen and TCP. Curiously, an initial lag phase was observed in the

proliferation of keratinocytes grown on Fib-Mat, before an exponential increase in proliferation occurred. As Fib-Mat is a more complex biological substrate than type I collagen, the acclimatisation of keratinocytes towards this platform may explain the initial slower proliferation. Collectively the data within **Chapter IV** indicated that keratinocytes grown on Fib-Mat were less differentiated than samples of the same keratinocyte population that had been grown on type I collagen or TCP. This is indicated by the expression of markers of undifferentiated keratinocytes, the smaller cell size, the persistent cell migration and the actin reorganisation. This study has shown that this xenogeneic culture system using Fib-Mat, may be an appropriate alternative to the existing protocol for the culture of undifferentiated keratinocytes for clinical applications.

Cell-ECM interactions play an important role in preserving the self-renewal ability of stem cells. This is especially so with cultured keratinocytes, as Adams and Watt[374] demonstrated that a loss of contact with the ECM by keratinocytes triggers terminal differentiation. This is consistent with our data and that of Coolen *et al.* [152], who showed that keratinocytes undergo terminal differentiation when grown on tissue culture plastic that lacked an ECM protein. As a result, ECM proteins such as type I collagen[153], type IV collagen[152] and fibronectin[87] have been used as substrates to culture keratinocytes. However, while using these ECM proteins enable the keratinocytes to adhere and proliferate, they do not sustain the long-term growth of keratinocytes[153,275]. In this reductionist approach, the synergistic impact of growth factors and ECM proteins and their coordinated signalling pathways in the keratinocytes is overlooked. Others have shown that even the combination of three matrix proteins can have a synergistic effect[297-299]. For example, Flaim *et al.* [297] demonstrated that the combination of type I collagen with laminin and type III collagen enabled embryonic stem (ES) cells to efficiently differentiate towards a liver progenitor lineage, although individually these matrix proteins were unable to promote liver progenitor cell differentiation. The impact of ECM proteins and growth factors acting synergistically to coordinate and activate the signalling pathways required for self-renewal is highlighted by our study. The microarray data (**Chapter V**) showed that keratinocytes grown on a native ECM rather than on type I collagen were able to elicit signalling pathways for self-renewal. Furthermore, gene ontology analysis indicated aberrant gene expression with no significant biological role when

keratinocytes grown on type I collagen. These data suggest that a native ECM is required to elicit the correct signalling pathways to facilitate the self-renewal capability of keratinocytes.

Another aspect of the ECM that has been shown to influence cell fate is its stiffness. This was first demonstrated by Engler *et al.*[375], who showed that the lineage specification of MSC can be changed according to the matrix stiffness. When MSCs were placed on a soft matrix that mimicked the ECM of the brain, they underwent differentiation along the neuronal lineage. As the stiffness of the matrix increased to mimic that of muscle or of bone, the MSCs were biased towards a myogenic or an osteogenic differentiation pathway respectively. In the case of keratinocytes, Trappmann *et al.*[376] have demonstrated that keratinocytes are induced to terminally differentiate when cultured on a soft matrix (0.5kPa). When the matrix increased in stiffness (>1 kPA-700kPa) keratinocytes were prevented from undergoing terminal differentiation. While the stiffness of the substrates used in this study were not measured, rigid surfaces such as TCP/EGC and type I collagen-coated TCP/EGC have been reported to be stiffer (>1GPa) than cell-derived matrices (200-600Pa) [294,295]. Our data have shown that keratinocytes were less likely to differentiate when grown on fibroblast-derived matrices, compared to TCP/EGC and type I collagen-coated TCP/EGC. The fibroblast-derived matrices were thick (6~8µm) and so cells seeded on these matrices were not as influenced by the stiffness of the underlying TCP. The fibroblast-derived matrices were likely to have provided a more physiologically compliant stiffness that assisted in suppressing, or down regulating keratinocyte differentiation pathways rather more than TCP/EGC or type I collagen-coated TCP/EGC. Taking these data, and that of Trappmann *et al.*[376] into account, and confining the consideration to substrate stiffness, it appears neither too soft (<0.5kPa as determined by Trappmann *et al.*[376]), or too stiff, is conducive for the maintenance of undifferentiated keratinocytes. Interestingly, the stiffness of the skin dermis was shown to range between 0.3kPa-19 kPa[377], which is close to the lower limit of less than 0.5kPa, which Trappmann *et al.*[376] claimed to be too soft. Thus, it is likely it is the combination of ECM composition and matrix stiffness within the fibroblast-derived matrices that regulates keratinocyte differentiation.

Substrate stiffness has been shown to correlate with Rho-associated kinase activity, with stiffer substrates leading to ROCK activation[293]. Upon activation, ROCK induces changes in the density and thickness of the actin fibre structures[47,292]. Interestingly, ROCK activity has also been associated with regulating keratinocyte differentiation. Various authors have demonstrated that the activation of ROCK is required for keratinocyte differentiation[45-47,291]. For example, Vaezi *et al*. [291] showed that following ROCK activation, thick circumferential actin structures could be observed, as the keratinocytes progressed through to terminal differentiation. Similar thick circumferential actin structures were seen in our keratinocytes cultured on TCP/EGC or type I collagen-coated TCP/EGC, and these cells were shown to have differentiated. Numerous research groups have demonstrated that the lifespan of *in vitro* cultured keratinocytes could be expanded by using a pharmacological inhibitor of ROCK, Y-27632[48-50,273,378]. Under the effect of Y-27632, keratinocytes were shown to have an increased proliferative capacity with less terminal differentiation[49,50]. The upregulation of genes associated with cell division and nucleic acid biosynthesis coupled with the downregulation of genes associated with keratinocyte differentiation were observed in keratinocytes grown with Y-27632[50]. However, the effect of Y-27632 on keratinocytes is shown to be conditional, as its removal caused these cells to undergo senescence and terminal differentiation. Moreover, keratinocytes cultured for a long period in Y-27632, were shown to undergo senescence quicker than those cultured for only a short period in Y-27632 before its removal[50]. These drawbacks question the usefulness of using Y-27632 as a way to culture keratinocytes for medical applications, as cells may not able to reepithelize the wound before they undergo senescence. Our studies have shown that the fibroblast-derived matrices modulated the expression of genes associated with cell division and differentiation similarly to that seen with Y-27632[50], and this was especially true for the matrices generated by foetal dermal fibroblasts. Hence, these dermal fibroblast matrices may be a good alternative to using Y-27632 when culturing keratinocytes for medical applications. However, it should be noted that long-term culture studies using these foetal matrices are still required to be conducted to determine the duration for which keratinocytes can be passaged without terminal differentiation.

Stem cell self-renewal is a tightly control process that is regulated not only by cell-matrix interactions, but also through signals arising from other cells in the close vicinity, a process termed intercellular feedback. The prime example of intercellular feedback occurs during haematopoiesis, whereby haematopoietic stem cells (HSCs) undergo a hierarchal differentiation: HSCs give rise to progenitor cells that follow different blood cell lineages, to eventually produce the full complement of mature blood cells[379]. The decision of the HSCs to self-renewal or to follow certain differentiation pathways is regulated by cross-talk from the neighbouring cell population, either through direct cell-cell interactions or through secreted factors[380]. Numerous pieces of evidence support the idea that mature blood cells suppress the proliferation and differentiation of progenitor cells, and progenitor cells correspondingly suppress the expansion of HSCs through a negative feedback loop. Together these processes regulate the HSC's fate and maintain homeostasis[379-382]. It is highly likely that a similar intercellular feedback loop maintains the homeostatic regulation of keratinocyte stem cells *in vivo*; whereby transient amplifying cells and terminally differentiated keratinocytes suppress the expansion of keratinocyte stem cells to prevent stem cell exhaustion. During *in vitro* culture, the inability of type I collagen to elicit the signalling pathway required for keratinocytes to fully differentiate (microarray data in **Chapter V**) may have disrupted the feedback loop required to maintain the keratinocyte stem cell population. Hence, the exhaustion of the keratinocyte stem cell population may have been the reason why long-term expansion of undifferentiated keratinocytes on type I collagen was not possible, as described by other authors[49,153,275]. Our microarray data indicated that matrices obtained from adult dermal fibroblasts probably triggered the required signalling pathways for the maturation of keratinocytes. It is also possible that a feedback loop to maintain the stem cell population during cell expansion was also triggered, although this aspect needs more investigation.

Studies have shown that foetal skin has an intrinsic regenerative ability to heal without scar formation. Differences in the ECM between the adult and the foetal dermis is said to be one of the factors in determining whether a wound will undergo scarring repair or scarless healing. Using quantitative proteomics, my study showed differences in type I collagen, type III collagen, type IV collagen, fibronectin, versican, biglycan, decorin and type VI level between foetal and adult dermal matrices. These findings

are consistent with the current literature[192,216,219-221,313,314,328,329]. Furthermore, the quantitative proteomics (**Chapter V**) revealed other ECM proteins that may also be involved in the regenerative repair of foetal skin, which have not yet been reported to have this role. Hence, it will be interesting to explore whether these ECM proteins contributes to scarless wound healing.

Current research is focused on transcription factors and epigenetic modification on regulating of cell behaviour[383]. However, it is now known that microenvironmental cues are also an important element in determining a cell's fate. For example, Bonfanti *et al*.[384] revealed that different environmental cues can instruct cells to adopt very different cell fates. This was demonstrated using *in vitro* cultured thymic epithelial cells (TECs), which were shown to integrate into the thymic network and differentiate into functional TECs, when transplanted into an embryonic thymus. Interestingly, when the *in vitro* cultured TECs were exposed to an inductive skin microenvironment, the TECs adopted an epidermal lineage[384]. This illustrates how the different microenvironments are able to influence cell fate. It is likely that differences in ECM composition of the thymus and skin microenvironments influences the direction of the differentiation pathway taken by the TECs. The microarray data in **Chapter V** highlighted the strong influence of extrinsic signals arising from ECM compositional differences on keratinocyte gene expression. Our data demonstrated that FT-MATs have an ECM composition that is permissive of cell division, whereas AD-MATs have an ECM composition that is appropriate for the homeostatic regulation of keratinocyte growth and differentiation. Hence, our data suggest that a thorough understanding of how ECM composition affects the transcriptional regulation of the gene expression may be necessary if a precise control of cell fate is to be achieved.

During normal embryonic development, undifferentiated stem cells are thought to follow a sequential and hierarchical progression towards physiologically mature cell types. This process (lineage commitment and cell differentiation) are thought to be unidirectional and irreversible[385]. Waddington[386] has perfectly illustrated this concept of lineage specification in his "epigenetic landscape" model. In this model, cells progressing through differentiation are segregated into different inescapable differentiation pathways and the pathway to which they become committed determines the final fate of the cells[385,387,388]. This model described how the differentiation of cells

into multiple different cell types is restricted during the progression of embryonic development[385]. Emerging evidence from genetic lineage tracing studies on epithelia from various organs indicates the existence of endogenous plasticity in cell fate determination (without genetic/epigenetic manipulation) [389]. This was demonstrated through ablation studies, which revealed that committed progenitor or terminally differentiated cells are able to dedifferentiate into more "stem-like" cells *in vivo* when the stem cell population was removed[390-392]. These "stem-like" cells regained an ability to proliferate. It has been suggested that extrinsic signals from the native microenvironment may trigger the dedifferentiation of committed progenitor cells into these "stem-like" cells[389]. The microarray data in **Chapter V** provide further evidence that the composition of the ECM may play an important role in providing the signal for differentiation and proliferation as demonstrated by the types of gene transcribed when keratinocytes were on grown foetal or adult dermal fibroblast-derived matrices. While it has yet to be demonstrated, it is possible that the keratinocytes may have dedifferentiated into proliferating committed progenitor cells or their transient amplifying cell status was maintained.

Barrandon *et al*[154] has emphasized the importance of maintaining keratinocytes in an undifferentiated state during long-term *in vitro* expansion, for these cells to be useful for cell therapy in a clinical setting. However, keratinocytes grown in the commonly used serum-free culture system have a more limited lifespan, showing diminished self-renewal capacity and an increased commitment towards differentiation or senescence. In **Chapter IV** of this thesis, dermal fibroblast-derived ECM was shown to be a key component for maintaining keratinocytes in an undifferentiated state in serum-free medium. Furthermore **Chapter V**, provided evidence that the composition of FT-Mats provide signals to promote keratinocyte self-renewal while AD-Mats contain signals for the regulation of keratinocyte differentiation and proliferation; presumably *in vivo* this matrix contributes to the maintenance of homeostasis in the epidermis. We envisage that the FT-Mats could be used for the long-term *in vitro* expansion of keratinocytes, as the microarray data indicates that this substrate enables the proliferation of keratinocytes in the undifferentiated state. Once a sufficient amount of keratinocytes are generated, these cells could be then be transferred to a scaffold containing AD-Mats, to provide the appropriate signals for epidermal differentiation, and so generate a functional graft to be transplanted onto a skin wound. As the

keratinocytes were grown in a serum-free culture system before grafting onto the host, the graft would contain no animal-derived proteins that could evoke an immunological response. Clearly this is an advantage in a clinical setting.

In conclusion, this study has highlighted the role of the ECM in the control of cell fate. Furthermore, the novel culture system developed in this thesis may serve as an appropriate alternative to the existing protocol for the serum-free culture of undifferentiated keratinocytes for clinical applications.

Reference

1. Fuchs, E. Scratching the surface of skin development. *Nature* **445,** 834–842 (2007).
2. Proksch, E., Brandner, J. M. & Jensen, J.-M. The skin: an indispensable barrier. *Experimental Dermatology* **17,** 1063–1072 (2008).
3. Hsu, Y.-C., Li, L. & Fuchs, E. Emerging interactions between skin stem cells and their niches. *Nat Med* **20,** 847–856 (2014).
4. Venus, M., Waterman, J. & McNab, I. Basic physiology of the skin. *Surgery* **28,** 469–472 (2010).
5. Nestle, F. O., Di Meglio, P., Qin, J.-Z. & Nickoloff, B. J. Skin immune sentinels in health and disease. *Nature Reviews Immunology* **9,** 679–691 (2009).
6. Powell, J. Skin physiology. *Surgery* **24,** 1–4 (2006).
7. Farage, M. A., Miller, K. W., Elsner, P. & Maibach, H. I. Structural Characteristics of the Aging Skin: A Review. *Cutaneous and Ocular Toxicology* **26,** 343–357 (2007).
8. Brincat, M. P., Muscat Baron, Y. & Galea, R. Estrogens and the skin. *Climacteric* **8,** 110–123 (2005).
9. LeBleu, V. S., MacDonald, B. & Kalluri, R. Structure and Function of Basement Membranes. *Experimental Biology and Medicine* **232,** 1121–1129 (2007).
10. Breitkreutz, D., Mirancea, N. & Nischt, R. Basement membranes in skin: unique matrix structures with diverse functions? *Histochem Cell Biol* **132,** 1–10 (2009).
11. Breitkreutz, D., Koxholt, I., Thiemann, K. & Nischt, R. Skin Basement Membrane: The Foundation of Epidermal Integrity—BM Functions and Diverse Roles of Bridging Molecules Nidogen and Perlecan. *BioMed Research International* **2013,** 1–16 (2013).
12. Fox, J. W. *et al.* Recombinant nidogen consists of three globular domains and mediates binding of laminin to collagen type IV. *The EMBO Journal* **10,** 3137 (1991).
13. Aumailley, M. *et al.* Nidogen mediates the formation of ternary complexes of basement membrane components. *Kidney international* **43,** 7–12 (2007).
14. Miner, J. H., Li, C., Mudd, J. L., Go, G. & Sutherland, A. E. Compositional

and structural requirements for laminin and basement membranes during mouse embryo implantation and gastrulation. *Development* **131,** 2247–2256 (2004).

15. Poschl, E. Collagen IV is essential for basement membrane stability but dispensable for initiation of its assembly during early development. *Development* **131,** 1619–1628 (2004).
16. Watt, F. M. Role of integrins in regulating epidermal adhesion, growth and differentiation. *The EMBO Journal* **21,** 3919–3926 (2002).
17. Sher, I. Targeting Perlecan in Human Keratinocytes Reveals Novel Roles for Perlecan in Epidermal Formation. *Journal of Biological Chemistry* **281,** 5178–5187 (2005).
18. Baranowsky, A. *et al.* Impaired wound healing in mice lacking the basement membrane protein nidogen 1. *Matrix Biology* **29,** 15–21 (2010).
19. Solanas, G. & Benitah, S. A. Regenerating the skin: a task for the heterogeneous stem cell pool and surrounding niche. *Nat Rev Mol Cell Biol* **14,** 737–748 (2013).
20. Benitah, S. A. & Frye, M. Stem cells in ectodermal development. *J Mol Med* **90,** 783–790 (2012).
21. Liu, S., Zhang, H. & Duan, E. Epidermal Development in Mammals: Key Regulators, Signals from Beneath, and Stem Cells. *IJMS* **14,** 10869–10895 (2013).
22. Mills, A. A. *et al.* p63 is a p53 homologue required for limb and epidermal morphogenesis. *Nature* **398,** 708–713 (1999).
23. Yang, A. *et al.* p63 is essential for regenerative proliferation in limb, craniofacial and epithelial development. *Nature* **398,** 714–718 (1999).
24. Koster, M. I., Kim, S., Mills, A. A., DeMayo, F. J. & Roop, D. R. p63 is the molecular switch for initiation of an epithelial stratification program. *Genes & Development* **18,** 126–131 (2004).
25. Shalom-Feuerstein, R. *et al.* Np63 is an ectodermal gatekeeper of epidermal morphogenesis. *Cell Death and Differentiation* **18,** 887–896 (2010).
26. Medawar, A. *et al.* ΔNp63 Is Essential for Epidermal Commitment of Embryonic Stem Cells. *PLoS ONE* **3,** e3441 (2008).
27. Romano, R.-A., Birkaya, B. & Sinha, S. A Functional Enhancer of Keratin14 Is a Direct Transcriptional Target of ΔNp63. *J Investig Dermatol* **127,** 1175–

1186 (2006).

28. Romano, R.-A., Ortt, K., Birkaya, B., Smalley, K. & Sinha, S. An Active Role of the ΔN Isoform of p63 in Regulating Basal Keratin Genes K5 and K14 and Directing Epidermal Cell Fate. *PLoS ONE* **4,** e5623 (2009).
29. De Rosa, L. *et al.* p63 Suppresses non-epidermal lineage markers in a bone morphogenetic protein-dependent manner via repression of Smad7. *Journal of Biological Chemistry* **284,** 30574–30582 (2009).
30. Koster, M. I. & Roop, D. R. Mechanisms Regulating Epithelial Stratification. *Annu. Rev. Cell Dev. Biol.* **23,** 93–113 (2007).
31. Laurikkala, J. p63 regulates multiple signalling pathways required for ectodermal organogenesis and differentiation. *Development* **133,** 1553–1563 (2006).
32. Zhao, Q. *et al.* Spatiotemporal Expression of p63 in Mouse Epidermal Commitment. *IJMS* **16,** 29542–29553 (2015).
33. Aberdam, D. *et al.* Key role of p63 in BMP-4-induced epidermal commitment of embryonic stem cells. *Cell Cycle* **6,** 291–294 (2007).
34. Nylander, K. *et al.* Differential expression of p63 isoforms in normal tissues and neoplastic cells. *J. Pathol.* **198,** 417–427 (2002).
35. Koh, L. F., Ng, B. K., Bertrand, J. & Thierry, F. Transcriptional control of late differentiation in human keratinocytes by TAp63 and Notch. *Experimental Dermatology* **24,** 754–760 (2015).
36. Mack, J. A., Anand, S. & Maytin, E. V. Proliferation and cornification during development of the mammalian epidermis. *Birth Defects Research Part C: Embryo Today: Reviews* **75,** 314–329 (2005).
37. Lai, E. C. Notch signaling: control of cell communication and cell fate. *Development* **131,** 965–973 (2004).
38. Artavanis-Tsakonas, S., Rand, M. D. & Lake, R. J. Notch signaling: cell fate control and signal integration in development. *Science* **284,** 770–776 (1999).
39. Nowell, C. & Radtke, F. Cutaneous Notch Signaling in Health and Disease. *Cold Spring Harbor Perspectives in Medicine* **3,** a017772–a017772 (2013).
40. Watt, F. M., Estrach, S. & Ambler, C. A. Epidermal Notch signalling: differentiation, cancer and adhesion. *Current Opinion in Cell Biology* **20,** 171–179 (2008).
41. Rangarajan, A. *et al.* Notch signaling is a direct determinant of keratinocyte

growth arrest and entry into differentiation. *The EMBO Journal* **20,** 3427–3436 (2001).

42. Nguyen, B.-C. *et al.* Cross-regulation between Notch and p63 in keratinocyte commitment to differentiation. *Genes & Development* **20,** 1028–1042 (2006).
43. Schwartz, M. Rho signalling at a glance. *J. Cell. Sci.* **117,** 5457–5458 (2004).
44. Murali, A. & Rajalingam, K. Small Rho GTPases in the control of cell shape and mobility. *Cell. Mol. Life Sci.* (2013). doi:10.1007/s00018-013-1519-6
45. Lock, F. E. & Hotchin, N. A. Distinct roles for ROCK1 and ROCK2 in the regulation of keratinocyte differentiation. *PLoS ONE* (2009). doi:10.1371/journal.pone.0008190.g001
46. McMullan, R. *et al.* Keratinocyte Differentiation Is Regulated by the Rho and ROCK Signaling Pathway. *Current Biology* **13,** 2185–2189 (2003).
47. Liebig, T. *et al.* RhoE Is required for keratinocyte differentiation and stratification. *Mol. Biol. Cell* **20,** 452–463 (2009).
48. Chapman, S., Liu, X., Meyers, C., Schlegel, R. & McBride, A. A. Human keratinocytes are efficiently immortalized by a Rho kinase inhibitor. *J. Clin. Invest.* **120,** 2619–2626 (2010).
49. Strudwick, X. L., Lang, D. L., Smith, L. E. & Cowin, A. J. Combination of Low Calcium with Y-27632 Rock Inhibitor Increases the Proliferative Capacity, Expansion Potential and Lifespan of Primary Human Keratinocytes while Retaining Their Capacity to Differentiate into Stratified Epidermis in a 3D Skin Model. *PLoS ONE* **10,** e0123651–12 (2015).
50. Chapman, S., McDermott, D. H., Shen, K., Jang, M. K. & McBride, A. A. The effect of Rho kinase inhibition on long-term keratinocyte proliferation is rapid and conditional. *Stem Cell Res Ther* **5,** 60 (2014).
51. Doupé, D. P. & Jones, P. H. Interfollicular epidermal homeostasis: dicing with differentiation. *Experimental Dermatology* **21,** 249–253 (2012).
52. Potten, C. S. The epidermal proliferative unit: the possible role of the central basal cell. *Cell Tissue Kinet* **7,** 77–88 (1974).
53. Mackenzie, J. C. Ordered structure of the stratum corneum of mammalian skin. *Nature* **222,** 881–882 (1969).
54. Mackenzie, I. C. Relationship between mitosis and the ordered structure of the stratum corneum in mouse epidermis. *Nature* **226,** 653–655 (1970).
55. Allen, T. D. & Potten, C. S. Fine-structural identification and organization of

the epidermal proliferative unit. (1974).

56. Mackenzie, I. C. & Bickenbach, J. R. Label-retaining keratinocytes and Langerhans cells in mouse epithelia. *Cell Tissue Res* **242,** 551–556 (1985).

57. Bickenbach, J. R. & Holbrook, K. A. Label-Retaining Cells in Human Embryonic and Fetal Epidermis. *J. Invest. Dermatol.* **88,** 42–46 (1987).

58. Mackenzie, I. C. Retroviral Transduction of Murine Epidermal Stem Cells Demonstrates Clonal Units of Epidermal Structure. *J. Invest. Dermatol.* **109,** 377–383 (1997).

59. Ro, S. & Rannala, B. A stop-EGFP transgenic mouse to detect clonal cell lineages generated by mutation. *EMBO Rep* **5,** 914–920 (2004).

60. Ro, S. & Rannala, B. Evidence from the stop-EGFP mouse supports a niche-sharing model of epidermal proliferative units. *Experimental Dermatology* **14,** 838–843 (2005).

61. Clayton, E. *et al.* A single type of progenitor cell maintains normal epidermis. *Nature* **446,** 185–189 (2007).

62. Doupé, D. P. *et al.* A single progenitor population switches behavior to maintain and repair esophageal epithelium. *Science* **337,** 1091–1093 (2012).

63. Doupé, D. P., Klein, A. M., Simons, B. D. & Jones, P. H. The Ordered Architecture of Murine Ear Epidermis Is Maintained by Progenitor Cells with Random Fate. *Developmental Cell* **18,** 317–323 (2010).

64. Mascré, G. *et al.* Distinct contribution of stem and progenitor cells to epidermal maintenance. *Nature* **489,** 257–262 (2013).

65. Jones, P. & Simons, B. D. Epidermal homeostasis: do committed progenitors work while stem cells sleep? *Nat Rev Mol Cell Biol* **9,** 82–88 (2008).

66. Hubmacher, D. & Apte, S. S. The biology of the extracellular matrix. *Current Opinion in Rheumatology* **25,** 65–70 (2013).

67. Frantz, C., Stewart, K. M. & Weaver, V. M. The extracellular matrix at a glance. **123,** 4195–4200 (2010).

68. Gattazzo, F., Urciuolo, A. & Bonaldo, P. Extracellular matrix: A dynamic microenvironment for stem cell niche. *BBA - General Subjects* **1840,** 2506–2519 (2014).

69. Theocharis, A. D., Skandalis, S. S., Gialeli, C. & Karamanos, N. K. Extracellular matrix structure. *Advanced Drug Delivery Reviews* **97,** 4–27 (2016).

70. Smith, L. T., Holbrook, K. A. & Madri, J. A. Collagen types I, III, and V in human embryonic and fetal skin. *Dev. Dyn.* **175,** 507–521 (1986).
71. Tracy, L. E., Minasian, R. A. & Caterson, E. J. Extracellular Matrix and Dermal Fibroblast Function in the Healing Wound. *Advances in Wound Care* **5,** 119–136 (2016).
72. Ricard-Blum, S. & Ruggiero, F. The collagen superfamily: from the extracellular matrix to the cell membrane. *Pathologie Biologie* **53,** 430–442 (2005).
73. Mienaltowski, M. J. & Birk, D. E. Structure, physiology, and biochemistry of collagens. *Progress in heritable soft connective tissue …* (2014). doi:10.1007/978-94-007-7893-1
74. Ricard-Blum, S. The collagen family. *Cold Spring Harbor Perspectives in Biology* **3,** a004978–a004978 (2011).
75. Hamill, K. J., Kligys, K., Hopkinson, S. B. & Jones, J. C. R. Laminin deposition in the extracellular matrix: a complex picture emerges. **122,** 4409–4417 (2009).
76. Domogatskaya, A., Rodin, S. & Tryggvason, K. Functional Diversity of Laminins. *Annu. Rev. Cell Dev. Biol.* **28,** 523–553 (2012).
77. Aumailley, M. The laminin family. *celladhesion* **7,** 48–55 (2013).
78. Smyth, N. *et al.* Absence of basement membranes after targeting the LAMC1 gene results in embryonic lethality due to failure of endoderm differentiation. *J. Cell Biol.* **144,** 151–160 (1999).
79. Li, S., Edgar, D., Fässler, R., Wadsworth, W. & Yurchenco, P. D. The role of laminin in embryonic cell polarization and tissue organization. *Developmental Cell* **4,** 613–624 (2003).
80. Uitto, J., Olsen, D. R. & Fazio, M. J. Extracellular Matrix of the Skin: 50 Years of Progress. *J. Invest. Dermatol.* **92,** 61S–77S (1989).
81. Pankov, R. & Yamada, K. M. Fibronectin at a glance. **115,** 3861–3863 (2002).
82. Halper, J. & Kjaer, M. in *Progress in Heritable Soft Connective Tissue Diseases* (ed. Halper, J.) **802,** 31–47 (Springer Netherlands, 2013).
83. Stoffels, J. M. J., Zhao, C. & Baron, W. Fibronectin in tissue regeneration: timely disassembly of the scaffold is necessary to complete the build. *Cell. Mol. Life Sci.* **70,** 4243–4253 (2013).
84. Chester, D. & Brown, A. C. The role of biophysical properties of provisional

matrix proteins in wound repair. *Matrix Biology* **60-61,** 124–140 (2017).

85. Brotchie, H. & Wakefield, D. Fibronectin: structure, function and significance in wound healing. *Australas. J. Dermatol.* **31,** 47–56 (1990).
86. Schultz, G. S., Ladwig, G. & Wysocki, A. Extracellular matrix: review of its roles in acute and chronic wounds. *World Wide Wounds* (2005).
87. Watt, F. M., Kubler, M. D., Hotchin, N. A., Nicholson, L. J. & Adams, J. C. Regulation of keratinocyte terminal differentiation by integrin-extracellular matrix interactions. **106,** 175–182 (1993).
88. Adams, J. C. & Watt, F. M. Changes in keratinocyte adhesion during terminal differentiation: reduction in fibronectin binding precedes alpha 5 beta 1 integrin loss from the cell surface. *Cell* **63,** 425–435 (1990).
89. Mithieux, S. M. & Weiss, A. S. Elastin. *Adv. Protein Chem.* **70,** 437–461 (2005).
90. Almine, J. F., Wise, S. G. & Weiss, A. S. Elastin signaling in wound repair. *Birth Defects Research Part C: Embryo Today: Reviews* **96,** 248–257 (2012).
91. Baldwin, A. K., Simpson, A., Steer, R., Cain, S. A. & Kielty, C. M. Elastic fibres in health and disease. *Expert Rev. Mol. Med.* **15,** e8 (2013).
92. Sherratt, M. J. Tissue elasticity and the ageing elastic fibre. *AGE* **31,** 305–325 (2009).
93. Bader, B. L. *et al.* Compound Genetic Ablation of Nidogen 1 and 2 Causes Basement Membrane Defects and Perinatal Lethality in Mice. *Molecular and Cellular Biology* **25,** 6846–6856 (2005).
94. Mokkapati, S. *et al.* Basement Membranes in Skin Are Differently Affected by Lack of Nidogen 1 and 2. *J Investig Dermatol* **128,** 2259–2267 (2008).
95. Preissner, K. T. Structure and biological role of vitronectin. *Annu. Rev. Cell Biol.* **7,** 275–310 (1991).
96. Leavesley, D. I. *et al.* Vitronectin-Master controller or micromanager? *IUBMB Life* **32,** n/a–n/a (2013).
97. Preissner, K. T. & Reuning, U. Vitronectin in vascular context: facets of a multitalented matricellular protein. *Semin. Thromb. Hemost.* **37,** 408–424 (2011).
98. Schvartz, I., Seger, D. & Shaltiel, S. Vitronectin. *Int. J. Biochem. Cell Biol.* **31,** 539–544 (1999).
99. Underwood, P. A. & Bennett, F. A. A comparison of the biological activities

of the cell-adhesive proteins vitronectin and fibronectin. *J. Cell. Sci.* **93 (Pt 4),** 641–649 (1989).

100. Mivamoto, Y., Izumi, M., Ishizaka, S. & Hayashi, M. Adsorption of Vitronectin in Human Serum onto Plastics is Augmented by Sodium Dodecyl Sulfate. *Cell Struct. Funct.* **14,** 151–162 (1989).
101. Steele, J. G., Johnson, G., Norris, W. D. & Underwood, P. A. Adhesion and growth of cultured human endothelial cells on perfluorosulphonate: role of vitronectin and fibronectin in cell attachment. *Biomaterials* **12,** 531–539 (1991).
102. Hyde, C., Hollier, B., Anderson, A., Harkin, D. & Upton, Z. Insulin-like Growth Factors (IGF) and IGF-Binding Proteins Bound to Vitronectin Enhance Keratinocyte Protein Synthesis and Migration. *J. Invest. Dermatol.* **122,** 1198–1206 (2004).
103. Clark, S. J., Bishop, P. N. & Day, A. J. The Proteoglycan Glycomatrix: A Sugar Microenvironment Essential for Complement Regulation. *Front. Immunol.* **4,** (2013).
104. Smith, M. M. & Melrose, J. Proteoglycans in Normal and Healing Skin. *Advances in Wound Care* **4,** 152–173 (2015).
105. Schaefer, L. & Schaefer, R. M. Proteoglycans: from structural compounds to signaling molecules. *Cell Tissue Res* **339,** 237–246 (2009).
106. Wight, T. N. Versican: a versatile extracellular matrix proteoglycan in cell biology. *Current Opinion in Cell Biology* **14,** 617–623 (2002).
107. Wight, T. N., Kinsella, M. G., Evanko, S. P., Potter-Perigo, S. & Merrilees, M. J. Versican and the regulation of cell phenotype in disease. *Biochimica et Biophysica Acta (BBA) - General Subjects* **1840,** 2441–2451 (2014).
108. Rahmani, M., Wong, B. W. & Ang, L. Versican: signaling to transcriptional control pathways This paper is one of a selection of papers published in this Special Issue, entitled Young Investigator's Forum. *Canadian journal of ...* (2006).
109. Wu, Y. J., La Pierre, D. P., Wu, J., Yee, A. J. & Yang, B. B. The interaction of versican with its binding partners. *Cell Res* **15,** 483–494 (2005).
110. Kuznetsova, S. A. *et al.* Versican-thrombospondin-1 binding in vitro and colocalization in microfibrils induced by inflammation on vascular smooth muscle cells. **119,** 4499–4509 (2006).

111. Evanko, S. P., Tammi, M. I., Tammi, R. H. & Wight, T. N. Hyaluronan-dependent pericellular matrix. *Advanced drug delivery …* **59,** 1351–1365 (2007).

112. Shirakata, Y. Regulation of epidermal keratinocytes by growth factors. *Journal of Dermatological Science* **59,** 73–80 (2010).

113. Zimmermann, D. R., Dours-Zimmermann, M. T., Schubert, M. & Bruckner-Tuderman, L. Versican is expressed in the proliferating zone in the epidermis and in association with the elastic network of the dermis. *J. Cell Biol.* **124,** 817–825 (1994).

114. Iozzo, R. V. & Schaefer, L. Proteoglycan form and function: A comprehensive nomenclature of proteoglycans. *Matrix Biology* **42,** 11–55 (2015).

115. Arikawa-Hirasawa, E., Watanabe, H., Takami, H., Hassell, J. R. & Yamada, Y. Perlecan is essential for cartilage and cephalic development. *Nat Genet* **23,** 354–358 (1999).

116. Reed, C. C. & Iozzo, R. V. The role of decorin in collagen fibrillogenesis and skin homeostasis. *Glycoconj J* **19,** 249–255 (2002).

117. Danielson, K. G. *et al.* Targeted Disruption of Decorin Leads to Abnormal Collagen Fibril Morphology and Skin Fragility. *J. Cell Biol.* **136,** 729–743 (1997).

118. Reese, S. P., Underwood, C. J. & Weiss, J. A. Effects of decorin proteoglycan on fibrillogenesis, ultrastructure, and mechanics of type I collagen gels. *Matrix Biology* 1–10 (2013). doi:10.1016/j.matbio.2013.04.004

119. Salbach, J. *et al.* Regenerative potential of glycosaminoglycans for skin and bone. *J Mol Med* **90,** 625–635 (2011).

120. Afratis, N. *et al.* Glycosaminoglycans: key players in cancer cell biology and treatment. **279,** 1177–1197 (2012).

121. Gandhi, N. S. & Mancera, R. L. The Structure of Glycosaminoglycans and their Interactions with Proteins. *Chemical Biology & Drug Design* **72,** 455–482 (2008).

122. Kim, S.-H., Turnbull, J. & Guimond, S. Extracellular matrix and cell signalling: the dynamic cooperation of integrin, proteoglycan and growth factor receptor. *J. Endocrinol.* **209,** 139–151 (2011).

123. Qiao, D., Meyer, K., Drew, S. A., Mundhenke, C. & Friedl, A. Heparan Sulfate Proteoglycans as Regulators of Fibroblast Growth Factor-2 Signaling

in Brain Endothelial Cells. Specific role for Glypican-1 in glioma angiogenesis. *Journal of Biological Chemistry* **278,** 16045–16053 (2003).

124. Tumova, S., Woods, A. & Couchman, J. R. Heparan sulfate proteoglycans on the cell surface: versatile coordinators of cellular functions. *Int. J. Biochem. Cell Biol.* **32,** 269–288 (2000).

125. Sun, Y., Chen, C. S. & Fu, J. Forcing Stem Cells to Behave: A Biophysical Perspective of the Cellular Microenvironment. *Annu. Rev. Biophys.* **41,** 519–542 (2012).

126. Watt, F. M., Jordan, P. W. & O'Neill, C. H. Cell shape controls terminal differentiation of human epidermal keratinocytes. *Proc. Natl. Acad. Sci. U.S.A.* **85,** 5576–5580 (1988).

127. Connelly, J. T. *et al.* Actin and serum response factor transduce physical cues from the microenvironment to regulate epidermal stem cell fate decisions. *Nature Cell Biology* **12,** 711–718 (2010).

128. Le, H. Q. *et al.* Mechanical regulation of transcription controls Polycomb-mediated gene silencing during lineage commitment. *Nature Cell Biology* **18,** 864–875 (2016).

129. Sun, Z., Guo, S. S. & Fässler, R. Integrin-mediated mechanotransduction. *J. Cell Biol.* **215,** 445–456 (2016).

130. Barczyk, M., Carracedo, S. & Gullberg, D. Integrins. *Cell Tissue Res* **339,** 269–280 (2009).

131. Brizzi, M. F., Tarone, G. & Defilippi, P. Extracellular matrix, integrins, and growth factors as tailors of the stem cell niche. *Current Opinion in Cell Biology* **24,** 645–651 (2012).

132. Anderson, L. R., Owens, T. W. & Naylor, M. J. Integrins in development and cancer. *Biophys Rev* **6,** 191–202 (2013).

133. Volk, S. W., Iqbal, S. A. & Bayat, A. Interactions of the Extracellular Matrix and Progenitor Cells in Cutaneous Wound Healing. *Advances in Wound Care* **2,** 261–272 (2013).

134. Adams, J. C. & Watt, F. M. Expression of beta 1, beta 3, beta 4, and beta 5 integrins by human epidermal keratinocytes and non-differentiating keratinocytes. *J. Cell Biol.* **115,** 829–841 (1991).

135. Ellis, S. J. & Tanentzapf, G. Integrin-mediated adhesion and stem-cell-niche interactions. *Cell Tissue Res* **339,** 121–130 (2009).

136. Margadant, C., Charafeddine, R. A. & Sonnenberg, A. Unique and redundant functions of integrins in the epidermis. *FASEB J.* **24,** 4133–4152 (2010).
137. Levy, L., Broad, S., Diekmann, D., Evans, R. D. & Watt, F. M. beta1 integrins regulate keratinocyte adhesion and differentiation by distinct mechanisms. *Mol. Biol. Cell* **11,** 453–466 (2000).
138. Chen, M., Przyborowski, M. & Berthiaume, F. Stem cells for skin tissue engineering and wound healing. *Crit Rev Biomed Eng* **37,** 399–421 (2009).
139. Horch, R. E., Kopp, J., Kneser, U., Beier, J. & Bach, A. D. Tissue engineering of cultured skin substitutes. *J. Cell. Mol. Med.* **9,** 592–608 (2005).
140. Priya, S. G., Jungvid, H. & Kumar, A. Skin Tissue Engineering for Tissue Repair and Regeneration. *Tissue Engineering Part B: Reviews* **14,** 105–118 (2008).
141. MacNeil, S. Progress and opportunities for tissue-engineered skin. *Nature* **445,** 874–880 (2007).
142. Rheinwald, J. G. & Green, H. Serial cultivation of strains of human epidermal keratinocytes: the formation keratinizin colonies from single cells. *Cell* **6,** 331–343 (1975).
143. Bello, Y. M., Falabella, A. F. & Eaglstein, W. H. Tissue-engineered skin. *American journal of clinical dermatology* **2,** 305–313 (2001).
144. Clark, R. A. F., Ghosh, K. & Tonnesen, M. G. Tissue Engineering for Cutaneous Wounds. *J Investig Dermatol* **127,** 1018–1029 (2007).
145. O'Connor, N. E. & Mulliken, J. B. Grafting of burns with cultured epithelium prepared from autologous epidermal cells. *Lancet* **1,** 75–78 (1981).
146. Hefton, J., Finkelstein, J., Madden, M. & Thomas Shires, G. Grafting of burn patients with allografts of cultured epidermal cells. *Lancet* **322,** 428–430 (1983).
147. Johnson, M. C., Meyer, A. A., deSerres, S., Herzog, S. & Peterson, H. D. Persistence of fetal bovine serum proteins in human keratinocytes. *J Burn Care Rehabil* **11,** 504–509 (1990).
148. Sun, T. *et al.* Developments in xenobiotic-free culture of human keratinocytes for clinical use. *Wound Repair Regen* **12,** 626–634 (2004).
149. Martin, M. J., Muotri, A., Gage, F. & Varki, A. Human embryonic stem cells express an immunogenic nonhuman sialic acid. *Nat Med* **11,** 228–232 (2005).
150. Badylak, S. F. & Gilbert, T. W. Immune response to biologic scaffold

materials. *Seminars in Immunology* **20,** 109–116 (2008).

151. Mujaj, S., Manton, K., Upton, Z. & Richards, S. Serum-free primary human fibroblast and keratinocyte coculture. *Tissue Eng Part A* **16,** 1407–1420 (2010).

152. Coolen, N. A. *et al.* Culture of keratinocytes for transplantation without the need of feeder layer cells. *Cell Transplant* **16,** 649–661 (2007).

153. Esteban-Vives, R. *et al.* In vitro keratinocyte expansion for cell transplantation therapy is associated with differentiation and loss of basal layer derived progenitor population. *Differentiation* 1–9 (2015). doi:10.1016/j.diff.2015.05.002

154. Barrandon, Y. *et al.* Capturing epidermal stemness for regenerative medicine. *Seminars in Cell and Developmental Biology* **23,** 937–944 (2012).

155. Fitzpatrick, L. E. & McDevitt, T. C. Cell-derived matrices for tissue engineering and regenerative medicine applications. *Biomater Sci* **3,** 12–24 (2015).

156. Zhang, W. *et al.* Cell-Derived Extracellular Matrix: Basic Characteristics and Current Applications in Orthopedic Tissue Engineering. *Tissue Engineering Part B: Reviews* **22,** 193–207 (2016).

157. Lu, H., Hoshiba, T., Kawazoe, N. & Chen, G. Autologous extracellular matrix scaffolds for tissue engineering. *Biomaterials* **32,** 2489–2499 (2011).

158. Marinkovic, M. *et al.* One size does not fit all: developing a cell-specific niche for in vitro study of cell behavior. *Matrix Biology* **52-54,** 426–441 (2016).

159. Sriram, G., Bigliardi, P. L. & Bigliardi-Qi, M. Fibroblast heterogeneity and its implications for engineering organotypic skin models in vitro. *European Journal of Cell Biology* **94,** 483–512 (2015).

160. Sorrell, J. M. & Caplan, A. I. Fibroblast heterogeneity: more than skin deep. **117,** 667–675 (2004).

161. Meigel, W. N., Gay, S. & Weber, L. Dermal architecture and collagen type distribution. *Arch Dermatol Res* **259,** 1–10 (1977).

162. Schönherr, E., Beavan, L. A., Hausser, H., Kresse, H. & Culp, L. A. Differences in decorin expression by papillary and reticular fibroblasts in vivo and in vitro. *Biochemical Journal* **290,** 893–899 (1993).

163. Sorrell, J. M., Baber, M. A. & Caplan, A. I. Site-matched papillary and reticular human dermal fibroblasts differ in their release of specific growth

factors/cytokines and in their interaction with keratinocytes. *J. Cell. Physiol.* **200,** 134–145 (2004).

164. Mine, S., Fortunel, N. O., Pageon, H. & Asselineau, D. Aging Alters Functionally Human Dermal Papillary Fibroblasts but Not Reticular Fibroblasts: A New View of Skin Morphogenesis and Aging. *PLoS ONE* **3,** e4066–13 (2008).

165. Janson, D., Saintigny, G., Mahé, C. & Ghalbzouri, A. E. Papillary fibroblasts differentiate into reticular fibroblasts after prolonged in vitroculture. *Experimental Dermatology* **22,** 48–53 (2012).

166. Driskell, R. R. *et al.* Distinct fibroblast lineages determine dermal architecture in skin development and repair. *Nature* **504,** 277–281 (2013).

167. Chen, C., Loe, F., Blocki, A., Peng, Y. & Raghunath, M. Applying macromolecular crowding to enhance extracellular matrix deposition and its remodeling in vitro for tissue engineering and cell-based therapies. *Advanced Drug Delivery Reviews* **63,** 277–290 (2011).

168. Minton, A. P. The Influence of Macromolecular Crowding and Macromolecular Confinement on Biochemical Reactions in Physiological Media. *Journal of Biological Chemistry* **276,** 10577–10580 (2001).

169. Zeiger, A. S., Loe, F. C., Li, R., Raghunath, M. & Van Vliet, K. J. Macromolecular Crowding Directs Extracellular Matrix Organization and Mesenchymal Stem Cell Behavior. *PLoS ONE* **7,** e37904 (2012).

170. Bateman, J. F., Cole, W. G., Pillow, J. J. & Ramshaw, J. A. Induction of procollagen processing in fibroblast cultures by neutral polymers. *Journal of Biological Chemistry* **261,** 4198–4203 (1986).

171. Lareu, R. R. *et al.* Collagen matrix deposition is dramatically enhanced in vitro when crowded with charged macromolecules: The biological relevance of the excluded volume effect. *FEBS Lett.* **581,** 2709–2714 (2007).

172. Satyam, A. *et al.* Macromolecular Crowding Meets Tissue Engineering by Self-Assembly: A Paradigm Shift in Regenerative Medicine. *Adv. Mater.* **26,** 3024–3034 (2014).

173. Rashid, R. *et al.* Novel Use for Polyvinylpyrrolidone as a Macromolecular Crowder for Enhanced Extracellular Matrix Deposition and Cell Proliferation. **20,** 994–1002 (2014).

174. Kumar, P. *et al.* Macromolecularly crowded in vitro microenvironments

accelerate the production of extracellular matrix-rich supramolecular assemblies. *Sci. Rep.* **5,** 8729–10 (2015).

175. Kumar, P. *et al.* Accelerated Development of Supramolecular Corneal Stromal-Like Assemblies from Corneal Fibroblasts in the Presence of Macromolecular Crowders. *Tissue Engineering Part C: Methods* **21,** 660–670 (2015).

176. Satyam, A., Kumar, P., Cigognini, D., Pandit, A. & Zeugolis, D. I. Low, but not too low, oxygen tension and macromolecular crowding accelerate extracellular matrix deposition in human dermal fibroblast culture. **44,** 221–231 (2016).

177. Gilbert, T., Sellaro, T. & Badylak, S. Decellularization of tissues and organs. *Biomaterials* 1–9 (2006). doi:10.1016/j.biomaterials.2006.02.014

178. Keane, T. J., Swinehart, I. T. & Badylak, S. F. Methods of tissue decellularization used for preparation of biologic scaffolds and in vivo relevance. *Methods* **84,** 25–34 (2015).

179. Nonaka, P. N. *et al.* Effects of freezing/thawing on the mechanical properties of decellularized lungs. *J. Biomed. Mater. Res.* **102,** 413–419 (2013).

180. Gilbert, T. W. Strategies for tissue and organ decellularization. *J. Cell. Biochem.* **113,** 2217–2222 (2012).

181. Yang, M., Chen, C.-Z., Wang, X.-N., Zhu, Y.-B. & Gu, Y. J. Favorable effects of the detergent and enzyme extraction method for preparing decellularized bovine pericardium scaffold for tissue engineered heart valves. *J. Biomed. Mater. Res.* **91B,** 354–361 (2009).

182. Chen, X.-D., Dusevich, V., Feng, J. Q., Manolagas, S. C. & Jilka, R. L. Extracellular Matrix Made by Bone Marrow Cells Facilitates Expansion of Marrow-Derived Mesenchymal Progenitor Cells and Prevents Their Differentiation Into Osteoblasts. *J Bone Miner Res* **22,** 1943–1956 (2007).

183. Lai, Y. *et al.* Reconstitution of marrow-derived extracellular matrix ex vivo: a robust culture system for expanding large-scale highly functional human mesenchymal stem cells. *Stem Cells and Development* **19,** 1095–1107 (2010).

184. Fu, X. *et al.* Establishment of Clinically Compliant Human Embryonic Stem Cells in an Autologous Feeder-Free System. *Tissue Engineering Part C: Methods* **17,** 927–937 (2011).

185. Kathju, S., Gallo, P. H. & Satish, L. Scarless integumentary wound healing in

the mammalian fetus: Molecular basis and therapeutic implications. *Birth Defects Research Part C: Embryo Today: Reviews* **96,** 223–236 (2012).

186. Walmsley, G. G. *et al.* Scarless Wound Healing. *Plastic and Reconstructive Surgery* **135,** 907–917 (2015).

187. Aarabi, S., Longaker, M. T. & Gurtner, G. C. Hypertrophic Scar Formation Following Burns and Trauma: New Approaches to Treatment. *PLoS Med* **4,** e234–7 (2007).

188. Staley, M., Richard, R., Billmire, D. & Warden, G. Head/face/neck burns: therapist considerations for the pediatric patient. *J Burn Care Rehabil* **18,** 164–171 (1997).

189. Penna, K. J. & Sadoff, R. S. *Prevention of microstomia following facial burns*. (British Journal of Oral and Maxillofacial …, 1998).

190. Fricke, N. B. *et al.* Skeletal and Dental Disturbances in Children After Facial Burns and Pressure Garment Use: A 4-Year Follow-Up. *Journal of Burn Care & Research* **20,** 239 (1999).

191. Leung, A., Crombleholme, T. M. & Keswani, S. G. Fetal wound healing. *Current Opinion in Pediatrics* **24,** 371–378 (2012).

192. Whitby, D. J. & Ferguson, M. W. The extracellular matrix of lip wounds in fetal, neonatal and adult mice. *Development* **112,** 651–668 (1991).

193. Adzick, N. S. & Longaker, M. T. Animal models for the study of fetal tissue repair. *Journal of Surgical Research* (1991).

194. Lorenz, H. P., Whitby, D. J., Longaker, M. T. & Adzick, N. S. Fetal wound healing. The ontogeny of scar formation in the non-human primate. *Annals of Surgery* **217,** 391–396 (1993).

195. Longaker, M. T. *et al.* Adult skin wounds in the fetal environment heal with scar formation. *Annals of Surgery* **219,** 65–72 (1994).

196. Lo, D. D., Zimmermann, A. S., Nauta, A., Longaker, M. T. & Lorenz, H. P. Scarless fetal skin wound healing update. *Birth Defects Research Part C: Embryo Today: Reviews* **96,** 237–247 (2012).

197. Ferguson, M. W. J. & O'Kane, S. Scar-free healing: from embryonic mechanisms to adult therapeutic intervention. *Philosophical Transactions of the Royal Society B: Biological Sciences* **359,** 839–850 (2004).

198. Helmo, F. R. *et al.* Fetal Wound Healing Biomarkers. *Disease Markers* **35,** 939–944 (2013).

199. Armstrong, J. R. & Ferguson, M. W. Ontogeny of the skin and the transition from scar-free to scarring phenotype during wound healing in the pouch young of a marsupial, Monodelphis domestica. *Developmental Biology* **169,** 242–260 (1995).

200. Lorenz, H. P. *et al.* Scarless wound repair: a human fetal skin model. *Development* **114,** 253–259 (1992).

201. Bullard, K. M., Longaker, M. T. & Lorenz, H. P. Fetal Wound Healing: Current Biology. *World Journal of Surgery* **27,** 54–61 (2003).

202. Leavitt, T. *et al.* Scarless wound healing: finding the right cells and signals. *Cell Tissue Res* 1–11 (2016). doi:10.1007/s00441-016-2424-8

203. Frantz, F. W. *et al.* Biology of fetal repair: the presence of bacteria in fetal wounds induces an adult-like healing response. *J. Pediatr. Surg.* **28,** 428–33–discussion 433–4 (1993).

204. Kumta, S., Ritz, M., Hurley, J. V., Crowe, D. & Romeo, R. Acute inflammation in foetal and adult sheep: the response to subcutaneous injection of turpentine and carrageenan. *British journal of plastic …* (1994).

205. Liechty, K. W., Adzick, N. S. & Crombleholme, T. M. Diminished Interleukin 6 (IL-6) production during scarless human fetal wound repair. *Cytokine* **12,** 671–676 (2000).

206. Liechty, K. W. E. A. Diminished Interleukin-8 (IL-8) Production in the Fetal Wound Healing Response. 1–5 (1998).

207. Gordon, A. *et al.* Permissive environment in postnatal wounds induced by adenoviral-mediated overexpression of the anti-inflammatory cytokine interleukin-10 prevents scar formation. *Wound Repair and Regeneration* **16,** 70–79 (2008).

208. Li, M., Zhao, Y., Hao, H., Han, W. & Fu, X. Theoretical and practical aspects of using fetal fibroblasts for skin regeneration. *Ageing Research Reviews* **36,** 32–41 (2017).

209. Shiraha, H., Gupta, K., Drabik, K. & Wells, A. Aging Fibroblasts Present Reduced Epidermal Growth Factor (EGF) Responsiveness Due to Preferential Loss of EGF Receptors. *Journal of Biological Chemistry* **275,** 19343–19351 (2000).

210. Schor, S. L., Schor, A. M., Rushton, G. & Smith, L. Adult, foetal and transformed fibroblasts display different migratory phenotypes on collagen

gels: evidence for an isoformic transition during foetal development. **73,** 221–234 (1985).

211. Coolen, N. A., Schouten, K. C. W. M., Boekema, B. K. H. L., Middelkoop, E. & Ulrich, M. M. W. Wound healing in a fetal, adult, and scar tissue model: A comparative study. *Wound Repair and Regeneration* **18,** 291–301 (2010).

212. Larson, B. J., Longaker, M. T. & Lorenz, H. P. Scarless Fetal Wound Healing: A Basic Science Review. *Plastic and Reconstructive Surgery* **126,** 1172–1180 (2010).

213. Farahani, R. M. & Kloth, L. C. The hypothesis of 'biophysical matrix contraction': wound contraction revisited. *International wound journal* **5,** 477–482 (2008).

214. Kishi, K., Okabe, K., Shimizu, R. & Kubota, Y. Fetal Skin Possesses the Ability to Regenerate Completely: Complete Regeneration of Skin. *Keio J. Med.* **61,** 101–108 (2012).

215. Estes, J. M. *et al.* Phenotypic and functional features of myofibroblasts in sheep fetal wounds. *Differentiation* **56,** 173–181 (1994).

216. Merkel, J. R., DiPaolo, B. R., Hallock, G. G. & Rice, D. C. Type I and type III collagen content of healing wounds in fetal and adult rats. *Proc. Soc. Exp. Biol. Med.* **187,** 493–497 (1988).

217. Burd, D. A., Longaker, M. T., Adzick, N. S., Harrison, M. R. & Ehrlich, H. P. Foetal wound healing in a large animal model: the deposition of collagen is confirmed. *Br J Plast Surg* **43,** 571–577 (1990).

218. Cuttle, L. *et al.* Collagen in the scarless fetal skin wound: detection with picrosirius-polarization. *Wound Repair Regen* **13,** 198–204 (2005).

219. Sorrell, J. M., Carrino, D. A., Baber, M. A. & Caplan, A. I. Versican in human fetal skin development. *Anat Embryol* **199,** 45–56 (1999).

220. Carrino, D. A., Sorrell, J. M. & Caplan, A. I. Age-related changes in the proteoglycans of human skin. *Arch. Biochem. Biophys.* **373,** 91–101 (2000).

221. Beanes, S. R. *et al.* Down-regulation of decorin, a transforming growth factor-beta modulator, is associated with scarless fetal wound healing. *J. Pediatr. Surg.* **36,** 1666–1671 (2001).

222. Mast, B. A. *et al.* Hyaluronic Acid is a Major Component of the Matrix of Fetal Rabbit Skin and Wounds: Implications for Healing by Regeneration. *Matrix Collagen and Related Research* **11,** 63–68 (1991).

223. Iocono, J. A., Ehrlich, H. P. & Keefer, K. A. Hyaluronan induces scarless repair in mouse limb organ culture. *J. Pediatr. Surg.* **33,** 564–567 (1998).

224. Minamide, L. S. & Bamburg, J. R. A filter paper dye-binding assay for quantitative determination of protein without interference from reducing agents or detergents. *Anal. Biochem.* **190,** 66–70 (1990).

225. Jarvelainen, H., Sainio, A., Koulu, M., Wight, T. N. & Penttinen, R. Extracellular Matrix Molecules: Potential Targets in Pharmacotherapy. *Pharmacological Reviews* **61,** 198–223 (2009).

226. Koumas, L., Smith, T. J., Feldon, S., Blumberg, N. & Phipps, R. P. Thy-1 expression in human fibroblast subsets defines myofibroblastic or lipofibroblastic phenotypes. *AJPA* **163,** 1291–1300 (2003).

227. Chang, Y., Li, H. & Guo, Z. Mesenchymal stem cell-like properties in fibroblasts. *Cell Physiol Biochem* **34,** 703–714 (2014).

228. Klingberg, F., Hinz, B. & White, E. S. The myofibroblast matrix: implications for tissue repair and fibrosis. *J. Pathol.* **229,** 298–309 (2012).

229. Desmoulière, A., Geinoz, A., Gabbiani, F. & Gabbiani, G. Transforming growth factor-beta 1 induces alpha-smooth muscle actin expression in granulation tissue myofibroblasts and in quiescent and growing cultured fibroblasts. *J. Cell Biol.* **122,** 103–111 (1993).

230. Naba, A. *et al.* The matrisome: in silico definition and in vivo characterization by proteomics of normal and tumor extracellular matrices. *Mol. Cell Proteomics* **11,** M111.014647–M111.014647 (2012).

231. Dewavrin, J.-Y. *et al.* Synergistic Rate Boosting of Collagen Fibrillogenesis in Heterogeneous Mixtures of Crowding Agents. *J. Phys. Chem. B* **119,** 4350–4358 (2015).

232. Uhlén, M. *et al.* Proteomics. Tissue-based map of the human proteome. *Science* **347,** 1260419–1260419 (2015).

233. Bliss, E., Heywood, W. E., Benatti, M., Sebire, N. J. & Mills, K. An optimised method for the proteomic profiling of full thickness human skin. *Biological Procedures Online* 1–7 (2016). doi:10.1186/s12575-016-0045-y

234. Janson, D. G., Saintigny, G., van Adrichem, A., Mahé, C. & Ghalbzouri, El, A. Different Gene Expression Patterns in Human Papillary and Reticular Fibroblasts. *J. Invest. Dermatol.* **132,** 2565–2572 (2012).

235. Desmoulière, A., Darby, I. A., Laverdet, B. & Bonté, F. Fibroblasts and

myofibroblasts in wound healing. *CCID* **Volume 7,** 301–11 (2014).

236. Darby, I. A., Zakuan, N., Billet, F. & Desmoulière, A. The myofibroblast, a key cell in normal and pathological tissue repair. *Cell. Mol. Life Sci.* **73,** 1145–1157 (2015).

237. Moulin, V., Auger, F. A., Garrel, D. & Germain, L. Role of wound healing myofibroblasts on re-epithelialization of human skin. *Burns* **26,** 3–12 (2000).

238. Tomasek, J. J., Gabbiani, G., Hinz, B., Chaponnier, C. & Brown, R. A. Myofibroblasts and mechano-regulation of connective tissue remodelling. *Nat Rev Mol Cell Biol* **3,** 349–363 (2002).

239. Hinz, B. The myofibroblast Paradigm for a mechanically active cell. *Journal of Biomechanics* **43,** 146–155 (2010).

240. Magno, V. *et al.* Macromolecular crowding for tailoring tissue-derived fibrillated matrices. *Acta Biomaterialia* 1–11 (2017). doi:10.1016/j.actbio.2017.04.018

241. Prewitz, M. C. *et al.* Extracellular matrix deposition of bone marrow stroma enhanced by macromolecular crowding. *Biomaterials* **73,** 60–69 (2015).

242. Steiglitz, B. M. *et al.* Procollagen C proteinase enhancer 1 genes are important determinants of the mechanical properties and geometry of bone and the ultrastructure of connective tissues. *Molecular and Cellular Biology* **26,** 238–249 (2006).

243. Hojima, Y., Behta, B., Romanic, A. M. & Prockop, D. J. Cleavage of type I procollagen by C- and N-proteinases is more rapid if the substrate is aggregated with dextran sulfate or polyethylene glycol. *Anal. Biochem.* **223,** 173–180 (1994).

244. Shalitin, N., Schlesinger, H., Levy, M. J., Kessler, E. & Kessler-Icekson, G. Expression of procollagen C-proteinase enhancer in cultured rat heart fibroblasts: Evidence for co-regulation with type I collagen. *J. Cell. Biochem.* **90,** 397–407 (2003).

245. Russell, S. B., Russell, J. D. & Trupin, K. M. Collagen synthesis in human fibroblasts: effects of ascorbic acid and regulation by hydrocortisone. *J. Cell. Physiol.* **109,** 121–131 (1981).

246. Kishimoto, Y. *et al.* Ascorbic acid enhances the expression of type 1 and type 4 collagen and SVCT2 in cultured human skin fibroblasts. *Biochemical and Biophysical Research Communications* **430,** 579–584 (2013).

247. Xing, Q. *et al.* Decellularization of Fibroblast Cell Sheets for Natural Extracellular Matrix Scaffold Preparation. *Tissue Engineering Part C: Methods* **21,** 77–87 (2015).

248. Farag, A. & Vaquette, C. Decellularized periodontal ligament cell sheets with recellularization potential. *Journal of dental …* (2014). doi:10.1177/0022034514547762

249. Perea-Gil, I., Uriarte, J. J. & Prat-Vidal, C. In vitro comparative study of two decellularization protocols in search of an optimal myocardial scaffold for recellularization. *American journal …* (2015).

250. Wu, Z. *et al.* The use of phospholipase A2 to prepare acellular porcine corneal stroma as a tissue engineering scaffold. *Biomaterials* **30,** 3513–3522 (2009).

251. Chaturvedi, V. *et al.* Interactions between Skeletal Muscle Myoblasts and their Extracellular Matrix Revealed by a Serum Free Culture System. *PLoS ONE* **10,** e0127675–27 (2015).

252. Badylak, S. F., Freytes, D. O. & Gilbert, T. W. Extracellular matrix as a biological scaffold material: Structure and function. *Acta Biomaterialia* **5,** 1–13 (2009).

253. Sellaro, T. L., Ravindra, A. K., Stolz, D. B. & Badylak, S. F. Maintenance of Hepatic Sinusoidal Endothelial Cell Phenotype In VitroUsing Organ-Specific Extracellular Matrix Scaffolds. *Tissue Eng.* **13,** 2301–2310 (2007).

254. Lysheden, A.-S. *et al.* Analysis of Gene Expression in Fibroblasts in Response to Keratinocyte-Derived Factors In Vitro: Potential Implications for the Wound Healing Process. *J. Invest. Dermatol.* **122,** 216–221 (2003).

255. Peehl, D. M. & Ham, R. G. Growth and differentiation of human keratinocytes without a feeder layer or conditioned medium. *In Vitro* **16,** 516–525 (1980).

256. Boyce, S. T. & Ham, R. G. Calcium-regulated differentiation of normal human epidermal keratinocytes in chemically defined clonal culture and serum-free serial culture. *J Investig Dermatol* (1983). doi:10.1111/1523-1747.ep12540422

257. Peng, Y. *et al.* Human fibroblast matrices bio-assembled under macromolecular crowding support stable propagation of human embryonic stem cells. *J Tissue Eng Regen Med* **6,** e74–e86 (2012).

258. Jiang, D. *et al.* Efficacy of tendon stem cells in fibroblast-derived matrix for tendon tissue engineering. *Journal of Cytotherapy* **16,** 662–673 (2014).

259. Ng, C. P. *et al.* Enhanced ex vivo expansion of adult mesenchymal stem cells by fetal mesenchymal stem cell ECM. *Biomaterials* **35,** 4046–4057 (2014).

260. Zhou, Y. *et al.* Effects of Human Fibroblast-Derived Extracellular Matrix on Mesenchymal Stem Cells. *Stem Cell Rev* 1–13 (2016). doi:10.1007/s12015-016-9671-7

261. Watt, F. M. & Green, H. Involucrin synthesis is correlated with cell size in human epidermal cultures. *J. Cell Biol.* (1981).

262. Bertolero, F., Kaighn, M. E., Camalier, R. F. & Saffiotti, U. Effects of serum and serum-derived factors on growth and differentiation of mouse keratinocytes. *In Vitro Cell Dev Biol* **22,** 423–428 (1986).

263. Svendsen, M. L., Daneels, G., Geysen, J., Binderup, L. & Kragballe, K. Proliferation and Differentiation of Cultured Human Keratinocytes is Modulated by 1,25(OH)2D3 and Synthetic Vitamin D3 Analogues in a Cell Density-, Calcium- and Serum-Dependent Manner*. *Basic & Clinical Pharmacology & Toxicology* **80,** 49–56 (1997).

264. Poumay, Y. & Pittelkow, M. R. Cell Density and Culture Factors Regulate Keratinocyte Commitment to Differentiation and Expression of Suprabasal K1/K10 Keratins. *J. Invest. Dermatol.* **104,** 271–276 (1995).

265. Lessard, J. C., Piña-Paz, S. & Rotty, J. D. Keratin 16 regulates innate immunity in response to epidermal barrier breach. in (2013). doi:10.1073/pnas.1309576110/-/DCSupplemental

266. Maruthappu, T. *et al.* Rhomboid family member 2 regulates cytoskeletal stress-associated Keratin 16. *Nature Communications* **8,** 1–11 (2017).

267. Pellegrini, G. *et al.* p63 identifies keratinocyte stem cells. *Proc. Natl. Acad. Sci. U.S.A.* **98,** 3156–3161 (2001).

268. Haase, I., Evans, R., Pofahl, R. & Watt, F. M. Regulation of keratinocyte shape, migration and wound epithelialization by IGF-1-and EGF-dependent signalling pathways. (2003). doi:10.1242/jcs.00610

269. Gregory, G. G., O'Connor, N. E. & Compton, C. C. *Permanent coverage of large burn wounds with autologous cultured human epithelium*. (N Engl J Med, 1984).

270. Dunnwald, M., Tomanek-Chalkley, A., Alexandrunas, D., Fishbaugh, J. & Bickenbach, J. R. Isolating a pure population of epidermal stem cells for use in tissue engineering. *Experimental Dermatology* **10,** 45–54 (2001).

271. Li, A., Pouliot, N., Redvers, R. & Kaur, P. Extensive tissue-regenerative capacity of neonatal human keratinocyte stem cells and their progeny. *J. Clin. Invest.* **113,** 390–400 (2004).

272. Kim, D. S., Cho, H. J., Choi, H. R., Kwon, S. B. & Park, K. C. Isolation of human epidermal stem cells by adherence and the reconstruction of skin equivalents. *Cell. Mol. Life Sci.* **61,** 2774–2781 (2004).

273. Cerqueira, M. T., Frias, A. M., Reis, R. L. & Marques, A. P. Boosting and Rescuing Epidermal Superior Population from Fresh Keratinocyte Cultures. *Stem Cells and Development* **23,** 34–43 (2014).

274. Horch, R. E., Debus, M., Wagner, G. & Stark, G. B. Cultured human keratinocytes on type I collagen membranes to reconstitute the epidermis. *Tissue Eng.* **6,** 53–67 (2000).

275. Youn, S. W. *et al.* Cellular senescence induced loss of stem cell proportion in the skin in vitro. *Journal of Dermatological Science* **35,** 113–123 (2004).

276. Lin, H., Yang, G., Tan, J. & Tuan, R. S. Influence of decellularized matrix derived from human mesenchymal stem cells on their proliferation, migration and multi-lineage differentiation potential. *Biomaterials* **33,** 4480–4489 (2012).

277. Rakian, R. *et al.* Native extracellular matrix preserves mesenchymal stem cell 'stemness' and differentiation potential under serum-free culture conditions. *Stem Cell Res Ther* 1–11 (2015). doi:10.1186/s13287-015-0235-6

278. He, F., Chen, X. & Pei, M. Reconstruction of an in vitro tissue-specific microenvironment to rejuvenate synovium-derived stem cells for cartilage tissue engineering. *Tissue Eng Part A* **15,** 3809–3821 (2009).

279. Pei, M., Zhang, Y., Li, J. & Chen, D. Antioxidation of Decellularized Stem Cell Matrix Promotes Human Synovium-Derived Stem Cell-Based Chondrogenesis. *Stem Cells and Development* **22,** 889–900 (2013).

280. Fuchs, E. & Green, H. Changes in keratin gene expression during terminal differentiation of the keratinocyte. *Cell* **19,** 1033–1042 (1980).

281. Coulombe, P. A., Kopan, R. & Fuchs, E. Expression of keratin K14 in the epidermis and hair follicle: insights into complex programs of differentiation. *J. Cell Biol.* **109,** 2295–2312 (1989).

282. Troy, T. C. & Turksen, K. In vitro characteristics of early epidermal progenitors isolated from keratin 14 (K14)-deficient mice: insights into the

role of keratin 17 in mouse keratinocytes. *J. Cell. Physiol.* **180,** 409–421 (1999).

283. Alam, H., Sehgal, L., Kundu, S. T., Dalal, S. N. & Vaidya, M. M. Novel function of keratins 5 and 14 in proliferation and differentiation of stratified epithelial cells. *Mol. Biol. Cell* **22,** 4068–4078 (2011).

284. Parsa, R., Yang, A., McKeon, F. & Green, H. Association of p63 with Proliferative Potential in Normal and Neoplastic Human Keratinocytes. *J. Invest. Dermatol.* **113,** 1099–1105 (1999).

285. King, K. E. *et al.* ΔNp63α functions as both a positive and a negative transcriptional regulator and blocks in vitro differentiation of murine keratinocytes. *Oncogene* **22,** 3635–3644 (2003).

286. Sun, T. T. & Green, H. Differentiation of the epidermal keratinocyte in cell culture: formation of the cornified envelope. *Cell* **9,** 511–521 (1976).

287. Barrandon, Y. & Green, H. Cell size as a determinant of the clone-forming ability of human keratinocytes. *Proc. Natl. Acad. Sci. U.S.A.* **82,** 5390–5394 (1985).

288. Izumi, K., Tobita, T. & Feinberg, S. E. Isolation of human oral keratinocyte progenitor/stem cells. *Journal of Dental Research* **86,** 341–346 (2007).

289. Li, J. *et al.* Enrichment of putative human epidermal stem cells based on cell size and collagen type IV adhesiveness. *Cell Res* **18,** 360–371 (2008).

290. Nanba, D. *et al.* Cell motion predicts human epidermal stemness. *J. Cell Biol.* **209,** 305–315 (2015).

291. Vaezi, A., Bauer, C., Vasioukhin, V. & Fuchs, E. Actin Cable Dynamics and Rho/Rock Orchestrate a Polarized Cytoskeletal Architecture in the Early Steps of Assembling a Stratified Epithelium. *Developmental Cell* **3,** 367–381 (2002).

292. Nanba, D. *et al.* Actin filament dynamics impacts keratinocyte stem cell maintenance. *EMBO Mol Med* **5,** 640–653 (2013).

293. Handorf, A. M., Zhou, Y., Halanski, M. A. & Li, W.-J. Tissue Stiffness Dictates Development, Homeostasis, and Disease Progression. *Organogenesis* **11,** 1–15 (2015).

294. Wells, R. G. The role of matrix stiffness in regulating cell behavior. *Hepatology* **47,** 1394–1400 (2008).

295. Kutys, M. L., Doyle, A. D. & Yamada, K. M. Regulation of cell adhesion and

migration by cell-derived matrices. *Exp. Cell Res.* **319,** 2434–2439 (2013).

296. Webb, A., Li, A. & Kaur, P. Location and phenotype of human adult keratinocyte stem cells of the skin. *Differentiation* **72,** 387–395 (2004).

297. Flaim, C. J., Chien, S. & Bhatia, S. N. An extracellular matrix microarray for probing cellular differentiation. *Nat Meth* **2,** 119–125 (2005).

298. Flaim, C. J., Teng, D., Chien, S. & Bhatia, S. N. Combinatorial Signaling Microenvironments for Studying Stem Cell Fate. *Stem Cells and Development* **17,** 29–40 (2008).

299. Malta, D. F. B. *et al.* Extracellular matrix microarrays to study inductive signaling for endoderm specification. *Acta Biomaterialia* **34,** 30–40 (2016).

300. Chacón-Martínez, C. A., Klose, M., Niemann, C., Glauche, I. & Wickström, S. A. Hair follicle stem cell cultures reveal self-organizing plasticity of stem cells and their progeny. *The EMBO Journal* **36,** 151–164 (2017).

301. Blanpain, C. & Fuchs, E. Epidermal Stem Cells of the Skin. *Annu. Rev. Cell Dev. Biol.* **22,** 339–373 (2006).

302. Chebotaev, D. V., Yemelyanov, A. Y., Lavker, R. M. & Budunova, I. V. Epithelial Cells in the Hair Follicle Bulge do not Contribute to Epidermal Regeneration after Glucocorticoid-Induced Cutaneous Atrophy. *J. Invest. Dermatol.* **127,** 2749–2758 (2007).

303. Barrandon, Y. & Green, H. Three clonal types of keratinocyte with different capacities for multiplication. *Proc. Natl. Acad. Sci. U.S.A.* **84,** 2302–2306 (1987).

304. Lyle, S. *et al.* The C8/144B monoclonal antibody recognizes cytokeratin 15 and defines the location of human hair follicle stem cells. *J. Cell. Sci.* **111 (Pt 21),** 3179–3188 (1998).

305. Michel, M. *et al.* Keratin 19 as a biochemical marker of skin stem cells in vivo and in vitro: keratin 19 expressing cells are differentially localized in function of anatomic sites, and their number varies with donor age and culture stage. *J. Cell. Sci.* **109 (Pt 5),** 1017–1028 (1996).

306. Ma, D. *et al.* Breast cancer resistance protein identifies clonogenic keratinocytes in human interfollicular epidermis. *Cell Cycle* 1–13 (2015). doi:10.1186/s13287-015-0032-2

307. Lamb, R. & Ambler, C. A. Keratinocytes Propagated in Serum-Free, Feeder-Free Culture Conditions Fail to Form Stratified Epidermis in a Reconstituted

Skin Model. *PLoS ONE* **8,** e52494 (2013).

308. Benny, P., Badowski, C., Lane, E. B. & Raghunath, M. Making More Matrix: Enhancing the Deposition of Dermal–Epidermal Junction Components In Vitroand Accelerating Organotypic Skin Culture Development, Using Macromolecular Crowding. *Tissue Eng Part A* **21,** 183–192 (2015).
309. Hu, M. S. *et al.* Tissue Engineering and Regenerative Repair in Wound Healing. *Ann Biomed Eng* **42,** 1494–1507 (2014).
310. Gawronska-Kozak, B., Bogacki, M., Rim, J.-S., Monroe, W. T. & Manuel, J. A. Scarless skin repair in immunodeficient mice. *Wound Repair and Regeneration* **14,** 265–276 (2006).
311. Manuel, J. A. & Gawronska-Kozak, B. Matrix metalloproteinase 9 (MMP-9) is upregulated during scarless wound healing in athymic nude mice. *Matrix Biology* **25,** 505–514 (2006).
312. Gawronska-Kozak, B. Scarless skin wound healing in FOXN1 deficient (nude) mice is associated with distinctive matrix metalloproteinase expression. *Matrix Biology* **30,** 290–300 (2011).
313. Longaker, M. T. *et al.* Studies in fetal wound healing, VI. Second and early third trimester fetal wounds demonstrate rapid collagen deposition without scar formation. *J. Pediatr. Surg.* **25,** 63–8– discussion 68–9 (1990).
314. Coolen, N. A., Schouten, K. C. W. M., Middelkoop, E. & Ulrich, M. M. W. Comparison between human fetal and adult skin. *Arch Dermatol Res* **302,** 47–55 (2009).
315. Knight, K. R. *et al.* Glycosaminoglycan composition of uninjured skin and of scar, tissue in fetal, newborn and adult sheep. *Res. Exp. Med.* **194,** 119–127 (1994).
316. David-Raoudi, M. *et al.* Differential effects of hyaluronan and its fragments on fibroblasts: Relation to wound healing. *Wound Repair Regen* **16,** 274–287 (2008).
317. Bartolini, B. *et al.* Iduronic Acid in Chondroitin/Dermatan Sulfate Affects Directional Migration of Aortic Smooth Muscle Cells. *PLoS ONE* **8,** e66704–11 (2013).
318. Thompson, A. *et al.* Tandem Mass Tags: A Novel Quantification Strategy for Comparative Analysis of Complex Protein Mixtures by MS/MS. *Anal. Chem.* **75,** 1895–1904 (2003).

319. Naba, A., Clauser, K. R., Mani, D. R., Carr, S. A. & Hynes, R. O. Quantitative proteomic profiling of the extracellular matrix of pancreatic islets during the angiogenic switch and insulinoma progression. *Sci. Rep.* 1–12 (2016). doi:10.1038/srep40495

320. Brink, H. E., Bernstein, J. & Nicoll, S. B. Fetal dermal fibroblasts exhibit enhanced growth and collagen production in two- and three-dimensional culture in comparison to adult fibroblasts. *J Tissue Eng Regen Med* **3,** 623–633 (2009).

321. Allison, D. B., Page, G. P., Beasley, T. M. & Edwards, J. W. *DNA Microarrays and Related Genomics Techniques*. (CRC Press, 2005).

322. Szklarczyk, D. *et al.* The STRING database in 2017: quality-controlled protein–protein association networks, made broadly accessible. *Nucleic Acids Res* **45,** D362–D368 (2017).

323. Takeo, M., Lee, W. & Ito, M. Wound healing and skin regeneration. *Cold Spring Harbor Perspectives in Medicine* **5,** a023267–a023267 (2015).

324. Schmidt, M. *et al.* Controlling the Balance of Fibroblast Proliferation and Differentiation: Impact of Thy-1. *J. Invest. Dermatol.* **135,** 1893–1902 (2015).

325. Walraven, M., Akershoek, J. J., Beelen, R. H. J. & Ulrich, M. M. W. In vitro cultured fetal fibroblasts have myofibroblast-associated characteristics and produce a fibrotic-like environment upon stimulation with TGF-β1: Is there a thin line between fetal scarless healing and fibrosis? *Arch Dermatol Res* **309,** 111–121 (2016).

326. Walraven, M., Gouverneur, M., Middelkoop, E., Beelen, R. H. J. & Ulrich, M. M. W. Altered TGF-β signaling in fetal fibroblasts: What is known about the underlying mechanisms? *Wound Repair Regen* **22,** 3–13 (2013).

327. Rauniyar, N. & Yates, J. R., III. Isobaric Labeling-Based Relative Quantification in Shotgun Proteomics. *J. Proteome Res.* **13,** 5293–5309 (2014).

328. Gosiewska, A. *et al.* Differential expression and regulation of extracellular matrix-associated genes in fetal and neonatal fibroblasts. *Wound Repair Regen* **9,** 213–222 (2001).

329. Smith, L. T. Patterns of type VI collagen compared to types I, III and V collagen in human embryonic and fetal skin and in fetal skin-derived cell cultures. *Matrix Biology* **14,** 159–170 (1994).

330. Lovvorn, H. N., Cheung, D. T., Nimni, M. E. & Perelman, N. Relative distribution and crosslinking of collagen distinguish fetal from adult sheep wound repair. *Journal of pediatric …* **34,** 218–223 (1999).

331. Wenstrup, R. J. *et al.* Type V collagen controls the initiation of collagen fibril assembly. *Journal of Biological Chemistry* **279,** 53331–53337 (2004).

332. Wilke, M. S. & Furcht, L. T. Human keratinocytes adhere to a unique heparin-binding peptide sequence within the triple helical region of type IV collagen. *J. Invest. Dermatol.* **95,** 264–270 (1990).

333. Bush, K. A., Downing, B. R., Walsh, S. E. & Pins, G. D. Conjugation of extracellular matrix proteins to basal lamina analogs enhances keratinocyte attachment. *J. Biomed. Mater. Res.* **80A,** 444–452 (2006).

334. Fujisaki, H., Adachi, E. & Hattori, S. Keratinocyte Differentiation and Proliferation are Regulated by Adhesion to the Three-Dimensional Meshwork Structure of Type IV Collagen. *Connect Tissue Res* **49,** 426–436 (2008).

335. Gaetani, M. *et al.* Unbiased and quantitative proteomics reveals highly increased angiogenesis induction by the secretome of mesenchymal stromal cells isolated from fetal rather than adult skin. *J Tissue Eng Regen Med* 1–34 (2017). doi:10.1002/term.2417

336. Bezakova, G. & Ruegg, M. A. New insights into the roles of agrin. *Nat Rev Mol Cell Biol* **4,** 295–309 (2003).

337. Burgess, R. W., Dickman, D. K., Nunez, L., Glass, D. J. & Sanes, J. R. Mapping sites responsible for interactions of agrin with neurons. *J. Neurochem.* **83,** 271–284 (2002).

338. Kim, N. *et al.* Lrp4 Is a Receptor for Agrin and Forms a Complex with MuSK. *Cell* **135,** 334–342 (2008).

339. Watt, F. M., Kubler, M. D., Hotchin, N. A., Nicholson, L. J. & Adams, J. C. Regulation of keratinocyte terminal differentiation by integrin-extracellular matrix interactions. **106 (Pt 1),** 175–182 (1993).

340. Ahn, Y., Sims, C., Logue, J. M., Weatherbee, S. D. & Krumlauf, R. Lrp4 and Wise interplay controls the formation and patterning of mammary and other skin appendage placodes by modulating Wnt signaling. *Development* **140,** 583–593 (2013).

341. Fujiwara, H., Gu, J. & Sekiguchi, K. Rac regulates integrin-mediated endothelial cell adhesion and migration on laminin-8. *Exp. Cell Res.* **292,** 67–

77 (2004).

342. Li, J. *et al.* Overexpression of Laminin-8 in Human Dermal Microvascular Endothelial Cells Promotes Angiogenesis-Related Functions. *J. Invest. Dermatol.* **126,** 432–440 (2006).

343. Ishikawa, T. *et al.* Laminins 411 and 421 differentially promote tumor cell migration via α6β1 integrin and MCAM (CD146). *Matrix Biology* **38,** 69–83 (2014).

344. Cox, T. R. & Erler, J. T. Remodeling and homeostasis of the extracellular matrix: implications for fibrotic diseases and cancer. *Disease Models & Mechanisms* **4,** 165–178 (2011).

345. Chen, W., Fu, X., Ge, S., Sun, T. & Sheng, Z. Differential expression of matrix metalloproteinases and tissue-derived inhibitors of metalloproteinase in fetal and adult skins. *Int. J. Biochem. Cell Biol.* **39,** 997–1005 (2007).

346. Okada, A. *et al.* Expression of Matrix Metalloproteinases during Rat Skin Wound Healing: Evidence that Membrane Type-1 Matrix Metalloproteinase Is a Stromal Activator of Pro-Gelatinase A. *J. Cell Biol.* **137,** 67–77 (1997).

347. Conway, S. J. *et al.* The role of periostin in tissue remodeling across health and disease. *Cell. Mol. Life Sci.* **71,** 1279–1288 (2013).

348. Walker, J. T., McLeod, K., Kim, S., Conway, S. J. & Hamilton, D. W. Periostin as a multifunctional modulator of the wound healing response. *Cell Tissue Res* 1–13 (2016). doi:10.1007/s00441-016-2426-6

349. Taniguchi, K. *et al.* Periostin Controls Keratinocyte Proliferation and Differentiation by Interacting with the Paracrine IL-1α/IL-6 Loop. **134,** 1295–1304 (2014).

350. Nishiyama, T. *et al.* Delayed Re-Epithelialization in Periostin-Deficient Mice during Cutaneous Wound Healing. *PLoS ONE* **6,** e18410–14 (2011).

351. Ontsuka, K. *et al.* Periostin, a matricellular protein, accelerates cutaneous wound repair by activating dermal fibroblasts. *Experimental Dermatology* **21,** 331–336 (2012).

352. Özdemir, C. *et al.* Periostin is temporally expressed as an extracellular matrix component in skeletal muscle regeneration and differentiation. *Gene* **553,** 130–139 (2014).

353. Kühn, B. *et al.* Periostin induces proliferation of differentiated cardiomyocytes and promotes cardiac repair. *Nat Med* **13,** 962–969 (2007).

354. Yamaguchi, Y. Periostin in Skin Tissue and Skin-Related Diseases. *Allergology International* **63,** 161–170 (2014).

355. Crawford, J., Nygard, K., Gan, B. S. & O'Gorman, D. B. Periostin induces fibroblast proliferation and myofibroblast persistence in hypertrophic scarring. *Experimental Dermatology* **24,** 120–126 (2015).

356. Mitchell, A. C., Briquez, P. S., Hubbell, J. A. & Cochran, J. R. Engineering growth factors for regenerative medicine applications. *Acta Biomaterialia* **30,** 1–12 (2016).

357. Whitby, D. J. & Ferguson, M. W. Immunohistochemical localization of growth factors in fetal wound healing. *Developmental Biology* **147,** 207–215 (1991).

358. Broker, B. J. *et al.* Comparison of growth factor expression in fetal and adult fibroblasts: a preliminary report. *Arch. Otolaryngol. Head Neck Surg.* **125,** 676–680 (1999).

359. Botchkarev, V. A. Bone Morphogenetic Proteins and Their Antagonists in Skin and Hair Follicle Biology. *J. Invest. Dermatol.* **120,** 36–47 (2003).

360. BRILL, S. The role of fetal and adult hepatocyte extracellular matrix in the regulation of tissue-specific gene expression in fetal and adult hepatocytes. *European Journal of Cell Biology* **81,** 43–50 (2002).

361. Sun, Y. *et al.* Rescuing replication and osteogenesis of aged mesenchymal stem cells by exposure to a young extracellular matrix. *The FASEB Journal* **25,** 1474–1485 (2011).

362. Li, J. *et al.* Rejuvenation of chondrogenic potential in a young stem cell microenvironment. *Biomaterials* **35,** 642–653 (2014).

363. Blanpain, C. & Fuchs, E. Epidermal homeostasis: a balancing act of stem cells in the skin. *Nat Rev Mol Cell Biol* **10,** 207–217 (2009).

364. Hustedt, N. & Durocher, D. The control of DNA repair by the cell cycle. *Nature Publishing Group* **19,** 1–9 (2017).

365. Torgovnick, A. & Schumacher, B. DNA repair mechanisms in cancer development and therapy. *Front. Genet.* **6,** 1–15 (2015).

366. Brazil, D. P., Church, R. H., Surae, S., Godson, C. & Martin, F. BMP signalling: agony and antagony in the family. *Trends Cell Biol.* **25,** 249–264 (2015).

367. Hayashi, Y. *et al.* BMP-SMAD-ID promotes reprogramming to pluripotency

by inhibiting p16/INK4A-dependent senescence. *Proc. Natl. Acad. Sci. U.S.A.* **113,** 13057–13062 (2016).

368. Qi, X. *et al.* BMP4 supports self-renewal of embryonic stem cells by inhibiting mitogen-activated protein kinase pathways. *Proc. Natl. Acad. Sci. U.S.A.* **101,** 6027–6032 (2004).
369. Gillan, L. *et al.* Periostin Secreted by Epithelial Ovarian Carcinoma Is a Ligand for αVβ3 and αVβ5 Integrins and Promotes Cell Motility. *Cancer Res* **62,** 5358–5364 (2002).
370. Cruet-Hennequart, S. *et al.* αv integrins regulate cell proliferation through integrin-linked kinase (ILK) in ovarian cancer cells. *Oncogene* **22,** 1688–1702 (2003).
371. Choi, H.-R. Niche interactions in epidermal stem cells. *WJSC* **7,** 495–8 (2015).
372. Ang, X. M. *et al.* Macromolecular Crowding Amplifies Adipogenesis of Human Bone Marrow-Derived Mesenchymal Stem Cells by Enhancing the Pro-Adipogenic Microenvironment. *Tissue Eng Part A* **20,** 966–981 (2014).
373. Lu, H. *et al.* Cultured cell-derived extracellular matrix scaffolds for tissue engineering. *Biomaterials* **32,** 9658–9666 (2011).
374. Adams, J. C. & Watt, F. M. Fibronectin inhibits the terminal differentiation of human keratinocytes. *Nature* **340,** 307–309 (1989).
375. Engler, A. J., Sen, S., Sweeney, H. L. & Discher, D. E. Matrix Elasticity Directs Stem Cell Lineage Specification. *Cell* **126,** 677–689 (2006).
376. Trappmann, B. *et al.* Extracellular-matrix tethering regulates stem-cell fate. *Nature Materials* **11,** 642–649 (2012).
377. Achterberg, V. F. *et al.* The Nano-Scale Mechanical Properties of the Extracellular Matrix Regulate Dermal Fibroblast Function. *J. Invest. Dermatol.* **134,** 1862–1872 (2014).
378. van den Bogaard, E. H. *et al.* Rho Kinase Inhibitor Y-27632 Prolongs the Life Span of Adult Human Keratinocytes, Enhances Skin Equivalent Development, and Facilitates Lentiviral Transduction. *Tissue Eng Part A* **18,** 1827–1836 (2012).
379. Kirouac, D. C. *et al.* Cell-cell interaction networks regulate blood stem and progenitor cell fate. *Mol. Syst. Biol.* **5,** 293 (2009).
380. Gaudet, S. Connecting cell fate decision networks in hematopoeisis from the outside in. *Mol. Syst. Biol.* **6,** 1–3 (2010).

381. Kirouac, D. C. *et al.* Dynamic interaction networks in a hierarchically organized tissue. *Mol. Syst. Biol.* **6,** 1–16 (2010).

382. Qiao, W. *et al.* Intercellular network structure and regulatory motifs in the human hematopoietic system. *Mol. Syst. Biol.* **10,** 741–741 (2014).

383. Roy, S. & Kundu, T. K. Gene regulatory networks and epigenetic modifications in cell differentiation. *IUBMB Life* **66,** 100–109 (2014).

384. Bonfanti, P. *et al.* Microenvironmental reprogramming of thymic epithelial cells to skin multipotent stem cells. *Nature* **466,** 978–982 (2011).

385. Ladewig, J., Koch, P. & Brüstle, O. Leveling Waddington: the emergence of direct programming and the loss of cell fate hierarchies. *Nat Rev Mol Cell Biol* **14,** 225–236 (2013).

386. Waddington, C. H. *The strategy of the genes. 1957*. (George Unwin & Unwin, 1957).

387. Takahashi, K. Cellular reprogramming--lowering gravity on Waddington's epigenetic landscape. *J. Cell. Sci.* **125,** 2553–2560 (2012).

388. Takahashi, K. Cellular Reprogramming. *Cold Spring Harbor Perspectives in Biology* **6,** a018606–a018606 (2014).

389. Tetteh, P. W., Farin, H. F. & Clevers, H. Plasticity within stem cell hierarchies in mammalian epithelia. *Trends Cell Biol.* **25,** 100–108 (2015).

390. van Es, J. H. *et al.* Dll1+ secretory progenitor cells revert to stem cells upon crypt damage. *Nature Cell Biology* **14,** 1099–1104 (2012).

391. Roth, S. *et al.* Paneth Cells in Intestinal Homeostasis and Tissue Injury. *PLoS ONE* **7,** e38965–15 (2012).

392. Tata, P. R. *et al.* Dedifferentiation of committed epithelial cells into stem cells in vivo. *Nature* **1,** 380–19 (2013).

Appendix A

Example of mass spectrometry proteomic dataset of protein composition of the acellular cell-derived ECM. Yellow highlights the ECM proteins

ACCENSION	DECRIPTION
P09382	Galectin-1 OS=Homo sapiens GN=LGALS1 PE=1 SV=2 - [LEG1_HUMAN]
P08670	Vimentin OS=Homo sapiens GN=VIM PE=1 SV=4 - [VIME_HUMAN]
P60709	Actin, cytoplasmic 1 OS=Homo sapiens GN=ACTB PE=1 SV=1 - [ACTB_HUMAN]
P63261	Actin, cytoplasmic 2 OS=Homo sapiens GN=ACTG1 PE=1 SV=1 - [ACTG_HUMAN]
P07437	Tubulin beta chain OS=Homo sapiens GN=TUBB PE=1 SV=2 - [TBB5_HUMAN]
P68371	Tubulin beta-4B chain OS=Homo sapiens GN=TUBB4B PE=1 SV=1 - [TBB4B_HUMAN]
Q9BUF5	Tubulin beta-6 chain OS=Homo sapiens GN=TUBB6 PE=1 SV=1 - [TBB6_HUMAN]
P01834	Ig kappa chain C region OS=Homo sapiens GN=IGKC PE=1 SV=1 - [IGKC_HUMAN]
P62736	Actin, aortic smooth muscle OS=Homo sapiens GN=ACTA2 PE=1 SV=1 - [ACTA_HUMAN]
P63241	Eukaryotic translation initiation factor 5A-1 OS=Homo sapiens GN=EIF5A PE=1 SV=2 - [IF5A1_HUMAN]
P04792	Heat shock protein beta-1 OS=Homo sapiens GN=HSPB1 PE=1 SV=2 - [HSPB1_HUMAN]
P04350	Tubulin beta-4A chain OS=Homo sapiens GN=TUBB4A PE=1 SV=2 - [TBB4A_HUMAN]
B1ALD8	Periostin OS=Homo sapiens GN=POSTN PE=2 SV=1 - [B1ALD8_HUMAN]
Q9BQE3	Tubulin alpha-1C chain OS=Homo sapiens GN=TUBA1C PE=1 SV=1 - [TBA1C_HUMAN]
P68363	Tubulin alpha-1B chain OS=Homo sapiens GN=TUBA1B PE=1 SV=1 - [TBA1B_HUMAN]
Q71U36	Tubulin alpha-1A chain OS=Homo sapiens GN=TUBA1A PE=1 SV=1 - [TBA1A_HUMAN]

Appendix B
Fibroblast-Derived Extracellular Matrix:
https://www.youtube.com/watch?v=n07aIy3atDU

Type I Collagen:
https://www.youtube.com/watch?v=Q8uEzmDJgI0

Tissue Culture Plastic:
https://www.youtube.com/watch?v=Q8uEzmDJgI0

Appendix C

Categorisation of gene ontology used for TreeMap in Fig. 5.20

TERM_ID	DESCRIPTION	LOG10PVALUE	CATEGORY
GO:0022402	cell cycle process	-7.7471	cell cycle process
GO:0007062	sister chromatid cohesion	-5.9318	cell cycle process
GO:0031577	spindle checkpoint	-4.0716	cell cycle process
GO:1903047	mitotic cell cycle process	-8.1993	cell cycle process
GO:0098813	nuclear chromosome segregation	-5.1079	cell cycle process
GO:0051301	cell division	-5.9706	cell cycle process
GO:0034501	protein localisation to kinetochore	-5.0066	protein localisation to kinetochore
GO:0044380	protein localisation to cytoskeleton	-4.3363	protein localisation to kinetochore
GO:0072698	protein localisation to microtubule cytoskeleton	-4.5686	protein localisation to kinetochore
GO:0090304	nucleic acid metabolic process	-6.0255	nucleic acid metabolism
GO:0019219	regulation of nucleobase-containing compound metabolic process	-5.1319	nucleic acid metabolism
GO:0046483	heterocycle metabolic process	-4	nucleic acid metabolism
GO:0006259	DNA metabolic process	-4.6216	nucleic acid metabolism
GO:0006139	nucleobase-containing compound metabolic process	-4.6383	nucleic acid metabolism
GO:0051783	regulation of nuclear division	-7.6615	regulation of nuclear division
GO:0051983	regulation of chromosome segregation	-4.2104	regulation of nuclear division
GO:0051276	chromosome organization	-4.8297	regulation of nuclear division
GO:0006996	organelle organization	-4.9957	regulation of nuclear division
GO:0000226	microtubule cytoskeleton organisation	-4.5901	regulation of nuclear division
GO:0007017	microtubule-based process	-5.4855	microtubule-based process
GO:0007059	chromosome segregation	-6.4413	chromosome segregation

Categorisation of gene ontology used for TreeMap in Fig. 5.21

TERM_ID	DESCRIPTION	LOG10PVALUE	CATEGORY
GO:0006629	lipid metabolic process	-10.5331	lipid metabolism
GO:0032787	monocarboxylic acid metabolic process	-4.7878	lipid metabolism
GO:0006066	alcohol metabolic process	-6.0511	lipid metabolism
GO:0090181	regulation of cholesterol metabolic process	-5.4622	lipid metabolism
GO:0044723	single-organism carbohydrate metabolic process	-5.6799	lipid metabolism
GO:0071702	organic substance transport	-4.6253	lipid metabolism
GO:0005975	carbohydrate metabolic process	-5.0164	lipid metabolism
GO:0044711	single-organism biosynthetic process	-4.58	lipid metabolism
GO:0044712	single-organism catabolic process	-4.3726	lipid metabolism
GO:0044710	single-organism metabolic process	-10.1391	lipid metabolism
GO:0044255	cellular lipid metabolic process	-7.3391	lipid metabolism
GO:0006438	valyl-tRNA aminoacylation	-4.083	lipid metabolism
GO:1902578	single-organism localization	-5.3947	lipid metabolism
GO:0006082	organic acid metabolic process	-5.025	lipid metabolism
GO:0044281	small molecule metabolic process	-6.0904	lipid metabolism
GO:0007155	cell adhesion	-4.2636	cell adhesion
GO:0098609	cell-cell adhesion	-4.1518	cell adhesion
GO:0008152	metabolic process	-4.857	metabolism
GO:0022610	biological adhesion	-4.209	biological adhesion
GO:0034976	response to endoplasmic reticulum stress	-4.9066	response to endoplasmic reticulum stress
GO:0071364	cellular response to epidermal growth factor stimulus	-4.0788	response to endoplasmic reticulum stress
GO:0098780	response to mitochondrial depolarization	-4.618	response to endoplasmic reticulum stress
GO:0051179	localization	-5.2958	localization
GO:0044238	primary metabolic process	-4.9318	primary metabolism
GO:0009056	catabolic process	-4.4672	catabolism
GO:0070268	cornification	-9.0788	cornification
GO:0012501	programmed cell death	-4.284	cornification
GO:0042119	neutrophil activation	-4.1186	neutrophil activation
GO:0071704	organic substance metabolic process	-4.8861	organic substance metabolism
GO:1901615	organic hydroxy compound metabolic process	-4.2147	organic hydroxy compound metabolism

Every reasonable effort has been made to acknowledge the owners of copyright material. I would be pleased to hear from any copyright owner who has been omitted or incorrectly acknowledged.